A fragment based approach to the development of novel antibacterial agents inspired by the natural product simocyclinone D8

Michael Jonathan Austin

School of Pharmacy

University of East Anglia

A thesis submitted for the degree of Doctor of Philosophy

August 2015

Declaration

This thesis is submitted to the University of East Anglia for the Degree of Doctor of Philosophy and has not been previously submitted at this or any University for assessment or for any other degree. Except where stated, and reference and acknowledgment is given, this work is original and has been carried out by the author alone.

Michael Jonathan Austin

Abstract

The novel mechanism of simocyclinone D8 (SD8) against DNA gyrase has inspired medicinal chemists for over a decade. The search for antibiotics with new mechanisms of action has never been more important with ever increasing prevalence of resistance. This project had three objectives. Firstly to contribute towards the total synthesis of SD8, by exploring chlorination reactions of dihydroxycoumarins and their corresponding starting reagents. Additionally, there was a need to establish a viable route towards the complex polyketide scaffold. Secondly, to generate a library of coumarins and screen for a low molecular weight fragment that could be taken forward as a lead compound. Thirdly, inspired by the bi-functional mode of action of SD8, the project sought to design and synthesise a coumarin-quinolone hybrid via a fragment-based approach.

Herein we exploit *ortho* and *para* directing effects of phenolic OH groups to selectively chlorinate starting materials. However, we show chlorination of reagents prior to forming a coumarin is not a viable synthetic strategy. This is due to the reduced nucleophilicity imparted by the halogen on adjacent atoms. Consequently, this abrogates any ring closure reaction.

We illustrate that a previously established Diels-Alder route can furnish a novel isomerised pericyclic adduct. This provides a good starting point for reaction optimisation and the onward enantioselective synthesis of the complex polyketide scaffold.

Lastly, 27 different coumarin fragments were synthesised and assessed for biological activity. We illustrate that simple coumarins lack inhibition in supercoiling assays against DNA gyrase. Furthermore, when ciprofloxacin is attached to a linker there is an attenuation of activity. Strikingly, when a simple coumarin is joined to ciprofloxacin, via a linker there is a restoration of activity. We show DNA gyrase inhibition is via cleavage stabilisation. Moreover, we demonstrate activity is related to the coumarin structure and not the presence of an aromatic ring.

Acknowledgments

'When I was a child, I spoke like a child; I thought like a child, I reasoned like a child: but when I became a man, I put away childish things'

(King James 2000 bible, 1 Corinthians 13:11)

I would like to thank Professor Mark Searcey and Dr Lesley Howell for giving me the opportunity to do a PhD. Their passion for science and medicinal chemistry inspired me to embark on this scientific adventure. No one else would have put up with my musical choices in the lab! Without their expertise and guidance this wouldn't have been possible.

I would also like to thank Professor Tony Maxwell for allowing me to work in his lab and for his guidance with the biological assays performed in this thesis. I also thank Steve Hearnshaw and Lesley Mitchenell for their help with the biological assays, and their unwavering patience when training me.

I would like to dedicate this thesis to my mother Suzanne Austin, her continued belief; support and encouragement sustained me over the years it took to complete. I also thank my Grandmother for helping with my early years of education. I want to thank my brothers and sisters in Christ, and the fellowship I have had from them. I am grateful for God's provision of joys, challenges and grace for growth.

Lastly, but not least I want to thank my lab buddies from the Medicinal Chemistry group. The banter, music and tears have all been worth it.

Table of Contents

Contents

Tables

Figures

Schemes

Abbreviations

Å	Angstrom
Ar	Aromatic
ATP	Adenosine Triphosphate
Boc	*tert*-butyloxycarbonyl
br	Broad
Conc.	Concentrated
°C	Degrees Celsius
CD	Circular Dichroism
Da	Dalton
DFT	Density Functional Theory

DMF	*N*-*N*-Dimethylformamide
DMSO	Dimethylsulfoxide
DNA	Deoxyribonucleic Acid
EDC	N-Ethyl-N'-(3-dimethylaminopropyl)Carbodiimide hydrochloride
ESI	Electrospray Ionisation
Eq.	Equivalent
EtOAc	Ethyl Acetate
EtOH	Ethanol
FDA	Food and Drug Administration
Gyr	Gyrase
h	Hour
Hz	Hertz

IR	Infrared Spectroscopy
M	Molar
MeCN	Acetonitrile
MHz	Megahertz
Min	Minutes
Mp.	Melting point
NADH	Nicotinamide Adenine Dinucleotide
NADPH	Nicotinamide Adenine Dinucleotide Phosphate
NMR	Nuclear Magnetic Resonance Spectroscopy
ppm	Parts Per Million
RNA	Ribonucleic Acid

rt	Room Temperature
SDS	Sodium Dodecyl Sulphate
SD4	Simocyclinone D4
SD8	Simocyclinone D8
TFA	Trifluroacetic Acid
TLC	Thin Layer Chromatography
Topo	Topoisomerase
UV	Ultra Violet
V	Volts

Chapter 1. Introduction

This chapter introduces bacteria, antimicrobial resistance (AMR) and orientates the reader to the arrangement of DNA, exemplifying the flexibility and conformational variation which gives rise to the unique biological properties of the building block of life. Additionally it examines DNA topology, topoisomerase enzymes and discusses the aminocoumarin and quinolone inhibitors. Lastly it highlights the simocyclinones (SD4 and SD8), whose novel mode of action and exquisite structure has inspired medicinal chemists for the last 15 years.

1.0 Gram-positive and Gram-negative bacteria

Hans Christian Gram developed the now widespread method of differentiating between two classes of bacteria based on the structural and physical characteristics of cell walls. Gram-positive organisms have a single membrane surrounded by a thick peptidoglycan layer (murine) that retains the dye, crystal violet (positive test result) giving them a purple appearance. Peptidoglycan is a rigid polymer lattice composed of two alternating sugars, *N*-acetylglucosamine (NAG) and *N*-acetyl muramic acid (NAM) linked by a β,1,4-glycosidic bond. The NAM carboxylic acid residues are further substituted with a pentapeptide cross-bridge.[1] This varies among species of Gram-positive and Gram-negative bacteria, but always terminates with two D-alanine residues.[2] Whilst the NAG and NAM units are linked together in the cell cytoplasm, their crosslinking takes place by membrane bound transpeptidase enzymes. They create a peptide bond between the D-alanine and the amine of L-lysine or pimelic acid in Gram-positive and Gram-negative bacteria respectively. As well as giving bacteria their shape, peptidoglycan also anchors cellular components, such as proteins, to its surface. Gram-positive bacteria contain lipoteichoic and teichoic acids that provide additional structural support and form pathogen associated molecular patterns (PAMP).

In contrast, Gram-negative organisms have a thin peptidoglycan layer that cannot retain crystal violet during the de-staining (negative test result). Instead it stains pink with a counterstain (fuchsine or safranin). The thin peptidoglycan layer is separated from the cell wall by the periplasmic space and is encapsulated by an outer membrane (OM).[3] In contrast to the cytoplasmic membrane, the OM is decorated mainly with lipopolysaccharides (LPS), as well as phospholipids and proteins termed outer membrane proteins (OMP). It should be noted that the OM, although containing phospholipids in its inner leaflet, is not a phospholipid bilayer.[4] LPS, which decorates the outer surface, has the ability to be recognised by the immune system and is an endotoxin.[5] It is comprised of 3 parts, an inner lipid, a core oligosaccharide (short sugar) and an outer polysaccharide (o-antigen, long sugar). The aqueous compartment in between the OM and cellular membrane is known as the periplasm. This contains hydrolytic enzymes, binding proteins, detoxifying enzymes and chemoreceptors not found in the cytoplasm.

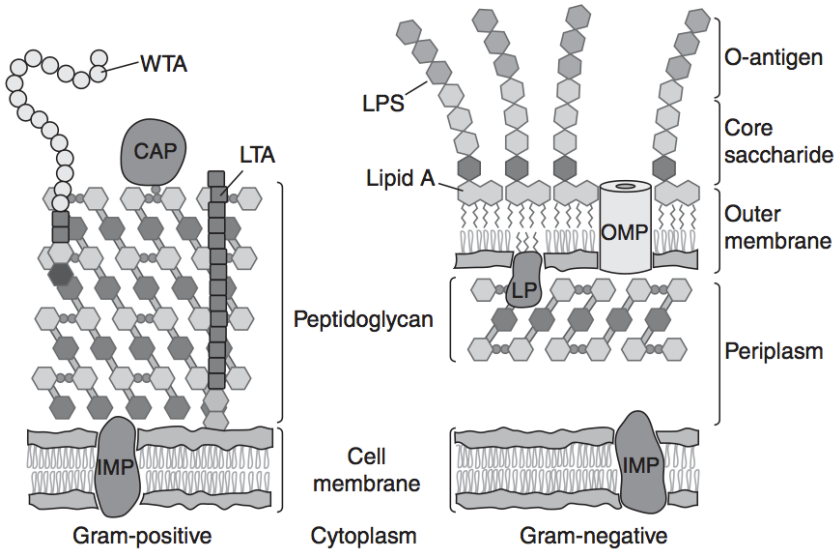

Figure 1. Structural differences between Gram-positive and Gram-negative bacteria. WTA = wall teichoic acid, CAP, covalently attached protein, LTA, lipoteichoic acid, IMP, integral membrane protein, LPS, lipopolysaccharide, OMP, outer membrane protein, LP, lipoprotein.[6]

The protective outer membrane of Gram-negative bacteria and the periplasm are partly responsible for the inherent difficulty in targeting these microorganisms with antibiotics. These structural differences are highlighted in Figure 1.

1.01 Antimicrobial resistance and mechanisms of resistance

The serendipitous discovery of penicillin in 1928 by Alexander Fleming serves as an example of how natural products can be harnessed as chemotherapeutic agents against bacteria, and marks the inauguration of modern antibiotics.[7,8] Unfortunately, multi-drug-resistance (MDR) to antibiotics has increased globally and is now considered one of the greatest threats to health.[8–10]

Resistance can be intrinsically present, having arisen through fortuitous mutations during replication of DNA or via the dissemination of DNA among bacteria. The use of antibiotics in society contributes to the problem by creating selection pressure, allowing resistant strains to dominate their non-resistant counterparts.

Intrinsic resistance is due to inbuilt structural or functional characteristics that prevent a microorganism being sensitive to a given drug.[11] Daptomycin, a lipopeptide, inserts itself into the cell membrane. This causes depolarisation that leads to the loss of vital intracellular components. This agent is only effective against Gram-positive bacteria. The reason for a lack of efficacy against Gram-negative organisms is due to a lower proportion of anionic phospholipids that consequently provides insufficient sites for calcium-mediated insertion of daptomycin into the cell membrane.[12]

Vancomycin is an additional example that is effective against Gram-positive microbes by inhibiting peptidoglycan synthesis. However, vancomycin has no effect on Gram-negative organisms, as it cannot cross the OM to reach the target transpepdidases in the periplasm.[13]

Acquired resistance arises through three main mechanisms: firstly by inactivation of the antibiotic, secondly through modification of the target site and thirdly those that can decease the intracellular concentration of the antibiotic.[11] An archetypal example of inactivation comes from the discovery of β-lactamase.[14] This class of enzyme hydrolyses the sterically strained β-lactam ring of penicillin, opening it up and abolishing its activity. Since their initial discovery, new improved antibiotics have come to market, but the ever-increasing group of β-lactamases that can inactivate a broad range of penicillins, structurally related cephalosporins and synthetic fluoroquinolones has also continued to develop. They are known as extended-spectrum beta-lactamases (ESBL) and over 200 have been identified.[15–17] Resistance can be disseminated among bacteria via plasmids encoding genes for ESBL or through domination of resistant species via Darwinian selection.[17]

Antibiotics will often bind to a specific region of their target; in the case of the fluoroquinolones, they bind to a specific site on a topoisomerase (topo) enzyme, DNA gyrase, as well as its structurally related family member topo IV (discussed in further detail in section 1.15). Resistance to this class of antibacterial is attributed to point mutations that often encode for a serine residue and aspartic/glutamic acid residues.[18] The loci of the specific genes are termed the quinolone resistance-determining region (QRDR).[19,20] This substitution in amino acid residues dramatically alters the efficacy of the drug by abrogating its binding to the target topo enzyme.

The physiology of Gram-negative organisms illustrates how decreasing antibiotic concentrations can confer resistance. The OM of Gram-negative species is inherently less permeable to antibiotics and serves as an intrinsic mechanical barrier. In addition, the OM contains porins, specialised channels that allow the movement of molecules through the OM into the periplasmic space. Down regulation and reduced expression of porins in the bacterial OM has been associated with resistance to carbapenams and chephalosporins.[21–23] Hydrolysing enzymes can target cephalosporins. This demonstrates the multi-faceted nature of resistance; often a combination of different mechanisms will confer an evolutionary advantage.

The injudicious use of antibiotics in humans and animals is the single most important factor for developing AMR. In the 1950's soon after the initial approval of antibiotics in livestock as growth promoters, concerns were raised regarding their use in intensive farming. Antibiotics were being used in livestock at sub-therapeutic doses, in the absence of disease, to enhance feeding and improve the growth of an animal (animal growth promotion termed AGP). In 1969, the British Government requested the Swann Committee to report on antibiotic usage in humans and animals. They concluded that animal feed antibiotics should not be used in humans due to the risk of

transmission of resistant strains. Furthermore, they recommended the Government should establish a permanent committee who would take responsibility for antibiotic usage.[24] However, it was another 30 years before the Specialist Advisory Committee on Antimicrobial Resistance (SACAR) was formed.[25] The link between antibiotic use in animals and subsequent transmission of resistant microbes to humans was established from investigations in oxytetracycline fed chickens and farm personnel. Oxytetracycline-fed chickens developed intestinal flora containing almost exclusively tetracycline-resistant organisms within one week of ingestion of the antibiotic. In correlation, farm members who were responsible for handling the animals and were not taking antibiotics, also developed increased numbers of tetracycline resistant intestinal bacteria. In contrast, their neighbours did not develop any change in microflora in this study.[26] Subsequently, a larger study looking at the streptothricin antibiotic, nourseothricin, in pig farming confirmed the earlier findings. Plasmid borne resistance to streptothricin was found in *E. coli* isolated from nourseothricin fed pigs, their handlers and the family members of the handlers. Additionally, in the larger study, resistance plasmids were detected in people in the surrounding community. These people had no contact with the pig farms but were present in areas where nourseothricin was used. This contrasted with a control territory where nourseothricin was not used, and no plasmid-encoded resistance was detected.[27] Sweden was the first European country to phase out AGP in 1986, followed by Denmark. In the UK, there has been a decrease in AGP since 1998 and the European Union (EU) banned antibiotic use as growth promoters in 2006.[28] Unfortunately, an estimated 70% of all antimicrobials continue to be used for non-therapeutic uses in agriculture in the USA.[29] The usage in developing nations such as Africa and India is currently unknown.[28] The ways in which antibiotics can disseminate into the environment are summarised Figure 2.

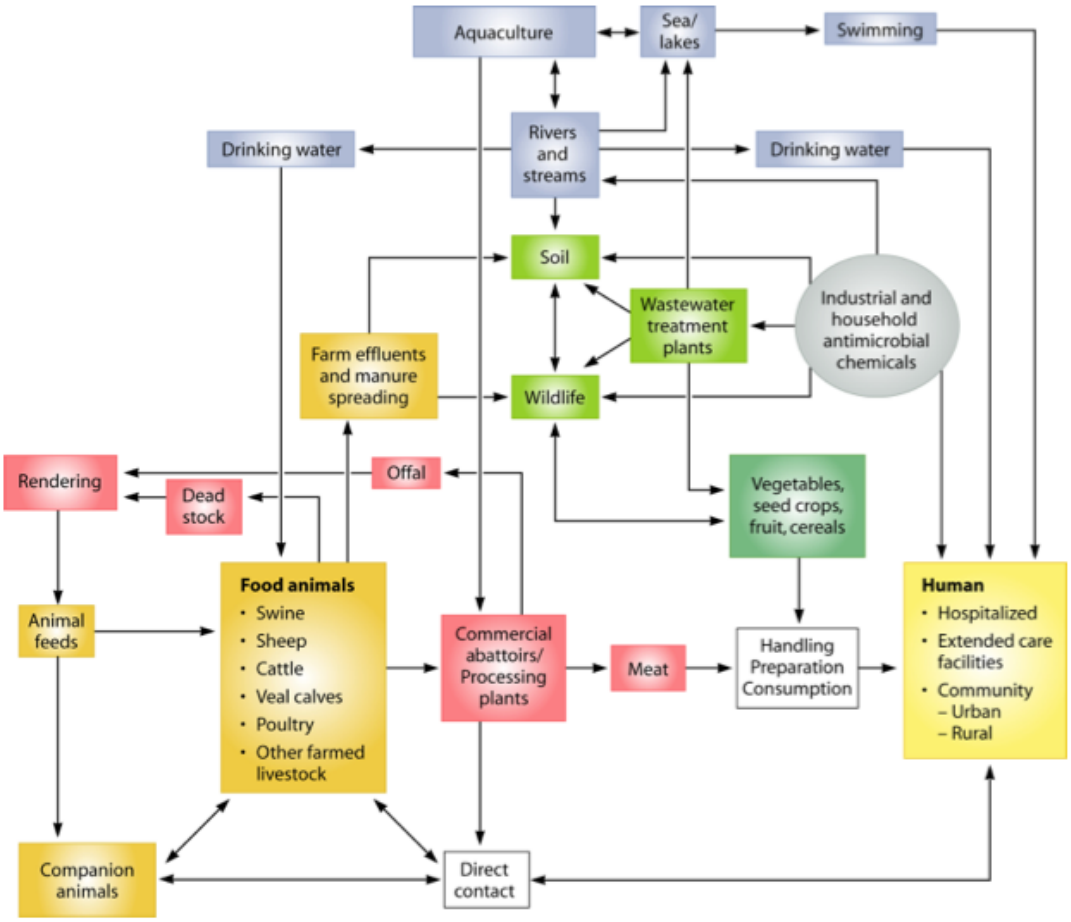

Figure 2. Dissemination of antibiotics into the environment.[30]

There is a positive correlation between human antibiotic consumption and microbial resistance.[31] Examples of inappropriate prescribing include: using antibiotics unnecessarily, ineffective doses, ineffective treatment duration or unsuitable antibiotic selection. Furthermore, problems arise from the way in which patients/animals take medicines. Inappropriate patient habits/animal administration include: not taking/giving antibiotics in accordance with a prescriber's instruction, missing doses and not completing prescribed courses. Antimicrobial stewardship (AMS) seeks to redress these anthropological derived problems. AMS, as defined by the Society for Healthcare Epidemiology of America (SHEA), Infectious Diseases Society of America (IDSA) and the Paediatric Infectious Diseases Society of America (PIDS) represents a co-ordinated effort to improve and measure appropriate utilisation of antibiotics.[32] Thus, the dwindling pool of efficacious antibiotics can be preserved for life threatening conditions. This can be achieved through the education and cultural change of healthcare professionals, patients and children.[33]

Cooperativity among countries is key to achieving the success of AMS as international travel, has forever changed the microbial landscape, eradicating physical barriers to transmission. Thus, international efforts are required to encourage a harmonised approach to antibiotic prescribing. A lack of antibiotic regulation in less economically developed countries is a contributing factor in the emergence of AMR; this includes lack of effective legislative enforcement, lack of financial resources and poor education and awareness of AMR.[34] Unfortunately, information regarding the unregulated sale of antibiotics and prescribing habits is scarce.

The interplay of factors that contribute to AMR is complex; the benefit of using an antibiotic comes with the price of introducing selective pressure that consequently drives resistance not only of the causative pathogen but also background microflora. The interplay between host, pathogen and indigenous microflora (commensal) is highlighted in Figure 3. Consequently, once a drug comes to market it is not long before resistant pathogens emerge (Table 1). AMR combined with a lack of antimicrobial investment from pharmaceutical companies has created a deficit of novel chemical entities coming to market. Drugs originally left undeveloped as lead compounds have been re-evaluated as conferring at least some advantage. Daptomycin is an example that was discovered in the 1980's by Eli Lily. It was originally shelved due to adverse side effects and what the company considered an unsatisfactory performance in clinical trials. In 1997, its patent was purchased by another company, Cubist, who considered the benefit outweighed the risk in an environment whereby an ever increasing proportion of resistant microbes were being identified.[35] The drug was subsequently approved by the FDA in 2003.

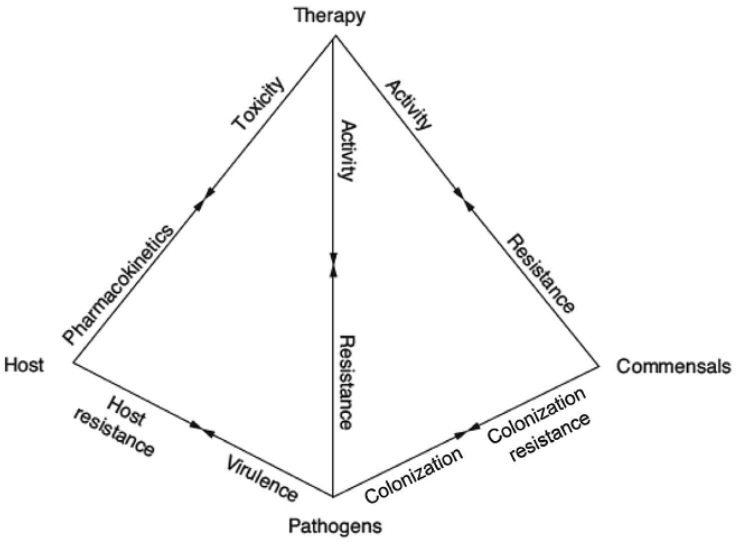

Figure 3. The infection pyramid: describes the relationship between humans (Host), bacteria (Pathogens, Commensals) and antibiotics (Therapy).[33]

Antibiotic class; example	Year of discovery	Year of introduction	Year resistance observed	Mechanism of action	Activity or target species
Sulfadrugs; prontosil	1932	1936	1942	Inhibition of dihydropteroate synthetase	Gram-positive bacteria
β-lactams; penicillin	1928	1938	1945	Inhibition of cell wall biosynthesis	Broad-spectrum activity
Aminoglycosides; streptomycin	1943	1946	1946	Binding of 30S ribosomal subunit	Broad-spectrum activity
Chloramphenicols; chloramphenicol	1946	1948	1950	Binding of 50S ribosomal subunit	Broad-spectrum activity
Macrolides; erythromycin	1948	1951	1955	Binding of 50S ribosomal subunit	Broad-spectrum activity
Tetracyclines; chlortetracycline	1944	1952	1950	Binding of 30S ribosomal subunit	Broad-spectrum activity
Rifamycins; rifampicin	1957	1958	1962	Binding of RNA polymerase β-subunit	Gram-positive bacteria
Glycopeptides; vancomycin	1953	1958	1960	Inhibition of cell wall biosynthesis	Gram-positive bacteria
Quinolones; ciprofloxacin	1961	1968	1968	Inhibition of DNA synthesis	Broad-spectrum activity
Streptogramins; streptogramin B	1963	1998	1964	Binding of 50S ribosomal subunit	Gram-positive bacteria
Oxazolidinones; linezolid	1955	2000	2001	Binding of 50S ribosomal subunit	Gram-positive bacteria
Lipopetides; daptomycin	1986	2003	1987	Depolarization of cell membrane	Gram-positive bacteria
Fidaxomicin (targeting *Clostridium difficile*)	1948	2011	1977	Inhibition of RNA polymerase	Gram-positive bacteria
Diarylquinolines; bedaquiline	1997	2012	2006	Inhibition of F_1F_O-ATPase	Narrow-spectrum activity (*Mycobacterium tuberculosis*)

Table 1. Timeline of discovery, coming to market and detection of antibiotic resistance.[36]

1.02 Current clinical targets for antibiotics

There are five main validated drug targets that are currently exploited in antimicrobial chemotherapy (Figure 4). A selection of drug structures that exploit these targets are shown in Figure 5. Disruption of cell wall synthesis is probably the most eminent drug target. Penicillin (amoxicillin, flucloxacillin, penicillin V) targets the enzymes involved in the synthesis of peptidoglycan, a cell wall component, by binding covalently to the active serine site of the transpeptidase enzymes (also termed a penicillin binding protein PBP).[37] Transpeptidases are a unique to bacteria and, therefore, a rational drug target. Penicillin and its derivatives are effective due to the highly reactive β-lactam ring that is structurally similar to D-alanine.[2] Consequently, the enzymes utilises the β-lactam as a substrate and become inactive, accordingly the enzyme is unable to cross-link the bacterial cell wall, resulting in cell lysis and death. Thus, the penicillins are

bactericidal in their mode of action. Similarly, cephalosporins (cephalexin, cefotazime, cefradine) contain a β-lactam ring fused to a dihydrothaizine ring; their mode of action is the same as the penicillins. The carbapenams (meropenem, ertapenem) also react with transpeptidase enzymes, entering cells via the OMP.[38,39] Due to the cell being unable to cross-link peptidoglycan, the bacteria burst under osmotic pressure. Analogously aztreonam exerts its effect by binding to the PBPs of mainly Gram-negative bacteria. However, unlike the previous classes of β-lactams it has no fused ring system.

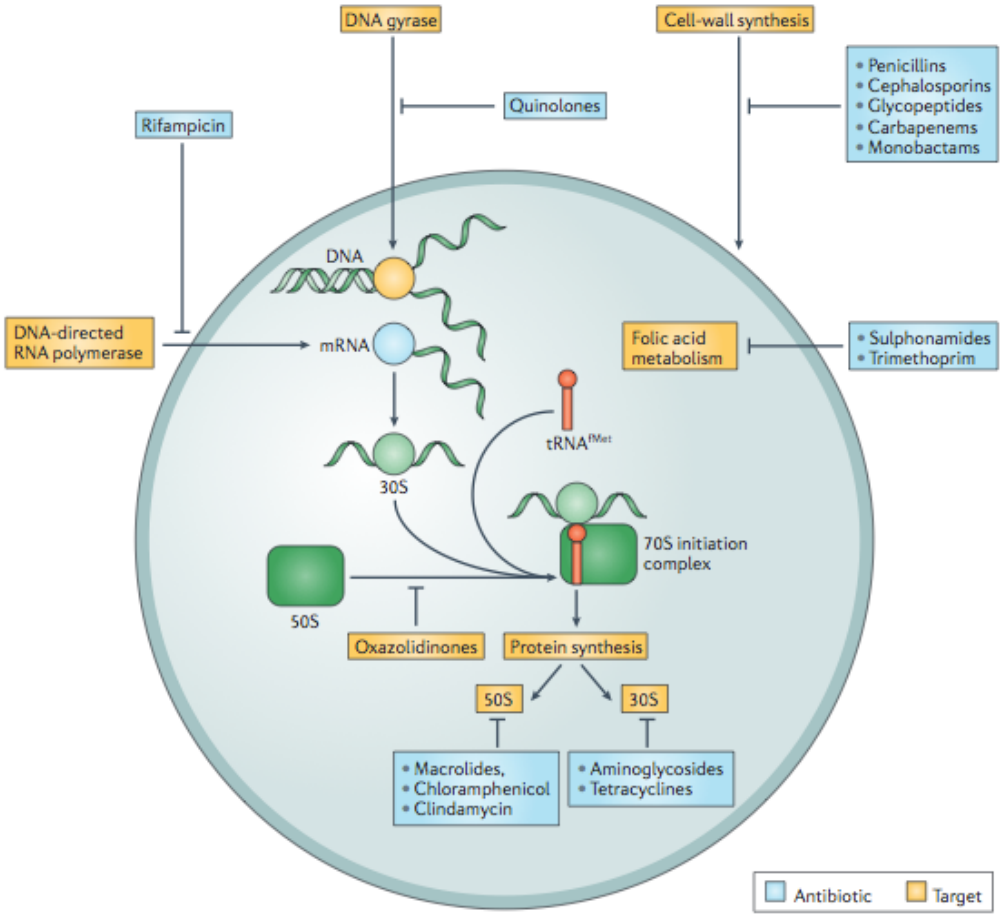

Figure 4. Clinically exploited antibiotic drug targets.[36]

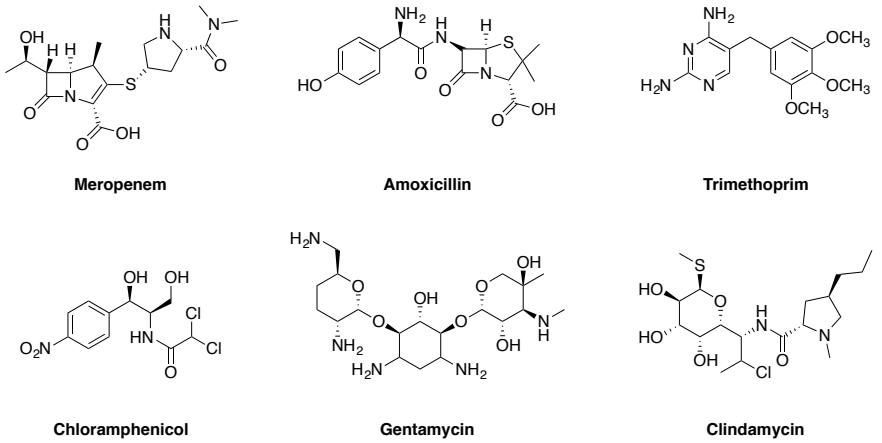

Figure 5. Examples of structures of clinically exploited antibiotics.

In contrast to the β-lactam antibiotics, the glycopeptide antibacterials (vancomycin, teicoplanin) are large complex molecules consisting of amino acids that can be decorated with halogens, OH groups, and sugars. The compounds disrupt a late stage in cell wall formation by binding to the D-Ala-D-Ala C-terminus of the disaccharide pentaptide repeating unit of the peptidoglycan.[40] The binding of the glycopeptide prevents the transpeptidase enzyme from binding to the amino acids, abrogating cross-linking of the cell wall, and thus inhibiting peptidoglycan formation.[41]

Protein synthesis is another heavily targeted bacterial process. The macrolides are lactone rings adorned with sugars. They target the 50S subunit of the bacterial ribosome, close to the peptidyl transferase centre.[42] This plays a vital role in the formation of peptide bonds during protein elongation. The binding sites of the macrolides (telithromycin) overlap with substrates of peptidyl transferase inhibiting the reaction.[43–45] The lincosamides (clindamycin), while structurally distinct, operate via a similar mechanism. Erythromycin is an exception, rather than inhibiting the peptidyl transferase reaction it sterically blocks the ribosomal tunnel through which newly created peptides exit the ribosome. Thus causing t-RNA to dissociate prematurely from the enzyme.[46,47] In contrast, chloramphenicol also binds to the 50S ribosomal subunit, but instead of sterically blocking the subunit, it irreversibly interacts with the receptor site to prevent amino acid transfer from peptidyl transferase.[48,49]

The aminoglycoside antibiotics (gentamycin, tobramycin) are amino sugars that bind to a conserved sequence of 16S ribosomal RNA (rRNA) in the 30S subunit of a ribosome.[50] The binding of the antibiotic stabilises a tRNA-mRNA interaction preventing the disassociation of tRNA. Consequently, this causes misreading of mRNA and the insertion of incorrect amino acids into polypeptides.[51] The tetracyclines (oxytetracycline, lymecycline) also target the 30S ribosome. They are composed of a linear fused tetracyclic scaffold decorated with a variety of functional groups, such as alcohols, amines and amides.[52] The tetracyclines prevent binding of aminoacyl tRNA with

the ribosome by sterically blocking tRNA binding.[53] Oxazolidinones (linezolid) are novel synthetic compounds that have a distinct mode of action that is not yet fully elucidated.[54] Structurally, linezolid contains an oxazolidinone ring, substituted with an acetyl protected primary amine. Furthermore, the oxazolidinone ring is coupled to a fluorinated aromatic ring with a morpholine substituent. Linezolid is only effective against Gram-positive bacteria. This antibiotic has been shown to bind to the 50S subunit and compete with chloramphenicol for binding. This suggests that the linezolid binding site is in close proximity to that of chloramphenicol.[55,56] However, the oxazolidinones do not inhibit peptidyl transferase or block the elongation or termination of peptide chains.

The sulphonamides and trimethoprim inhibit a pathway which produces tetrahydrofolate, a crucial precursor to the thymidine that is used in bacterial DNA synthesis. However, the two compounds exert their modes of action at different points in the pathway. The sulphonamides (sulfamethoxazole) are competitive antagonists of para-aminobenzoic acid (PABA) and prevent substrate binding to dihydropteroate synthetase. They all contain a sulphonamide functional group; although it should be mentioned that other non-antibacterial agents can also contain this moiety. This is attached to an aniline scaffold. The compound achieves its competitive inhibition due to its structural similarity with the natural metabolic substrate. It is noteworthy that whilst not broad spectrum, the drug has good Gram-positive activity. Trimethoprim binds to dihydrofolate reductase, an enzyme that catalyses the reduction of dihydrofolic acid to tetrahydrofolic acid, a later step in the tetrahydrofolate pathway. Often trimethoprim and sulfamethoxazole are given together to try and reduce the chances of resistance emerging.

Rifampicin is a semisynthetic compound derived from the rifamycins. The family of compounds can contain either naphthalene, napthoquinone, benzene or benzoquinone aromatic cores with an alkyl chain that forms a closed system.[57] Rifampicin has Gram-positive activity and some Gram-negative activity. It works by selectively inhibiting bacterial RNA synthesis via an interaction with RNA polymerase.[58]

The quinolones are synthetic compounds that inhibit both DNA gyrase and topo IV. These enzymes are crucial for resolving DNA topological complications that arise during cellular events such as replication. Subsequent generations of analogues have yielded successful broad-spectrum antibiotics. Their history and mode of action is discussed in detail in section 1.15-1.16. In order to understand this class of antibiotic fully, it is first necessary to review some fundamental aspects of DNA and its structure.

1.03 DNA

While growing resistance drives the need for development of new antibiotics, focusing on DNA topology is necessary in order to understand the biochemical processes that take place at a cellular level. Deoxyribonucleic acid (DNA) is the hereditary unit by which genetic information is stored and passed on. The pioneering discovery of its structure in 1953 at Cambridge University by James Watson and Francis Crick subsequently allowed information relating to it's organisation and function to be elucidated.[59]

DNA is composed of repeating nucleic acid monomers termed nucleotides. Nucleotides have three components, a sugar, a phosphate group and one of four nitrogen heterocyclic bases: the purines adenine (A) and guanine (G), or pyrimidines, cytosine (C) and thymine (T). Individual nucleoside constituents are linked; bases via the 1 position of the sugar ring and the phosphate groups in the 3' and 5' positions (Figure 6), forming a nucleotide, the repeating unit of DNA, the blueprint of life.

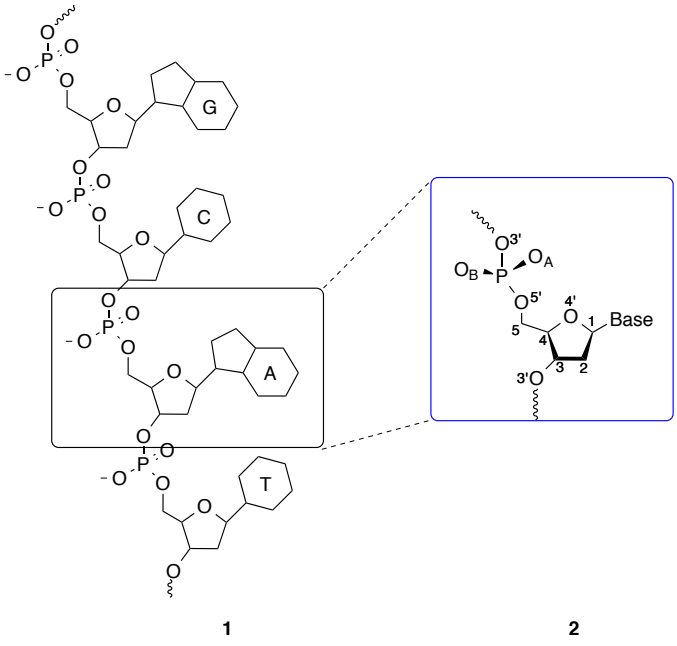

Figure 6. A polynucleotide chain **1**, demonstrating the 5'-3' phosphodiester linkages.[60] Magnified view of a polynucleotide **2** demonstrating atom numbering of a polynucleotide (blue box).[61]

Hydrogen bonding affinities between bases creates specificity; adenine and thymine are linked by two hydrogen bonds whereas guanine and cytosine have three hydrogen bonding interactions (Figure 7). This allows for the sequence specific storage of information that can be read (translated) by highly specialised enzymes to direct protein formation, via an RNA intermediate. Transcription is the term for this first step of gene expression in which RNA is synthesised from the DNA template. Genes are the names given to defined areas of DNA, which can be translated into a

protein product. The collection of genes that make up a human genome are compacted down into more manageable sizes. This condensation of genetic matter forms a chromosome.

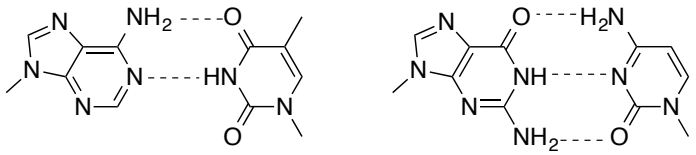

3 **4**

Figure 7. Hydrogen bonding between nucleobases **3** (A.T) **4** (G.C) illustrating Watson-Crick pairing.

The five membered 2-deoxy-D-ribose sugar ring of DNA is not planar, instead it has twist and strain. This is the first example of how rotation and flexibility affects the geometry of DNA. The twisting or 'puckering' is a result of steric interactions. Thus the ring adopts the most energetically favourable conformation in which substituents are as distant as possible from each other. The most frequent spatial arrangement encountered is C2' *endo* puckering whereby the C2 atom of the sugar diverges above the plane of the ring or conversely C3' *endo* where it is the C3 carbon (Figure 8).

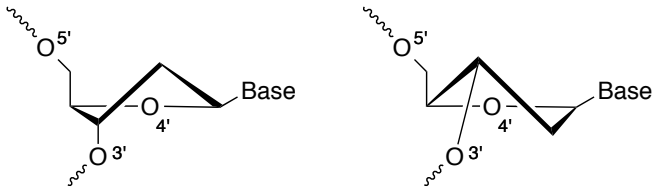

5 **6**

Figure 8. Sugar puckering **5** C2' endo **6** C3' endo arrangements.[61]

In an analogous fashion the stereochemistry at the anomeric C1' position is assigned. The glycosylated bond can orientate below the sugar (axial), termed an α-nucleoside, or above (equatorial) termed a β-nucleoside. This classification is included for completeness, as *in vivo* nucleotides only exist in β form. Moreover, nucleobases have free rotation around the n-glycosylated bond (χ) uniting the sugar ring to the base at the N-9 and N-1 position for purines and pyrimidines, respectively. Bases can therefore exist in two different states termed *anti* and *syn* (Figure 9).

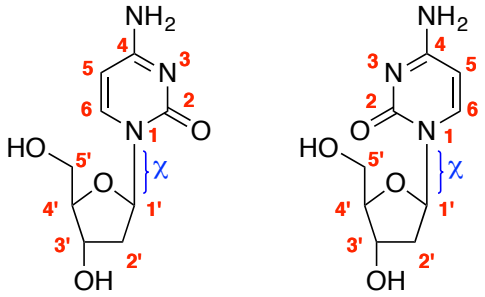

Figure 9. Example of *anti* **7** and **8** *syn* conformation of pyrimidine nucleoside.

Purine bases (A/G), like the sugar, are not co-planar; rather they sit almost at right angles to the sugar. They are permitted to rotate into either the *syn* or *anti* conformation. However pyrimidine bases (C/T) if *syn* to the sugar ring, experience steric clashing between their carbonyl group and the hydrogen at the C2' position of the sugar. Therefore, they predominate in the more energetically favourable *anti* conformation. Strain is not confined internally to the sugar ring (τ_0-τ_4), the phosphodiester backbone also experiences rotation around each of the sp^3 hybridised sigma bonds (Figure 10).

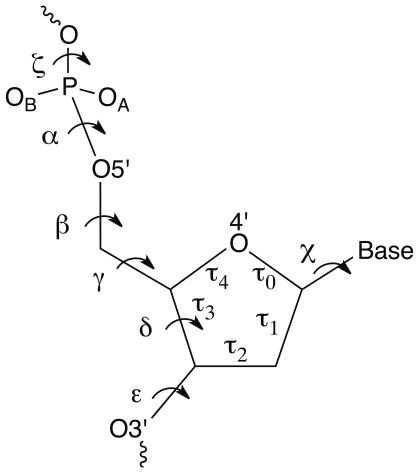

Figure 10. Positions of free rotation in DNA.[61]

Accordingly the free rotation means a helical axis is not straight; instead possessing intrinsic curvature, contributing to its biological function. Protein-DNA interactions in the major or minor groove provide an example of the relationship between shape, recognition and function. Ultimately, the flexibility of the components of DNA directly influences the higher order structures that can form *in vivo* and *in vitro*.

1.04 DNA higher order structures

B-form DNA is the most common arrangement of DNA within cells (Figure 11). It consists of a right-handed anti-parallel α-helix with Watson-Crick pairing. The sugar phosphate backbone exhibits C2' *endo* puckering with *anti* glycoside bond angles (χ). Each 360° turn contains 10.5 base pairs, with a separation of 3.4 Å between base pairs (helical rise) and a helical diameter of 20 Å. The helical nature of B-form DNA is the most energetically favourable conformation due to the orientation of the hydrophobic base pairs relative to their environment and the bond angles (α-ζ) of the sugar phosphate backbone. When double stranded DNA is separated into individual strands, water molecules hydrogen bond in place of a complementary base. As individual strands re-associate, water is eliminated from the central helical core, increasing the disorder and hence entropy of the system. This thermodynamically favourable reaction contributes to the overall stability of the helix. Stabilisation also comes from π-π stacking interactions of the planar bases above each other so that they are orientated approximately perpendicular to the helical axis.

A-form DNA represents an alternative conformation able to form *in vitro* (Figure 11). Rosalind Franklin illustrated using X-ray fibre diffraction studies that as the water content of DNA was reduced its structure transformed.[62] A-form DNA is also a right-handed α-helix with Watson-Crick pairing. Contrasting with B-form, it is shorter and broader with an extra base pair per turn. Important differences exist in the orientation of the sugar rings between A and B-form DNA. A-form is C3' *endo* whereas B-form is C2'-*endo*. Due to the twist of the sugar, the base pairs are tilted away from the central helix in A-form DNA, and consequently less hydrogen bonding interactions occur with the sugar phosphate backbone and its surroundings. Thus the A-form preferentially emerges in a dehydrated state.

In 1979 crystallographic studies of an alternating guanine-cytosine oligonucleotide revealed an unconventional structure compared to A and B-form DNA. This new assembly was termed Z-form DNA due to the zigzag profile of the sugar phosphate backbone (Figure 11). This structure uniquely possesses a left-handed helix and has no major groove. The shape of the backbone is due to strain generated by alternating *syn-anti* conformations of the nucleobases.

After Watson and Crick published their seminal paper on the structure of DNA they quickly realised separation of double stranded (duplex) DNA would be associated with helical rotation, resulting in strain. When two strands of DNA are separated, rotation ahead and behind the replication fork occurs resulting in over twisting (supercoiling). This supercoiling needs to be resolved before replication can resume. To surmount this barrier to cellular processes topoisomerase enzymes catalyse transient breaks into DNA allowing resolution of the strain.

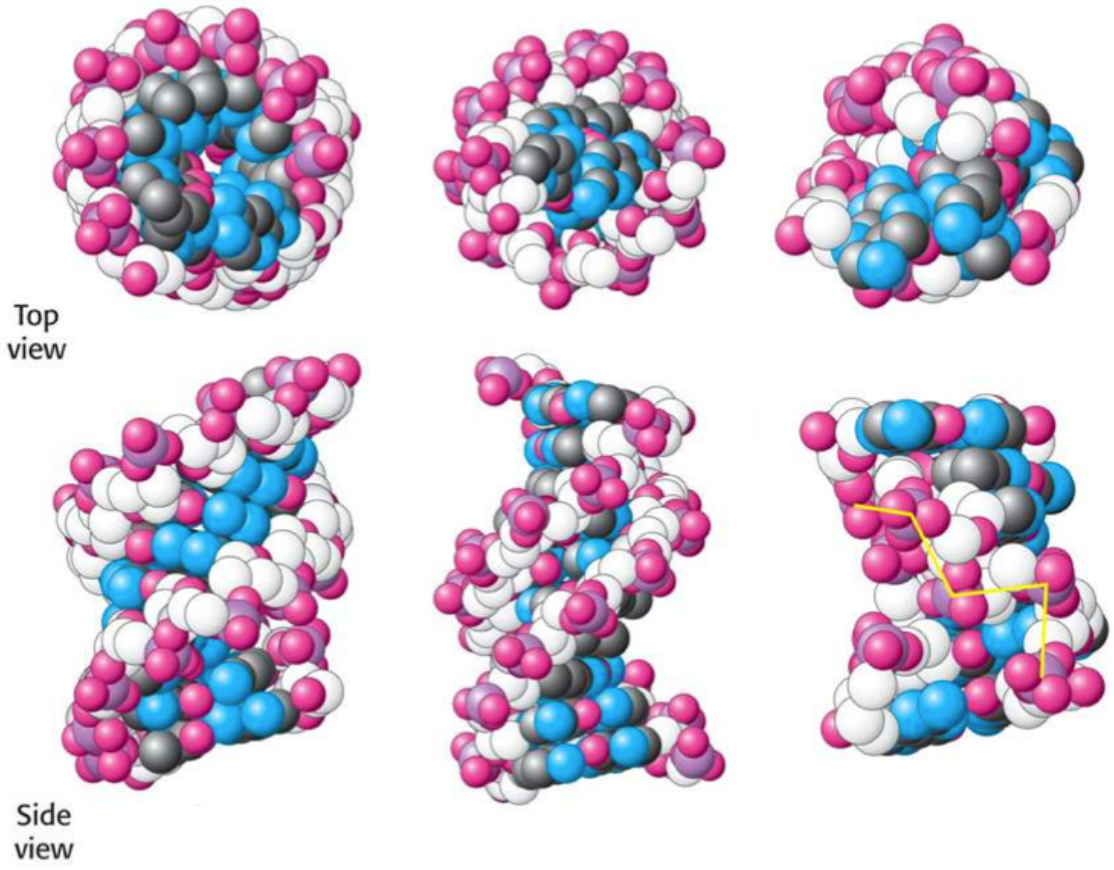

Figure 11. Structures of A-, B- and Z-form DNA respectively.[63]

1.05 Topology and geometry of DNA

To understand how topoisomerase enzymes function it is essential to appreciate the arrangement of DNA in space and how we describe this geometrically. DNA is supercoiled through over or under winding; the term twist (***Tw***) is used to describe the number of times one strand crosses over another. The amount of twist a molecule has is the same in both its linear and circular form. The term writhe (***Wr***) indicates the number of times that double stranded DNA crosses over itself to form supercoils. The linking number (***Lk***) is an integer that mathematically describes the topological changes that occur within a molecule, it is the sum of the twist and the writhe (Equation 1). The linking number cannot change within a closed system (such as a bacterial plasmid) without introducing breaks into the DNA strands. Put simply, the linking number is the number of times one strand would need to be passed through another in order for separation to occur.[60]

$$Lk = Tw + Wr$$

Equation 1. Relation of linking number to twist and writhe.

$$\Delta Lk = Lk - Lk_0$$

Equation 2. Change in linking number.

In addition to the linking number it is common to report the ΔLk. This quantitatively expresses the linking difference, termed Lk_0, when compared to a relaxed DNA molecule (Equation 2).

1.06 DNA replication in Prokaryotes

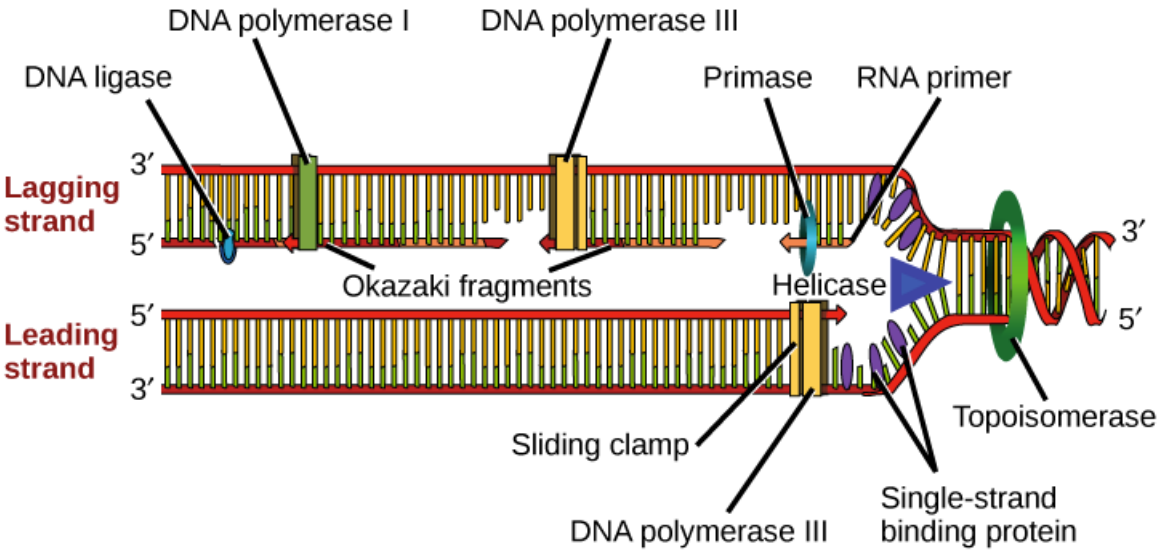

Figure 12. DNA replication.[64]

To access information stored within the base sequences of DNA, strand separation must occur. DNA helicase breaks hydrogen bonds between base pairs allowing complementary strands to disconnect and form a replication fork. This creates a leading strand, where DNA polymerase binds to a 3' end and synthesises a new daughter strand continuously in a 5' to 3' direction (Figure 12). The lagging strand requires DNA primase to add primers for the addition of RNA by polymerase III. Subsequently this is converted into DNA by polymerase I whilst DNA ligase re-anneals the free 3'-OH to the 5'-sugar phosphate backbone permitting DNA synthesis to occur in a discontinuous fashion. Topological changes occur in front and behind the replication fork. As replication progresses the proportion of unreplicated DNA ahead of the fork diminishes whilst the amount of strain and thus supercoiling increases (+ supercoiling). Crucially, there is an ever-decreasing amount of space in which to contain the supercoils. Strain is not confined to the unreplicated region of DNA, rather it can disseminate into the replicated region, culminating in the inter-winding of daughter strands to form "precatenanes", termed because they precede catenanes.

1.07 Topoisomerase enzymes

Topo enzymes regulate the topology of DNA. Separation of DNA causes rotation, creating topological strain. The problem of strain is a result of the double helix architecture of DNA. Consequently, if unresolved this would impede cellular processes. To overcome this topo enzymes resolve supercoiling by transiently cleaving and annealing DNA. The topoisomerase nomenclature is complex with overlap between the numbers denoting the type of enzyme and numbering denoting the time of discovery. The first topoisomerase (ω-protein) was isolated from *E. coli* in 1971.[65] The enzyme was able to relax negative supercoiled λ bacteriophage DNA. A year later a second topoisomerase from mouse embryo cells was found which unlike the ω-protein, could remove both positive and negative supercoils.[66] Both enzymes were evolutionary unrelated and mechanistically distinct.[67] They introduced single strand breaks (topoisomerase I) and are classified as topoisomerase IA and IB. Topoisomerase V remains discovered in a single species and is classified separately under topo IC as it is structurally distinct from IA and IB but has a single strand breakage mechanism. This forms the basis of topoisomerase I classification. Similarly to the topo IA and B family, type II topoisomerases, which introduce double strand breaks, are further differentiated based on architecture and mechanism. The following gives a brief description of each with an in depth focus on DNA gyrase, a type IIA topoisomerase.

1.08 Type IA

Type IA enzymes have an elongated toroid structure with a lumen large enough to accommodate B-form DNA.[67,68] They regulate DNA topology via a mechanism that ligates a single strand and then passes a second strand through the opening.[69] Subsequently, after the strand passage event, the ligated strand is re-annealed. Strand cleavage is mediated by tyrosine that hydrolyses the sugar phosphate backbone forming a covalent intermediate. This class of enzyme attacks the 5' end and releases a 3'-OH group.[70] Topo I, III and reverse gyrase are all members of this category; topo I and III are ATP independent whereas reverse gyrase requires ATP to perform its cellular reactions. The main function of topo I is to relax negatively supercoiled DNA, in contrast, topo III catenates and decatenates replicating daughter DNA molecules.[71] Lastly, reverse gyrase is unique to hyperthermophiles, it introduces positive supercoils and renatures DNA.[72,73]

1.09 Type IB

The type IB enzymes contain four domains that transiently clamp around DNA.[74] They can remove positive and negative supercoils. Unlike type IA enzymes, they relax DNA by nicking a single strand of duplex DNA by forming a covalent intermediate at the 3' end. This allows the 5'-OH strand end to rotate with respect to the intact strand. However, this is not unhindered, the

mechanism is torque sensitive involving a swivel mechanism where there is friction between the rotating DNA and the enzyme.[66,75]

1.10 Type IC

Topo V is the only member of this family.[76] Similar to topo IB enzymes, it functions by a nicking-swivelling mechanism relaxing both positively and negatively supercoiled DNA.[77] It is structurally divergent at its catalytic site compared to topo IB.[78] A summary of all type I topo enzymes is shown in Figure 13.

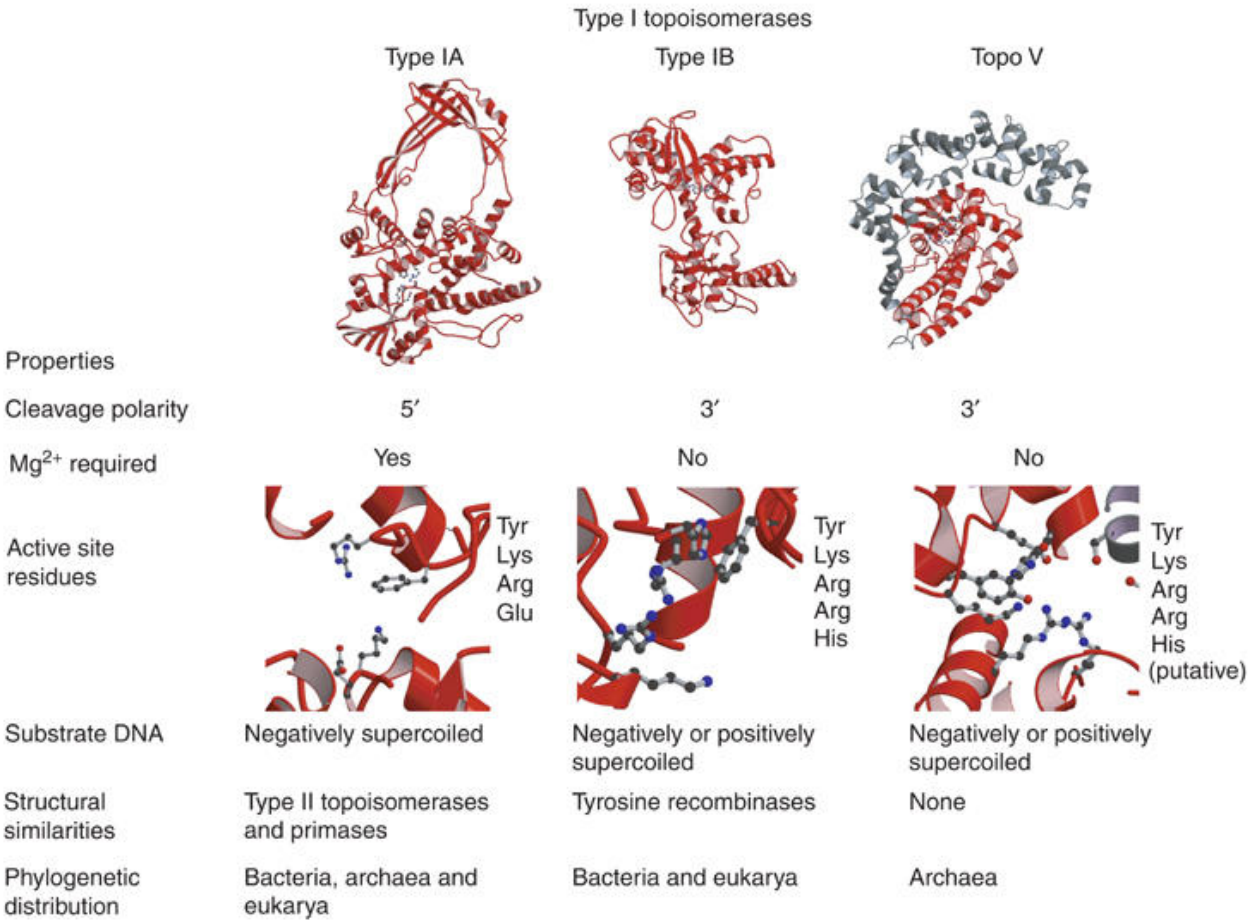

Figure 13. Comparisons of type I topoisomerase enzymes. Topo 1A (PDB 1I7D), Topo 1B (PDB 1A31) Topo V (PDB 2CSB, 2CSD).[78]

1.11 Type IIA (DNA gyrase)

Type IIA enzymes have a strand passage mechanism like the type IA enzymes. However they introduce two transient breaks into DNA instead of one and pass an unbroken strand through the opening of the cleaved strand. They can relax positive and negative supercoiled DNA and perform catenation/decatenation reactions. The mechanism of DNA gyrase, a prokaryotic type IIA topo, is discussed in detail in section 1.13. Topo IV is a structural homologue to DNA gyrase, consisting of a parC (84-kDa) domain and a parE (70-kDa) domain which forms a C_2E_2 heterotetramer. The topo IV mechanism is similar to gyrase but with an important difference, it does not wrap DNA around itself.[79]

1.12 Type IIB

The topo IIB enzymes (also called topo VI) are analogous to IIA and have two subunits that associate into a heterotetramer. The B subunit contains a conserved nucleotide binding fold (Bergerat fold) that is evolutionarily related to the IIA enzymes.[67,80–82] Two crucial distinctions are made in the mechanism of IIB compared to IIA enzymes. Firstly, cleavage is dependent on ATP. Secondly, the double strand breaks only have a 2 base pair overhang. Whilst the A subunit has no sequence similarity to IIA enzymes, sequence similarities for eukaryotic Spo11 protein from *S. cerevisiae* and Archaeal topo VI A subunit exist.[80]

1.13 Mechanism of DNA gyrase supercoiling

The mechanism by which DNA gyrase achieves negative supercoiling has yet to be fully elucidated. However, a model termed the 'two-gate mechanism' is supported by crystallographic and biochemical data.[83] DNA gyrase is a prokaryotic type II topoisomerase, the active enzyme associated with DNA has a heterotetramer (A_2B_2) structure.[84] GyrA has been shown to be a dimer in solution whereas GyrB is a monomer by x-ray scattering data (Figure 14. **1**).[85,86] This strongly agrees with *in vivo* data that shows most GyrA and GyrB molecules are not associated together but randomly distributed throughout the cytoplasm of the cell.[87] There is a conformational change in the presence of DNA. DNA (Gated/G-segment) binds to the N-terminal domain of the GyrA subunit (97-kDa) and the metal binding topo/primase (TOPRIM) domain of GyrB.[88] The DNA is folded around the C-terminal domain in a right-handed supercoil of ~130 base pairs.[89,90] X-ray crystallography of the GyrA C-terminal domain from *Borrelia burgdorferi* consists of a six bladed β-pinwheel containing the 'GyrA box' the part of the enzyme responsible for bending DNA to 180°, which if deleted abrogates supercoiling activity.[91,92] The right-handed wrapping of DNA facilitates a secondary segment from the same DNA molecule (transported/T-segment) to reach the N gate above the G-segment (Figure 14. **2**) in a positive crossover. The association of ATP to the N-terminal domain of GyrB causes dimerisation of the N gate on the B subunit (90-kDa) trapping the

T-segment within the active site.[93,94] A tyrosine residue (Try122) hydrolyses the DNA backbone (Figure 15), creating a double strand break in the G-segment to form a covalently linked intermediate to GyrA.[95] This requires magnesium ions as a divalent co-factor in order to occur. [96,97] A conformational change segregates the two hydrolysed G-segment strands of DNA, allowing the intact T-segment to pass through the cleaved opening into the GyrA cleft. The cleaved strands are subsequently re-annealed. The free energy from ATP hydrolysis is utilised to drive forward the energetically unfavourable procedure.[98] The strand is then able to leave via the exit gate. The overall effect is to alter the linking number (Lk) of DNA by -2 consequently resolving topological strain. One supercoiling cycle introduces two negative supercoils; this requires energy from two ATP molecules. When no ATP is present DNA gyrase can relax negatively supercoiled DNA by the reverse mechanism.

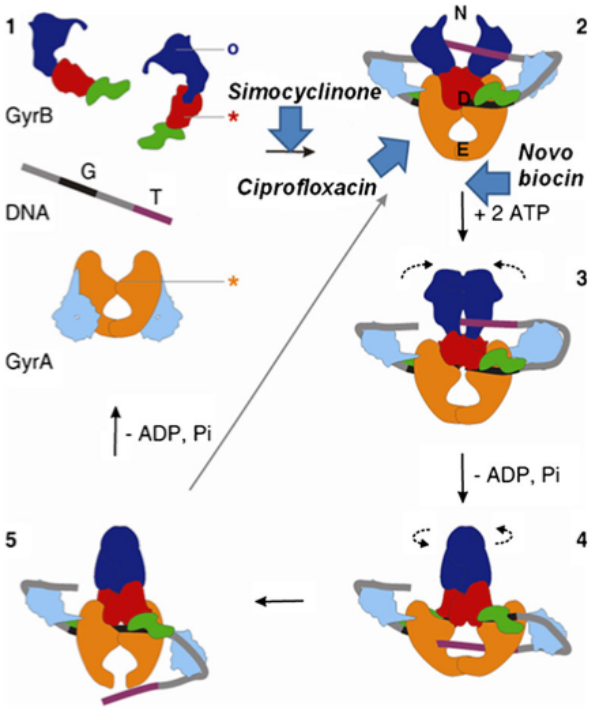

Figure 14. DNA gyrase mechanism: **1** proteins in their free state, **2** association of DNA around the C-terminal domain in a right handed manner presents the T segment above the G-segment, **3** GyrB dimerization in the presence of ATP transiently cleaving the G-segment, **4** GyrB rotates, the GyrA cleft widening and transportation of the T-segment through the G-segment driven by ATP hydrolysis, **5** re-annealing of G-segment and the introduction of two negative supercoils, release of T-segment and resetting of the enzyme.[86] Symbols indicate: Circle; ATP binding pocket, Star; position of residues involved in DNA cleavage. Colour coding: Orange; GyrA59 N-terminal domain, Cyan; GyrA C-terminal domain, Navy Blue; GyrB43 N-terminal domain, Red; TOPRIM domain, Green; tail domain, Purple; T-segment, Black; G-segment. The locations of gates: N; N-gate, D; DNA gate, E, Exit gate.[99]

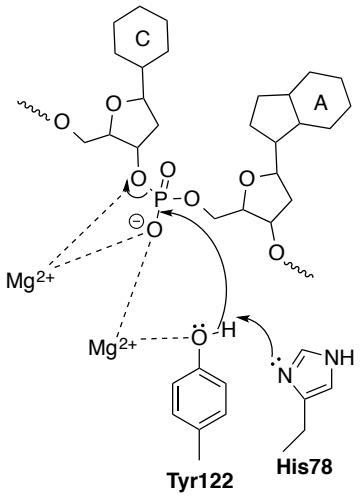

Figure 15. DNA cleavage by tyrosine in the presence of Mg^{2+} cations.[96]

At multiple points in the DNA gyrase catalytic cycle there are opportunities for small molecule ligands to interfere: with (i) DNA binding (ii), ATP hydrolysis (iii) and DNA ligation (Figure 14). Validated antimicrobial agents that target DNA gyrase include the aminocoumarin antibiotics; the quinolones, and more recently, the discovery of the simocyclinone D8 (SD8), a new class of angucycline antibiotics. SD8 has a novel mode of action and has therefore reignited interest in developing lead compounds both due to its bi-functional structure and its novel mode of action.

1.14 Aminocoumarin antibiotics

The aminocoumarins novobiocin, clorobiocin (also called chlorobiocin) and coumermycin A_1 are natural products derived from *Streptomyces*. Novobiocin was first discovered in 1965 subsequently followed by coumermycin A_1 (Kawaguchi, H.; Naito, T.; Tsukiura, H.,1965, Berger, J., *et al* 1966 cited Fedorko, J.; Katz, S.; Allnoch, H., 1969) and clorobiocin (Ninet, L., *et al* 1972 cited Maxwell, A., 1993).[100–106] All have structural similarities, notably a 4,7-dihydroxylated 3-aminocoumarin centre with a noviose sugar (Figure 16). Clorobiocin is similar to novobiocin except it contains a chlorine atom at the 8-position instead of a methyl group and has a 5-methyl-pyrrole ring instead of a carbamoyl group at the 3 prime position of the noviose sugar. Both novobiocin and chlorobiocin have a prenylated phenolic benzoic acid at the 3 position of the coumarin. Coumermycin A_1 is a dimer linked by a 3-methyl-2,4-dicarboxyl pyrrole linker. It has the same substituted sugar as chlorobiocin.

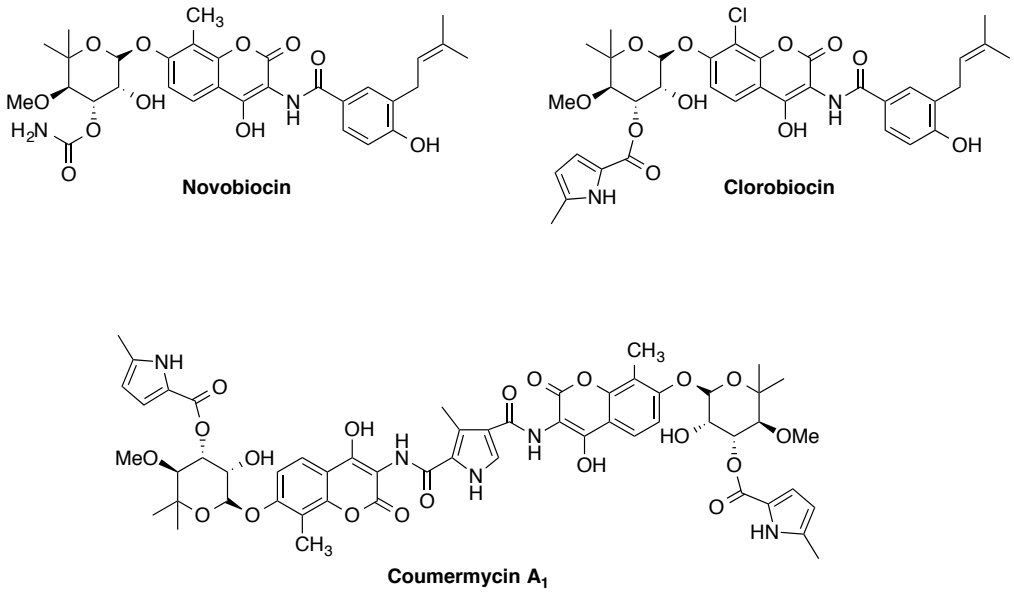

Figure 16. Aminocoumarin antibiotics.

Initial observations with *S. aureus* showed the accumulation of uridine nucleotide precursors as well as inhibition of protein and nucleic acid synthesis in the presence of novobiocin.[107] This was later extended to inhibition of DNA synthesis in *E. coli*.[108] While early theories predicted hindered cell wall formation, analogous to penicillin, this was later recanted.[109] The observation that novobiocin had an ability to bind magnesium, led to an additional hypothesis of induced magnesium ion deficiency which in turn compromised membrane integrity, this was also subsequently disproved.[110,111]

Insight into their true intracellular target came from the identification of clorobiocin resistance which mapped to the GyrB locus.[112] With the seminal discovery of DNA gyrase, it was revealed the aminocoumarins inhibited DNA gyrase catalysed supercoiling via competitive inhibition of ATP.[113–115] This was unexpected due to the lack of structural parity between aminocoumarins and ATP. The aminocoumarins bind tightly to a 24-kDa N-terminal domain on the GyrB subunit.[116] X-ray crystallography illustrated that while novobiocin bound to a region independent of ATP, the noviose sugar overlapped the ATP binding domain, thus acting as a steric block.[117] A year later a high-resolution structure of clorobiocin bound to the same 24-kDa GyrB subunit was published.[118] This structure shows the coumarin and prenyl group make important contacts around a Pro79 residue. The prenyl group is folded back onto the coumarin, reducing the hydrophobic surface of the molecule as well as making contacts with the protein. This had previously been observed with the novobiocin-GyrB24-kDa structure. The amide bond is *cis*, creating a bent 'staple'-like conformation in the crystal structure and in solution. This was confirmed by nuclear overhauser effect spectroscopy (NOESY) and total correlation spectroscopy (TOCSY) data from radiolabelled ^{15}N,^{13}C-GyrB24-novobiocin.

Arg136 was identified as critical for hydrogen bonding to the exocyclic carbonyl group of the coumarin. This supported earlier mutational data that showed abrogation of inhibitory activity towards aminocoumarins in mutants lacking this residue.[119] In contrast to novobiocin, the pyrrole group of chlorobiocin displaces water from the pocket. However, no conformational changes were seen in the protein. The difference in enthalpy from this displacement is not significant, as conveyed by isothermal titration calorimetry (ITC) experiments. However, it should be noted, binding of novobiocin and clorobiocin to gyrase is enthalpy driven at 25 °C. The relative stoichiometric binding of aminocoumarins is 1:1 for novobiocin and clorobiocin. In contrast coumermycin A_1 has a 0.5:1 ratio of drug to GyrB43-kDa subunit.[120] To date no crystal structure exists of coumermycin A_1 bound to DNA gyrase. Curiously the results suggest coumermycin A_1 must induce a different DNA gyrase dimer in order for the coumarin moieties to occupy the same pockets on the GyrB subunit as novobiocin and clorobiocin.[121] Despite strong inhibition *in vitro* the aminocoumarins have had limited clinical applications due to their poor water solubility, poor stability, low activity against Gram-negative organisms and toxicity towards eukaryotic cells.[106,122]

1.15 Quinolone antibiotics history and SAR

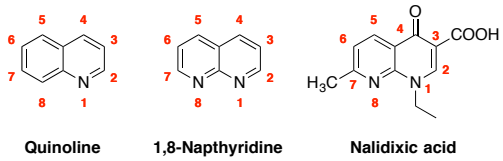

Figure 17. Quinoline, napthyridine and nalidixic acid.

Nalidixic acid was the first quinolone antibiotic identified serendipitously in 1962 as a by product of chloroquine synthesis.[123] This origin distinguishes quinolones from other antibiotics that are largely derived from, or metabolites of, natural products.[124–126] Chemically speaking nalidixic acid does not posses a quinoline scaffold, that is, two fused heterocycles with one containing nitrogen (Figure 17). Instead, this forerunner to the fluoroquinolones contains a 1,8-naphthyridine core (Figure 17). However, successive generations of quinolones derived from the parent quinoline scaffold see different structural motifs and spectrums of activity. Their classification is non-standardised and arbitrary. Several attributes have previously been taken into account including their date of marketing, clinical indication, SAR, and spectrum of activity. More recently they have been classified according to their *in vitro* activity and clinical indications.[127,128] The major SAR is discussed below, and a selection of drugs is shown in Figure 18. First generation quinolones had limited potency and activity against Gram-negative bacteria, they had a short half life and were highly protein bound. Their poor pharmacokinetic profiles restricted clinical usage to community-acquired urinary tract infections.[129]

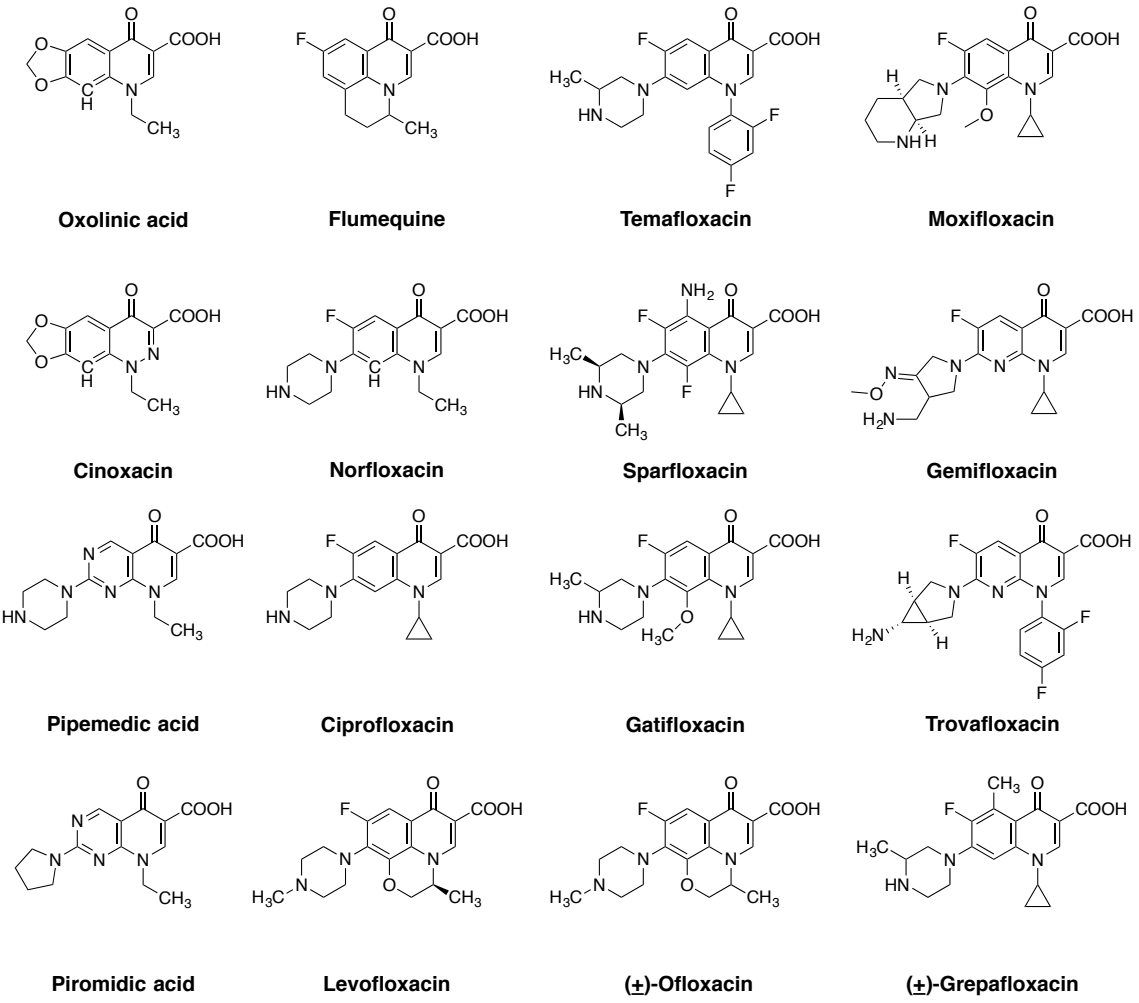

Figure 18. Structures of quinolone antibiotics

Examples are oxolinic acid, cinoxin, pipemidic acid, and flumequine. These agents provided slight improvements over nadilixic acid but still lacked broad-spectrum activity or high bioavailability.[130–132] Flumequine was the first example of a fluorinated quinolone.[133] It was utilised briefly until it was shown to have adverse ocular toxicity.[134] Whilst not routinely used for human treatment it found applications in the animal and fishing industry along side other quinolones.[135–137] Pipemedic acid and piromidic acid are early examples whereby the introduction of a basic nitrogen alongside a five or six membered ring was favourable for enhancing the spectrum of activity, penetration and bioavailability.[138] Moreover, it demonstrated the degree of variability that can be accommodated at this position.[139] Alkylation of the ring system increased activity against Gram-positive organisms and increased the half-life of the drug. Norfloxacin, a second-generation quinolone, showed improved activity against Gram-negative bacteria and resistant strains of *Pseudomonas aeruginosa* and MRSA.[140] However, little enhancement was observed against Gram-positive or anaerobic organisms.[132] Norfloxacin combined successful structural modifications from the first generation quinolones, a fluorine at position 6, and a piperazine ring at the 7 position and a carbon instead of

a nitrogen at the 8 position. Significantly enhanced activity was attributable to the introduction of a fluorine atom at the 6' position and represents one of the major SAR findings.[139,140] The enhanced action has been linked with improved cell penetration. Alkylation of the N1 position with a cyclopropyl group was more beneficial than ethyl or isopropyl groups. This modification resulted in the hugely successful ciprofloxacin, which outperformed all previous compounds and is often used as a benchmark comparator when evaluating efficacy. The incorporation of an oxygen-containing fused ring connecting the N1 and C8 position, reminiscent of flumequine gave the racemic second-generation ofloxacin. It was later shown that the *S*-isomer was twice as potent as the *R*-isomer leading to the development of levofloxacin.[141,142] Functionalisation of the 2 and 3-position is seldom undertaken and associated with poor SAR.[138] This is reflected in the successfully marketed quinolones which all contain a free carboxylic acid.

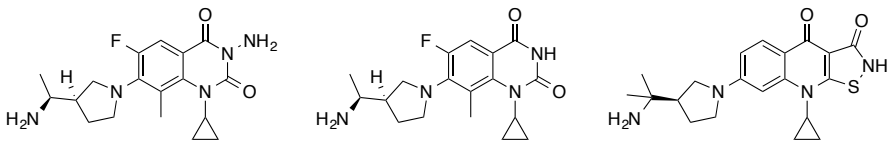

Figure 19. Potent inhibitors with functionalisation at the 3 position.

Two notable exceptions are the discovery of the 2,4 diones (PD 0305970 and PD 0326448), and ACH-702 an isothiazolequinolone (Figure 19). Both are structurally related to quinolones, and have dual inhibition of DNA gyrase and topo IV with potent broad spectrum of activities as well as efficacy against fluoroquinolone resistant isolates.[143–146] The mechanism of action of the 2,4 diones is distinct from traditional quinolones and is discussed further in section 1.16 below. The isothiazolequinolones mechanism of action remains to be elucidated.

1.16 Quinolone mechanism of action

In addition to being one of the most clinically successful classes of antibiotics, the quinolones also delivered fundamental insight into topoisomerase structure and function. It was demonstrated with nalidixic acid and oxolinic acid that, unlike the aminocoumarins, the quinolones inhibited both negative supercoiling and relaxation of DNA gyrase.[148] It was successively found that inhibition also extended to the homologous topo IV enzyme.[149] Our mechanistic understanding of the quinolone drugs was improved indirectly from biochemical experiments that showed they formed a drug-DNA-enzyme complex.[148,150] From these early observations it was predicted the mechanism was via intercalation between DNA bases.[151] More recently a crystal structure of moxifloxacin, levofloxacin and clinafloxacin with *Streptococcus pneumoniae* topo IV shows the quinolones interrupt the cleavage-religation process by intercalating themselves between DNA bases at both scissile bonds (Figure 20).[147] These are staggered and consequently two quinolone drug molecules intercalate

separated by 4 base pairs. This data; showed that interaction of the 3-carboxylic acid end of the quinolones with a Ser79 and Asp83 is important for binding. These residues are frequently mutated in quinolone-resistant bacteria and were in agreement with previous work. It is worth noting that the exact location of C7 substituent was different in all three structures.

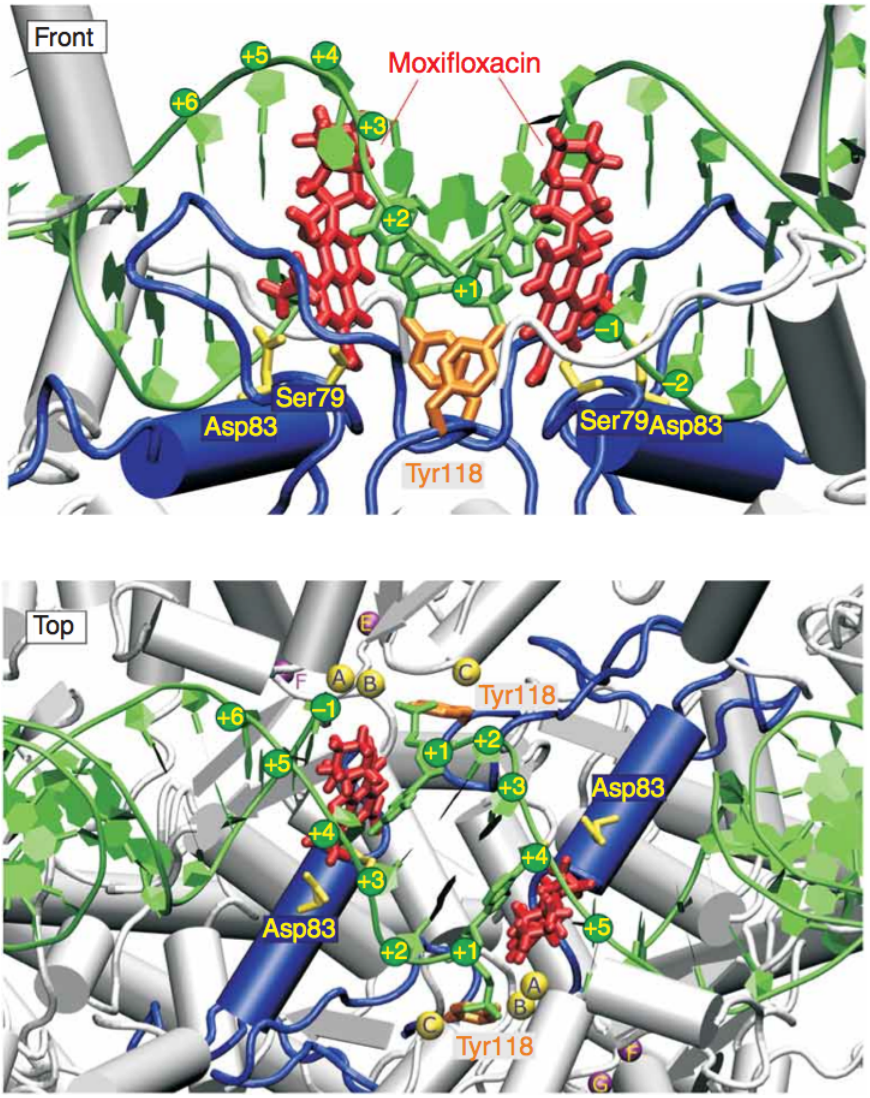

Figure 20. Topo IV with moxifloxcain (red) intercalated into DNA (green). Tyrosine is denoted in orange. Front and top views (PDB 3FOE and 3FOF).[147]

A subsequent crystal structure using dione PD0305970 and levofloxacin with the same *S. pneumoniae* topo IV enzyme showed both compounds intercalated into DNA twice, with Mg^{2+} playing a role in facilitating this interaction by interacting with tyrosine177 and the DNA backbone (Figure 21).[152] In both structures the compounds are orientated with their carboxylic acids facing downwards towards the α4 helix of ParC (corresponds to GyrA in DNA gyrase) and the 7-ring orientated towards the TOPRIM domain (corresponds to GyrB in DNA gyrase).

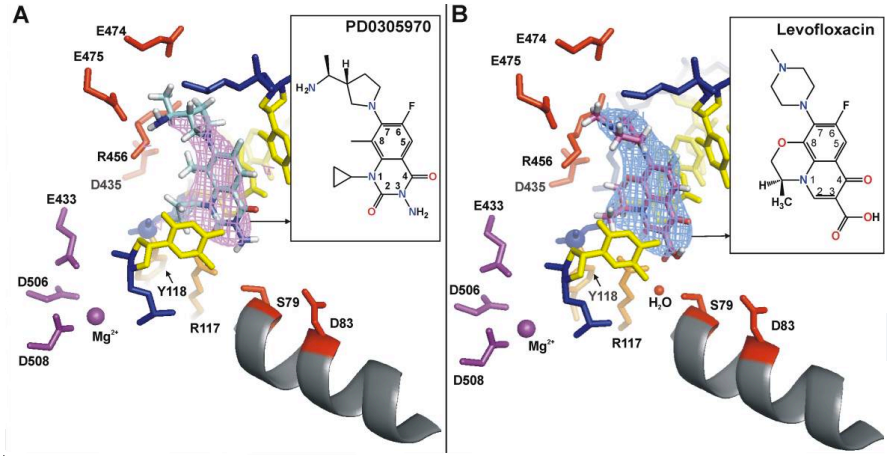

Figure 21. PD 0305970 (PDB 3LTN) and levofloxacin (PDB 3K9F) intercalated into DNA. DNA backbone (navy blue), the bases/sugars (yellow). Topoisomerase active site tyrosine (orange) and drug mutation sites (red). Magnesium ion co-ordination (purple).[152]

A separate crystal structure of moxifloxacin in complex with *Acinetobacter baumannii* supports previous observations that two quinolone compounds are intercalated into the DNA with a 4 bp gap mediated by van der Waals and π-π stacking interactions (Figure 22).[153] Additionally, a non-catalytic magnesium ion with an octahedral coordination sphere composed of two oxygen atoms from the quinolone carbonyl groups, and four water molecules mediates the interaction between the protein and drug. The water molecules were in close enough proximity to hydrogen bond with serine and the acidic aspartate and glutamate residues. The authors concluded this water-ion interaction bridged the drug to the enzyme. The orientation of the quinolone is unlike the structure obtained with moxifloxacin (Figure 20) but is similar in orientation to structures obtained with levofloxacin (Figure 21) but without the non-catalytic magnesium ion bound.

Functional studies show that mutation of either the serine or the acidic residues decreases the number of metal ions that can participate in quinolone activity. Decreased affinity of the drug-enzyme complex for the non-catalytic magnesium ion is also observed. Mutation at either residue was detrimental to quinolone binding, and complete abrogation of activity is seen when both mutations are present.[154,155] These findings indicate that the interaction of quinolones for type II topoisomerase is via the water-metal ion bridge. This helps to rationalise historic SAR showing the detrimental effect of modifying the 3 position and accounts for the large tolerance to functionalisation at the 7 and 8 position. Comparison of human and bacterial topoisomerases shows human enzymes lack the residues necessary to form the water-metal ion bridge (Figure 23).[18,156] This disparity accounts for the preferential way quinolones target bacterial enzymes.[156]

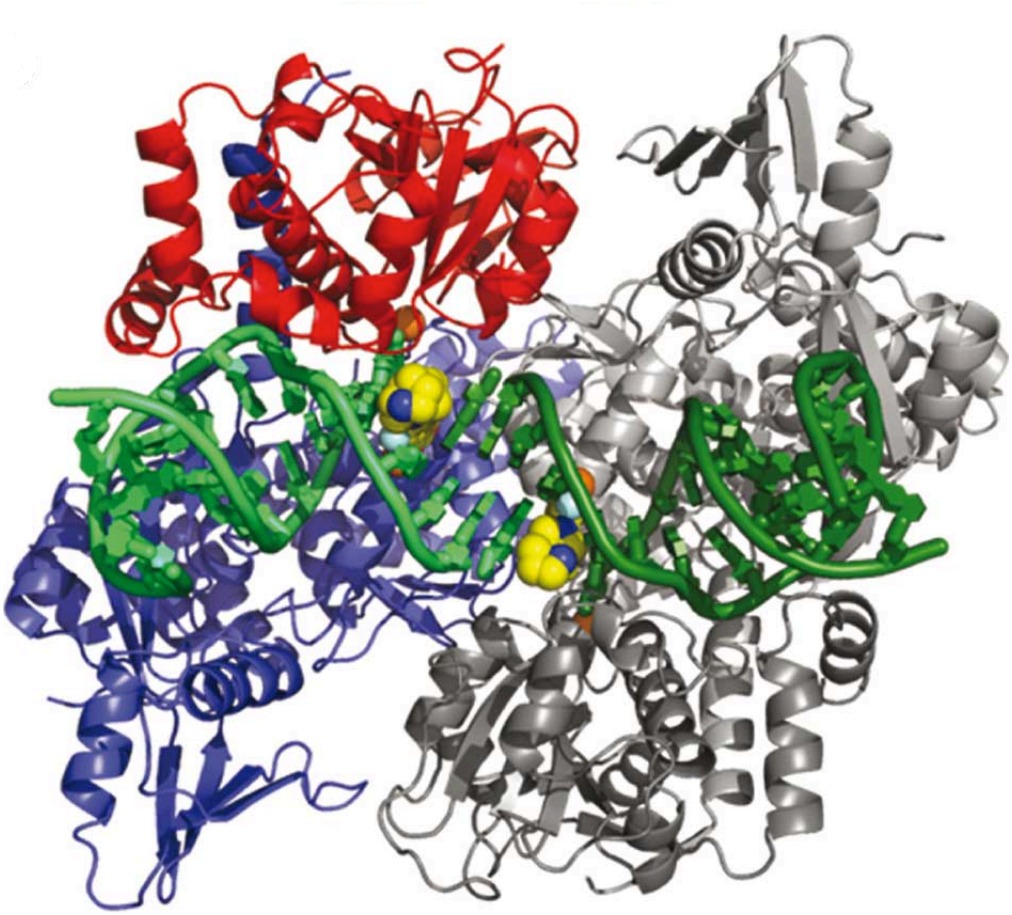

Figure 22. A crystal structure of moxifloxacin (yellow) intercalated into DNA (green), in complex with ParC (red) and ParE (Blue) of *Acinetobacter baumannii* topo IV (PDB 2XKK).[153]

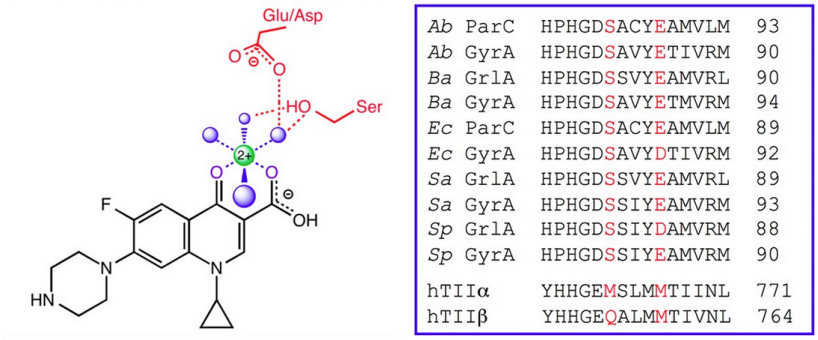

Ab ParC	HPHGDSACYEAMVLM	93
Ab GyrA	HPHGDSAVYETIVRM	90
Ba GrlA	HPHGDSSVYEAMVRL	90
Ba GyrA	HPHGDSAVYETMVRM	94
Ec ParC	HPHGDSACYEAMVLM	89
Ec GyrA	HPHGDSAVYDTIVRM	92
Sa GrlA	HPHGDSSVYEAMVRL	89
Sa GyrA	HPHGDSSIYEAMVRM	93
Sp GrlA	HPHGDSSIYDAMVRM	88
Sp GyrA	HPHGDSSIYEAMVRM	90
hTIIα	YHHGEMSLMMTIINL	771
hTIIβ	YHHGEQALMMTIVNL	764

Figure 23 Water-metal ion bridge (left) between ciprofloxacin and the Ser and Glu/Asp residues. Alongside contrasting sequences (blue box) of *A. baumannii* (Ab), *Bacillus anthracis* (Ba), *E. coli* (Ec) *Staphylococcus aureus* (Sa) and *S. pneumonia* (Sp) DNA gyrase (GyrA) and topoisomerase IV (ParC/GrlA). The homologous regions of human topoisomerase hTIIα and hTIIβ are shown for comparison.[18]

Interestingly the 2,4 quinazolinedione PD 0305970 cannot efficaciously form the C3/C4 water-metal ion bridge and its action must therefore be dependent on other structural components providing significant interactions with the enzyme. Mutation of serine, the acidic residues, or both, does not affect quinazolinedione affinity for topo IV or DNA gyrase.[154] The quinazolinediones are potent inhibitors *in vitro* and *in vivo* with a broad spectrum of activity against Gram-positive and Gram-negative bacteria.[146] Despite the ability to overcome quinolone resistance, this class has been shown to have undesirable cross reactivity to human topoisomerase IIα (hTIIα). This is ascribable to the 3'-(aminomethyl)-or 3'-aminoethylpryrrolidinyl moiety at the 7 position.[156] No clinically utilised quinolones to date contain this motif. A future challenge for the 2,4 diones is to design structures to minimise cross reactivity to human topoisomerase whilst retaining antibacterial activity.

1.17 Cellular response to quinolones

The mechanisms through which quinolones exert their lethal effect are complex and not yet fully elucidated. It was theorised that collision of replication forks with DNA-drug-enzyme complexes caused fork breakage and DNA release, and that this was the mechanism by which the quinolones exerted their therapeutic effect.[157] However, experiments showed that despite nalidixic acid having a pronounced effect arresting DNA replication, it did not alter the biological integrity of the DNA.[158] Cells exposed to nalidixic acid for 3 hours were able to recover after the drug was removed demonstrating that whilst the quinolones bound to DNA this binding was not tight. Moreover cleavage complex formation was reversible. The association between cell death and inhibition of DNA synthesis therefore warranted further investigation. Bacteriostatic concentrations of oxolinic acid had been shown to trap the DNA gyrase enzyme and prevent ligated DNA from being released from the enzyme. The release of fragmented DNA only occurred at high concentrations. Furthermore the release of DNA and consequent cell death at high concentrations was blocked by chloramphenicol, a known inhibitor of protein synthesis. The authors concluded that additional protein synthesis is required in order to free the broken DNA from the enzyme. Interestingly, ciprofloxacin could act independently in the presence of chloramphenicol, and was postulated to be able to cause dissociation of gyrase subunits.[159,160] Thus, it became apparent the quinolones could not only have a bacteriostatic but bactericidal effect depending on their structure and concentration. First generation nalidixic acid acid cannot kill *E. coli* in the presence of chloramphenicol or under anaerobic conditions. However, norfloxacin could maintain cell lethality in anaerobic conditions provided chloramphenicol was not present. In contrast, ciprofloxacin can kill cells regardless of the presence of anaerobic conditions or chloramphenicol. It was noted however, that higher concentrations of ciprofloxacin were required under the anaerobic conditions.[161] Therefore, the rapid killing of bacterial cells is currently described as a two-step process. Step one is the reversible formation of a drug-DNA-gyrase complex containing DNA breaks. The second is the release of DNA breaks from the enzyme which causes chromosome fragmentation and cell death.

The requirement for continuing protein synthesis in order for chromosome fragmentation to occur with certain quinolones is poorly understood. Current predictions include break down of DNA gyrase by protease, cleavage of the cleaved complex by nuclease and denaturation of the enzyme mechanisms by which broken DNA is released from the enzyme.[162]

1.18 Contribution of ROS to cell death

Following the addition of norfloxacin to *E. coli* it has been shown that levels of hydroxyl radicals increase.[163] In addition, agents that reduce levels of hydroxyl radicals (thiourea and 2,2'-bipyridyl) also reduced norfloxacin lethality. A separate group showed norfloxacin was not as lethal to an *E. coli* mutant lacking superoxide dismutase A (*sodA*) and B (*sodB*). This is consistent with the observation that cellular stress leads to increased levels of superoxide which can be converted into peroxide and ultimately form toxic hydroxyl radicals.[164] Thus, oxidative stress also plays a role in contributing to the quinolones lethal action. Interestingly thiourea and 2,2'-bipyridyl also inhibited oxolinic acid, a quinolone that works via the chloramphenicol sensitive pathway. However, as this did not prevent chromosome fragmentation; this step must precede ROS formation. Moreover, the same experiments with PD161144 a C8 methoxy derivative which kills anaerobically and via the chloramphenicol independent pathway (i.e. without the need for additional protein synthesis) was unaffected even though this quinolone stimulated hydroxyl radical formation (Figure 24).[165] Since their discovery over 50 years ago we are still unravelling insights into the full quinolone mechanism of action. The validity of targeting the DNA-cleavage-reunion cycle is eloquently exemplified by their pharmaceutical success. A new class of inhibitor with a completely separate mode of action against DNA gyrase has created further interest in exploiting this unique enzyme. The remainder of this chapter explores the literature regarding simocyclinone and our current understanding of its action.

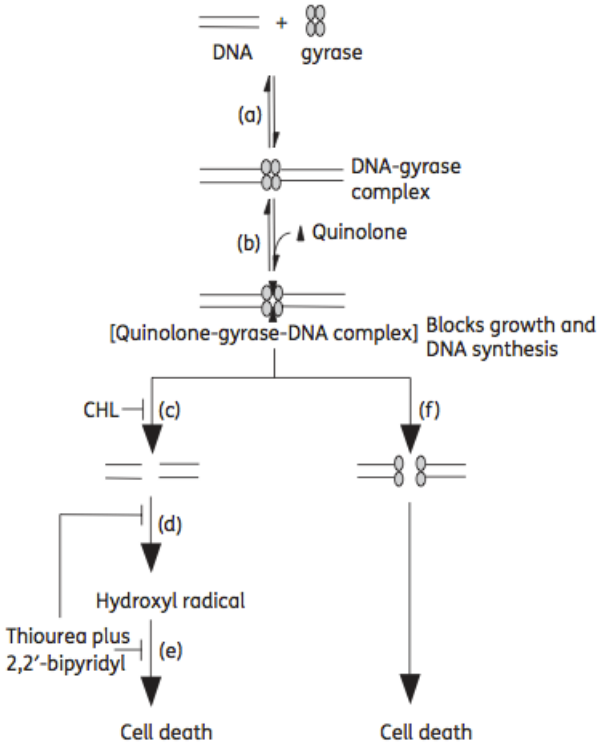

Figure 24. Quinolone mediated lethality and ROS: **(a)** DNA and gyrase associate to form a complex, **(b)** quinolones form a complex with DNA and gyrase; DNA is broken and constrained thus inhibiting DNA replication and growth, **(c)** chromosomal fragmentation that can be blocked by chloramphenicol (CHL) a known inhibitor of protein synthesis, **(d)** chromosome fragmentation increases reactive oxygen species and eventual hydroxyl radical formation **(e)**, **(f)** quinolones can also kill via a protein synthesis-independent, ROS-independent chromosomal fragmentation pathway.[165]

1.19 Isolation of the simocyclinone antibiotics

SD8 was first identified from a soil sample of Argentinean origin using high performance liquid chromatography with diode array detection and mass spectrometry (HPLC-DAD-MS).[166] An extract using ethyl acetate and methanol was compared to an in-house antibiotic database. The UV peaks of interest that were considered novel were then further investigated by mass spectrometry and two new compounds, termed simocyclinone D4 (SD4) and D8 (SD8) were revealed (Figure 25).

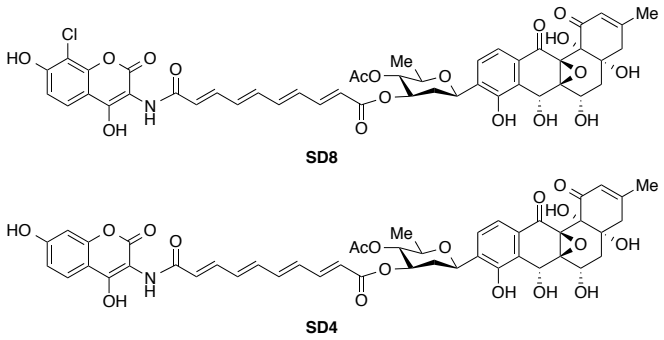

Figure 25. Structure of the simocyclinones.

It was recognised that the simocyclinones contained structural motifs reminiscent of other antibacterial agents. The polyketide had a classical aglycone moiety with angularic oxygens and a C-glycosidic bond to a D-olivose sugar similar to the napthoquinone aquayamycin; the unsaturated tetraene linker was known to be present in the antibiotic fumagillin and the chlorinated dihydroxylated coumarin was present in the aminocoumarin antibiotic chlorobiocin.[167,168] Thus, the simocyclinones themselves are considered natural product hybrids.

The simocyclinones were isolated from a *Streptomyces* genus. This was founded on the composition of the peptidoglycan layer of the bacteria, morphology, pigmentation and sporulation characteristics. Analysis of carbon utilisation allowed strain *Tü 6040* to be differentiated from *S. naganishii* and assigned as a *S. antibioticus* species. This was in accordance with standardised procedures for the chemotaxonomic classification of *Streptomyces*.[169] This first report of the simocyclinones also evaluated their biological activities. The authors found that as well as activity against Gram-positive bacteria, SD4 and SD8 could cytostatically inhibit cancer cells. Inhibition of growth in MCF-7 (breast cancer) cells occurred with an IC_{50} of 5.6 μM, 0.95 μM respectively. Additionally the IC_{50} for HMO-2 (gastric cancer) cells was 0.3 μM, 0.5 μM respectively.

1.20 Fermentation and classification of simocyclinones

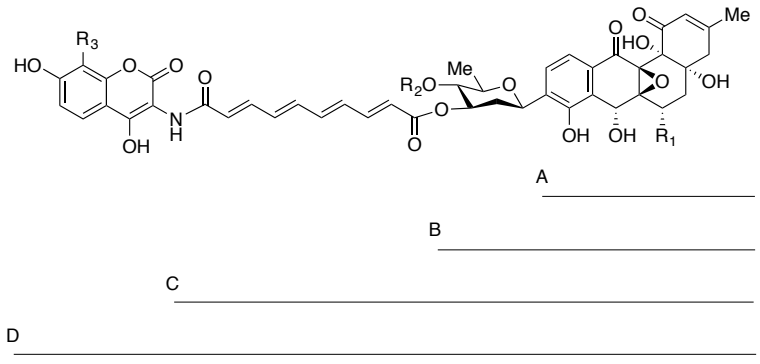

Figure 26. Classification of simocyclinones A-D.

	A1	B2	C2	C4	D6	D4	D8	D7
R_1	H	OH	OH	OH	OH	OH	OH	H
R_2	-	H	H	$COCH_3$	H	$COCH_3$	$COCH_3$	$COCH_3$
R_3	-	-	-	-	H	H	Cl	Cl

Table 2. Classification of simocyclinones A-D.

Investigation of the medium composition on antibiotic production contributed interesting results. A combination of glycerol and L-lysine or L-arginine produced the highest yield of SD8 with the optimal carbon:nitrogen ratio being 20. Variation of K_2HPO_4, NaCl and $MgSO_4$ concentrations did not affect cellular growth. However, maximum metabolite production occurred at concentrations previously reported.[166] Variation of the carbon and nitrogen sources allowed for the isolation of different structural elements of the simocyclinones. The authors categorised the structural motifs into four series from A-D (Figure 26 & Table 2). Confusion may arise because the nomenclature used to describe the contiguous rings of the polyketide is also denoted from A-D. Attention is drawn to the polyketide A1, which could only be isolated from a combination of mannitol and L-lysine. Additionally the linker, sugar, polyketide fragment (SC4) was solely isolated when grown in the presence of glycerol and L-arginine.[170]

Later investigations showed the addition of NaCl shifted the production of metabolites towards SD8. Conversely use of NaI exclusively constructed the dechlorinated SD4 analogue. This early work formed the foundation to the pioneering exploitation of *S. antibioticus* as a tool to produce new analogues for antibacterial screening. Moreover, the elucidation of different constituent intermediates of SD8 meant predictions about the biosynthetic pathways involved could start to be made.

1.21 Structural elucidation of SD4 and SD8

SD4 and SD8 were later fully assigned based on ^{1}H NMR, ^{13}C NMR, COSY and HMBC.[171] Although elemental analysis and MS confirmed the number of carbons as 46 for SD4 and SD8, the quaternary epoxide carbon 12a was not observed in NMR experiments. The authors attributed this phenomenon to parameters of the NMR experiments that made it unfavourable to measure this signal (Kalinowsk, H. O.; Berger, S.; Braun, S.; 1984 cited Holzenkämpfer, M.; Walker, M.; Zeeck, A.; Schimana, J.; Fiedler, HP., 2001).

An alternative to a distortionless enhancement by polarisation transfer (DEPT) experiment, an attached proton test (APT) was used to differentiate between carbons of the simocyclinones. Unlike DEPT, which supresses quaternary signals after multiple acquisitions, the APT displays these as a negative signal. The APT experiment showed the polyketide contained two carbonyl groups as indicated by the largely downfield chemical shifts and negative signals. The APT results differentiated between the aromatic carbons and the carbons attached to oxygen. The methyl group appeared as a distinctive positive signal in an upfield region. In contrast, the two CH_2 groups appeared as negative signals alongside the quaternary carbons. The sugar was identified as β-D-olivose via a combination of coupling constants and homonuclear correlation spectroscopy (COSY) analysis as the aglycone moiety at the anomeric centre is above the plane of the sugar. Ester groups mask the 3' and 4'-OH groups, HMBC revealed through bond coupling of the C1" carbon of the tetraene linker to the 3'-axial proton of the β-D-olivose sugar confirming the presence of an ester linkage. Due to restricted rotation around the C=C bonds of the tetraene linker each double bond carbon is attached to a univalent carbon. Thus, the fixed geometrical configuration of the double bonds can be assigned. The ^{3}J value of 15 Hz signifies an all-*E* stereochemistry. In contrast, if a *Z* configuration were present a smaller ^{3}J value would have been observed. Lastly, a coumarin chromophore is the only arrangement possible whereby the 13"-OH can be chelated from the carbonyl of the linker. This structure was also supported by the upfield signal of the quaternary C12". As a secondary substantiation, the chemical shifts of the coumarin were concordant with values of novobiocin. The ^{13}C NMR for SD4 and SD8 are identical except for the replacement of a protonated carbon for a quaternary signal. A more deshielded position characteristic of a halogen, is present in SD8.

1.22 Radiolabelled feeding experiments

Studies had suggested the angucyclic core could be synthesised from acetate. Additionally classical angucyclinones were postulated to be derived from decaketides initiated by acetyl-CoA and elongated by 9-malonyl-CoA units. Radiolabelled feeding experiments had shown the side chain of fumagillin could be produced from acetate. However, acetate itself was known to abolish the production of simocyclinones. Consequently malonic acid-2-^{13}C, malonic acid-1,3-$^{13}C_2$ were used instead to probe the biosynthetic pathways. As predicted, when fed to *S. antibioticus*, radiolabelled carbon was present in both the polyketide and linker. Further experiments with L-tyrosine-^{13}C illustrated exclusive incorporation into the aminocoumarin scaffold.

1.23 SD8 a novel mode of action

The simocyclinones were compared with novobiocin by varying the concentration of ATP in a supercoiling assay. At low ATP concentrations novobiocin showed strong inhibition, conversely at high ATP concentrations inhibition was abrogated. In contrast, SD8 had no change in its IC_{50} with

varying ATP, illustrating that its effect is independent of competition with ATP for binding. Interestingly, DNA-dependent ATPase activity, which is stimulated in the presence of DNA, was prevented by SD8, whereas DNA independent ATPase activity remained unaffected.[172] A ten-fold increase in IC_{50} value for SD8 was observed with a quinolone resistant mutant gyrase.[172,173] The Ser-83 to Trp point mutation on GyrA occurred in a region thought to be adjacent to the site of DNA cleavage (Heddle, J. G.; Barnard, F. M.; Wentzell, L. M.; Maxwell, A.; 2000 cited Flatman et al 2005).[172] Concomitant resistance to SD8 and ciprofloxacin indicated the involvement of this area in SD8 binding. Importantly, while the quinolones stabilised DNA after cleavage, no such observations were found with SD8. Furthermore, it was shown that SD8 could prevent ciprofloxacin and Ca^{2+} induced cleavage of supercoiled DNA. Surface plasmon resonance (SPR) showed SD8 blocked the association of DNA to the gyrase enzyme. Subsequent analysis with a GyrB43 subunit showed no interaction. Additionally, only a small response was elicited from GyrA59. The authors attributed the lack of response in GyrA59 as a limitation that arose from the SPR experiment not being representative of what occurs in solution.

ITC was used as a supplementary experiment, unlike the SPR data, ITC showed an interaction between SD8 and GyrA but not for GyrB. A binding constant of 50 to 100 nM indicated a 1:1 stoichiometry. These results suggested two molecules of SD8 bind to each A_2B_2 heterotetramer in solution. To ascertain if SD8 inhibition was unique to DNA gyrase, assays were performed on the closely related topoisomerase IV (topo IV) and eukaryotic topoisomerase I, II (topo I, topo II). No inhibition was observed with topo IV or topo I at 40 μM. However strong inhibition was seen in topo II decatenation concordant with earlier observations of a cytostatic effect on tumour cells.[166] In contrast, both aminocoumarins and quinolones acted on topo IV. This work was later expanded to show SD8 was a potent catalytic inhibitor of human topo II *in vitro*, against non small cell lung cancer (NSCLC) and mesothelioma (MM).[174] Unlike other inhibitors such as etoposide, which form a DNA-drug-enzyme ternary complex preventing strand religation, analogous to ciprofloxacin's effect on gyrase, SD8 did not induce DNA cleavage. Subsequent efforts demonstrated that high concentrations of SD8 (100 μM) could inhibit topo I in relaxation assays.[175] Similar to topo II, this did not induce cleavage. The concentrations at which inhibition were observed were higher than the original 40 μM investigated.[172] As previously noted, no relaxed topoisomers were visible at 50 μM. This raises an interesting unanswered question as to how SD8 exerts its affect on topo I, due to the fact it does not share structural similarity with type II topoisomerase enzymes.

1.24 Crystal structure of SD8 bound to N-terminal GyrA59

The first crystal structure of SD8 bound to an N-terminal fragment of GyrA59 from *E. coli* at a resolution of 2.6 Å was published in 2009.[176] This structure showed GyrA59 dimers bound to four SD8 molecules. The data showed that two distinct pockets existed on the GyrA59 subunit; an aminocoumarin pocket and a polyketide pocket. No conformational change to the enzyme was

observed after subtracting the ligand-bound structure from the unbound breakage-reunion domain of gyrase.[177] While two SD8 molecules had been isolated on each subunit, it was recognised that a single SD8 molecule could be modelled in a 'bent' arrangement to connect with both the aminocoumarin and polyketide pockets on the same subunit at the same time sustaining the contacts seen in the crystal structure (Figure 27 & 28). Analytical ultracentrifugation was used as a method of quantitative analysis, giving insight into the size of protein in solution.[178] When SD8 was absent or at low concentrations, the MW of GyrA59 was ~120 kDa, suggesting a dimer. Conversely, at high ligand to protein ratios of greater than 4:1, GyrA59 had a molecular weight of ~250 kDa which would be consistent with a tetramer (Figure 27). These observations were also confirmed by nanoelectrospray ionisation mass spectrometry (nanoESI MS) indicating that this was not an artefact of the crystallisation process. The full implication of these findings is not yet completely understood.

The crystal structure revealed critical information about intermolecular interactions. Lys42 was important for hydrogen bonding interactions with the amide carbonyl group of SD8. Similarly Ser172 and Arg91 were hydrogen bonded to the lactone ring carbonyl and the 4'-OH group respectively. The Asn165 residue was observed to be hydrogen bonded to the 7-OH group whilst the halogen interacted with a Gly170 residue. Non-bonding interactions were attributed to Leu98 and His45 with the aromatic ring of the coumarin. The polyketide portion was seen to be associated with Mg^{2+} ions complexing with the OH groups of the A, C and D ring. Lastly, hydrogen-bonding contacts were formed between the ketone of the C ring and the epoxide by arginine residues (Figure 28).

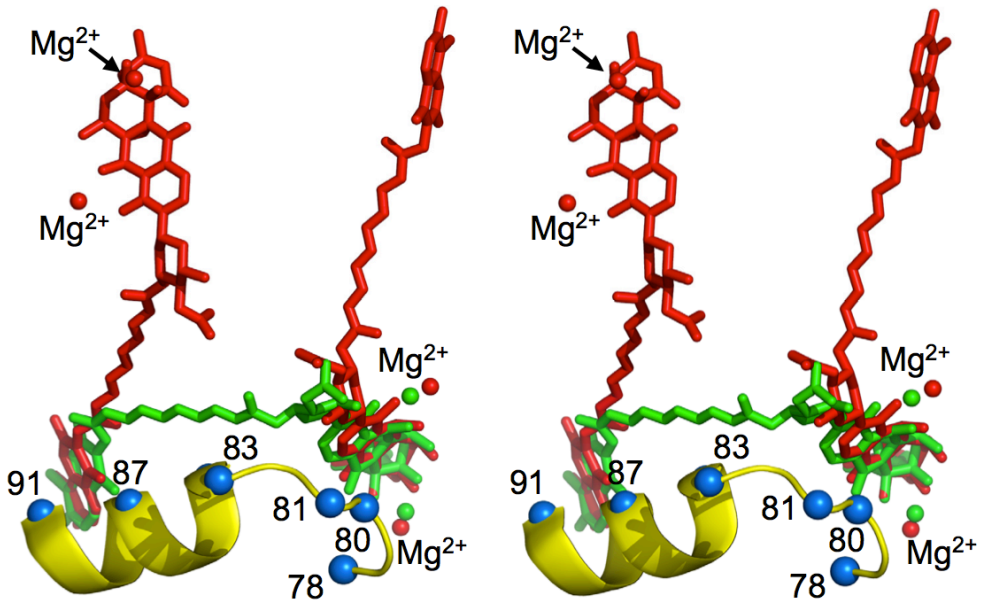

Figure 27. SD8 bound as two separate molecules (red) on each subunit (yellow). A single SD8 molecule bound in a 'bent' conformation (green) with Magnesium counter ions as spheres.[176]

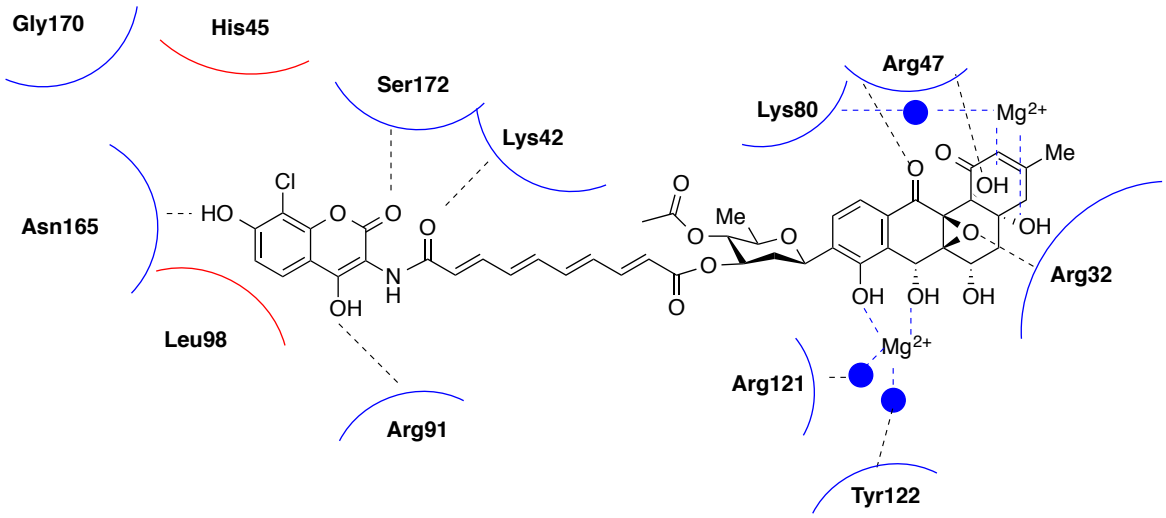

Figure 28. Key bonding interactions for SD8 bound in a 'bent' conformation. Dashed black bonds represent hydrogen bonding, dashed blue lines represent magnesium co-ordination, solid red lines represent hydrophobic interactions, solid blue circles are shown for water molecules.[176]

Accompanying investigations were performed with spontaneous resistant *E. coli* mutants with a permeable strain (NR698) that possessed a deletion in the increased membrane permeability gene (*imp*). The authors found 31 mutants, with 22 containing mutations to the gyrA region. The other 9 isolates were resistant to bile salts and consequently postulated to have secondary site mutations which had restored their *imp* function; thus they were not explored further.[179] All of the amino acid changes were in residues in close proximity to the purported binding site of SD8 based on the crystal structure data. Based on these findings the authors performed selected site directed mutations in GyrA59. Mutation to the aminocoumarin pocket at His^{45} or Arg^{91} or the polyketide pocket at His^{80} and Gly^{81} had a detrimental affect on supercoiling. Moreover, mutation to H78A on the polyketide produced an inactive enzyme; SPR showed a reduced affinity of SD8 for the mutant over the wild type. Circular dichroism (CD) demonstrated that the enzyme was correctly folded with a near identical spectrum obtained for the mutant and wild type. It is noteworthy that excluding the inactive mutant, all mutations to the aminocoumarin or polyketide conferred susceptibility to quinolones. Conversely, mutations to the quinolone resistance determining region (QRDR), which lies in close proximity to the SD8 binding area, reduced the inhibitory effect of SD8.

To explore the role of each functional unit of SD8 constituent fragments SC4 and MGD8N2A were analysed for their ability to inhibit supercoiling compared to the parent compound IC_{50} of 0.6 μM (Figure 29). Fascinatingly the individual fragments of SD8 showed only modest inhibition in supercoiling assays at 70 μM and 50 μM respectively. This indicated that while both functional groups could exert modest inhibition individually, when combined they had a synergistic effect resulting in potent inhibition. An eloquent example of nature's own fragment based drug.

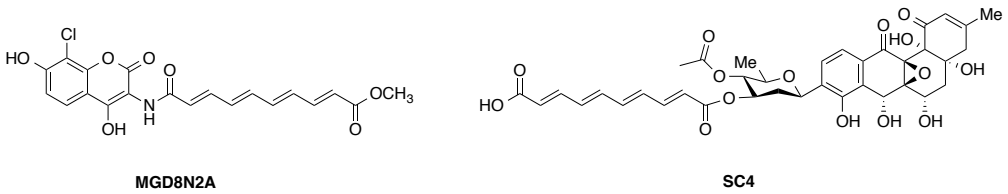

Figure 29. Structures of constituent fragments of SD8.

1.25 Mass spectrometry studies into SD8 binding

As a complementary technique to investigate SD8 binding, mass spectrometry was employed. Nano electrospray ionisation (nanoESI) mass spectrometry of the Gyr59-SD8 complex supported previous findings that a stoichiometry of 1:1 SD8 ligand:subunit exists at pharmacologically relevant concentrations.[180] Tetramer formation was also seen when a large molar excess of SD8 was used, consistent with previous observations from the original crystal structure of SD8 binding. Interestingly, the data indicated a preference for SD8 molecules to bind as a pair to one GyrA dimer (Figure 30 **c**) even at low concentrations rather than one molecule binding (Figure 30 **b**) to one subunit of a dimer. This preference indicated positive cooperativity in binding. Statistically, it is more likely that occupancy of independent sites would bind in a manner depicted in Figure 30 **(b)**, particularly at low concentrations.

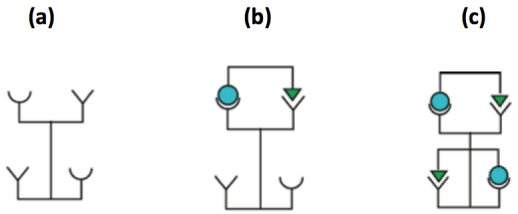

Figure 30. SD8 occupancy of Gyr59 dimer. **(a)** represents an unoccupied Gyr59 dimer, **(b)** one molecule of SD8 bound to one subunit of a dimer, **(c)** two SD8 molecules bound to the same dimer. Adapted from Edwards et al 2011.[180]

Deployment of the fragments SC4 and MGD8N2A revealed a difference in affinities, with the polyketide having a 5 fold greater binding affinity compared to the aminocoumarin. However, there is no enhancement observed when the individual fragments were used concomitantly. Consequently it can be unequivocally stated that the tight binding of SD8 is a consequence of both fragments being linked together as a single molecule. This was in agreement with the previous body of work by the same authors and also supported the hypothesis of SD8 binding in a 'bent' conformation to occupy sites on the same monomer.

1.26 Evidence of binding to Gyrase B

Circular dichroism (CD) can be a useful technique for studying protein-ligand interactions. Many molecules, including proteins, exhibit chirality in their structure. CD measures the difference in polarised light that has been passed through a solution of the molecules of interest. When a ligand or small molecule binds to the protein of interest it can induce a conformational change, this causes a change in the CD signal termed an "induced circular dichroism" (ICD). However, if no structural perturbation occurs then there is no change in the CD signal.[181] The addition of SD8 to reconstituted gyrase (A_2B_2 heterotetramer) showed no significant changes in the 200-250 nm range, indicating a distinct lack of conformational change to the enzyme structure upon SD8 binding.[182] Similarly when SD8 was added to individual GyrA, GyrA59, GyrB and GyrB43 no ICD was observed in agreement with the A_2B_2 behaviour.

To further probe SD8 interaction, protein thermal stability experiments were performed with ciprofloxacin, SD8, novobiocin and adenylyl imidodiphosphonate (ADPNP), a non-hydrolysable form of ATP. Ciprofloxacin was the only compound that was able to shift the T_m of GyrA as previously noted.[183] As expected ADPNP and novobiocin, which are known to bind to the B subunit, also failed to give an increased T_m for the GyrA and GyrA59 proteins. In contrast, SD8 modestly increased the T_m at low concentrations (10 μM) by 5.5 °C. When the concentration of SD8 was plotted against T_m, a sigmoidal curve was obtained indicating two molecules of SD8 having a co-operative effect, supporting previous observations. More surprisingly, all the ligands except for ciprofloxacin showed a concentration dependent increase on GyrB T_m. There were differences observed in the shifts, the T_m with ADPNP was entirely dependent on magnesium ion concentration whereas novobiocin and SD8 effects were independent of the Mg^{2+} concentration. An interaction for SD8 was only found at the C-terminal domain of GyrB47 and showed a stabilisation of its natural conformation This contrasted with the GyrB43 N-terminal domain where no effect was seen. It is important to note that the GyrB47 C-terminal domain does not contain the ATP or coumarin-binding site but instead is involved in DNA binding. This was substantiated with proteolytic cleavage assays using trypsin in which SD8 delayed the appearance of a 25-kDa degradation product of the C-terminal fragment.

The changes in T_m in the simultaneous presence of multiple ligands gave further insight into the respective binding domains of each compound. Novobiocin showed an ability to displace GyrB-ADPNP complex. When ADPNP was added to a GyrB-SD8 complex an increased thermal shift that was larger than the T_m of each individual ligand was noted. This signified a synergistic stabilisation of the subunit. Similar results were obtained with the addition of novobiocin to GyrB-SD8 complex. The same was true for a GyrB-novobiocin complex when SD8 was added. The authors then switched their attention to observing these effects on supercoiling. ADPNP and novobiocin both act to prevent the association of ATP to the gyrase B subunit, denying the release of energy from the

hydrolysis of the sugar phosphate backbone. This abolishes the enzymes ability to introduce negative supercoils into the bacterial DNA. The two ligands are unable to block the ATP-independent relaxation of supercoiled DNA. However, because SD8 can block the binding of DNA, it can abolish both supercoiling and relaxation of DNA. No effects were seen on the inhibitory activity of SD8 when either ADPNP or novobiocin were used simultaneously. Consequently, this body of work demonstrated the binding sites for aminocoumarins and SD8 are distinct. The authors concluded, based on the data indicated by the melting experiments, that SD8 has a higher affinity for GyrA over GyrB. Interestingly, the overall increased melting point is more pronounced for the full A_2B_2 tetramer of gyrase than the individual subunits, indicating two interaction events contributing to the observed activity. The overall implications of two binding sites for SD8 are not fully understood and further investigation is required to elucidate the full mode of action.

1.27 A new crystal structure gives fresh insight into SD8 binding

In 2014 a new crystal structure was obtained that consisted of SD8 bound to a N-terminal 55-kDa fragment.[184] The purpose of the shorter gyrase fragment was to obtain a crystal structure with SD8 bound in way that was more representative of its binding in solution at low concentration. The key differences between this fragment and its predecessor, GyrA59, were that 10 of the 12 amino acid residues recognised as stabilising the tetramer at dimer-dimer interface were missing as well as the N-terminal alpha helix. CD spectra and ITC of the new 55-kDa GyrA fragment supported previous data obtained from the GyrA59 fragment indicating that the new truncated gyrase had formed the correct tertiary protein structure. Strikingly, the conformation of SD8 in the crystal structure of the Gyr55-SD8 complex was different to the previously published structure. The structure revealed SD8 bound within one homodimer with the polyketide spanning two GyrA55 monomers. Hydrogen bonding occurs from Met120 of an adjacent monomer as well as direct hydrogen bonding from His80 and Gly81 (Figure 31). Indirect bonding via water comes from Pro79 and Asp87. The aminocoumarin pocket was fundamentally the same as previously reported.[176] However, the orientation of the coumarin in the pocket was different. The key residues implicated in both crystal structures are Lys42 hydrogen bonding to the carbonyl group of the lactone, Ser172 hydrogen bonding to the 4-OH group and Arg91 hydrogen bonding to the exocyclic carbonyl group of the lactone ring. Hydrophobic contacts from Val44 and His78 were now apparent as well as hydrogen bonding from His80 to the ester of the tetraene linker.

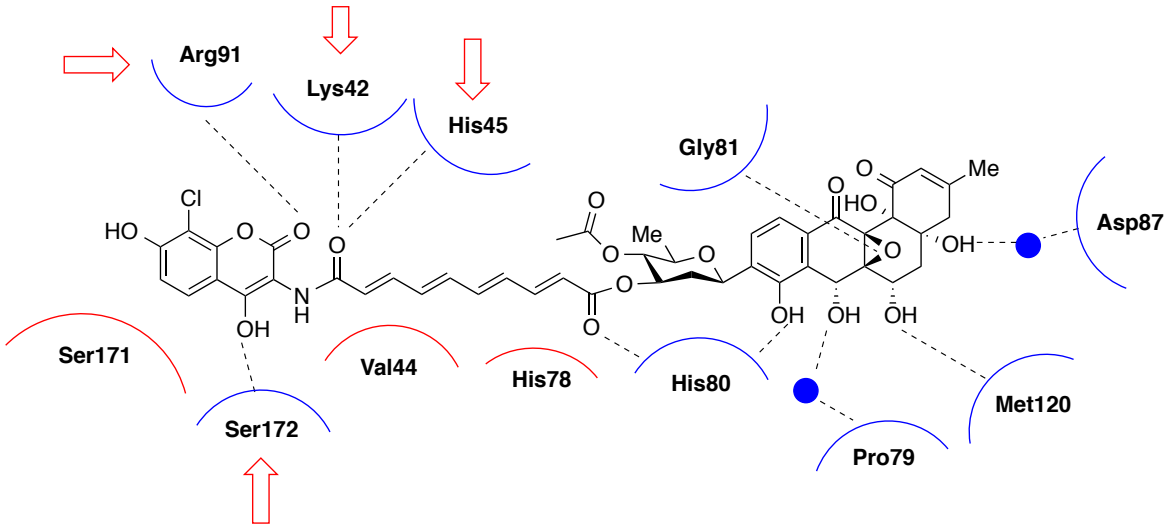

Figure 31. New crystal structure data for SD8 binding to a 55-kDa fragment, the amino acid residues that are present in both crystal structures but their orientation is different are highlighted with red arrows.[184]

Previously, mutation data for the GyrA59-SD8 complex was not completely understood. The new crystal structure helped to illuminate some of the formerly unanswered questions. Substitutions at the Arg32 and Arg47 residues were initially identified as important for binding the polyketide terminus. However, no changes were observed for these mutants as indicated by supercoiling assays and surface plasmon resonance compared to the wild type. The new orientation indicates that two arginine residues are away from the polyketide scaffold, showing they are not involved in binding. In contrast, changes to Gly81 and Asp87 bestowed resistance with no obvious explanation as to the residues responsible for this in the GyrA59-SD8 complex. This new structure shows the epoxide of SD8 hydrogen bonds to Gly81 and water hydrogen bonds to a hydroxyl group via Asp87, thus providing an answer to this mystery.

To confirm the authenticity of the new GyrA55-SD8 complex, three further mutants were created and tested. Changes were made at the Lys42 residue in the aminocoumarin pocket, Met120 in the polyketide pocket and the Ala85 residue in the α-helix 4 that runs parallel to the tetraene linker. As predicted, the mutations to the aminocoumarin and polyketide binding site dramatically altered susceptibility to SD8 (50 fold and 60 fold respectively). Interesting to note is that the increased α-helix 4 had no effect on activity, the authors concluded that it must adopt a conformation that does not interfere with binding. Crucially, this new structure illustrated that SD8 positions itself to “staple” the dimer interface closed and prevent the DNA gate from opening, which is a necessary step for allowing DNA binding and strand passage to occur. The α-helix 4 residues are held in place by the hydrogen bonding occurring from the polyketide. Furthermore, the catalytic tyrosine residue responsible for DNA ligation cannot arrange itself in the correct position due to preclusion by the

polyketide. The aminocoumarin contact at Arg91 would prevent the stabilisation of DNA during association between the DNA and the enzyme (Figure 32). Lastly, ITC experiments agreed with previous work, that a 1:1 stoichiometry occurred *in vitro* upon the addition of SD8 to GyrA55.

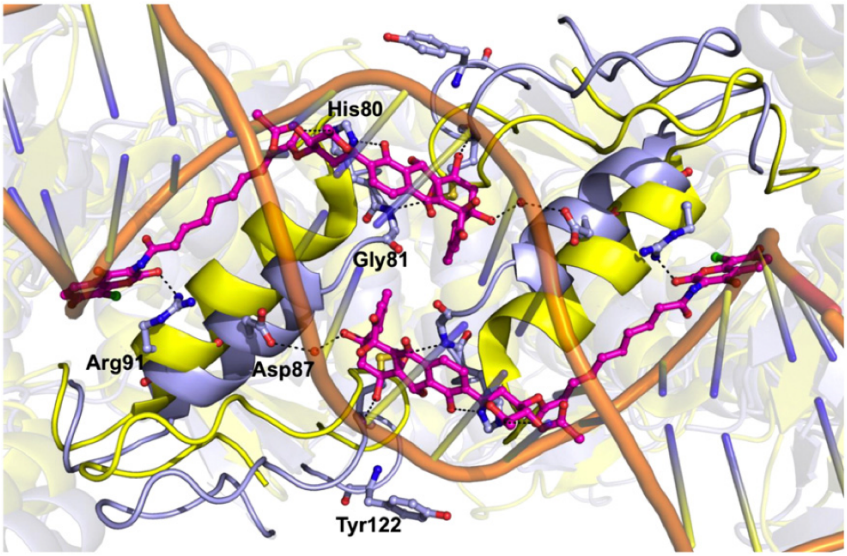

Figure 32. Superposition of the DNA gates of GyrA55-SD8 (blue) and *S. aureus* GyrA-DNA-GSK299423 (ligand not shown, yellow).[184]

1.28 Significance of the polyketide

In 2015 a new simocyclinone derivative termed "7-oxo-SD8" was isolated from investigations into the function of the SimC7 enzyme (Figure 33).[185] Due to difficulties in creating mutants of *S. antibioticus*, the authors cloned the *sim* gene cluster and analysed it in a heterologous system using *S. coelicolor* M1152 as the host.

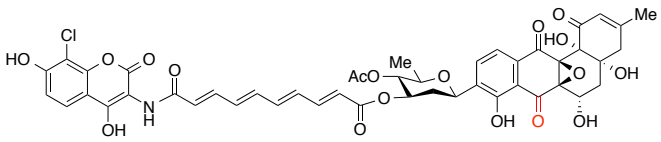

Figure 33. Structure of 7-oxo-SD, the different substituent to SD8 is highlighted in red.

This advantageously gave a simplified metabolite profile and improved production of secondary metabolites. Strikingly, an in-frame deletion of the SimC7 gene resulted in a novel simocyclinone being produced. The new compound had a different retention time, as assessed by HPLC to SD8. Assessment using high-resolution mass spectrometry and NMR confirmed the compound contained a ketone at the C7 position of the polyketide instead of an OH group. Thus, it transpired the true function of SimC7 is as a NAD(P)H-dependent ketoreductase. To test this hypothesis, His-

tagged SimC7 *in E. coli* was purified and incubated with 7-oxo-SD8. This readily converted into SD8 using NADH or NADPH for the reduction. Of more significance is the consequential effect seen on biological activity. To test for 7-oxo-SD8's ability to inhibit bacterial growth, a permeable strain of *E. coli* NR698 was used. This contains an in-frame deletion in the increased membrane permeability (*imp*) gene. Without this mutation the simocyclinones cannot penetrate into Gram-negative bacteria. SD8 exhibited an IC_{50} of 0.3 μM, in contrast the bacterial strain continued to grow in the presence of 7-oxo-SD8 up to a concentration of 17.5 μM. This indicated the binding of the 7-oxo-SD8 had been compromised. Supercoiling assays substantiated the *in vivo* data, showing 7-oxo-SD8 had an IC_{50} of 50-100 μM, contrasting with the normal 0.1-0.5 μM for SD8. Similarly, much higher concentrations of 7-oxo-SD8 were required for cleavage stabilisation to be observed. SPR was only able to detect non-specific binding to gyrase, confirming the abrogation in activity. The authors predict the reduced activity is due to an inability to hydrogen bond with Arg121 and Pro79, mediated via a water molecule as indicated by the GyrA55 crystal structure (Figure 31).[184] Furthermore, the adjacent phenolic OH would be expected to have reduced binding to His80 an important amino acid for polyketide binding. This study eloquently highlights the importance of the polyketide for the potent action of SD8.

1.29 Fragment based drug design

Traditionally methods such as high throughput screening (HTS) or combinatorial chemistry have been used to screen large libraries of compounds in order to identify potent hits that can be taken forward for development.[186] Furthermore, the use of *in silico* ligand screening can help to streamline the number of compounds required for analysis and inform decision making as to potential lead compounds.[187] Imatinib (Gleevec), a tyrosine-kinase inhibitor serves as an example of the successes that can be achieved by employing these methods in drug design. Despite development of these technologies, the attrition rates of novel chemical entities remain high.[188,189] Fragment based drug design (FBDD) is an alternative method whereby low affinity fragments are identified during screening and used to optimise lead drug design. Its founding principles are that a drug can be considered a function of its different binding fragments.[190,191] The advantages over HTS are a more diverse chemical space can be covered and ligand efficiency can be improved. HTS often focuses on large MW compounds with potent activity, however this has not always proved fruitful as the average MW of a drug decreases at each checkpoint towards coming to market.[192] Conversely, FBDD uses relatively low MW fragments typically in the 140-300 Da range.[193] This is in accordance with ligand efficiency that suggests the energy contributed by each ligand atom to the overall binding energy is inversely proportional to the MW.[193,194] With this in mind, FBDD serves as a useful method for developing potential novel inhibitors of DNA gyrase by exploring the inhibition with different low molecular weight fragments.

1.30 Aims of the study

The structure of SD8 and the body of literature investigating its bi-functional mode of action indicate two key binding pockets. These are well defined, with evidence from both x-ray crystallography and mutational data. Crucially, synergy from both fragments is fundamental for the observed potent activity. Having outlined the need for new antibiotics, the biological importance of DNA topology, and the validity of DNA gyrase as a therapeutic target, the aims of this study are as follows:

1. To make synthetic efforts towards constructing the chlorinated dihydroxylated coumarin chromophore present in SD8 as well as developing and validating a viable pathway for synthesis of the polyketide scaffold (Figure 34 red and green highlighted areas).

2. To synthesise a range of 3-aminocoumarin compounds with increasing steric bulk at the 3'-position. Subsequently evaluate their potential as small molecule, low affinity fragments for inhibiting activity of DNA gyrase using established supercoiling assays as a measurement of activity (Figure 34 blue highlighted areas)

3. To synthesise a coumarin-quinolone hybrid and investigate its biological activity. This would be achieved by combining an identified low affinity coumarin ligand and coupling it to the established quinolone ciprofloxacin as an example of a fragment based approach to developing new inhibitors (Figure 34 highlighted in orange).

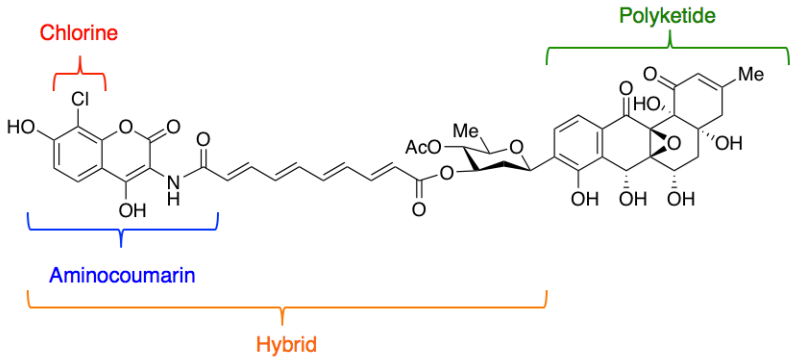

Figure 34. Aims of the study: chlorination of the coumarin (red), synthesis of aminocoumarins (blue) and synthetic efforts towards the polyketide (green) and construction of coumarin hybrids (orange).

Chapter 2. Synthetic efforts towards key fragments of SD8

The generation of the aminocoumarin (AC) and polyketide (PK) moieties of simocyclinone D8 (SD8) is synthetically challenging. Despite the isolation of SD8 over a decade ago, successful synthetic methodologies for the compound have not been reported. This has justified the exploration and development of viable procedures to synthesise both constituent fragments. This work was undertaken to investigate the contribution, if any, of the chlorinated AC chromophore on DNA gyrase inhibition. Furthermore, this would facilitate synthetic access to other analogues such as chlorobiocin, for which no total synthesis has yet been described. Consequently, this work would contribute to the overall total synthesis of two natural products. This chapter introduces the coumarin chromophore and describes efforts towards the synthesis of the chlorinated dihydroxylated AC found in SD8. Additionally, it investigates the use of a Diels-Alder methodology to generate the polyketide scaffold.

2.1 Coumarin and related heterocycles

The word coumarin finds its etymological origin from 'cumaru' the indigenous name for *Dipteryx odorata*, a tree native to South America.[195] It is the tonka bean seeds produced by the tree from which the compound was first extracted in the 19th century.[196,197] Coumarin and chromone are examples of plant-derived oxygen-containing heterocycles that belong to the benzopyrone family. Structurally the parent benzopyran core termed a chromene scaffold by the International Union of Pure and Applied Chemistry (IUPAC) consists of an aromatic benzene ring fused to either a 2H- or 4H-pyran ring system (Figure 35).[198]

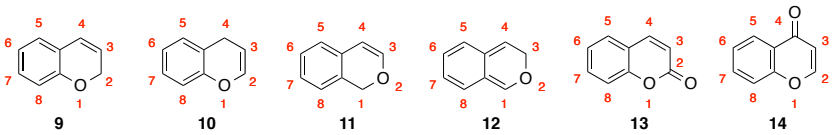

Figure 35. Numbering of 2H-chromene **9**, 4H-chromene **10**, 1H-isochromene **11**, 3H-isochromene **12**, coumarin **13** and chromone **14**.

The location of the oxygen atom in the benzopyran core can have two locations, resulting in two isomers, chromene (1-benzopyran) **9** and isochromene (2-benzopyran) **11**. The numbering denotes the position of the oxygen in the six-membered ring (Figure 35). The same nomenclature is used to describe architecturally related compounds where the *sp*^{3}-hybridised carbon, either adjacent or opposite to the oxygen, is replaced with a carbonyl group. Substitution at the 2-position results in coumarin **13** (2H-chromen-2-one), an α-benzopyrone. Substitution at the 4-position, however, gives chromone **14** (4H-chromen-4-one), a γ-benzopyrone and a structural isomer of coumarin (Figure 35). A distinguishing functional feature of coumarin is the presence of the cyclic ester termed a lactone. In contrast, chromone has no such feature.

2.2 Classification of coumarins

Six categories have been described in the literature to classify coumarins: simple coumarins, pyranocoumarins, furanocoumarins, dimeric/trimeric coumarins and isocoumarins.[197,198] 7-hydroxycoumarin, has been proposed as the parent structure for more complex compounds (Keating, G.; O'Kennedy, R.; 1997 cited Lacey, A.; O'Kennedy, R., 2004). Subdivisions of compound classification exist which are dependent on the substitution pattern within the framework and this is indicated by numbering.[199] Assemblies with additional rings are differentiated according to the site of fusion and described as either angular or linear.[198,200] The structural diversity of coumarins means they may come under more than one heading.[201] This classification is not definitive and will need updating as the field of coumarins progresses.

2.3 Dihydroxylated coumarins

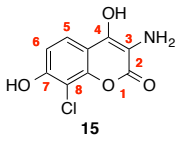

Figure 36. Target compound 8-chloro-4,7-dihydroxy-2H-chromen-2-one.

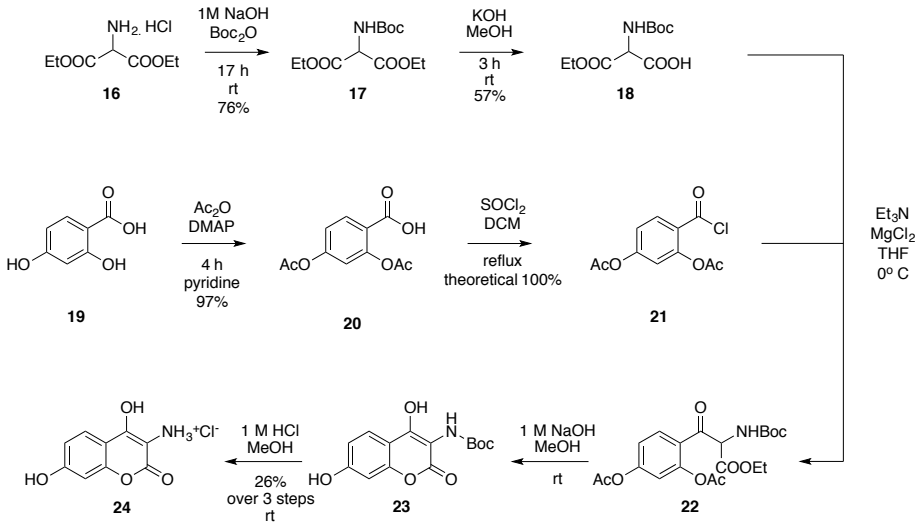

Scheme 1. Synthetic methodology to access the dihydroxylated coumarin scaffold.[202,203]

The overall goal was to establish a route to the target chloro-substituted AC **15** (Figure 36). In order to access this scaffold it was envisaged that an existing procedure could be utilised (scheme 1). The first method explored uses an acetyl protected 2,4-dihydroxybenzoic acid **20**, which is converted into the corresponding acyl chloride **21** and coupled to a *tert*-butyl carbamate (Boc) protected malonate group. Subsequently, the intermediate is cyclised to form the Boc-protected

coumarin **23**. The Boc group can then be removed using acid to give the corresponding coumarin salt **24** (Scheme 1) as previously described.[202,203] It was predicted that chlorination of the dihydroxylated scaffold **24** or the starting benzoic acid **19** could provide a viable synthetic strategy for generating the AC chromophore. The first priority was to validate the previously described procedure by repeating the work.

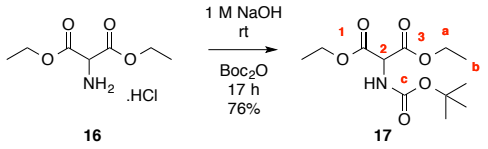

Scheme 2. Synthesis of 1,3-diethyl 2-{[(*tert*-butoxy) carbonyl] amino} propanedioate.

Commercially available diethyl aminomalonate **16** can have a carbamate-protecting group introduced onto the free amine using Boc_2O (Scheme 2).[204–206] Compound **17** was isolated as a colourless oil. ^{1}H NMR showed a doublet at 7.63 ppm (J = 8.0 Hz) assigned as the nitrogen proton and confirmed by HSQC. A doublet at 4.86 ppm was correlated to the 2-H, a reciprocal J value of 8.0 Hz, confirmed its interaction with the N-H proton. A complex multiplet was observed between 4.22-4.11 ppm for the CH_2 groups, this was ascribed to the free rotation of the sigma bond of the Boc protected nitrogen. The integration corroborated this assignment (4 H). A large singlet at 1.39 ppm (9 H) was confirmatory of the introduction of the Boc group. A triplet at 1.20 ppm occurred for the CH_3 signals. ^{13}C NMR showed 7 resolved signals. Due to the chemical equivalence of the CH_2, CH_3 and Boc groups. Downfield signals at 166.6 ppm and 155.1 ppm were ascribed to carbonyl groups. A triple height signal at 28.0 ppm was attributed to the Boc group. IR analysis showed a medium intensity absorption at 3371 cm^{-1} ascribed as the CON-H stretch. Additional absorptions at 2979 cm^{-1} and 2941 cm^{-1} were ascribed to the CH_3 and CH_2 stretches. Two strong absorptions at 1745 cm^{-1} and 1714 cm^{-1} were assigned as two carbonyl groups. The broad peak meant it likely masked one of the unaccounted for carbonyl absorptions. An absorption at 1368 cm^{-1} was attributed to the C-N stretch. Two prominent absorptions at 1182 cm^{-1} and 1158 cm^{-1} were attributed to C-O stretches of both esters. An accurate high-resolution mass of 276.1442 $[M+H]^+$ was found.

Saponification of one ester was achieved using a strong base (Scheme 3).[202] Compound **18** was isolated as a colourless powder. ^{1}H NMR showed a doublet at 7.47 ppm for the N-H proton. The 2-H signal at 4.71 ppm also appeared as a doublet. The a-H_2 signal remained a multiplet between 4.18-4.10 ppm, but the integration had changed (2 H), indicating the loss of the ethyl group. The Boc signal showed as a singlet at 1.38 ppm. An upfield triplet at 1.19 ppm was assigned to the CH_3 of the ester. ^{13}C NMR showed 8 well-resolved signals. The most downfield signal at 167.8 ppm was assigned to the C1 of the carboxylic acid. The next most de-shielded signal at 167.3 ppm was

ascribed to the C3 of the ester. In contrast, the carbon of the carbamate carbonyl had more electron density due to conjugation with the adjacent nitrogen atom and therefore had a more upfield signal at 155.1 ppm. IR analysis showed a medium intensity absorption at 3272 cm^{-1} assigned to the CON-H stretch. Absorptions at 2980 cm^{-1} and 2933 cm^{-1} were ascribed to the CH_3 and CH_2 stretches. These overlapped a broad OH stretch of the carboxylic acid. Intense absorptions at 1747 cm^{-1}, 1723 cm^{-1} and 1650 cm^{-1} were ascribed to the carbonyl stretches. Two strong absorptions at 1182 and 1154 cm^{-1} were assigned to the C-O stretches. An accurate high-resolution mass of 248.1129 $[M+H]^+$ was found.

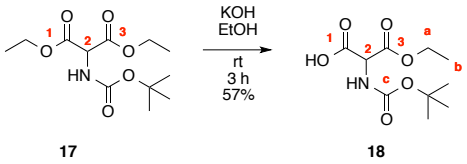

Scheme 3. Synthesis of 2-{[(*tert*-butoxy) carbonyl] amino}-3-ethoxy-3-oxopropanoic acid.

Commercially available 2,4-dihydroxybenzoic acid **19** can be acetylated to form the key intermediate **20**. Phenolic OH groups can be deprotonated using an organic base, such as pyridine. Nucleophilic attack of acetic anhydride by the phenoxy anion will acetylate the corresponding OH groups. DMAP is often included as a catalyst to facilitate the reaction. This step was found to be troublesome, as cited in the literature. Often a mixture of mono or di-acetylated product would be obtained. ^{1}H NMR illustrated a progressive loss of an acetyl singlet over a 24 h period. A corresponding increase in an acetic acid peak is also noted. Consequently, and in subsequent reactions the mixture was covered to protect it form light exposure. Additionally, the acetic anhydride was added dropwise to limit the release of exothermic energy, minimising the degradation of the product, facilitating the near complete conversion into the desired product (Scheme 4).

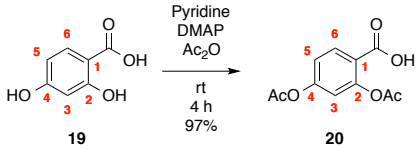

Scheme 4. Synthesis of 2,4-bis(acetyloxy) benzoic acid.

Compound **20** was isolated as an off white powder. ^{1}H NMR showed a broad singlet at 13.13 ppm for the carboxylic acid peak. A doublet at 7.92 ppm was attributed to the 6-H proton, and a doublet of doublets at 7.18 ppm to the 5-H position. A doublet at 7.08 ppm was ascribed to the 3-H proton, a *J* value of 2.4 Hz, indicated *meta* coupling. Two upfield singlets at 2.29 ppm and 2.24 ppm were ascribed to the acetate CH_3 groups. ^{13}C NMR showed 11 resolved peaks, signals at 168.9 ppm,

168.6 ppm and 164.9 ppm were indicative of the three carbonyl groups. The upfield signals at 20.8 ppm and 20.7 ppm were ascribed to the CH_3 groups of both acetates. IR analysis showed medium absorptions at 2981 cm^{-1} and 2941 cm^{-1} attributable to CH_3 stretches. Absorptions at 2645 cm^{-1} and 2539 cm^{-1} were ascribed as aromatic C-H stretches. Three prominent signals at 1773 cm^{-1}, 1681 cm^{-1} and 1607 cm^{-1} were assigned to the carbonyl stretches. A high-resolution accurate mass of 237.0405 $[M-H]^-$ was observed.

Subsequently, the acetylated benzoic acid was refluxed in thionyl chloride and anhydrous DCM to generate the corresponding acyl chloride **21** (Scheme 5). The sulfur atom is electron-deficient due to the electronegativity of the chlorine atom. Nucleophilic attack of the chloride on **20 c** leads to the formation of an unstable tetrahedral intermediate **20 d** which then decomposes to generate the acyl chloride **21**. This reaction is not in equilibrium as HCl and SO_2 gas are generated as side products which are lost from the reaction mixture, and therefore is entropically favourable (Scheme 6).

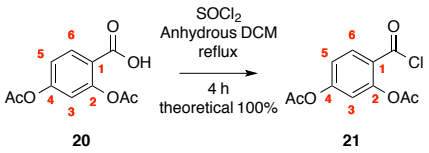

Scheme 5 Synthesis of 3-(acetyloxy)-4-(carbonochloridoyl) phenyl acetate.

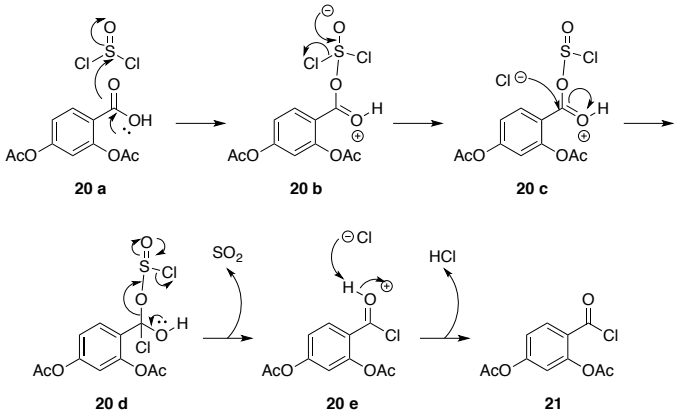

Scheme 6. Mechanism of acyl chloride formation.

The acyl chloride **21** was carried directly forward into the next reaction and added to a solution of Boc protected malonate **18** in anhydrous THF to form intermediate **22** (Scheme 7). The predicted mechanism is shown in Scheme 7. The acidic proton at the 2 position of the malonate **18 a** is removed by an organic base, such as triethylamine. Consequently, a negative charge can resonate through the carbonyl group. The magnesium cation likely co-ordinates the negative charge onto the oxygen atom in intermediate **18 b**. Addition of the acyl chloride **21** permits a nucleophilic 1,4-conjugate addition to occur. Subsequently, an acidic work up generates the desired compound **22**.

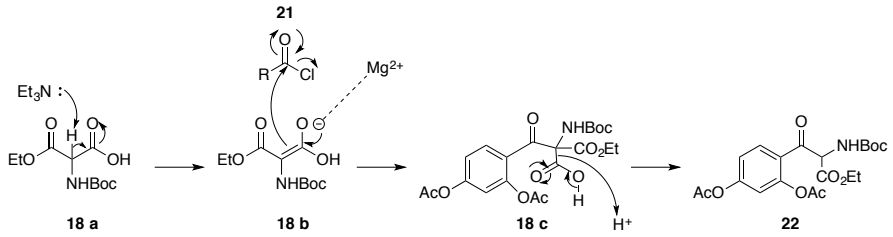

Scheme 7. Conjugate addition to acid chloride.

The intermediate **22** was not purified but used crude in the next reaction by adding it to a solution of NaOH in methanol. The strong base was predicted to remove an acetate group, forming a phenoxide anion intermediate **22 b** (Scheme 8). The lone pair of electrons is free to attack the carbonyl group of the nearby ester to form the lactone ring **22 c**. Protonation of the carbonyl group in the 4-position is likely to be driven by the resultant thermodynamically favourable α,β-conjugation within the coumarin ring **23** (Scheme 9).

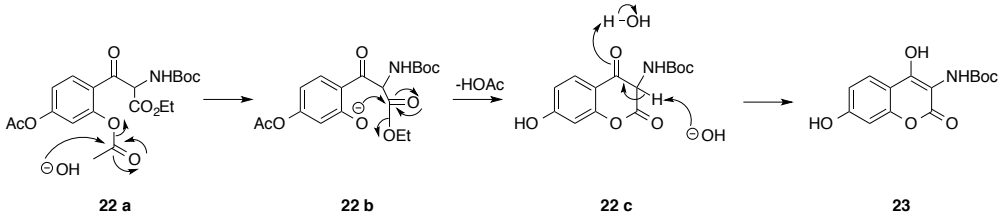

Scheme 8. Synthesis of *tert*-butyl N-(4,7-dihydroxy-2-oxo-2H-chromen-3-yl) carbamate.

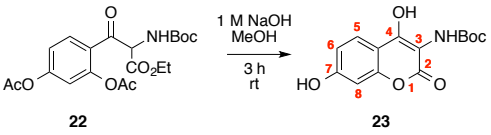

Scheme 9. Synthesis of *tert*-butyl N-(4,7-dohydroxy-2-oxo-2H-chromen-3-yl) carbamate.

Aminocoumarin **23** was reacted with ethereal HCl to remove the *tert*-butyl protecting group. This worked well to remove impurities that had been carried forward, as assessed by TLC. The desired compound **24** was isolated as an orange brown precipitate (Scheme 10). ^{1}H NMR of compound **24** showed a downfield doublet at 7.88 ppm (1 H) that correlated to the 5-H, followed by a doublet of doublets at 6.90 ppm ascribed to the 6-H (J_1 = 8.8 Hz, J_2 = 2.4 Hz, 1 H). The reciprocal *J* values confirmed the *ortho* coupling to the 5-H and *meta* coupling to the 8-H that appeared as a doublet at 6.77 ppm (J = 2.0 Hz). ^{13}C NMR showed 9 resolved peaks as expected. Signals at 126 ppm, 115 ppm and 104 ppm were all protonated as shown by HSQC and were therefore assigned as the C5, C6 and C8 signals respectively. IR analysis showed two broad absorptions at 3345 cm^{-1} and 2929 cm^{-1} assigned as the two OH groups. This was likely masking the N-H stretch. A strong

absorption at 1710 cm^{-1} was attributed to the carbonyl group of the lactone. An absorption at 1639 cm^{-1} was ascribed as N-H bending. Medium absorptions at 1564 cm^{-1} and 1526 cm^{-1} were attributed to C=C aromatic stretches. A high-resolution accurate mass of 192.0303 $[M-H]^-$ was observed.

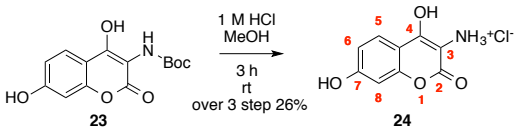

Scheme 10. Synthesis of 4,7-dihydroxy-2-oxo-2H-chromen-3-aminium chloride.

2.4 Sodium hypochlorite as a chlorinating agent

A key feature of the AC found in SD8 and chlorobiocin is the presence of a chlorine substituent in the 8-position. A key objective of the work in this chapter was to develop a viable route to correctly place this substituent within the AC framework. The ease of handling and cheap cost of NaOCl made it an attractive reagent, compared to alternatives such as Cl_2 and N-chlorosuccinimide (NCS). Sodium hypochlorite reacts with water (Equation 3) to generate hypochloric acid (HOCl) and sodium hydroxide (NaOH).

$$NaOCl + H_2O \longrightarrow HOCl + NaOH$$

$$HOCl \rightleftharpoons H^+ + {}^-OCl$$

Equation 3. Formation of hypochloric acid and dissociation into hypochlorite anion.

Hypochloric acid has a pKa of ~7.5, therefore under basic conditions equilibrium will be driven towards the dissociation of the proton from the hypochlorite anion ($^-$OCl).[207,208] Consequently, only a small proportion of hypochloric acid will be free for reaction at any given time. Crucially, this allows for control of the chlorination process. In contrast, no such control exists when using Cl_2 as a chlorinating agent and this is a disadvantage of this alternative methodology. Control was necessary to prevent chlorination occurring at multiple sites on the coumarin ring. Hypochloric acid will react with a nucleophile allowing electrophilic substitution of an aromatic ring to take place. The AC found in SD8 contains two hydroxyl moieties. It was theorised the *ortho* and *para*-directing effect, of the OH groups, could be used to introduce the halogen in the desired location.

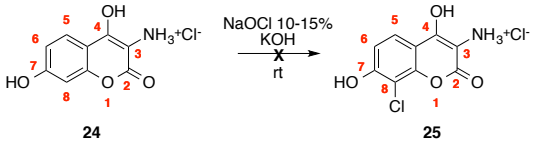

Scheme 11. Attempted synthesis of 8-chloro-4,7-dihydroxy-2-oxo-2H-chromen-3-aminium chloride.

Several attempts were made to chlorinate coumarin **24** directly in the 8-position using sodium hypochlorite and basic conditions to obtain compound **25** (Scheme 11).[209] The reaction produced multiple spots by TLC with no major product spot. Attempts to purify the mixture by flash column chromatography failed to yield the desired product. It was theorised the strong oxidising conditions were responsible for the multiple reaction products observed by TLC. Similarly, attempts were made to chlorinate the starting reagent of 2,4-dihydroxybenzoic acid (Scheme 12). The two hydroxyl groups are *ortho* and *para*-directing making the 3-and 5-position the most favourable sites for substitution to take place. However, no chlorinated product was isolated. ^{1}H NMR and TLC showed a complex mixture of products.

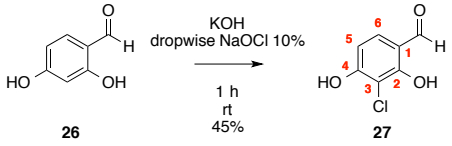

Scheme 12. Synthesis of 3-chloro-2,4-dihydroxybenzaldehyde.

Successful chlorination of 2,4-dihydroxybenzaldehyde **26** had previously been reported.[210] We therefore turned our attention to chlorinating an aldehyde derivative and oxidising the compound to the corresponding carboxylic acid. This could then, in turn, be used in the previously validated dihydroxycoumarin procedure (Scheme 12).[209] Compound **27** was isolated as colourless crystals after being purified by flash column chromatography and recrystallised from DCM. This two-step purification process was necessary as the reaction generated a black “tar” like side product. ^{1}H NMR showed a singlet at 9.69 ppm assigned to the aldehyde proton. A doublet at 7.49 ppm was ascribed as the 6-H as it was more de-shielded relative to the 5-H. A doublet at 6.59 ppm was attributed to the 5-H. ^{13}C NMR showed 7 individual carbon signals. A signal at 195.8 ppm was characteristic of a carbonyl, due to its downfield chemical shift. Two further de-shielded signals at 162.6 ppm and 160.8 ppm were assigned as the C2 and C4 atoms respectively. IR analysis showed absorptions at 3294 cm^{-1} and 3084 cm^{-1} assigned to the OH stretches. An absorption at 2878 cm^{-1} was assigned as an aromatic C-H stretch. A prominent signal at 1618 cm^{-1} was assigned as the carbonyl stretch. A high-resolution accurate mass of 173.0000 [M+H] was found.

This side product formation was attributed to the effect of the strong oxidiser, HOCl, which is generated *in situ*. A short reaction time was found to give moderate yields and facilitate efficient purification. This is due to limiting the amount of oxidative side reactions that can take place. Moreover, the reaction needed to be carefully monitored as over-chlorination was observed which resulted in the di-chlorinated benzaldehyde **28** (Scheme 13).

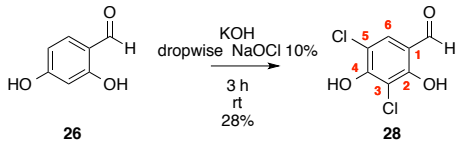

Scheme 13. Synthesis of 3,5-dichloro-2,4-dihydroxybenzaldehyde.

Compound **28** was isolated as an off white solid. ^{1}H NMR showed a broad downfield signal at 11.48 ppm ascribed to the OH signal. Unusually, the other OH signal was not visible in the spectrum. A singlet at 9.88 ppm was attributed to the aldehyde proton. A singlet at 7.77 ppm was assigned to the 6-H proton, as confirmed by HSQC. ^{13}C NMR showed 7 individually resolved peaks. A signal at 192.6 ppm was the most downfield in the spectra, and assigned as the carbonyl group of the aldehyde. Two signals at 156.9 ppm and 156.1 ppm were attributed to the C4 and C2 atoms respectively. The signal at 130.8 ppm was assigned as the 6-H, as confirmed by HSQC. IR analysis showed no peak for the OH groups, however an absorption at 2941 cm^{-1} was assigned as an aromatic C-H stretch. A strong absorption at 1623 cm^{-1} was ascribed to the carbonyl of the aldehyde. A peak at 741 cm^{-1} and 714 cm^{-1} was attributed to the C-Cl stretches. A high-resolution accurate mass of 204.9461 $[M-H]^-$ was observed, alongside the isotopic m/z pattern of $[M+2]^+$ and $[M+4]^+$. The splitting pattern was in a ratio of 9:6:1 indicating the presence of two chlorine atoms. The predicted mechanism for chlorination by hypochloric acid is shown below (Scheme 14).

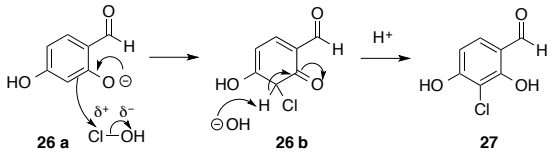

Scheme 14. Proposed mechanism of chlorination by hypochloric acid.

Chlorination with NaOCl is an example of electrophilic aromatic substitution with the hypochloric acid being the active species. The reaction is under basic conditions in order to deprotonate the –hydroxyl-salicylaldehyde, so that it is soluble in the aqueous reaction mixture. Additionally, deprotonation of the phenol groups increases electron density at the aromatic centre. The chlorine atom of the hypochloric acid will have a positive molecular dipole due to the lower electronegativity

compared to the adjacent oxygen atom **26 a**. This allows electrophilic substitution to take place *ortho* or *para* to the phenol. The observation of the formation of **27** and **28** support this hypothesis.

One approach to oxidise an aldehyde into a carboxylic acid is to use peroxide. The use of Cu(II) in the presence of peroxide is predicted to occur via a free radical mechanism. It has been reported that Cu(II) and H_2O_2 can react together via a one electron redox process that converts H_2O_2 into the highly reactive free radical species ($O_2^{\bullet-}$).[211] A method for the oxidation of chlorinated aldehydes to carboxylic acids had previously been identified. This procedure used a catalytic amount of $Cu(II)Br_2$ in the presence of *tert*-butyl hydroperoxide solution.[212] A hypothesised mechanism is shown in Scheme 15.

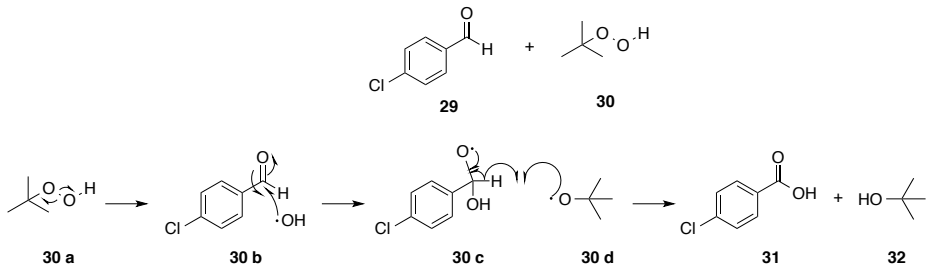

Scheme 15. Predicted aldehyde oxidation via a hydroxyl radical mechanism.

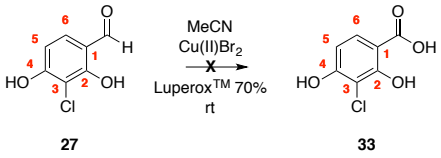

Scheme 16. Attempted oxidation to 3-chloro-2,4-dihydroxybenzoic acid.

The direct conversion of aldehyde **27** into the corresponding carboxylic acid **33** using *tert*-butyl hydroperoxide (Luperox™ 70%) did not succeed (Scheme 16), with multiple products visible by TLC analysis. It has been described that under oxidative conditions, free phenolic OH groups can form *ortho* and *para*-linked dimeric and polymeric products.[213] Thus, a protecting group was introduced to prevent the nucleophilic character interfering with the oxidation step. Iodomethane was utilised to mask the alcohols as alkyl ethers (Scheme 17).

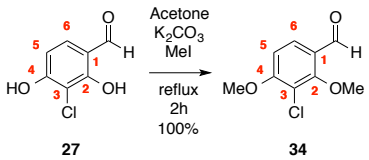

Scheme 17. Synthesis of 3-chloro-2,4-dimethoxybenzaldehyde.

Compound **34** was isolated as a colourless solid. ^{1}H NMR showed a downfield singlet at 10.17 ppm for the aldehyde. Two doublets at 7.72 ppm and 6.79 ppm were ascribed to the 6-H and 5-H signals respectively. They showed a reciprocal coupling constant of 8.8 Hz. Two singlets at 3.94 ppm and 3.93 ppm (3 H) indicated the successful methylation of the OH groups. ^{13}C NMR showed 9 resolved signals. The successful methylation was apparent with two signals at 63.0 ppm and 56.7 ppm for the alkyl ethers of the C2 and C4 atoms. IR showed the presence of ethers with two absorptions at 2950 cm^{-1} and 2869 cm^{-1} as well as a carbonyl stretch at 1673 cm^{-1}. A correct high-resolution accurate mass of 201.0313 $[M+H]^{+}$ was found.

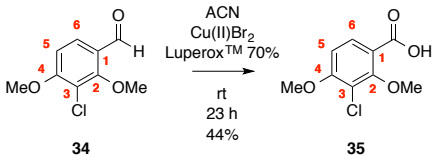

Scheme 18. Synthesis of 3-chloro-2,4-dimethoxybenzoic acid.

Compound **35** was isolated as a colourless solid (Scheme 18). ^{1}H NMR showed a carboxylic acid peak as a singlet at 12.82 ppm, and a corresponding loss in the aldehyde peak. The carboxylic acid was much more deshielded than the parent aldehyde **34**. This signified the oxidation had been successful. The 6 and 5-H protons appear as two doublets at 7.75 ppm and 6.99 ppm. The two methyl groups appear as two singlet's at 3.90 ppm and 3.80 ppm. ^{13}C NMR showed 9 carbons were still present in the molecule. IR confirmed the insertion of the oxygen atom with a broad absorption at 2564 cm^{-1} for the OH stretch. A carbonyl stretch appeared at 1664 cm^{-1} whilst the two C-O stretches occur at 1284 cm^{-1} and 1221 cm^{-1} respectively. An accurate high-resolution mass of 217.0261 $[M+H]^{+}$ was observed.

Boron tribromide (BBr_3), a strong Lewis acid, was used to remove the methoxy protecting groups (Scheme 19). The trivalent boron has an empty *p* orbital that accepts a lone pair of electrons from the oxygen atom of the aryl ether **37 a**. This forms an oxonium cation intermediate that can then undergo nucleophilic S_N2 attack by a bromine anion. An aqueous organic work up generates boronic acid and hydrobromic acid as water-soluble side products.

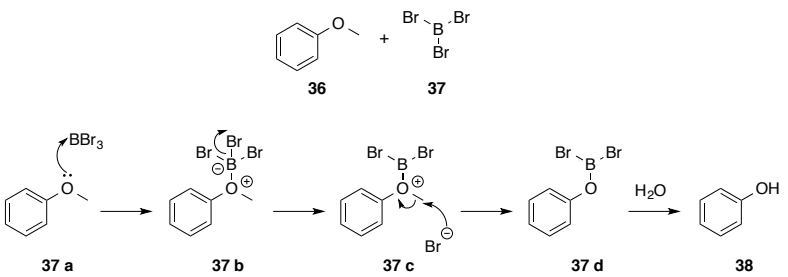

Scheme 19. BBr_3 mediated O-demethylation.

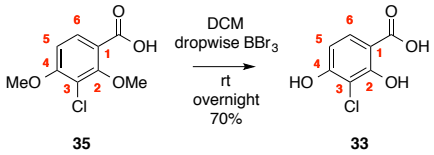

Scheme 20. Synthesis of 3-chloro-2,4-dihydroxybenzoic acid.

The desired product **33** was obtained as a colourless solid in good yield (Scheme 20), this key intermediate had not been previously described in the literature. ^{1}H NMR showed a doublet at 7.64 ppm (1 H), assigned as the 6-H because of its more deshielded location, relative to the remaining doublet at 6.47 ppm (1 H). Consequently, the remaining doublet at 6.47 ppm was assigned as the 5-H. A coupling constant of 8.0 Hz, confirmed the reciprocal *ortho* coupling to each other. The remaining phenolic OH groups and carboxylic acid protons were not visible due to the presence of H_2O in the deuterated MeOH solvent. ^{13}C NMR showed 7 individually resolved carbon signals. The loss of the methyl groups was highlighted by the lack of signals at 61 ppm and 56 ppm, confirming the deprotection was successful. IR analysis showed a broad signal at 3445 cm^{-1} assigned to the O-H stretch. An additional absorption at 3056 cm^{-1} was ascribed to the carboxylic acid O-H stretch. A strong absorption at 1643 cm^{-1} was representative of the carbonyl stretch. A high-resolution accurate mass of 188.9947 $[M+H]^{+}$ was observed.

Subsequently, the chlorinated dihydroxylated benzoic acid **33** was subjected to the same reaction conditions as 2,4-dihydroxybenzoic acid to acetylate both alcohols. This intermediate was predicted to be critical to the reaction pathway. Knowing that the product was unstable and sensitive to light, the same procedural modifications were used; namely, protecting the reaction from light and adding the acetic anhydride dropwise (Scheme 21).

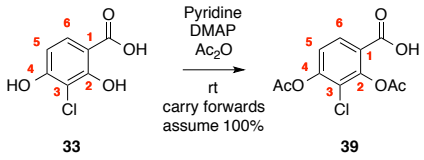

Scheme 21. Synthesis of 2,4-bis(acetyloxy)-3-chlorobenzoic acid.

^{1}H NMR showed a doublet at 7.96 ppm ascribed to the 6-H. A more upfield doublet at 7.40 ppm was assigned as the 5-H. Two singlets at 2.37 ppm and 2.33 ppm were indicative of the acetate groups. The product was labile with rapid decomposition into either mono-acetylated compound or the starting material. Therefore, no ^{13}C NMR was obtainable for compound **39**. A high-resolution accurate mass of 271.0016 $[M-H]^{-}$ was observed. No IR or MP analysis was performed due to the instability of the product. Several attempts were made to react the di-acetylated compound onwards. However, the harsh conditions of refluxing in $SOCl_2$ were considered inappropriate for the

unstable intermediate. To surmount this barrier a switch was made to oxalyl chloride at room temperature with a catalytic amount of DMF (Scheme 22). Multiple spots were seen at each step with no one major product formation observable by TLC. No Boc protected chlorinated AC was isolated.

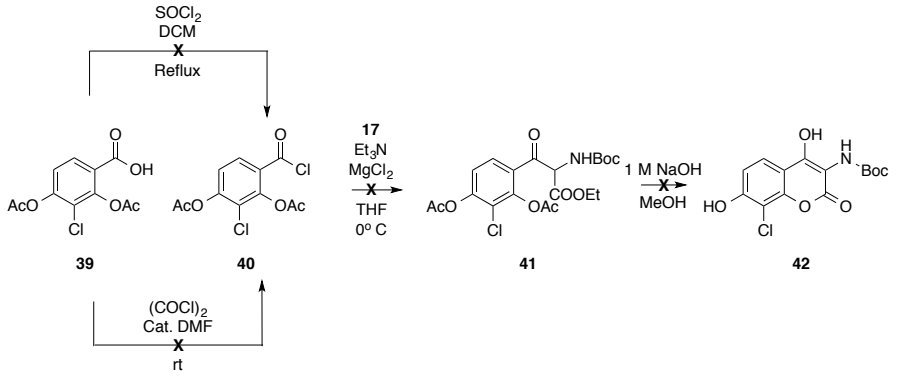

Scheme 22. Synthesis of *tert*-butyl N-(8-chloro-4,7-dihydroxy-2-oxo-2H-chromen-3-yl) carbamate.

The intrinsic instability of **39** likely arises due to the deactivating effect of the chlorine atom. Due to the nature of the procedure, whereby the product is assumed to have formed and carried forward into each subsequent reaction it is difficult to ascertain which step is problematic. However, it is highly likely the instability of di-acetylated **39** means the difficulty is with the acid chloride and conjugation to the malonate derivative. If a free OH group is present, then nucleophilic attack to the acid chloride in an intermolecular fashion can take place.

An alternative method for generating the desired chlorinated AC chromophore was explored using a 2,4-dihydroxyacetephenone derivative. Previously, this methodology had successfully been used to create the 3-methyl-4,7-dihydroxycoumarin present in novobiocin (scheme 23).[214] This protected one of phenols leaving one unprotected. Subsequently, the authors took advantage of the directing effect from the free OH group, to selectively nitrate in the 3-position. The procedure performed a simultaneous zinc reduction and acetate protection of the formed amine. It was theorised that the starting hydroxy-acetephenone could be chlorinated selectively in the 8-position after the benzyl protection step. Subsequently, the product could be reacted onwards to give the chlorinated coumarin scaffold. It was predicted the presence of a singular OH group would reduce the formation of di-chlorinated product.

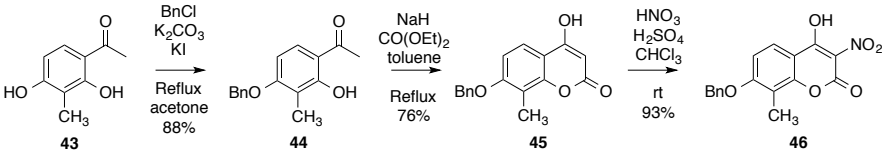

Scheme 23. Synthetic pathway described for novobiocin.[214]

To validate the pathway, 2-hydroxyacetephenone **47** was employed as a model reactant.[215] The reaction likely relies on a base preferentially deprotonating the acidic phenol. The phenolate anion is then able to act as a nucleophile towards the carbonyl group of diethyl carbonate **47 a**. Ethoxide can act as a good leaving group due to its ability to stabilise a negative charge. A basic species is then able to remove an α-H, generating an enolate at the ketone carbonyl **47 c**. Subsequently, this can attack the carbonyl group of the diethyl carbonate giving the dione **47 f**. The acidic proton in the 3-position can be removed with a base to generate the conjugated coumarin structure **48**. The predicted mechanism is shown below (Scheme 24).

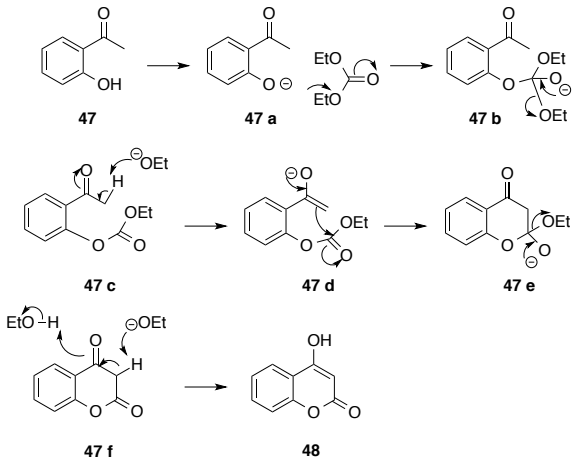

Scheme 24 Predicted mechanism for coumarin formation with diethyl carbonate.

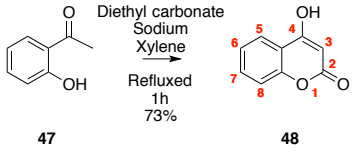

Scheme 25. Synthesis of 4-hydroxy-2H-chromen-2-one.

Compound **48** was obtained as a cream powder in good yield (Scheme 25). ^{1}H NMR showed a broad singlet at 12.62 ppm (1 H) assigned as the 4-hydroxyl proton. This was confirmed by HSQC. A doublet of doublets at 7.82 ppm was assigned to the 5-H. The remaining aromatic protons appeared as multiplets between 7.66-7.62 ppm (1 H) and 7.37-7.32 ppm (2 H). The most

deshielded multiplet was assigned as the 6-H, due to the electron distribution within the coumarin system. The carbon had through bond coupling to the adjacent 5-H but had no signal for the 8-H, confirming the assignment. The 7 and 8-H signals were in similar environments and thus overlapped each other. This give a multiplet that was more upfield. A singlet at 5.65 ppm was indicative of the 3-H. ^{13}C NMR showed 9 individually resolved carbon signals. The presence of the 3-H allowed the determination of the C2 through observed through-bond coupling in the HMBC experiment. The signal at 161.9 ppm was the only quaternary carbon not visible to protonated carbons other than the 3-H. This, therefore, must have been the carbonyl signal. The more downfield signal at 165.7 ppm was assigned as the C4. IR analysis showed absorptions at 2941 cm^{-1} and 2555 cm^{-1} ascribed to the aromatic protons. This was overlapped by a broad signal at 2896 cm^{-1} assigned as the OH group. An absorption at 1608 cm^{-1} was attributed to the carbonyl group of the lactone. Three medium intensity absorptions at 1556 cm^{-1}, 1562 cm^{-1} and 1504 cm^{-1} were ascribable to the C=C aromatic stretches. A signal at 1273 cm^{-1} was assigned to the O-H bend. A high-resolution accurate mass of 161.0244 $[M-H]^-$ was observed.

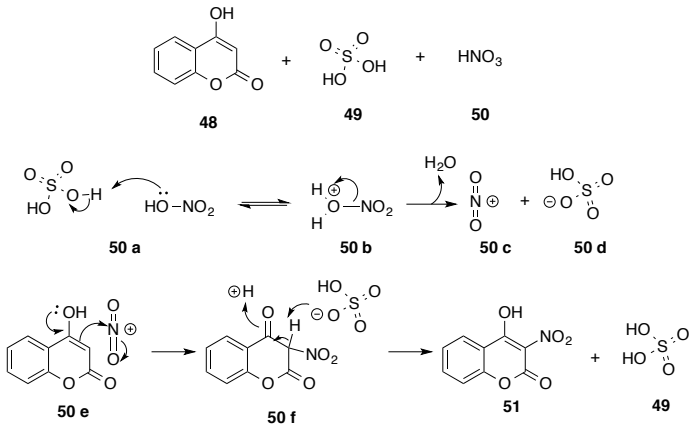

Scheme 26. Nitration of 4-hydroxycoumarin.

A crucial step for introducing the amino group functionality was to nitrate selectively in the 3-position (Scheme 26). This was found to be difficult to achieve without nitrating the aromatic ring. Despite the presence of an OH group to direct electron-density to the 3-position, and help facilitate aromatic substitution at this carbon, low yields were obtained. A short reaction time was needed, otherwise no product was generated, based on experimental observation. Furthermore, it was found that reproducibility was problematic. The optimum conditions developed were stirring for 1 hour in an ice bath. The nitrating mixture was also cooled to zero degrees and premixed prior to the addition to the coumarin. This is an example of electrophilic substitution. The premixing of the sulphuric acid with the nitric acid generates the electrophilic nitronium cation **50 c**. Subsequently, electrophilic attack from the electrons at the C3-C4 position, adds the NO_2 group to the C3 carbon of coumarin **50 e**. The removal of the proton restores conjugation to the system.

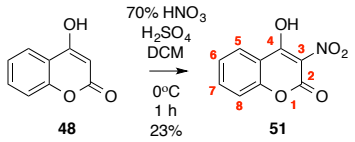

Scheme 27. Synthesis of 4-hydroxy-3-nitro-2H-chromen-2-one.

Compound **51** was obtained as a yellow powder (Scheme 27). ^{1}H NMR showed a doublet of doublets at 7.89 ppm ascribed to the 5-H. A deshielded multiplet between 7.55-7.50 ppm was attributed to the 6-H. A multiplet at 7.24-7.17 ppm was assigned as the 7 and 8-H protons. The loss of a singlet confirmed that nitration had taken place in the 3-position. ^{13}C NMR showed 9 individually resolved peaks. The most downfield signal at 166.8 ppm was assigned as the C4. Two proton signals had through bond coupling to this signal, therefore it was not the C2 of the carbonyl group. A signal at 157.3 ppm and 120.7 ppm had no though bond coupling to any other signals. These were ascribed to the C2 and C3 respectively. Signals at 132.6 ppm, 125.6 ppm, 123.3 ppm, and 116.2 ppm were assigned as the aromatic protonated carbons, as confirmed by HSQC. In the preceding parent compound the C3 carbon appeared at 91 ppm, as determined by HSQC. In contrast, the product had no such signal. Further confirming the correct product has been obtained. IR analysis showed absorptions at 2941 cm^{-1} and 2555 cm^{-1} ascribed to the aromatic proton stretches. This was overlapped by a broad OH signal. The strong absorption at 1605 cm^{-1} was attributed to the carbonyl group of the lactone. The strong absorption at 1422 cm^{-1} was ascribed to the N-O asymmetric stretch, whereas a strong absorption at 1144 cm^{-1} was assigned to the N-O symmetric stretch. The lower than usual wavenumbers for the asymmetric and symmetric stretch was likely a result of enhanced deshielding due to the extended conjugation of the coumarin.

Having synthesised the model 4-hydroxycoumarin, efforts where focused on taking advantage of this route as a means of generating the chlorinated AC scaffold. The first step was to selectively protect one phenol. This was achieved by refluxing 2,4-dihydroxyacetaphenone **52** in acetone, in the presence of a mild base, with benzyl bromide (Scheme 28). This is an example of an S_N2 nucleophilic substitution reaction. The observed selectivity for the 4-hydroxyl group over the 2-hydroxyl group is likely due to steric hindrance from the adjacent ketone. Additionally, it is likely that the carbonyl group of the ketone is hydrogen bonded to the *ortho* OH group, consequently preventing it from reacting.

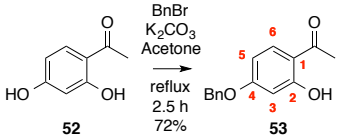

Scheme 28. Synthesis of 1-[4-(benzyloxy)-2-hydroxyphenyl] ethan-1-one.

Compound **53** was obtained as colourless crystals (Scheme 28). ^{1}H NMR showed a downfield singlet at 12.63 ppm that was characteristic of a phenolic OH group. A downfield doublet at 7.84 ppm (1 H) was ascribed to the 6-H. A large multiplet occurred between 7.46-7.32 ppm (5 H), this was indicative of the benzyl aromatic group. The similar environment experienced by each proton resulted in overlapping signals. A doublet of doublets at 6.60 ppm (1 H) was attributed to the 5-H. This was experiencing *ortho* coupling from the 6-H and *meta* coupling from the 3-H. This was illustrated in the coupling constants of 8.0 Hz and 2.4 Hz. A more upfield doublet at 6.56 ppm was assigned as the 3-H. A singlet at 5.19 ppm (2 H) was ascribed to the CH_2 group of the benzyl moiety. A prominent upfield singlet at 2.55 ppm (3 H) was indicative of the CH_3 group. ^{13}C NMR showed 13 individually resolved carbon signals. The benzyl group had a plane of symmetry running through it, therefore only 4 signals were observed instead of 6 due to chemical equivalence. These signals were recognisable by their double height at 128.5 ppm and 127.8 ppm. The most downfield signal at 203.1 ppm was characteristic of the carbon of the ketone moiety. IR analysis showed absorptions at 3026 cm^{-1}, 3002 cm^{-1} and 2937 cm^{-1} ascribed to the aromatic C-H stretches. A prominent absorption at 1617 cm^{-1} was assigned to the carbonyl of the ketone. A strong absorption 1363 cm^{-1} was attributed to a C-O stretch. A high-resolution accurate mass of 243.1018 $[M+H]^{+}$ was found.

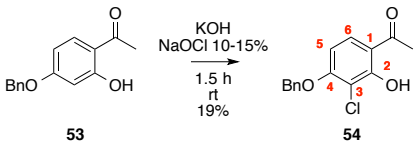

Scheme 29. Synthesis of 1-[4-(benzyloxy)-3-chloro-2-hydroxyphenyl] ethan-1-one.

Sodium hypochlorite was deployed using the previously validated conditions, to selectively chlorinate the 3 position (Scheme 29). Compound **54** was obtained as fuchsia crystals in moderate yield. ^{1}H NMR showed a downfield singlet at 13.14 ppm ascribed to the 2-hydroxyl proton. A doublet at 7.94 ppm was assigned to the 6-H. A multiplet between 7.49-7.33 ppm (5 H) was attributed to the benzyl group. A doublet at 6.91 ppm was assigned to the 5-H. Based on the presence of two doublets the chlorine was confidently assigned as having been added to the 3-H position. If substitution had occurred onto the *para* 5-H position, the 6 and 3-H would appear as singlets. A singlet at 5.36 ppm was attributed to the CH_2 group and the singlet at 2.62 ppm the CH_3

group.[13]C NMR showed 12 individually resolved carbon signals. 7 protonated carbons were noted in the HSQC and DEPT135 experiment. One quaternary signal was not visible in the NMR spectra. This was rationalised as an artefact of the experimental NMR conditions. IR analysis showed absorptions at 3048 cm^{-1}, 3029 cm^{-1}, 2940 cm^{-1} and 2881 cm^{-1} assigned to the aromatic C-H stretches. A strong absorption at 1627 cm^{-1} was ascribed to the carbonyl stretch. An absorption at 1277 cm^{-1} was attributed to the C-O stretch. A strong absorption at 1055 cm^{-1} was assigned to the C-O stretch. A medium intensity absorption at 919 cm^{-1} was ascribed to the O-H bend. An absorption at 840 cm^{-1} was assigned as the C-Cl stretch. A high-resolution accurate mass of 277.0628 $[M+H]^+$ was observed.

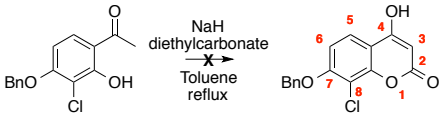

54 55

Scheme 30. Synthesis of 7-(benzyloxy)-8-chloro-4-hydroxy-2H-chromen-2-one.

When intermediate **54** was refluxed in the presence of diethyl carbonate, no formation of product was observed by TLC (Scheme 30). Comparable to the previous synthetic route this lack of coumarin formation was rationalised as a consequence of the deactivating properties of the halogen. At the same time as these investigations, a body of work probing the same procedures to access the SD8 chromophore was published.[216] Similarly, when a chlorine atom was inserted into the 3 position of either a 2,4-dihdroxybenzoic acid or 2,4-dihydroxyacetaphenone derivative no ring closure was achieved. Interestingly, iodine was also explored as an alternative to chlorine due to its reduced electronegativity. However, attempts to iodinate the 3-position were not successful. The work presented here is concordant with the observations that the chlorine substituent reduces the nucleophilicity of the hydroxyl groups and therefore, precludes any ring closure event from taking place. Having explored the possibility of generating a dihydroxylated chlorinated coumarin, efforts were shifted to making streamlined mono-substituted analogues. The shorter reaction pathway meant a library of different coumarins could be made quickly and efficiently. Moreover screening a diverse library was hoped to provide SAR insight that could be used to design new inhibitors (Chapter 3). Additionally this would give a pool of starting AC from which novel hybrids could be made (Chapter 4). These findings demonstrate that a new approach is required inorder to access the elusive chlorinate AC moiety. One solution to accessing the chlorinated AC could be to degrade the natural product SD8 and isolate the desired AC, this could then be biologically evaluated to determine if it possesses any intrinsic inhibition for DNA gyrase. Whilst not answering the question of how to access the scaffold, it would potentially answer the question of its necessity for biological activity.

2.5 Polyketide synthesis

The polyketide portion of SD8 **56** is a highly complex angucyclic core, with 6 contiguous stereocenters (Figure 37). Therefore, in order to access the desired scaffold we sought to use a modified intermolecular Diels-Alder methodology as a proof of principle methodology. Previous unpublished work within the Searcey group had found the Diels-Alder problematic with no successful adducts isolated. The Diels-Alder procedure is a type of concerted pericyclic reaction to generate a heterocycle. The diene is an important component of the reaction, there is a requirement for the substrates to be able to adopt a s-cis conformation in order for orbital overlap to occur. Similarly, the dienophile commonly has an electron-withdrawing group present. This is conjugated to the alkene and has the effect of enhancing the reactivity by lowering the HOMO/LUMO energy barrier.

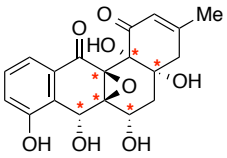

56

Figure 37. The polyketide portion of SD8 with stereocenters marked with a red asterisk.

The synthetic strategy is outlined in Scheme 31. The aim was to use commercially available 5-hydroxy-1,4-naphthoquinone as a chiral dienophile. The presence of the two ketone groups makes the double bond in the naphthoquinone particularly electron-deficient, and thus is a useful substrate for this type of reaction. The dienophile has a partially fixed s-cis arrangement ascribable to the double bonds reducing free rotation into the unreactive s-trans conformation. In order to test the validity of the Diels-Alder approach to accessing the benzo[*a*]anthracene nucleus the synthesis of ochromycinone was performed as outlined in Scheme 31.

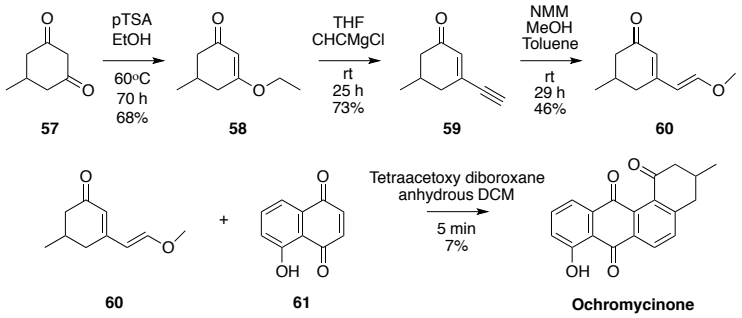

Scheme 31. Synthetic pathway to the polyketide scaffold.[217–220]

The first step was an acid catalysed conjugate addition using *para*-toluenesulfonic acid and EtOH.[217–219] The dione **57** can exist in either a keto or corresponding enol form. The C=O bond (720 KJ mol) is much stronger than the C=C (620 KJ mol). This difference in bond energies explains why the keto tautomer predominates. Compound **57** obeys the Erlenmeyer rule which states that alcohols which are directly bonded to a C=C double bond will preferentially exist in their keto form. The presence of an acid shifts this equilibrium from the keto to enol form (Scheme 32). Protonation of the oxygen of the carbonyl group of **57 a** creates an electrophilic centre. Subsequently, the alcohol can act as a nucleophile performing an addition to the α,β-unsaturated double bond. A rearrangement then takes place, consequently eliminating water, and the α,β-unsaturated system is regenerated to give **58**.

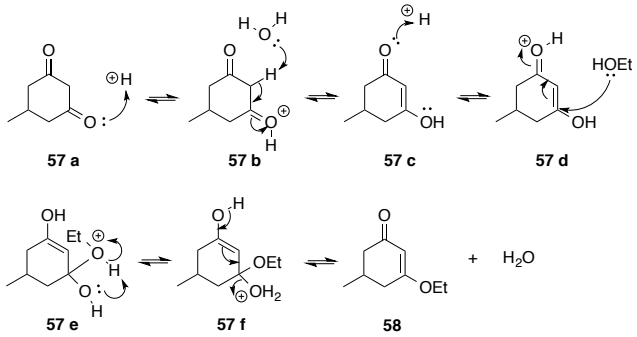

Scheme 32. Acid catalysed conjugate addition mechanism.

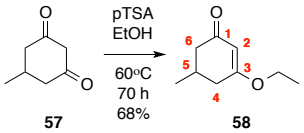

Scheme 33. Synthesis of (±) 3-ethoxy-5-methylcyclohex-2-ene-1-one.

Compound **58** was isolated as a yellow oil (Scheme 33). ^{1}H NMR showed a singlet at 5.30 ppm ascribed to the 2-H. The deshielded signal was due to the conjugation of the double bond to the adjacent ketone. A multiplet between 3.90-3.83 ppm was attributed to the CH_2 group of the ethoxy moiety. The unusual highly complex splitting was postulated to be a consequence of free rotation and interaction with the 2-H and 4-H_2 protons (Figure 38). HSQC illustrated the correlation of the carbon signal to a proton, thus the CH_2 and CH_3 carbons of the ethoxy group could be determined. The multiplet between 3.90-3.83 ppm possessed through bond coupling to a carbon signal at 14.2 ppm, assigned as the adjacent CH_3 group and 177.4 ppm for the C3 position. In contrast to the CH_2 signal, the CH_3 showed an expected triplet at 1.33 ppm and reciprocal through-bond coupling to the carbon of the CH_2 signal.

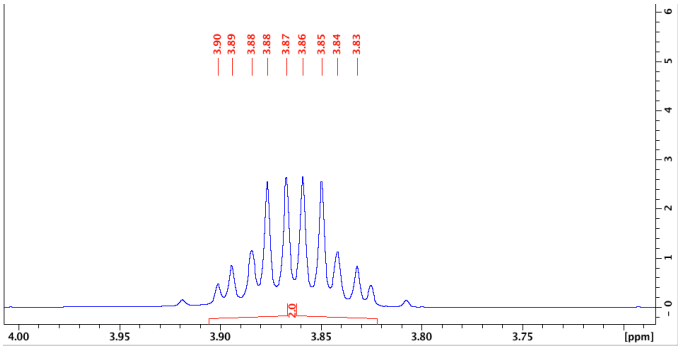

Figure 38. Splitting pattern for the ethoxy CH_2 moiety.

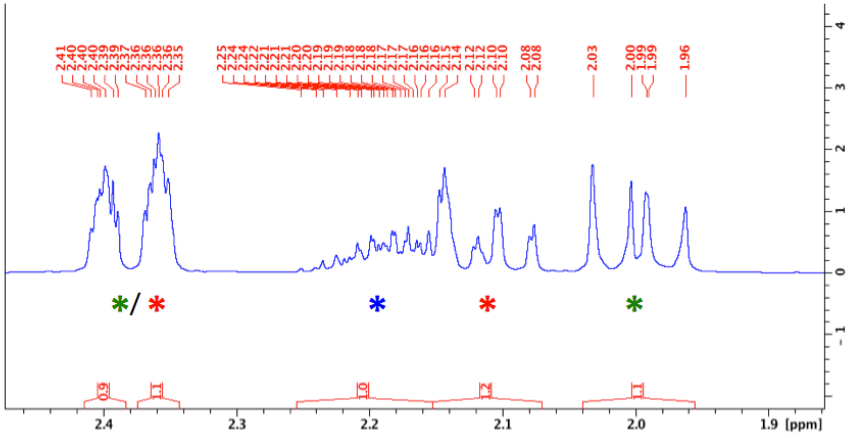

Figure 39. Cyclic protons marked with an asterisk. Green = 6-HH_2, Red = 4-HH_2, Blue = 5-H.

The CH_2 groups of the alkyl ring also displayed complex splitting due to their diasterotopic nature (Figure 39). Two multiplets between 2.41-2.39 ppm and 2.37-2.35 ppm were ascribable as either the 4-HH_2 or the 6-HH_2 protons. Due to the overlapping carbons signals, these protons could not be differentiated by HMBC or HSQC. A multiplet between 2.25-2.16 ppm was determined by HSQC as the 5-H. The 5-H signal overlapped a multiplet between 2.15-2.08 ppm for the remaining 4-HH_2 signal. HMBC analysis showed the multiplet had through bond coupling to a quaternary carbon at 177.6 ppm assigned as the C3. Therefore, this proton was confidently assigned as the 4-HH_2. Lastly, the multiplet between 2.03-1.96 ppm was assigned as the remaining 6-HH_2. A confirmatory through bond coupling to a quaternary carbon at 199.9 ppm, assigned as the C1 ketone was observed. A doublet at 1.04 ppm (3 H) was characteristic of the 5-CH_3. ^{13}C NMR showed 9 individually resolved signals. IR analysis showed absorptions at 2973 cm^{-1} and 2872 cm^{-1} attributed to the CH_3 and CH_2 stretches. A strong absorption at 1650 cm^{-1} was indicative of a carbonyl stretch. An absorption at 1597 cm^{-1} was seen for the C=C bond stretch. A high-resolution accurate mass of 155.1063 $[M+H]^+$ was observed.

Subsequently, ethynyl magnesium chloride was utilised in a 1,4 conjugate addition reaction (Scheme 34).[219] A lone pair of electrons on the ethoxy group of **58** co-ordinates to the Lewis acidic magnesium atom of a Grignard reagent. Consequently, nucleophilic attack preferentially takes place at the C3 rather than the C1 position. The ethoxide anion is a good leaving group and is formed as a by-product due to the reformation of the conjugated system.

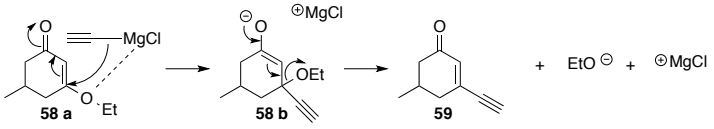

Scheme 34. Mechanism of a 1,4-conjugate addition using a Grignard reagent.

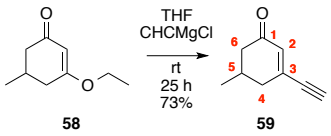

Scheme 35. Synthesis of (±) 3-ethynyl-5-methylcyclohex-2-en-1-one.

Compound **59** was isolated as a yellow oil (Scheme 35). ^{1}H NMR showed a singlet at 6.25 ppm for the 2-H. A prominent singlet at 3.52 ppm (1 H) was attributed to the alkyne proton. Two multiplets between 2.52-2.50 ppm and 2.48-2.46 ppm were ascribed to either the 4-HH_2 or the 6-HH_2 protons. A multiplet between 2.28-2.20 ppm was attributed to the 5-H. A coalesced multiplet from 2.19-2.05 ppm was for the remaining 4-HH_2 or the 6-HH_2 protons. A doublet at 1.07 ppm was for the 5-H_3. ^{13}C NMR showed 9 well resolved signals. IR analysis showed an absorption at 3242 cm^{-1} assigned as the alkyne C-H stretch. Absorptions at 2956 cm^{-1} and 2876 cm^{-1} were attributed to CH_3 and CH_2 stretches. The alkyne carbon-carbon stretch appeared as a weak signal at 2092 cm^{-1}. A strong absorption at 1658 cm^{-1} was for the carbonyl of the ketone. An absorption at 1592 cm^{-1} was ascribed as the C=C stretch. A high-resolution accurate mass of 135.0803 $[M+H]^+$ was found.

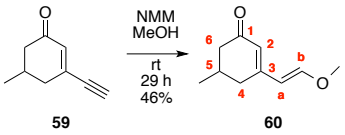

Scheme 36. Synthesis of (±) 3-[(E)-2-methoxyethenyl]-5-methylcyclohex-2-en-1-one.

A conjugate addition with methanol to the terminus of the alkyne generated compound **60** as a yellow oil (Scheme 36).[219] This compound was found to be very unstable and therefore only short NMR experiments could be performed on the compound. The product was made fresh and used straight away in the next reaction step. ^{1}H NMR showed a doublet at 7.03 ppm for the a/b-H of the

alkene double bond. A singlet at 5.83 ppm was assignable as the 2-H. A further doublet at 5.64 ppm was ascribable to the other a/b-H. A prominent singlet at 3.70 ppm was for the OCH_3. A multiplet between 2.54-2.43 ppm was for the 4/6-HH_2. A multiplet between 2.27-2.15 ppm was characteristic of the 5-H, based on the preceding parent structure this was confidently assigned. A multiplet between 2.11-2.01 ppm was for the 4/6-HH_2. A doublet at 1.09 ppm was for the 5-CH_3. ^{13}C NMR showed 10 individual signals. IR showed absorptions at 2952 cm^{-1} and 2835 cm^{-1} for the CH_3 and CH_2 stretches. A strong signal at 1613 cm was attributed to the carbonyl stretch. An absorption at 1227 cm^{-1} was assigned as a C-O stretch. Due to its instability no accurate mass was obtained for this product. The compound was used directly into the next modified Diels-Alder reaction.[219,220]

To access ochromycinone the diene **60** was added dropwise to a light protected mixture of commercially available 5-hydroxy-1,4-naphthoqinone **61** and tetraacetoxy diboroxane in anhydrous DCM. Attempts to react the dienophile and diene without the tetraacetoxy diboroxane did not generate any product. Upon addition, an instantaneous colour change was noted. The reaction was quenched with ice water, extracted with DCM and the solvent removed under reduced pressure. The crude product was purified by flash column chromatography immediately. Two products were visible by TLC analysis. Previous reports using this procedure documented that ochromycinone formed via an unstable intermediate that underwent spontaneous aerial oxidation and aromatisation.[219] Interestingly two products were isolated, ochromycinone and a pericyclic adduct **62** not previously described. The new pericyclic adduct is a rearrangement product whereby the double bond migrates to become conjugated with the ketone. This conjugation would give greater stability and therefore can be rationalised as thermodynamically favourable to form.

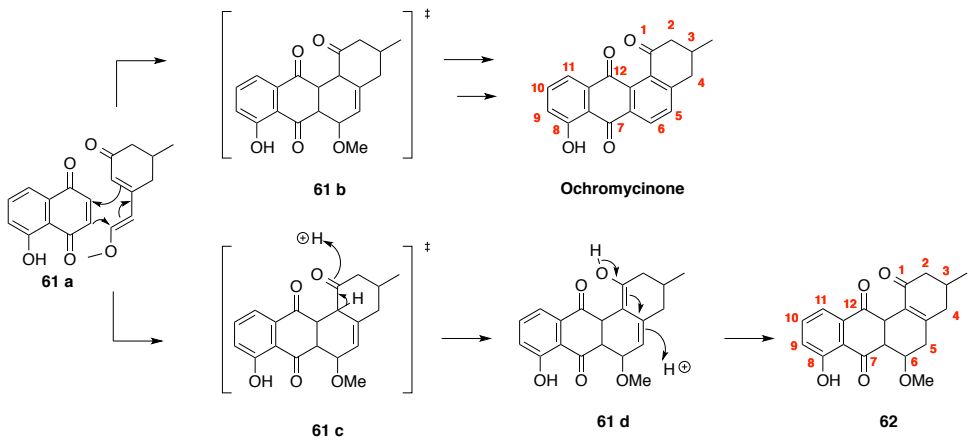

Scheme 37. Diels-Alder reaction pathways.

Ochromycinone was isolated as an orange powder in a 7% yield (Scheme 37). ^1H NMR showed a singlet at 12.28 ppm for the OH group. A downfield doublet at 8.28 ppm (1 H) was attributable to

the 6-H of the B ring. A multiplet (2 H) between 7.69-7.64 was ascribable to the 9/10-H protons, from the D ring. These are the most deshielded protons of the D ring due to the neighbouring phenolic OH group. A doublet at 7.55 ppm was attributed to the 5-H, this showed reciprocal coupling to the 6-H (8.0 Hz). The interaction was confirmed by COSY analysis. A doublet of doublets at 7.27 ppm was assignable as the 11-H. A multiplet between 3.06-2.98 ppm (2 H) was attributable to the 4-H_2 alkyl protons. A doublet of doublets at 2.50 ppm and 2.61 ppm was ascribed to the 2-H_2. A multiplet between 2.52-2.42 ppm was characteristic of the 3-H. An upfield doublet at 1.21 ppm was indicative of the CH_3 group. ^{13}C NMR showed 19 resolved carbon signals. The most downfield signal at 199.3 ppm was attributed to the C1 carbonyl position. Two additional downfield signals at 187.7 ppm and 183.2 ppm were also indicative of carbonyl groups, however the C7/C12 positions could not be discriminated and therefore were not assignable. A deshielded signal at 162.2 ppm was attributed to the C8. A signal at 21.6 ppm was characteristic of the CH_3 group. IR analysis showed absorptions between 2955 cm^{-1} and 2872 cm^{-1} assigned as the aromatic C-H stretches. These overlapped an OH peak. Absorptions at 1698 cm^{-1}, 1666 cm^{-1} and 1631cm^{-1} were attributed to C=O stretches. A high-resolution accurate mass of 307.0965 $[M+H]^+$ was observed.

Alongside ochromycinone another compound was characterised. Compound **62** was isolated as an orange-brown solid in an 8% yield. ^1H NMR showed a singlet at 12.20 ppm for the phenolic OH group. A triplet at 7.61 ppm was assigned as the 10-H of the aromatic ring. A de-shielded doublet of doublets at 7.47 ppm was ascribed to the 9-H aromatic. A doublet of doublets at 7.19 ppm was attributed to the 11-H aromatic. A doublet at 4.34 ppm was attributed to the 12a-H. A multiplet between 4.00-3.98 ppm was ascribed to the 6-H. A doublet of doublets at 3.07 ppm was attributed to the 7a-H. A prominent singlet at 3.00 ppm (3 H) was indicative of the OCH_3 group. A multiplet between 2.61-2.42 ppm was attributable to the overlapping signals of the 4-H_2 and 5-H_2. A multiplet between 2.33-2.22 ppm was for the 2-H_2 and the 3-H. A doublet at 1.13 ppm (3 H) was assigned as the CH_3 group. ^{13}C NMR showed 20 individually resolved signals. Deshielded signals at 205.0 ppm, 197.8 ppm and 193.4 ppm were assigned as quaternary carbons of the three carbonyl groups C7, C10 and C18. IR analysis showed absorptions at 2953 cm^{-1} and 2871 cm^{-1} ascribed to the CH_3 and CH_2 groups. This was overlapped by a broad OH signal. Strong absorptions at 1698 cm^{-1}, 1667 cm^{-1} and 1633 cm^{-1} were characteristic of carbonyl stretches. A high-resolution accurate mass of 341.1381 $[M+H]^+$ was observed.

Having isolated the novel pericyclic adduct **62** it was decided to shift the focus away from the synthesis of the AC and PK moieties. This work successfully established a starting point for the PK synthesis, so efforts were concentred towards the generation of coumarin fragments for biological screening. It was predicted that the pursuit of coumarin fragments would generate lead compounds that could be identified rapidly for eventual asymmetric analogue development. In contrast, the

onward synthesis of the PK moiety represented a significant challenge in its own right and would not lend itself to the rapid synthesis of small molecule inhibitors.

2.6 Conclusions

This work demonstrates that selective chlorination of phenolic aldehydes and ketones with NaOCl is feasible. Concordant with the findings of Gaskell 2013, this simultaneous investigation showed whilst chlorination of hydroxylated aldehydes and ketones is possible, this inherently deactivates the adjacent OH groups.[169] Consequently, the cyclisation of a lactone ring is problematic. This can be explained as a function of reduced nucleophilic character, due to induction of electron density away from the OH group and into the aromatic ring system by the chlorine atom.

Future work would focus on introducing the chlorine once the coumarin has been formed. One such approach could be to form the coumarin via the diethyl carbonate methodology and then selectively protect the 4-OH group as methyl ether. Selective debenzylation would generate the free 7-OH group analogue. Consequently, a directing effect to the 6 and 8-position would occur. Chlorination of this intermediate could be attempted with a subsequent reduction of the nitro group to give the SD8 chromophore.

This work highlights the utility of the Diels-Alder approach to creating a polyketide scaffold from which further stereoselective synthesis can take place. Future work will focus on optimising the reaction conditions to find the best possible yield for the isomerised pericyclic adduct. This can then be taken forward for enantioselective dihydroxylation. Furthermore, the phenolic OH can be taken advantage of as a co-ordinating atom for the selective reduction of the C ring ketone. The efforts towards the total synthesis of SD8 eloquently demonstrate that nature is a superlative natural product chemist. The exquisite structure and novel mechanism of action of SD8 will continue to inspire medicinal chemists in the coming years.

Chapter 3. Synthesis and biological evaluation of coumarin fragments

The AC chromophore is present in SD8, chlorobioicin, novobiocin and coumermycin A1. The crystal structure data, elucidated using SD8 and novobiocin, shows a well-defined pocket for AC binding. Moreover, the observation that inhibition is retained with the AC fragment MGD8N2A, warranted additional investigation into screening simplified aminocoumarin fragments against DNA gyrase. It was hypothesised that this would illustrate further the contribution that the aminocoumarin moiety makes, to DNA gyrase inhibition. Furthermore, this would facilitate the design of future novel inhibitory compounds. The effect of acetate, carbamate and free amine groups, at the 3-position, on DNA gyrase supercoiling activity was explored. This chapter introduces the Perkin, Pechmann and Knoevenagel reactions as classic methods for preparing simple coumarins. It culminates with the synthesis and biological evaluation of a library of 3-aminocoumarin fragments, synthesised via a modified Perkin reaction.

3.10 Perkin reaction

In 1868 William Henry Perkin first reported the condensation of an aromatic aldehyde with an anhydride in the presence of a mild base to give coumarin.[221,222] The publication was followed by the observation that the same reaction could form α,β-unsaturated carboxylic acids. It was originally suggested that the phenolic group of the 2-hydroxybenzaldehyde is acetylated by acetic anhydride and subsequent deprotonation occurs to generate an acetal anion. This anion can attack the carbonyl group of the formyl moiety in an intramolecular fashion, eliminating water and furnishing coumarin (Scheme 38). Evidence against the intramolecular reaction comes from the observation that when 2-formylphenyl acetate is heated in the presence of sodium acetate only trace amounts of coumarin are obtained.[223] Similar results are noted when varying bases, solvents and dehydrating agents. Conversely, when acetic anhydride is added to a mixture of 2-formylphenyl acetate and sodium acetate, coumarin readily forms. These results support investigations, using benzaldehyde, that show condensation occurs between an anhydride and a formyl group in the presence of an alkali salt. The base is predicted to catalyse the formation of cinnamic acid, an α,β-unsaturated carboxylic acid.[224,225] An alternative mechanism is for the enolate to be derived from the anhydride. The enolate attacks the formyl group, followed by a cyclisation and loss of water to form the lactone (Scheme 39).

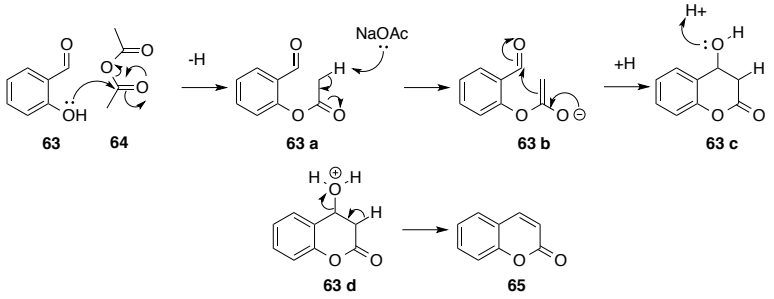

Scheme 38. Perkin condensation intramolecular hypothesis.

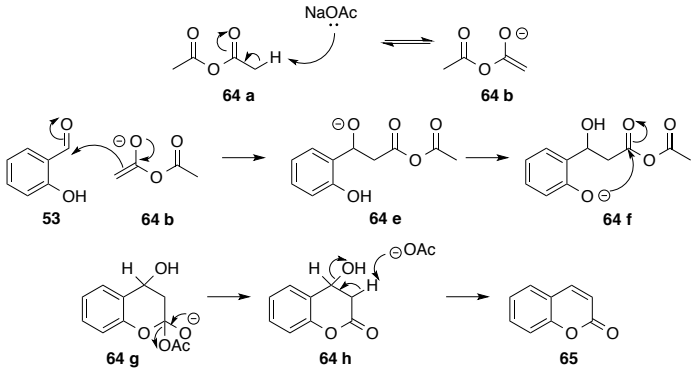

Scheme 39. Perkin condensation coumarin formation.

Isolation of geminal diacetate from a variety of aldehydes opposes the dogma of the generation of enolate from the anhydride species.[226] However, this was observed in the presence of catalytic amounts of BF_3 or anhydrous $FeCl_3$ in the reaction mixture.[227,228] The suggestion that the nucleophilic species could arise from a geminal-diacetate of the aromatic aldehyde is speculative (Scheme 40). It has been demonstrated that when benzal diacetate is refluxed in the presence of potassium acetate then cinnamic acid is obtained in high yield. This supports the hypothesis of the enolate arising from the geminal diacetate. Similarly, when benzaldehyde is refluxed with acetic anhydride, cinnamic acid is generated. Furthermore, if the benzal diacetate is refluxed in the presence of acetic anhydride, the results are unchanged, with cinnamic acid being the major product. Despite its discovery over a century ago and widespread use, the exact mechanism of the Perkin reaction remains unknown. It likely proceeds via the base catalysed formation of an enolate derivative with acetic anhydride participating in the reaction.

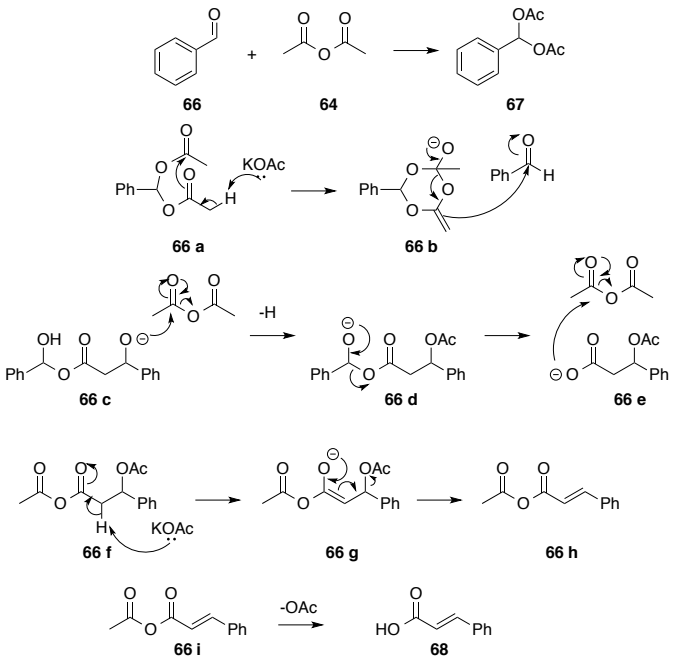

Scheme 40. Geminal-diacetate mediated enolate mechanism.[173]

3.11 Pechmann reaction

Coumarins can also be synthesised by condensing phenol with a β-keto ester in the presence of sulphuric acid (Pechmann, H.; & Duisberg, C., 1883, cited Clayden, J.; Greeves, N.; Warren, S., 2013). The efficiency of the reaction is dependent on the condensing agent, phenol and β-keto ester used. A variety of condensing agents promote the reaction, such as $ZnCl_2$, $POCl_3$ and $AlCl_3$.[229,230] Monohydric phenols give poor yields; conversely activated aromatic compounds, such as resorcinol are more favoured. The enhanced reactivity is attributed to increased electron density at the 4 and 6 position of the benzene ring.[201] Experimental evidence shows that electronegative groups in the alkyl portion of the ester improve reactivity; this is predicted to facilitate enolisation of the carbonyl group. In contrast, increasing steric bulk in the α-position of the β-keto ester generally impedes reactions. However, a degree of alkylation can be tolerated.[231] Debate still surrounds the mechanism which is theorised to involve trans-esterification, water elimination and cyclisation steps (Scheme 41). It is unknown if the ester is in its keto or enol tautomer. Intriguingly, density functional theory (DFT) calculations predict a high-energy barrier for the enolic route over the oxo form which is contrary to experimental evidence.[232]

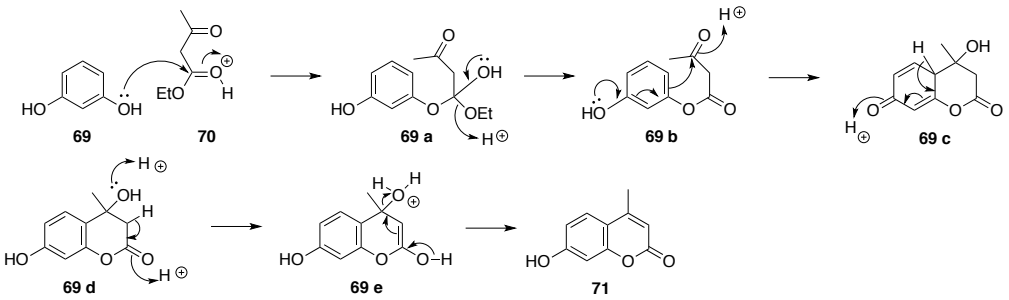

Scheme 41. A predicted Pechmann mechanism.

3.12 Knoevenagel reaction

The Knoevenagel reaction uses functionalised *o*-hydroxybenzaldehydes and dicarbonyl compounds, such as diethyl malonate or malonic acid, in the presence of a mild base, such as piperidine. This promotes the reaction between the aldehyde and enolate but prevents self condensation of the aldehyde.[233] The nucleophilic base deprotonates the acidic α-H from the 1,3-dicarbonyl compound, to create a resonance stabilised enolate anion. Nucleophilic attack on the carbonyl group of the aldehyde by the base forms an imine intermediate, that in turn undergoes nucleophilic attack from the α carbon of the keto-enol tautomer. Lastly, trans-esterification with the OH group of the *o*-hydroxybenzaldehyde generates the lactone with alcohol as the side product (Scheme 42).

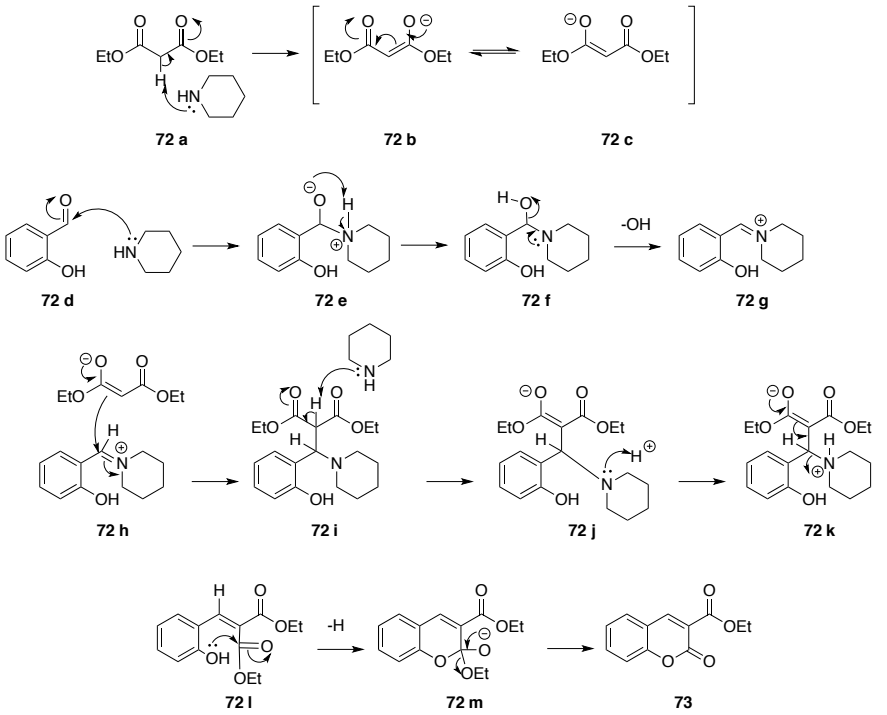

Scheme 42. Knoevenagel condensation of salicylaldehyde and diethyl malonate.

Importantly, this is an alternative method for placing a functional handle in the 3-position of the coumarin. Examples include: ester, carboxylic acid, nitrile and phenyl derivatives.[234–237] The reaction also lends itself to solid phase synthesis with the enolate derivative attached to the support resin.[238]

3.13 Formylation of phenols

A formyl reaction can be used in order to access the desired starting materials for the generation of coumarin analogues. A Reimer-Tiemann reaction is one such example that can introduce an aldehyde group *ortho* or *para* to a phenolic hydroxyl moiety. Normally, chloroform is used with an aqueous base such as sodium hydroxide. The strong base removes a proton from chloroform forming a carbon anion. Chlorine can act as a good leaving group to generate a stable dichlorocarbene **74 c**, this is an electron deficient species having only 6 electrons, and thus is short of a full octet. The electrophilic carbene reacts with a phenolate in a substitution reaction. Subsequently, an intramolecular proton transfer takes place, reforming the aromatic ring. Next, a chlorine atom leaves intermediate **74 g**. A hydroxide anion attacks the sp^2-hybridised carbon bonded to a single chlorine, introducing an alcohol group. Successively, an additional chlorine atom leaves. Further nucleophilic attack of the OH group abstracts a proton resulting in formyl functional group. Lastly, an acidic work up reprotonates the phenol moiety to give the desired product **63** (Scheme 43).

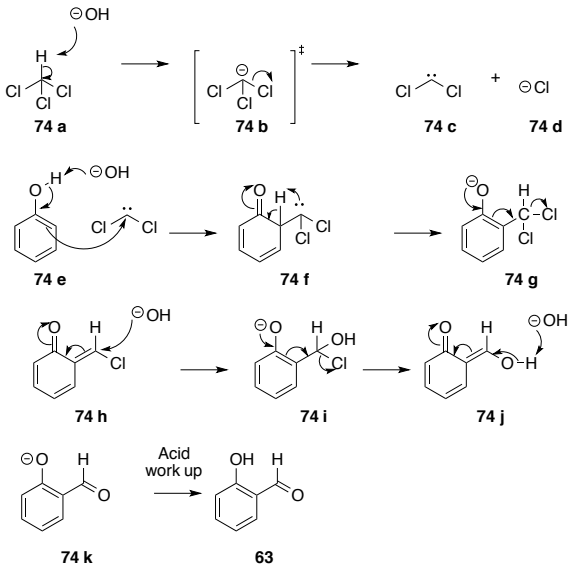

Scheme 43. Mechanism of the Reimer-Tiemann reaction.

Due to the immiscibility of chloroform and aqueous base, heat and vigorous stirring is required to instigate the formylation reaction. However, the highly exothermic nature of the reaction makes thermal runaway a safety concern.[239] Alternatively, THF can be used with $MgCl_2$ as a coordinating

ion and triethylamine as an organic base in the presence of paraformaldehyde to give two regioisomers.[240] This reaction preferentially produces the less sterically hindered product, and is safer than using chloroform. The theorised mechanism involves triethylamine deprotonating the phenol allowing it to form the aryloxymagnesium chloride salt. This species reacts with formaldehyde, which is formed from the parent paraformaldehyde at elevated temperatures. Interestingly, without magnesium chloride, no formyl products are obtained. A cyclohexadieneone scaffold is generated which in turn gives an alcohol intermediate. A redox reaction can subsequently take place to furnish the desired benzaldehyde with methanol as a side product (Scheme 44).[241]

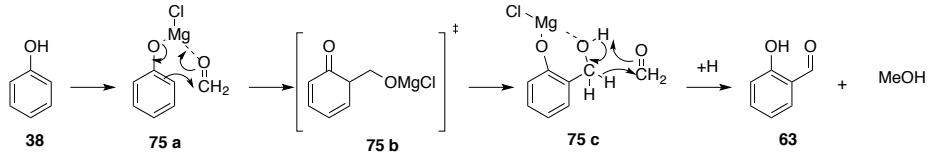

Scheme 44. Formylation using magnesium, Et_3N and monomeric formaldehyde.

3.14 Modified Perkin reaction

Limited routes exist for the synthesis of 3-aminocoumarins. These molecules are interesting because both the aminocoumarin antibiotics and SD8 both contain this moiety. Three strategies were proposed to access this scaffold: 1) to nitrate a coumarin in the three position and reduce to an amine or use a starting reagent with a nitro group already in place.[242–245] 2) Introduce a nitrile group and reduce to an amine.[246,247] 3) Use a starting reagent with a protected amine and cyclise to form coumarin.[248] For simplicity, and ease of synthesis, the latter method was chosen. A previously described method uses different salicylaldehyde derivatives with N-acetylglycine to give the amine protected coumarin scaffold using a modified Perkin reaction.[248] One predicted mechanism involves a glycine anhydride intermediate **76 c** that reacts with the phenol of the salicylaldehyde **76**. The acetyl group can leave as acetic acid, crucially forming the beginning of the lactone ring. A key step for ring closure would be the removal of an acidic proton in the α-position by the weak base sodium acetate. This forms a double bond that can cyclise with the formyl group to close the ring and form the coumarin framework (Scheme 45). However, in agreement with the previously discussed mechanisms, the more likely pathway is via the enolate derived from the acetic anhydride attacking the formyl group **78 b** as shown in the scheme 46.

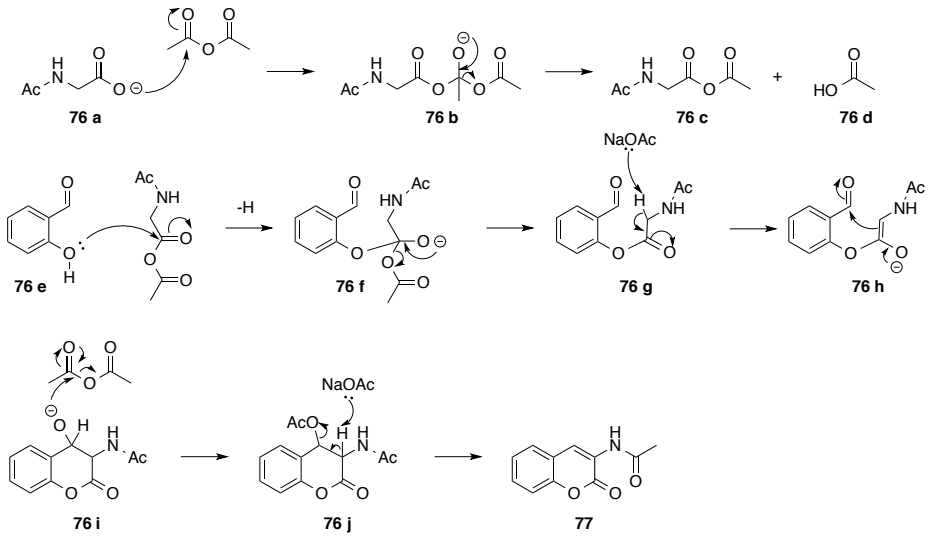

Scheme 45. A possible mechanism of the modified Perkin reaction.

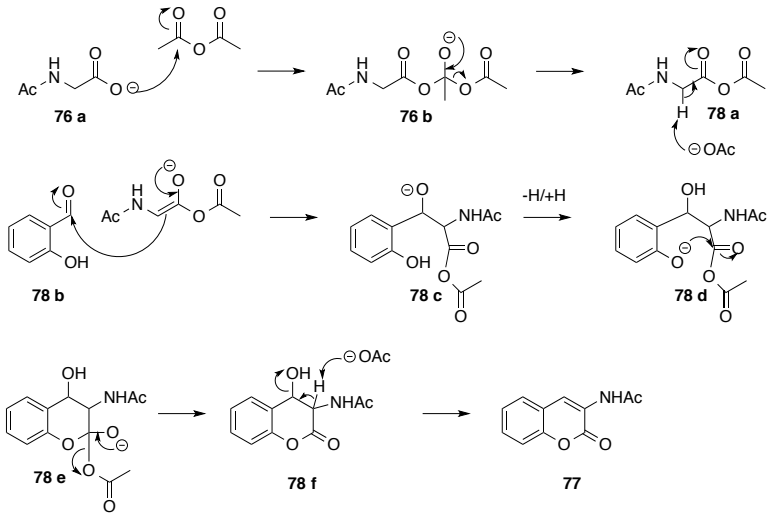

Scheme 46. Alternative mechanism of modified Perkin reaction.

3.15 Acetate protected coumarins

The formation of acetate protected 3-aminocoumarins created a series of parent structures, from which further derivatives could be synthesised. Briefly, salicylaldehyde was used as the starting reagent, and refluxed in acetic anhydride at 120 ºC, in the presence of anhydrous sodium acetate and the amino acid N-acetylglycine. The reaction was quenched with ice water to remove any remaining anhydride. After cooling to room temperature the reaction mixture would often form a sticky solid. This was difficult to work with and it was found trituration with large amounts of water allowed the dissolution of the sodium acetate salt. Addition of ethyl acetate (EtOAc) would cause

the product to precipitate in the organic layer. Filtration and washing with aliquots of solvent removed acetic acid from the product; no further purification was necessary.

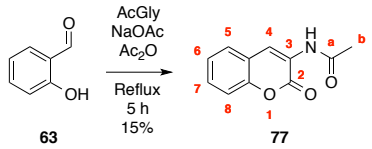

Scheme 47. Synthesis of N-(2-oxo-2H-chromen-3-yl) acetamide.

Compound **77** was isolated as a yellow powder (Scheme 47). ^{1}H NMR showed a singlet at 9.76 ppm attributable to the amide proton. A less deshielded singlet at 8.60 ppm occurred for the 4-H. The strong electronegative effect of the neighbouring carbonyl groups withdraws electron density away from both protons. Consequently, this exposes both environments to a stronger magnetic field, giving two downfield signals. The remaining aromatic protons appeared more shielded as a doublet of doublets at 7.69 ppm for the 5-H. A coupling constant of 8.0 Hz, and 1.6 Hz indicated *ortho* and *meta* coupling to the 6-H and 7-H protons. A triplet of doublets at 7.50 ppm was assigned as the 6-H. An apparent doublet appeared at 7.38 ppm (1 H), instead of the predicted doublet of doublets, ascribed to the 8-H. The poorly resolved signal was likely due to coincidental overlap. Lastly, a triplet of doublets at 7.33 ppm was attributed to the 7-H. IR analysis showed an absorption at 3328 cm^{-1} for the CON-H stretch. Two absorptions at 1707 cm^{-1} and 1680 cm^{-1} were assigned as the lactone and amide carbonyls respectively. The ^{13}C NMR showed 11 resolved peaks for the coumarin scaffold. A high-resolution accurate mass of 204.0655 $[M+H]^{+}$ was observed.

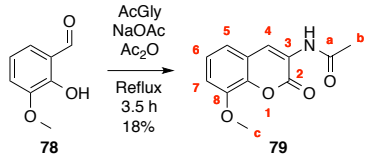

Scheme 48. Synthesis of N-(8-methoxy-2-oxo-2H-chromen-3-yl) acetamide.

Compound **79** was isolated as a yellow powder (Scheme 48). ^{1}H NMR showed a singlet at 8.65 ppm (1 H) for the 4-H. HSQC confirmed there was no correlation to a carbon. The amide proton appeared as a broad singlet at 8.08 ppm. A triplet at 7.23 ppm was ascribable to the 6-H. The coupling constant of 8.0 Hz was due to *ortho* coupling of the adjacent aromatic protons. A doublet of doublets at 7.09 ppm and 7.01 ppm were assigned as the 5-H and 7-H signals respectively. A sharp singlet at 3.97 ppm (3 H) was characteristic of the deshielded methoxy group. In contrast, a more upfield singlet at 2.23 ppm was assignable to the acetate of the amide.^{13}C NMR showed 12 individually resolved carbons. IR analysis showed an absorption at 3333 cm^{-1} for the

CON-H stretch. Absorptions at 3087 cm^{-1} and 2893 cm^{-1} represented Ar-H stretches. Two absorptions at 1707 cm^{-1} and 1676 cm^{-1} were assigned as the lactone and acetate carbonyl groups respectively. Absorptions at 1607 cm^{-1}, 1577 cm^{-1} and 1530 cm^{-1} were assigned as the aromatic C=C stretches. A high-resolution accurate mass of 234.0756 $[M+H]^+$ was found.

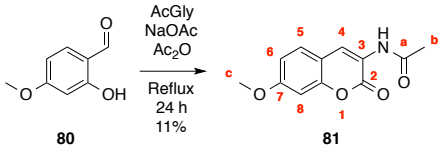

Scheme 49. Synthesis of N-(7-methoxy-2-oxo-2H-chromen-3-yl)acetamide.

Compound **81** was obtained as a yellow powder (Scheme 49). ^1H NMR showed a sharp singlet at 8.63 ppm attributed to the 4-H. A broadened singlet at 7.98 ppm was ascribed to the nitrogen proton. This assignment was confirmed by HSQC. A doublet at 7.40 ppm was assigned as the 5-H proton. A doublet of doublets occurred at 6.88 ppm for the 6-H. A doublet at 6.81 ppm was attributable to the 8-H. The methoxy group appeared as a prominent singlet at 3.86 ppm showing the slightly deshielded environment. ^{13}C NMR showed 12 individual carbons. IR analysis gave a strong absorption at 3347 cm^{-1} for the CON-H stretch. A weak absorption at 3060 cm^{-1} was assigned as the $COCH_3$ stretch. This overlapped absorptions at 2949 cm^{-1} and 2843 cm^{-1} for the sp^3C-H stretches. Two signals at 1702 cm^{-1} and 1676 cm^{-1} were the lactone and amide carbonyls respectively. Three absorptions of medium intensity at 1523 cm^{-1}, 1519 cm^{-1} and 1504 cm^{-1} were assigned as the aromatic C=C stretches. A high-resolution accurate mass of 234.0762 $[M+H]^+$ was observed.

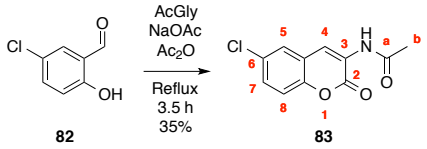

Scheme 50. Synthesis of N-(6-chloro-2-oxo-2H-chromen-3-yl) acetamide.

The novel compound **83** was isolated as a yellow powder in a reasonable yield (Scheme 50). Due to the poor solubility of compound **83** it was necessary to obtain carbon spectral data on a 800 MHz NMR machine. ^1H NMR showed a deshielded singlet at 9.82 ppm for the N-H, HSQC confirmed the assignment. The singlet at 8.60 ppm was ascribed to the 4-H proton. A doublet at 7.87 ppm was attributed to the 5-H (J = 2.4 Hz). A doublet of doublets at 7.52 ppm (J_1 = 8.8 Hz, J_2 = 2.8 Hz) was ascribed to the 7-H. A doublet at 7.42 ppm was assigned to the 8-H. A reciprocal J coupling of 8.8 Hz to the 7-H was observed. The CH_3 moiety gave an expected singlet at 2.17 ppm. HSQC allowed the assignment of the protonated carbons. The C4 was observed at 121.1 ppm, C5

at 127.1 ppm, C7 at 129.7 ppm and the C8 at 117.9 ppm. The C4 carbon was correlated to 6 signals, two of which had no through bond coupling to any other protonated carbon. Thus, allowing the assignment of the C2 at 158.4 ppm and C3 at 125.0 ppm. The remaining signals were quaternary, the C5 and C7 both had through bond coupling to a signal at 130.7 ppm. Consequently, this must be attributed to the C6 position. All protonated carbons had through bond coupling to signals at 148.3 ppm and 121.9 ppm. Based on the electronegativity of the adjacent oxygen atom the signal at 148.3 ppm was likely the C8a carbon, whereas the signal at 121.9 ppm was the C4a carbon. ^{13}C NMR showed 11 individual carbon signals. IR analysis showed an absorption at 3337 cm^{-1} for the CON-H stretch. Weak absorptions at 3093 cm^{-1}, 3056 cm^{-1} and 3030 cm^{-1} were assigned as Ar-H stretches. Two absorptions at 1711 cm^{-1} and 1676 cm^{-1} were assigned as the lactone and amide carbonyl respectively. Three medium signals at 1568 cm^{-1}, 1537 cm^{-1} and 1524 cm^{-1} were assigned as the aromatic C=C stretches. A prominent absorption at 828 cm^{-1} was assigned to the C-Cl stretch. A high-resolution accurate mass of 238.0265 [M+H]$^{+}$ was observed.

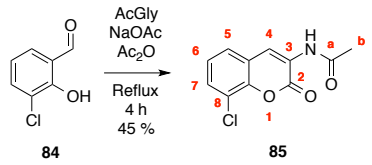

Scheme 51. Synthesis of N-(8-chloro-2-oxo-2H-chromen-3-yl) acetamide.

Compound **85** was isolated as a colourless powder (Scheme 51). ^{1}H NMR showed a broad singlet at 9.87 ppm for the N-H. HSQC confirmed the assignment. The previous 6-chlorocoumarin, **83,** paralleled the observed chemical shift. A singlet at 8.64 ppm was assigned to the 4-H. A deshielded doublet of doublets at 7.66 ppm was ascribed to the 5-H (J_1 = 7.6 Hz, J_2 = 1.2 Hz), consistent with previously assigned compounds. A doublet of doublets at 7.61 ppm was attributed to the 7-H (J_1 = 8.0 Hz, J_2 = 1.6 Hz). Due to the neighbouring electronegative chlorine, the 7-H signal was more deshielded than normal. A triplet at 7.33 ppm was ascribed to the 6-H. A singlet at 2.18 ppm was ascribed to the acetate group. ^{13}C NMR showed 11 carbon signals. IR analysis showed an absorption at 3337 cm^{-1} for the CON-H stretch. Two absorptions at 1711 cm^{-1} and 1676 cm^{-1} were assigned as the lactone and amide carbonyl, respectively. A strong signal at 767 cm^{-1} was assigned as the C-Cl stretch. A high-resolution accurate mass of 238.0265 [M+H]$^{+}$ was found.

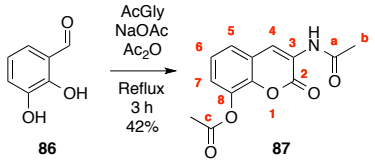

Scheme 52. Synthesis of 3-acetamide-2-oxo-2H-chromen-8-yl acetate.

The novel compound **87** was isolated as an off white powder (Scheme 52). ^{1}H NMR showed a singlet at 8.68 ppm, ascribed to the 4-H. Conversely, a broad singlet at 8.06 ppm was assigned as the N-H. HSQC shows no correlation to carbon, confirming the assignment. HMBC analysis allowed discrimination between the 5-H and 7-H signals of the coumarin that both appeared as doublet of doublets. The 5-H proton had through bond coupling to the C4 position, whereas the 7-H did not. Moreover, the 7-H had through bond coupling to the quaternary C8 position. This was not seen in the sister doublet. Therefore the first downfield doublet of doublets at 7.39 ppm was ascribed to the 5-H proton. A coupling constant of 8.0 Hz was noted for the 6-H. While a coupling of 1.6 Hz was observed for the 5-H. A triplet at 7.28 ppm was, as predicted, for the 6-H proton. A *J* value of 8.0 Hz was consistent with *ortho* coupling. The remaining doublet of doublets at 7.20 ppm was assigned as the 7-H. This designation was consistent with the observation of the 4-H and 5-H positions being areas of diminished electron density. ^{13}C NMR shows 13 resolved signals. Bond coupling to the quaternary C8 carbon made it possible to determine the acetate group signal. Thus, the signal at 2.42 ppm in the ^{13}C NMR was the ester and the signal at 2.25 ppm was the amide. IR analysis showed an absorption at 3284 cm^{-1} for the CON-H stretch. Absorptions at 1773 cm-^{1}, 1711 cm^{-1} and 1676 cm^{-1} were characteristic for the carbonyl stretch signals. The similarity of the values for the lactone and the ester carbonyl groups meant they cannot be assigned. The amide was assigned as the 1676 cm^{-1} absorption. A high-resolution accurate mass of 262.0712 $[M+H]^{+}$ was observed.

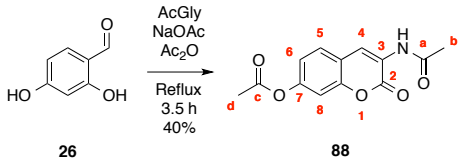

Scheme 53. Synthesis of 3-acetamido-7-acetoxy-2H-chromen-2-one.

Compound **88** was isolated as a pale yellow powder (Scheme 53). ^{1}H NMR showed the 4-H was a singlet downfield at 8.67 ppm. A broad singlet at 8.03 ppm was assigned as the N-H. HSQC showed no correlation to a carbon, confirming the assignment. A doublet at 7.51 ppm (*J* = 8.0 Hz), was assigned as the 5-H. The coupling constant was indicative of *ortho* coupling, to the 6-H position. A doublet at 7.13 ppm was ascribed to the 8-H. A *J* value of 2.4 Hz is consistent with the

expected *meta* coupling to the 6-H. A doublet of doublets at 7.07 ppm was attributed to the 6-H. HMBC analysis did not reveal any through bond coupling from the amide proton, nor did the 4-H proton have through bond coupling to the Ca carbon. Therefore, differentiation between acetate groups was not possible. ^{13}C NMR showed 13 resolved carbons. IR analysis showed a strong absorption at 3340 cm^{-1} for the CON-H stretch. A weak absorption at 3079 cm^{-1} was assigned as an Ar-H stretch. A broadened and strong absorption at 1532 cm^{-1} was attributed to the aromatic C=C stretches, it is likely this peak masks the other two signals. Three carbonyl absorptions at 1757 cm^{-1}, 1716 cm^{-1} and 1678 cm^{-1} confirmed the correct product been isolated. The signals at 1757 cm^{-1} and 1716 cm^{-1} were ascribed for the ester and lactone. However, due to their similar values they cant specifically be assigned. The amide was assigned as the absorption at 1678 cm^{-1}. A high-resolution accurate mass of 262.0715 $[M+H]^+$ was found.

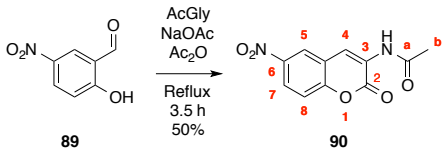

Scheme 54. Synthesis of N-(6-nitro-2-oxo-2H-chromen-3-yl) acetamide.

Compound **90** was isolated as an off white powder at the highest yield for this set of analogues (Scheme 54). This provides evidence in support of the mechanism proposed earlier whereby the enolate attacks the formyl group. The presence of the nitro-group would withdraw electron density away from the formyl carbonyl through induction making it more electropositive. Furthermore, the nitro-group would help stabilise a negative charge on the oxygen of the formyl carbonyl. ^{1}H NMR showed a deshielded singlet at 8.76 ppm for the 4-H. This is an electron poor region of the molecule due to the adjacent acetamide, and the electronegative effect of the nitro group. A doublet at 8.44 ppm (J = 2.6 Hz) was attributed the 5-H proton with *meta* coupling to the 7-H. A doublet of doublets at 8.30 ppm represents the 7-H (J_1 = 8.0 Hz, J_2 = 2.4 Hz). A broad singlet at 8.08 ppm was assigned as the N-H. HSQC showed no carbon was correlated with this signal, confirming the assignment. A singlet at 2.28 ppm was ascribed to the CH_3 group. ^{13}C NMR showed 11 resolved peaks for the coumarin framework. IR analysis showed an absorption at 3372 cm^{-1} for the CON-H stretch. Two weak absorptions at 3096 cm^{-1} and 3080 cm^{-1} were attributed to Ar-H stretches. Two carbonyl absorptions occurred at 1722 cm^{-1} and 1686 cm^{-1} for the lactone and amide, respectively. Additionally, absorptions at 1519 cm^{-1}, 1515 cm^{-1} and 1504 cm^{-1} were ascribed to the aromatic C=C stretches. A prominent absorption at 1332 cm^{-1} is attributed to the C-NO_2 stretch. A high-resolution accurate mass of 307.0920 $[M+H]^+$ was observed.

3.16 Boc protected coumarins

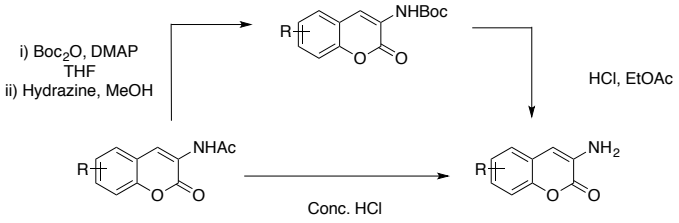

Scheme 55. Routes for acetate removal.[248,249]

Acetate removal can be problematic as the lone pair of electrons on the nitrogen atom is. Delocalised through the amide bond. Two approaches to acetate removal were pursued (Scheme 55). The first was via Boc group protection and Boc removal to give the corresponding free amine. The second was via direct cleavage with acid (discussed in section 3.17). A common technique to facilitate acetyl removal is to Boc protect the nitrogen atom first. This removes the ability of the lone pair of electrons to be fully available for conjugation, consequently allowing the acetate to be removed with a strong base. The *tert*-butyl carbamate is base stable but acid labile. In contrast, the acetate group can be removed under both basic and acidic conditions. To encourage nucleophilic attack from the remaining lone pair of electrons of the acylated nitrogen atom, N,N-dimethylaminopyridine (DMAP) can be used (Scheme 56). Pyridine itself has nucleophilicity because the lone pair of electrons are orthogonal to the *p*-orbitals of the ring system. Thus, they cannot become delocalised. The dimethyl amino group is a strong electron-donator via inductive effects. This enhances the nucleophilic character of the pyridine-based compound. Normally, it is sufficient to use catalytic amounts of DMAP for carbamate or acetyl protection. However, the nucleophilic character of the acylated nitrogen in coumarin is reduced by cross conjugation. Thus, five equivalents of DMAP are used to promote the protection step.

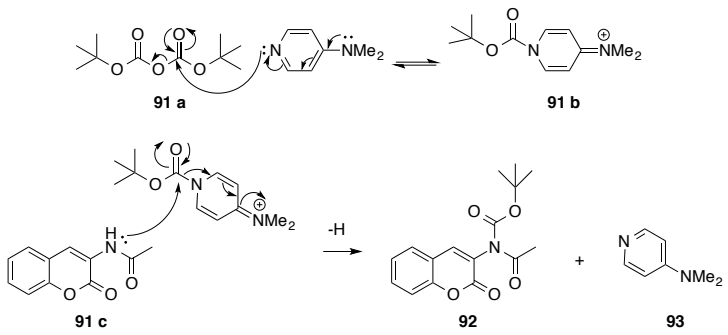

Scheme 56. Boc protection of acetylated coumarin.

The likely mechanism for acetate removal is via nucleophilic attack; the lone pair of electrons on the nitrogen of the hydrazine would attack the acetate carbonyl of the coumarin (Scheme 57). This

generates a negative charge on the electronegative oxygen atom of the acetate group. Subsequently, the bond between the Boc protected nitrogen atom and the hydrazine adduct breaks and the side product acetyl hydrazine leaves. A proton transfer onto the nitrogen atom of the liberated Boc protected coumarin would allow for the conservation of charge. This is likely a concerted reaction. The carbamate group is more stable due to electron induction into the bond from the alkyl group, as well as the lone pair of electrons being present on the adjacent oxygen and nitrogen atoms. Consequently, this reduces the overall dipole moment experienced by the carbon of the carbonyl group and makes nucleophilic attack from hydrazine less favourable. Furthermore, the sterically hindered environment contributes to the stability of the carbamate moiety. Generation of *tert*-butyl protected compounds allowed investigation of the effect introducing larger steric functionalities would have on the coumarin compounds. All of the Boc protected coumarins were more soluble in organic solvents than the parent acetylated compounds.

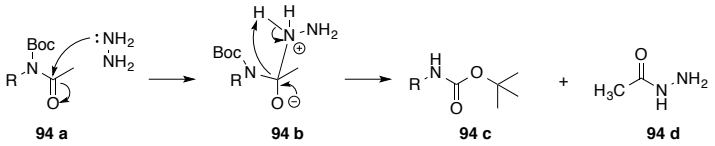

Scheme 57. Acetate removal with hydrazine.

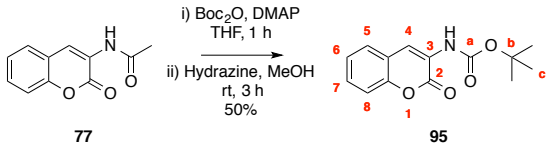

Scheme 58. Synthesis of *tert*-butyl N-(2-oxo-2H-chromen-3-yl)carbamate.

Compound **95** was isolated as a colourless powder (Scheme 58). ^{1}H NMR showed a broad singlet at 8.27 ppm for the 4-H. HSQC analysis confirmed this signal was coupled to a carbon and therefore ruled out amide proton assignment. A doublet of doublets at 7.45 ppm occurred for the 5-H. Coupling constants of 7.6 Hz and 1.6 Hz indicated *ortho* and *meta* coupling of the 5-H to the 6-H and 7-H protons respectively. A triplet of doublets at 7.41 ppm (2 H) represented the signal for the 6-H as well as the overlapping amide proton. In comparison to the acetylated parent material, the proton of the nitrogen moiety was far more shielded due to the neighbouring oxygen atom of the carbamate group. This was reflected in the lower chemical shift. A reciprocal coupling constant of 7.2 Hz and 1.6 Hz confirmed the interaction with the 5-H. Importantly, HSQC analysis revealed one signal was correlated with a carbon. An overlapping multiplet between 7.31-7.25 ppm (2 H) accounted for the remaining 7-H and 8-H aromatic protons. A singlet at 1.54 ppm was characteristic of the Boc CH_3 group. ^{13}C NMR showwed 12 individually resolved carbons. The methyl groups of the *tert*-butyl moiety are homotropic, being in the same environment. Thus, a

large singlet at 28.4 ppm was observed. The chemical shift of the carbonyl group of the carbamate at 152.6 ppm was significantly lower than the acetylated carbonyl of the parent compound (170.2 ppm). This highlighted the difference in dipole moment experienced by these quaternary carbon atoms experimentally. IR analysis showed two absorptions at 3415 cm^{-1} and 3321 cm^{-1} ascribed to the CON-H stretches. Absorptions at 2997 cm^{-1}, 2973 cm^{-1} and 2924 cm^{-1} were attributed to sp^3C-H stretches. Two almost overlapping absorptions were seen at 1702 cm^{-1} and 1698 cm^{-1} for the lactone and carbamate carbonyl groups respectively. A large coalesced absorption at 1519 cm^{-1} was ascribed as the aromatic C=C stretches. A high-resolution accurate mass of 262.1071 $[M+H]^+$ was found.

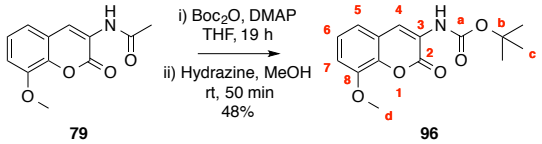

Scheme 59. Synthesis of *tert*-butyl N-(8-methoxy-2-oxo-2H-chromen-3-yl) carbamate.

Compound **96** was isolated as a yellow powder (Scheme 59). ^{1}H NMR showed a broad singlet at 8.22 ppm (1 H) attributed to the 4-H. HSQC showed this was correlated to a carbon, thus confirming the assignment. A broad singlet at 7.42 ppm was ascribed to the N-H. A triplet at 7.18 ppm (J = 8.0 Hz), represented the 6-H. A doublet of doublets at 7.02 ppm and 6.95 ppm was assigned to the 5-H and 7-H protons respectively (J_1 = 8.0 Hz and J_2 = 1.2 Hz). A singlet at 3.94 ppm was characteristic of the methoxy moiety.^{13}C NMR showed 13 resolved carbons, the methyl groups of the *tert*-butyl group are equivalent due to a uniform environment, showing as a single peak at 28.3 ppm. IR analysis showed an absorption at 3317 cm^{-1} for CON-H stretch. Two absorptions at 1728 cm^{-1} and 1698 cm^{-1} were ascribed to the carbonyl groups of the lactone and carbamate respectively. A high-resolution accurate mass of 292.1178 $[M+H]^+$ was observed.

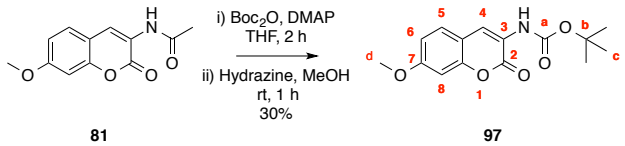

Scheme 60. Synthesis of *tert*-butyl N-(7-methoxy-2-oxo-2H-chromen-3-yl) carbamate.

Compound **97** was isolated as a colourless powder (Scheme 60). ^{1}H NMR showed a singlet at 8.23 ppm ascribed to the 4-H proton. HSQC showed this was not correlated with a carbon, confirming the assignment. A doublet at 7.35 ppm (J = 8.0 Hz), was attributed to the 5-H. A broad singlet at 7.28 ppm was assigned as the N-H. A doublet of doublets at 6.86 ppm and doublet at 6.81 ppm were ascribed to the 6-H and 8-H respectively. A singlet at 3.85 ppm (3 H) was attributed to the methoxy group. A prominent singlet at 1.52 ppm (9 H) unequivocally represented the Boc

group. ^{13}C NMR correctly showed 13 resolved peaks for the product. IR analysis showed absorptions at 3423 cm^{-1} for the CON-H stretch. Three absorptions at 2985 cm^{-1}, 2937 cm^{-1} and 2831 cm^{-1} were attributed to sp^3C-H stretches. Two absorptions were seen at 1713 cm^{-1} and 1615 cm^{-1} for the lactone and carbamate carbonyl groups. The two medium intensity absorptions at 1515 cm^{-1}, and 1505 cm^{-1} were assigned to the aromatic C=C stretches. The unaccounted for C=C signal was likely masked by the first peak at 1515 cm^{-1}. A strong absorption at 1130 cm^{-1} was ascribed as the methoxy ether bend. Unlike the acetylated parent compound, the $COCH_3$ stretch was not visible. This is not unexpected, as the bending signal is often weak. A high-resolution accurate mass of 282.1182 $[M+H]^+$ is observed.

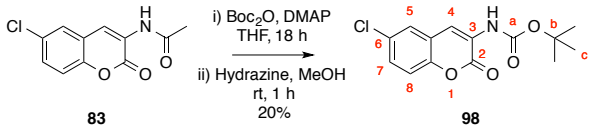

Scheme 61. Synthesis of *tert*-butyl N-(6-chloro-2-oxo-2H-chromen-3-yl) carbamate.

The novel compound **98** was obtained as colourless powder (Scheme 61). ^1H NMR showed a down field singlet at 8.13 ppm (1 H) assigned as the 4-H. A singlet at 7.39 ppm (1 H) was ascribed to the N-H. HSQC confirmed no correlation to a carbon atom. A doublet at 7.37 ppm was attributed to the 5-H. A doublet of doublets at 7.29 ppm was ascribed to the 7-H. The most shielded proton at position 8-H was assigned to a doublet at 7.19 ppm. Removal of the acetate was confirmed by the loss of a singlet (3 H) and the appearance of a larger singlet at 1.50 ppm (9 H) for the Boc moiety. ^{13}C NMR showed 12 resolved carbons. IR analysis showed an absorption at 3403 cm^{-1} for the CON-H stretch. A weak absorption at 3095 cm^{-1} was ascribed to the Ar-H stretch, whereas absorptions at 2986 cm^{-1} and 2929 cm^{-1} were indicative of sp^3C-H stretches. A broad, strong absorption was seen at 1706 cm^{-1} and this was assigned as one of the carbonyl stretches. It likely overlaid the other C=O that was expected for this compound, masking it. Similarly, a broad absorption at 1507 cm^{-1} was observed, this was likely overlaying the other two absorptions expected for the aromatic C=C moieties. A further strong absorption at 767 cm^{-1} was attributable to the C-Cl stretch. A high-resolution accurate mass of 296.0688 $[M+H]^+$ was observed. A $[M]^+$ and $[M+2]^+$ pattern in a 3:1 ratio was noted in the mass spectrum, and confirmed the presence of a chlorine substituent.

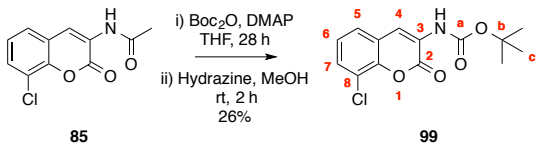

Scheme 62. Synthesis of *tert*-butyl N-(8-chloro-2-oxo-2H-chromen-3-yl) carbamate.

Compound **99** was obtained as a colourless powder (Scheme 62). ^{1}H NMR showed a broad singlet at 8.26 ppm ascribed to the 4-H. A doublet of doublets at 7.45 ppm was assigned as the 5-H (J_1 = 8.0Hz and the J_2 = 1.6 Hz). A broad singlet at 7.43 ppm was ascribed to the N-H and this was confirmed by HSQC. A doublet of doublets at 7.36 ppm was attributed to the 7-H. The signal displayed a reciprocal coupling interaction with the 6-H and 5-H protons. Lastly, a triplet at 7.21 ppm (J = 8.0 Hz) occurred for the 6-H. A singlet at 1.53 ppm was characteristic of the CH_3 groups. ^{13}C NMR showed 12 resolved carbons. IR analysis showed an absorption at 3326 cm^{-1} for the CON-H stretch. Absorptions at 2983 cm^{-1}, 2961 cm^{-1} and 2924 cm^{-1} were ascribable to the sp^3C-H stretches. Absorptions bands at 1597 cm^{-1}, 1567 cm^{-1} and 1526 cm^{-1} were assigned as aromatic C=C stretches. Two absorptions at 1731 cm^{-1} and 1702 cm^{-1} were assigned to the lactone and the carbamate respectively. A strong absorption at 759 cm^{-1} was attributed to the C-Cl stretch. A high-resolution accurate mass of 296.0686 $[M+H]^+$ was found. A confirmatory $[M]^+$ and $[M+2]^+$ pattern in a 3:1 ratio was noted in the spectrum, indicating the presence of a chlorine substituent.

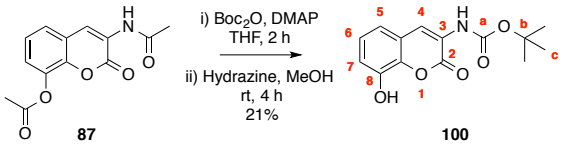

Scheme 63. Synthesis of *tert*-butyl N-(8-hydroxy-2-oxo-2H-chromen-3-yl) carbamate.

Compound **100** was obtained as a colourless powder (Scheme 63). ^{1}H NMR showed a singlet at 8.30 ppm ascribed to the 4-H. A broad singlet at 7.37 ppm was assigned to the N-H. Two doublets of doublets appeared at 7.04 ppm and 7.01 ppm for the 7-H and 5-H respectively. The interaction was confirmed by constants of 8.0 Hz and 1.6 Hz, typical for *ortho* and *meta* coupling. For this compound, hydrazine monohydrate had also deacetylated the 8 position. However, due to the hygroscopic properties of chloroform, it was not possible to see a phenolic OH group in the ^{1}H NMR spectrum. The lack of an acetyl signal in the ^{1}H NMR supports the conclusion that successful removal of both protecting groups had occurred simultaneously. A prominent singlet occurred at 1.54 ppm attributed to the CH_3 groups. ^{13}C NMR showed 12 resolved signals. IR analysis showed an absorption at 3419 cm^{-1} for the CON-H stretch. This was overlapped by a broad absorption at 3398 cm^{-1} that was indicative of an alcohol group. A weak intensity band at 2970 cm^{-1} was ascribed as the sp^3C-H stretch. One broad, strong absorption was seen at 1707 cm^{-1} assigned as a C=O band. This likely overlaid the other unaccounted for C=O signal. Three medium absorptions at 1591 cm^{-1}, 1518 cm^{-1} and 1515 cm^{-1} were attributed to the aromatic C=C stretches. A high-resolution accurate mass of 300.9845 $[M+Na]^+$ was found.

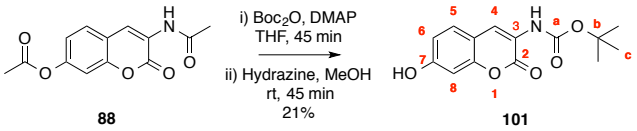

Scheme 64. Synthesis of *tert*-butyl N-(7-hydroxy-2-oxo-2H-chromen-3-yl) carbamate.

Compound **101** was isolated as a colourless powder (Scheme 64). ^{1}H NMR showed a broad singlet at 8.14 ppm was attributed to the 4-H as confirmed by HSQC. A doublet at 7.34 ppm was assigned as the 5-H. A doublet of doublets occurred at 6.77 ppm (J_1 = 8.0 Hz, J_2 = 2.4 Hz) for the 6-H. This signal showed coupling to the 5-H and 8-H positions. A doublet at 6.68 ppm was attributed to the 8-H. ^{13}C NMR showed 12 individually resolved signals. The Boc peak appeared at an upfield position of 1.52 ppm, commensurate with other analogues of this class. The lack of a signal for the 7-OH group is attributed to the hygroscopic CD_3OD solvent used to obtain the proton ^{1}H NMR spectrum. IR analysis showed a broad absorption at 3316 cm^{-1} for the OH group, this masked the signal for the CON-H stretch. A weak absorption at 3079 cm^{-1} was assigned as an Ar-H stretch. Further absorptions at 2978 cm^{-1} and 2929 cm^{-1} represented *sp*^{3}C-H stretches. Two absorptions at 1702 cm^{-1} and 1684 cm^{-1} were assigned as the lactone and carbamate groups respectively. Three medium signals at 1607 cm^{-1}, 1534 cm^{-1} and 1510 cm^{-1} were assigned as aromatic C=C stretches. A high-resolution accurate mass of 278.1028 was observed $[M+H]^{+}$.

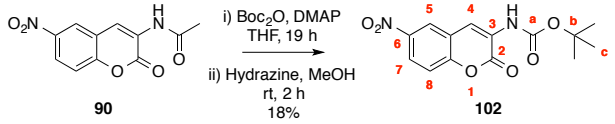

Scheme 65. Synthesis of *tert*-butyl-N-(6-nitro-2-oxo-2H-chromen-3-yl) carbamate.

Compound **102** was obtained as an off white powder (Scheme 65). ^{1}H NMR showed a doublet at 8.38 ppm, this was ascribed to the 5-H proton. The electron-withdrawing nitro-group adjacent to the 5-H aromatic proton accounted for the observed downfield chemical shift. A coupling constant of 2.4 Hz was noted, and signified *meta* coupling of the 5-H to the 7-H proton. A singlet at 8.35 ppm was attributed to the 4-H. A doublet of doublets at 8.25 ppm was ascribed to the 7-H. The observed coupling constants of 8.0 Hz and 2.4 Hz, were concordant with coupling to the 5-H and 8-H protons. A doublet at 7.43 ppm was assigned as the 8-H.^{13}C NMR showed 12 resolved signals. IR analysis showed an absorption at 3409 cm^{-1} for the CON-H stretch. An absorption at 3075 cm^{-1} was assigned as an Ar-H stretch. Whereas the band at 2976 cm^{-1} was attributed to a *sp*^{3}C-H stretch. A strong absorption at 1715 cm^{-1} was indicative of a carbonyl and likely masked the other unaccounted for C=O band. Two medium intensity absorptions at 1526 cm^{-1} and 1509 cm^{-1} were ascribed as aromatic C=C stretches. A strong band at 1338 cm^{-1} was attributable to the C-NO_2 stretch. A high-resolution accurate of mass of 307.0920 $[M+H]^{+}$ was observed.

3.17 Synthesis of 3-aminocoumarins

Tert-butyl carbamate groups can be removed under acidic conditions (Scheme 66). Although the original described procedure used TFA as its proton source, a higher yield was obtained using ethereal HCl.[248] Under acidic conditions the oxygen atom of carbamate **103 a** becomes protonated. Subsequently, this allows the *tert*-butyl cation to leave in an E1 elimination reaction step. The carbocation is stabilised via inductive effects of the adjacent alkyl groups. Decarboxylation gives the coumarin product **103 c** as the free amine, which forms the corresponding salt **104 a** in the presence of acid.

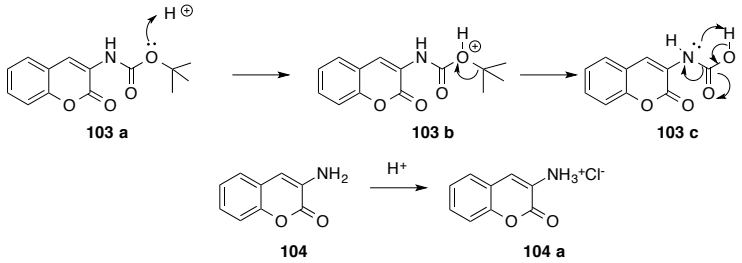

Scheme 66. Boc removal under acidic conditions.

To maximise the quantity of 3-aminocouamrin that could be obtained, the acid stable coumarin chromophore could be refluxed in concentrated HCl to remove the acetate group (Scheme 67).[249] The acetate group **105 a** under the acidic conditions becomes protonated. Nucleophilic attack from water hydrolyses the acetate group. The product **105 e** was obtained as the free amine by adjusting the pH of the reaction mixture to natural with a suitable aqueous base. The product was filtered off as a solid and washed with small aliquots of ethanol, with no further purification necessary. This procedure obviated the need to Boc protect the product and removed a reaction and purification step. Thus, the synthesis of the 3-aminocoumarin analogues was streamlined.

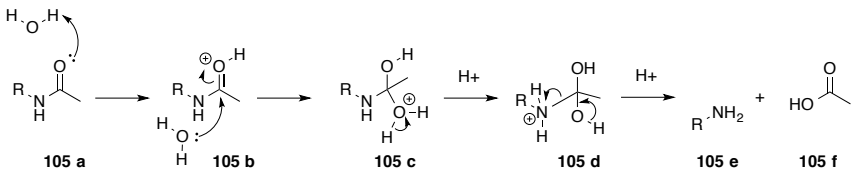

Scheme 67. Acetate removal with acid.

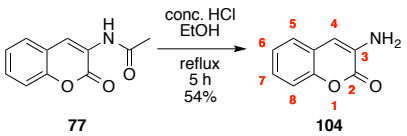

Scheme 68. Synthesis of 3-amino-2H-chromen-2-one.

Compound **104** was isolated as a yellow powder (Scheme 68). ^{1}H NMR showed a complex splitting pattern. Multiplets appeared between 7.42-7.40 ppm (1 H), 7.28-7.24 ppm (1 H) and 7.22-7.17 ppm (2 H). However, the 4-H was ascribed to a singlet at 6.71 ppm, as confirmed by HSQC. A broad singlet at 5.69 ppm (2 H), was attributed to the N-H_2. ^{13}C NMR showed 9 resolved carbons. IR analysis showed absorptions at 3425 cm^{-1} and 3313 cm^{-1} assigned to the N-H_2 asymmetric and symmetric stretches respectively. Weak absorptions at 3054 cm^{-1} and 3022 cm^{-1} were ascribed to Ar-H stretches. A strong carbonyl signal was observed for the lactone at 1702 cm^{-1}. A medium absorption at 1633 cm^{-1} was assigned as N-H_2 scissoring. A further medium intensity absorption at 1331 cm^{-1} was attributed to the C-N stretch. A strong absorption at 888 cm^{-1} was ascribed as the N-H_2 wagging signal. A high-resolution accurate mass of 162.0550 [M+H] was found.

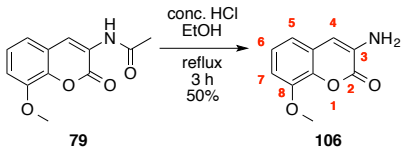

Scheme 69. Synthesis of 3-amino-8-methoxy-2H-chromen-2-one.

Compound **106** was isolated as a brown powder (Scheme 69). ^{1}H NMR showed a triplet at 7.13 ppm (1 H) and two sets of doublet of doublets at 6.97 ppm and 6.92 ppm respectively, each with the same integration (1 H). The 4-H signal was a singlet at 6.68 ppm followed by the N-H_2 at 5.69 ppm. Lastly, the a-H_3 of the methoxy group appeared as a singlet at 3.86 ppm. The ^{13}C NMR showed 10 resolved signals. IR analysis showed two absorptions at 3360 cm^{-1} and 3338 cm^{-1} for the N-H asymmetric and symmetric stretches respectively. Weak absorptions at 2997 cm^{-1}, 2969 cm^{-1} and 2941 cm^{-1} were attributed to *sp*^{3}C-H stretches of the methoxy group. An intense absorption at 1686 cm^{-1} was assigned to the carbonyl group of the lactone. An equally strong absorption at 1633 cm^{-1} was ascribed as N-H_2 scissoring. Medium intensity absorptions at 1608 cm^{-1}, 1593 cm^{-1} and 1571 cm^{-1} were attributed to C=C stretches. A broad absorption at 763 cm^{-1} was assigned as the N-H wagging vibration. A high-resolution accurate mass of 192.0654 [M+H]$^{+}$ was found.

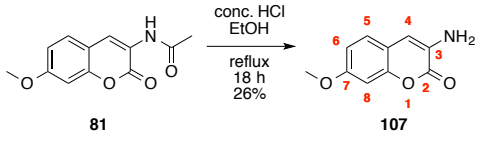

Scheme 70. Synthesis of 3-amino-7-methoxy-2H-chromen-2-one.

Compound **107** was isolated as a yellow powder (Scheme 70). ^{1}H NMR displayed a doublet at 7.19 ppm (1 H) ascribed to the 8-H proton, followed by a multiplet between 6.83-6.80 ppm (2 H) for

the remaining 6 and 5-H aromatic protons. The 4-H appeared as a singlet at 6.70 ppm. A broad singlet at 4.06 ppm was for the N-H_2. ^{13}C NMR showed 10 resolved signals. IR analysis showed absorptions at 3419 cm^{-1} and 3355 cm^{-1} for the N-H_2 asymmetric and symmetric stretches respectively. Weaker absorptions at 3091 cm^{-1} and 3006 cm^{-1} were assigned as Ar-H stretches. Absorptions at 2744 cm^{-1}, 2669 cm^{-1} and 2498 cm^{-1} were indicative of sp^3C-H stretches of the methoxy group. A prominent absorption at 1707 cm^{-1} was ascribed to the carbonyl of the lactone. Three medium intensity absorptions at 1556 cm^{-1}, 1543 cm^{-1} and 1510 cm^{-1} were assigned as C=C stretches. A strong absorption at 1250 cm^{-1} was ascribed as a C-N stretch. A strong absorption at 1607 cm^{-1} was attributed to N-H_2 scissoring. A broad absorption at 753 cm^{-1} was assigned as an N-H wagging absorption. A high-resolution accurate mass of 192.0653 $[M+H]^+$ was found.

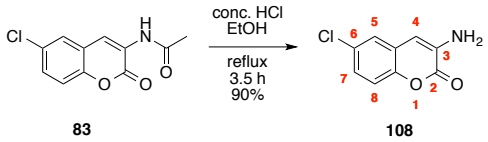

Scheme 71. Synthesis of 3-amino-6-chloro-2H-chromen-2-one.

Compound **108** was isolated as a yellow powder (Scheme 71). ^{1}H NMR showed a doublet at 7.54 ppm ascribed to the 5-H with a *J* value of 2.4 Hz, this was more deshielded than normal due to the electronegativity of the neighbouring chlorine atom. The 8-H proton appeared as a doublet at 7.29 ppm with a *J* value of 8.8 Hz, the adjacent 7-H signal was a doublet of doublets at 7.21 ppm. This proton showed long range coupling to the 5-H with *J* values of 8.4 Hz and 2.4 Hz respectively. A singlet at 6.66 ppm was characteristic of the 4-H. ^{13}C NMR showed 9 resolved signals. IR analysis showed two absorptions at 3407 cm^{-1} and 3322 cm^{-1} attributed to the asymmetric and symmetric N-H_2 stretches. Weak absorptions at 2916 cm^{-1} and 2847 cm^{-1} were indicative of Ar-H stretches. A strong absorption at 1708 cm^{-1} was ascribed to the carbonyl group of the lactone. A broad, medium-intensity absorption at 1644 cm^{-1} was assigned as the N-H_2 scissoring. Three signals at 1614 cm^{-1}, 1592 cm^{-1} and 1561 cm^{-1} were ascribed to the aromatic C=C stretches. A broad. medium-intensity absorption at 1169 cm^{-1} was characteristic of a C-N stretch. An absorption at 887 cm^{-1} was assigned as N-H_2 wagging. Lastly, a strong, sharp absorption at 806 cm^{-1} was ascribed to the C-Cl stretch. A high-resolution accurate mass of 196.0159 $[M+H]^+$ was found.

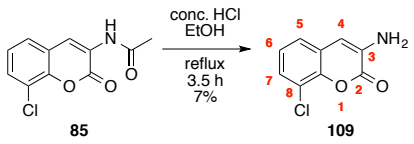

Scheme 72. Synthesis of 3-amino-8-chloro-2H-chromen-2-one.

Compound **109** was isolated as a white solid (Scheme 72). ^{1}H NMR showed two doublets of doublets at 7.32 ppm and 7.19 ppm. The more deshielded signal at 7.32 ppm was assigned as the 7-H. HMBC confirmed the assignment, as the 7-H proton had no through bond coupling to the 4-H signal. In contrast, the other doublet of doublets at 7.19 ppm did, and this is therefore unequivocally was assigned as the 5-H. A triplet at 7.13 ppm was attributed to the 6-H. A singlet at 6.67 ppm was assigned as the 4-H. Lastly, a broad singlet at 4.35 ppm was indicative of the N-H_2, as confirmed by HSQC. ^{13}C NMR showed 9 individually resolved signals. IR analysis showed absorptions at 3416 cm^{-1} and 3334 cm^{-1} for the asymmetric and symmetric N-H_2 stretches respectively. A strong absorption at 1712 cm^{-1} was assigned to the carbonyl of the lactone. A medium absorption at 1638 cm^{-1} was ascribed to N-H_2 scissoring. Additional medium intensity absorptions at 1591 cm^{-1} and 1556 cm^{-1} were assigned as C=C aromatic stretches. A broadened absorption at 1152 cm^{-1} was attributed to the C-N stretch. A further absorption at 898 cm^{-1} was ascribed to N-H_2 wagging. Lastly, a prominent absorption at 764 cm^{-1} was assigned as the C-Cl stretch. A high-resolution accurate mass of 196.0160 $[M+H]^+$ was observed.

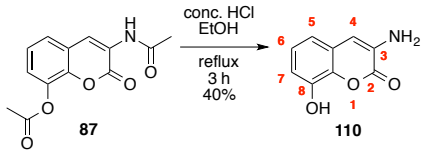

Scheme 73. Synthesis of 3-amino-8-hydroxy-2H-chromen-2-one.

Compound **110** was isolated as a brown solid (Scheme 73). ^{1}H NMR showed a broad singlet at 9.94 ppm for the OH group, a triplet at 6.68 ppm for the 6-H position and two doublet of doublets, as expected, for the 5-H and 7-H at 6.80 ppm and 6.75 ppm, respectively. The 4-H was shielded, compared to its aromatic counter part at 6.66 ppm. HMBC allowed the unequivocal assignment of the doublet of doublets, only one pair had through bond coupling to the 4-H singlet, this had to be the 5-H as the 7-H was more than 4 bonds away. ^{13}C NMR showed 9 well-resolved signals, confirming the successful simultaneous deprotection of both the ester and acetate moieties. IR analysis showed two absorptions at 3454 cm^{-1} and 3456 cm^{-1} assigned as the N-H_2 asymmetric and symmetric stretches respectively. A broad absorption at 3364 cm^{-1} was ascribed to the OH group. A strong absorption at 1704 cm^{-1} was consistent with the carbonyl group of the lactone. A similarly strong absorption at 1697 cm^{-1} was assigned as the N-H_2 scissoring. Three signals at 1611 cm^{-1}, 1594 cm^{-1} and 1567 cm^{-1} are attributed to the C=C aromatic bond stretches. A strong sharp absorption at 1174 cm^{-1} was assigned as the C-O stretch. In contrast, a broadened absorption at 1144 cm^{-1} was representative of the C-N stretch. A strong absorption at 761 cm^{-1} was attributable to the N-H_2 wagging vibration. A high-resolution accurate mass of 178.0496 $[M+H]^+$ was found.

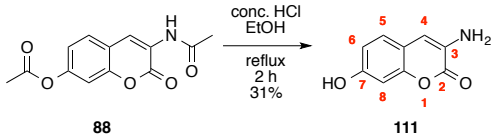

Scheme 74. Synthesis of 3-amino-7-hydroxy-2H-chromen-2-one.

Compound **111** was isolated as a yellow powder (Scheme 74). ^{1}H NMR showed a doublet at 7.33 ppm ascribed to the 5-H. A singlet at 7.26 ppm was attributable to the 4-H. The N-H_2 signal was not visible as exchange occurred with water present in the CD_3OD, consequently masking the signal. A doublet of doublets at 6.80 ppm was ascribed to the 6-H (J_1 = 8.0 Hz, J_2 = 2.4 Hz). The 6-H proton experienced splitting from the 5 and 8-H protons. Lastly, a doublet at 6.73 ppm (J_1 = 2.4 Hz), was assigned as the 8-H. The coupling constant was typical for a long-range *meta* coupling to the 6-H. ^{13}C NMR showed 9 well resolved signals. IR analysis showed two absorptions at 3435 cm^{-1} and 3344 cm^{-1} for the asymmetric and symmetric N-H_2 stretches respectively. A broad absorption at 3214 cm^{-1} was assignable as the phenolic O-H stretch. A strong absorption at 1678 cm^{-1} was for the carbonyl of the lactone. A broad medium absorption at 1608 cm^{-1} was ascribed to N-H_2 scissoring. An absorption at 1557 cm^{-1} and 1507 cm^{-1} was attributed to C=C aromatic stretches. The preceding broad scissoring signal for the NH_2 likely masked one the C=C bond signals. A broad and strong absorption at 1285 cm^{-1} was attributed to the C-N stretch. A strong absorption at 1125 cm^{-1} was ascribed as the C-O stretch. A medium absorption at 686 cm^{-1} was attributed to N-H_2 wagging. A high-resolution accurate mass of 178.0498 $[M+H]^+$ was observed.

3.18 Supercoiling activity of DNA gyrase

DNA gyrase activity is determined using a supercoiling assay. The individual A and B Gyrase subunits can be overexpressed, purified and mixed together to give an active species.[250] The A_2B_2 heterotetramer is incubated with relaxed plasmid DNA topoisomers, that is, plasmid DNA with different linking numbers. The experiment is performed in the presence of 1 mM of ATP at 37 °C for 30 minutes. In the absence of an inhibitor, the enzyme will supercoil the relaxed DNA, altering the linking number and therefore changing the topological state. The reaction is arrested using a mixture of chloroform and iso-amyl alcohol (24:1) with STEB buffer. This aqueous-organic extraction allows the segregation of DNA into the aqueous layer leaving the enzyme protein in the organic solvent. After centrifuging the sample DNA is loaded onto a 1% agarose gel. The supercoiled form of plasmid DNA migrates differently through the gel; the condensed arrangement allows the DNA to migrate more quickly compared to its relaxed counterpart. Thus, the level of supercoiling, or lack thereof, can be determined visually. This is achieved by resolving relaxed and supercoiled DNA by electrophoresis, staining with ethidium bromide and imaging under UV light.

The (4.3-Kb) plasmid pBR322 is derived from *E. coli* and has become a standard substrate for the assay.[251] The crystal structure of SD8 bound to DNA gyrase was obtained using *E. coli,* gyrase, and as such, this became our organism of choice for screening our compounds.

3.19 Biological evaluation of coumarin analogues

The coumarin analogues were screened at a concentration of 50 μM. Compounds identified with inhibition below this concentration were predicted to serve as a good lead to progress forward with. The results are shown below (Figures 40-42). All of the controls show a good response with a strong presence of different topoisomers in the negative control and a strong visible supercoiling band in the positive control. SD8 a control inhibitor shows strong inhibition at 1 μM. None of the 23 analogues show appreciable inhibition of supercoiling activity.

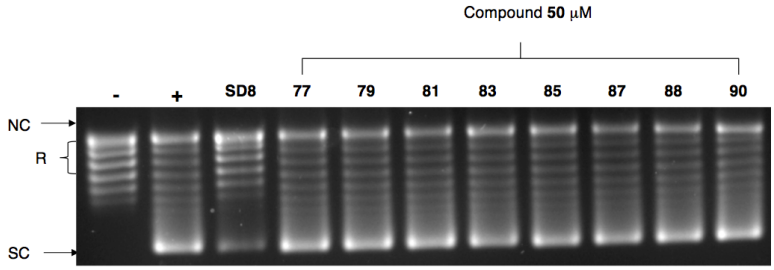

Figure 40. Effects of acetyl protected coumarins on DNA supercoiling by wild type *E. coli* gyrase. Relaxed pBR322 plasmid DNA is used as a negative control (-), and incubated in the presence of gyrase as a positive control (+). SD8 is used as a comparator at a concentration of 1 μM. NC indicates nicked circle DNA; R, relaxed DNA; SC, supercoiled DNA.

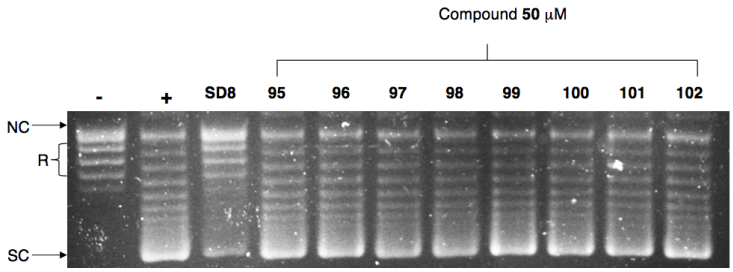

Figure 41. Effects of Boc protected coumarins on DNA supercoiling by wild type *E. coli* gyrase. Relaxed pBR322 plasmid DNA is used as a negative control (-), and incubated in the presence of gyrase as a positive control (+). SD8 is used as a comparator at a concentration of 1 μM. NC indicates nicked circle DNA; R, relaxed DNA; SC, supercoiled DNA.

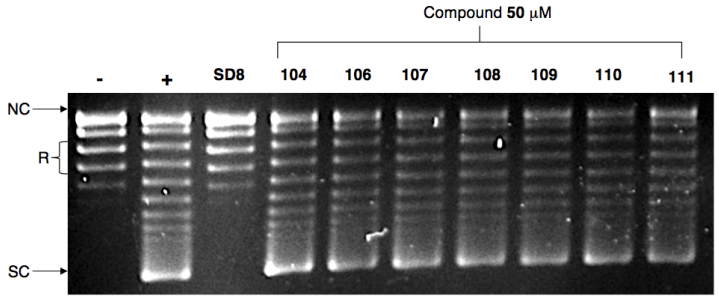

Figure 42. Effects of free amine coumarins on DNA supercoiling by wild type *E. coli* gyrase. Relaxed pBR322 plasmid DNA is used as a negative control (-), and incubated in the presence of gyrase as a positive control (+). SD8 is used as a comparator at a concentration of 1 μM. NC indicates nicked circle DNA; R, relaxed DNA; SC, supercoiled DNA.

3.20 Conclusions

This work shows the modified Perkin reaction with N-acetylglycine can be applied to a variety of starting salicylaldehyde derivatives to furnish 3-aminocoumarins. It was observed that functional groups with deactivating-inductive effects, such as nitro groups, have enhanced yields in the modified Perkin reaction. This needs to be considered when evaluating the suitability of this route for coumarin synthesis. Additionally, this work demonstrates the broad applicability of refluxing in HCl to deprotect aminocoumarins as a viable route to streamline access to a variety of 3-aminocoumarins.

This work adds to previous findings with the synthesis and biological evaluation of twenty three diverse coumarin analogues using established and validated procedures. Four of the analogues are novel (**83**, **87**, **98** and **100),** which is noteworthy. This is the first body of work to evaluate small coumarin fragments with minimal steric bulk on the aromatic ring and 3 position for intrinsic inhibition of DNA gyrase to GyrA. They showed no efficacious inhibition at the concentration screened. It is highly likely that the inhibitory effect described with the constituent coumarin fragment (MGD8N2A) of SD8 is a result of the rigid tetraene linker still having an ability to sterically interfere with DNA binding. However, the original paper did not perform cleavage stabilisation to confirm the preclusion of a DNA binding event. The dihydroxylated aminocoumarin likely plays a crucial part in directing the positioning of the linker through the geometry of its binding. Thus, the lack of inhibitory effect can be rationalised as a result of the minimal steric functionalisation at the 3 position.

Additionally, this work demonstrates that the presence of a coumarin on its own is unlikely to be useful as an inhibitor. CD shows that when SD8 binds there is no conformational change in the protein. Therefore, one can deduce that the AC pocket is a well-defined binding area and no

modulation of enzyme function occurs upon coumarin binding. It is difficult to evaluate whether the coumarins synthesised here bind to the pocket without additional experimental results. One such example could be to investigate if a binding event is seen upon addition of the ligands to the DNA gyrase enzyme using SPR. However, a limitation of SPR is that a binding event with a small MW ligand is more difficult to detect.

The structure of the aminocoumarin on its own is not favourable for the biological assay conditions. In relation to SD8 the presence of two OH groups likely enhances the physiochemical characteristics of the compound, alongside the sugar. In contrast, the small, low molecular weight analogues tested here do not have favourable physiochemical characteristics for water solubility. They can under go π-π stacking and precipitate in the conditions of the assay. This highlights the balancing act between lipophilic and hydrophilic characteristics needed for a useful inhibitor.

Like the constituent fragments of SD8, we were interested to determine whether a coumarin could be used to anchor/direct a drug to the DNA gyrase surface. This had not been described in the literature and thus warranted further investigation. Individual fragments used in FBDD, derived from the parent natural product, often have weak affinity for their target. Thus, the lack of an inhibition observed with the coumarin analogues screened did not rule out using the coumarin as a low MW fragment. Consequently, we turned our attention to incorporating the coumarin structure into part of a larger hybrid molecule. SD8 and its individual fragments with their modest activity individually serve as a paradigm for the idea of synergy. The combined effect for the ‘bi-functional’ molecule is potent inhibition, with this in mind a proof of concept was to take a simple un-functionalised coumarin as a base template and to conjugate it to a pre-existing inhibitor to see if a streamlined ‘bi-functional’ inhibitor could be discovered.

Chapter 4. Coumarin-quinolone hybrids as potential dual inhibitors of DNA gyrase

This chapter discusses the literature with respect to quinolone antibiotic hybrids, subsequently describing the synthesis and biological evaluation of a coumarin-quinolone hybrid and control analogues. The chapter goes on to outline a preliminary exploration into understanding their mode of action, followed by the conclusion.

4.00 Oxazolidinone-quinolone hybrids

The idea of tethering two chromophores together to give a dual targeting hybrid is not new. Previously quinolones have been tethered to the oxazolidinone class of antibiotics to generate dual hybrids.[252] As formerly discussed (Chapter 1), the oxazolidinones target the bacterial 50S ribosomal subunit and interfere with protein synthesis. However, their spectrum of activity is limited to Gram-positive organisms.[253,254] The lack of clinical efficacy against Gram-negative pathogens is ascribable to their inability to permeate the cytoplasm at sufficient concentrations. In contrast, quinolones can traverse the OM in Gram-negative organisms. The hybrids were linked through the C7 piperazine, taking advantage of the cyclic amine present in both classes of antibacterial. Additionally, investigations were made into conjugation at the N1 position (Figure 43, structures **112-115**). The hybrids were screened for antimicrobial activity to determine their minimum inhibitory concentrations (MICs) according to the National Committee for Clinical Laboratory Standards (NCCLS) guidelines.[255] The strains tested were: *S. aureus*, including a linezolid and ciprofloxacin resistant strain, *E. faecium*, linezolid and ciprofloxacin resistant strains, *H. influenza* and *M. catarrhalis* the last two being Gram-negative. Linezolid and ciprofloxacin were used individually as control comparator compounds. Strikingly, the hybrids linked through the N1 position displayed severely abrogated activity for all strains tested. This is in agreement with quinolone SAR. In contrast, hybrids joined through the C7 piperazine showed potent activity against Gram-positive strains. This activity was superior to either parent compound on its own. As an example compound **112** had a MIC of 0.25 μg/mL for *S. aureus,* more active compared to ciprofloxacin (0.5 μg/mL) and linezolid (4 μg/mL). It is important to note when the free carboxylic acid of the quinolone **114** was masked as an ester **115,** the activity was severely attenuated, consistent with previously discussed quinolone SAR. As an example **114** had an MIC of 0.5 μg/mL against *S. aureus* whereas **115** had an MIC of 8 μg/mL. No improvement was observed against Gram-negative pathogens with the hybrids compared to parent compounds. However, the C7 hybrids displayed improved activity against all Gram-positive resistant strains. The authors attribute the lack of improved efficacy against Gram-negative organisms as an effect of the sub-optimal pKa of the distal nitrogen of the C7 piperazine ring in the hybrids. Building upon this body of work, a separate group tethered quinolones and oxazolidinones through the C7 piperazine linker and explored the effect of adding an additional pyrrolidinyl or amino azetidyinyl spacer (Figure 43, structures **116-118**).[256] As well as looking at MICs against selected strains, the group evaluated the ability to inhibit *in vitro* supercoiling activity and protein synthesis.

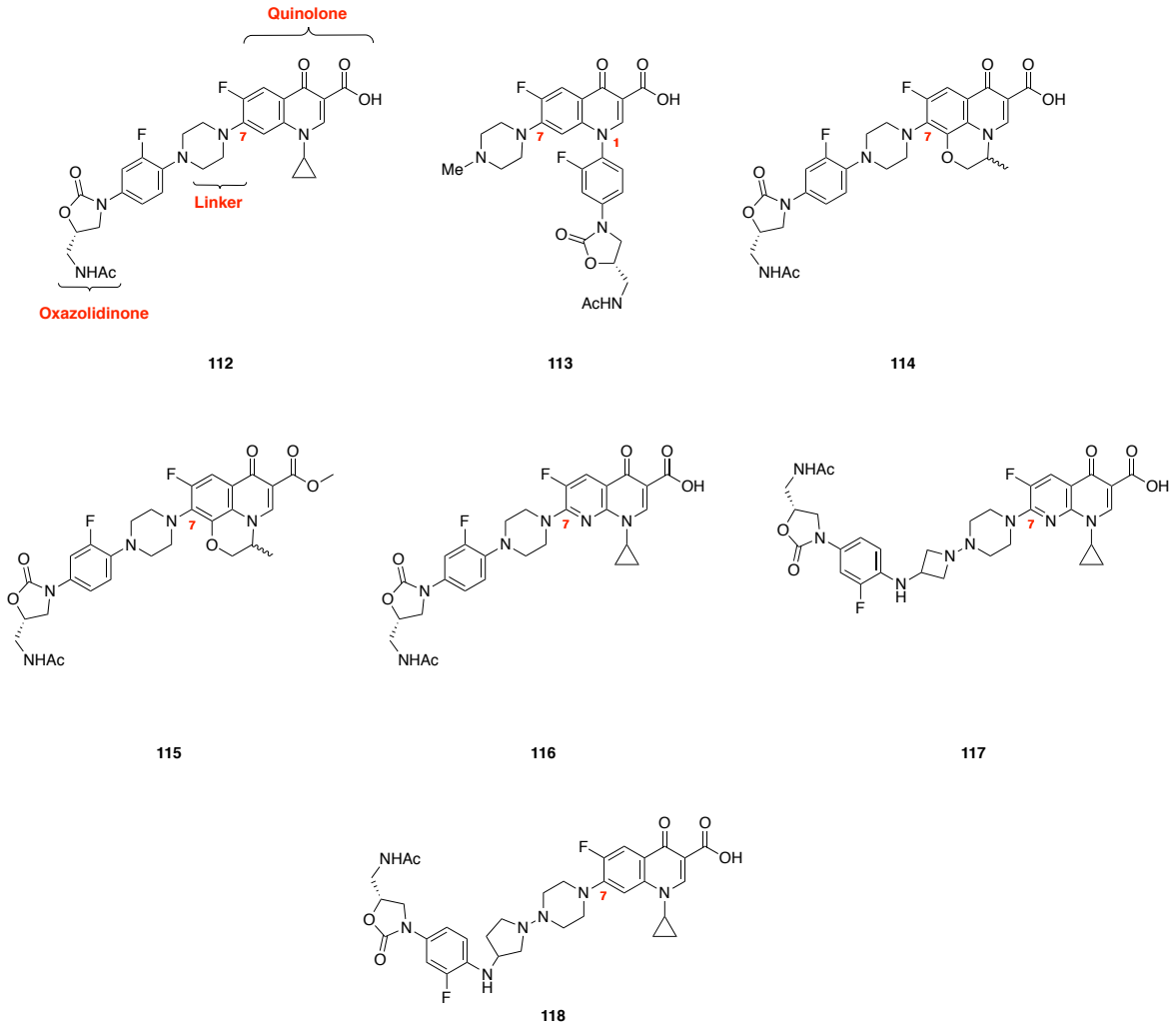

Figure 43. Quinolone-oxazolidinone hybrids.

Hybrids **112** and **116** with a piperazine linker to the oxazolidinone overcame quinolone resistance to *S. aureus* with MIC of 0.25 μg/mL and 0.125 μg/mL respectively. This outperforms the parent ciprofloxacin (32 μg/mL). Similarly, the compounds overcame linezolid-resistant *S. aureus* with MICs of 4 μg/mL and 8 μg/mL respectively compared to 64 μg/mL of the parent linezolid. Hybrids **117** and **118** with additional spacers also displayed good activity against the same quinolone resistant strains. Intriguingly, the authors noted differing effects on supercoiling and protein synthesis. The piperazine-linked **112** and **116** compounds showed reasonable supercoiling inhibition against DNA gyrase (IC_{50} 20 μM and 50 μM respectively) as well as topo IV (IC_{50} 50 μM and 10 μM respectively) compared to ciprofloxacin (0.5 μM DNA gyrase and 5 μM topo IV). Nevertheless, they were also able to inhibit protein synthesis both having an IC_{50} of 2.8 μM compared to linezolid (IC_{50} 4.1 μM). This is in contrast to compound **118** that displays excellent supercoiling inhibition, with an IC_{50} of 0.2 μM and 1 μM for gyrase and topo IV but poor inhibition of protein synthesis with an IC_{50} above 20 μM. The results demonstrated that piperazine-linked

compounds are capable of dual targeting. This also highlighted that the introduction of the amino-pyrrolidinyl moiety conferred a preference for quinolone activity. Furthermore, the work substantiated previous findings of dual targeting via these two classes of antimicrobial and strengthened the quinolone-SAR relationships.

4.01 Macrolide-quinolone hybrids

The quinolone scaffold has been successfully joined at the C6 and C7 positions to the macrolides erythromycin, clarithromycin and telithromycin via an ester linkage at the 4" position.[257,258] With alykylamine chains the authors probed the effect of linker length on antimicrobial activity using seven or nine atoms and varying the substituents at the N1 and C6 position. The strains tested were macrolide-resistant *S. aureus*, *S. pneumonia*, *S. pyogenes*. Additionally, β-lactamase-negative ampicillin-resistant *H. influenzae* was also investigated as a Gram-negative standard. Several general SAR trends were noted with the compounds (Figure 44). Hybrids **119** and **120** showed enhanced activity over all strains tested compared to clarithromycin on its own. The shorter linked hybrid **119** possessed improved activity with an MIC of 0.5 μg/mL in a macrolide-resistant efflux-mediated *S. aureus* strain compared to the longer linked compound **120** (2 μg/mL). Interestingly, a 7-atom linker with a chlorine substituent at the C7 (**121**) displayed enhanced activity against all strains tested compared to hybrid **119** and the clarithromycin control. However, exceptionally, **119** was worse against *S. pyrogens* (<0.125 μg/mL) compared to telithromycin (0.06 μg/mL).

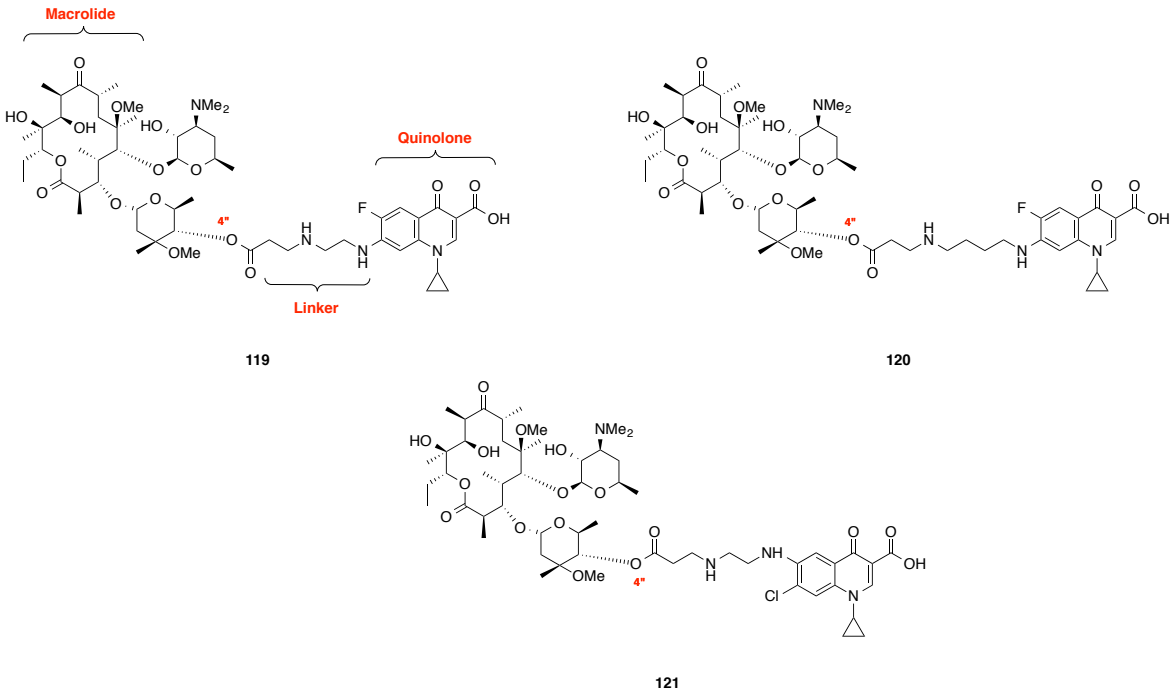

Figure 44. Clarithromycin-quinolone hybrids.

The same study noted the benefit of a halogen substituent at the C6 position in erythromycin quinolone hybrids and illustrated the improved potency of having a cyclopropyl group at the N1 position. These observations were consistent with previous assessment of quinolone SAR. This study demonstrated that a large complex molecule can be tethered to a quinolone molecule without deleterious effects on macrolide activity. Moreover, they demonstrated resistance to macrolides can be overcome with the addition of a quinolone. A subsequent body of work using novel C4"-substituted azithromycin macrolides attached to quinolones at the C6 and C7 position provided further insight with respect to potential dual targeting.[258] This work added to the previous study by assessing ciprofloxacin-resistant strains and performing DNA supercoiling assays against DNA gyrase and topo IV. The authors utilised a free amine at the end of their chosen linker to facilitate coupling of the quinolones to macrolides using HBTU. This resulted in good yields of 60-90%. Subsequently, the hybrid compounds were tested against macrolide-susceptible and macrolide-resistant strains: *S. aureus*, *S. pneumonia*, *S. pyogenes* as well as *M. catarrhalis*, and *H. influenzae* standards provided by the Pliva Research Institute culture collection.[258] The quinolone analogues **122**-**128** (Figure 45) displayed no appreciable activity (MIC > 64 μg/mL) against any of the strains. Furthermore, they had no activity against ciprofloxacin resistant *S. aureus*. In contrast, two azithromycin-quinolone hybrids **129**, and **130**, displayed improved activity against all strains including macrolide resistant bacteria when compared to azithromycin and ciprofloxacin on their own. The improvement of **129** and **130** against Gram-negative *M. catarrhalis* (<0.125 μg/mL and, 0.125 μg/mL respectively) and *H. influenzae* (both 0.5 μg/mL) compared to azithromycin (0.25 μg/mL and 1 μg/mL respectively) or ciprofloxacin (0.125 μg/mL and, < 0.125 μg/mL respectively) is notable.

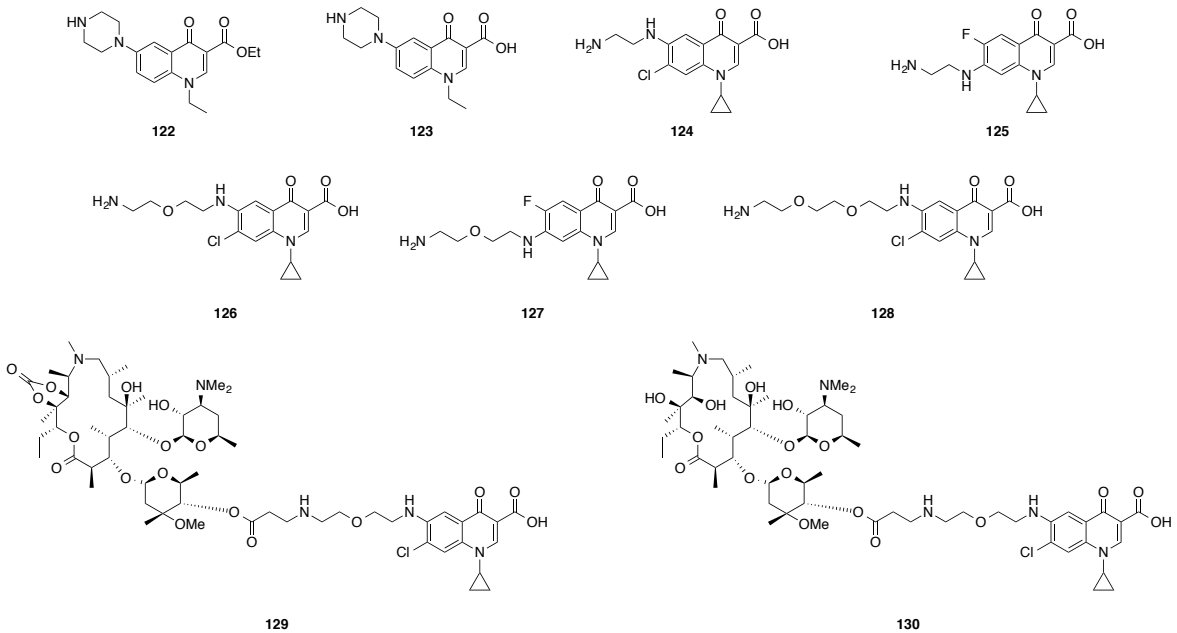

Figure 45. Quinolone linker analogues and azithromycin-quinolone hybrids.

Interestingly, when the authors probed for bi-functional activity they found that the lead compounds **129** and **130** lacked the ability to effectively inhibit *E. coli* DNA gyrase (IC_{50} 70 and 60 μM respectively) or topo IV (60 and 50 μM respectively). Contrasting with this, **129** and **130** could act as potent inhibitors of protein synthesis with IC_{50} values of 0.28 μM and 0.35 μM compared to telithromycin (0.23 μM). Crucially this work shows a short linker can abolish quinolone activity. Furthermore, substitution of the C6 position with a piperazine ring in **123** abrogates quinolone activity. The results show that the hybrids demonstrate improved macrolide activity with respect to Gram-negative organisms. This is likely not due to dual targeting; rather the presence of the quinolone could enhance the ability of the hybrid to traverse the OM of Gram-negative pathogens.

4.02 Aminoglycoside-quinolone hybrids

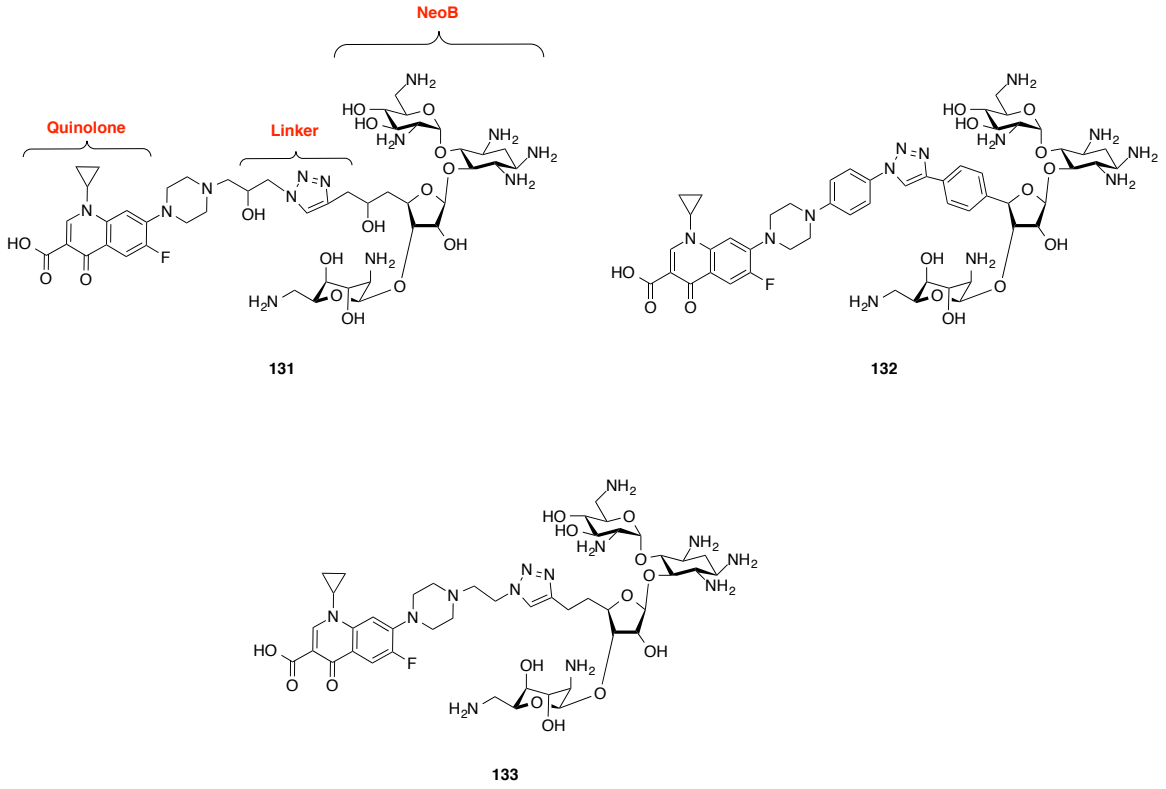

Figure 46. NeoB-ciprofloxacin hybrid structures.

Tethering fluoroquinolones to aminoglycoside antibiotics yields bi-functional hybrids.[259] It was thought that the strategy of coupling a quinolone to Neomycin B (neoB) would overcome resistance. The authors predicted that the positive charge of neoB would be beneficial to quinolone binding by facilitating contacts to DNA and/or the DNA-protein interface. The hybrids were joined through a 1,2,3, triazole group with spacers on either side (Figure 46). Additionally, commercially available ciprofloxacin was alkylated at the C7 piperazine substituent with the appropriate spacer-azide. In a reverse approach three different alkyne groups were also introduced on the neoB

molecule at the 5-OH group. Subsequently, the hybrids were prepared via click chemistry under microwave irradiation conditions to give the desired compounds. The hybrids were evaluated for their biological activity *in vitro*, against susceptible and resistant strains with both ciprofloxacin and neoB as controls. The study utilised *E. coli*, *B. subtilis* and *MRSA*. The majority of hybrids displayed good activity, with better inhibition than neoB on its own against Gram-negative *E.coli* which included the aminoglycoside-resistant AG100A and AG100B strains. However, none of the hybrids were more potent than ciprofloxacin. Compound **132** was the most potent inhibitor across all strains tested. The majority of these hybrids were less efficacious than the controls against the Gram-positive *B. subtilis*. However, they displayed improved activity against aminoglycoside-resistant MRSA. To further investigate the hybrids mode of action, the authors checked for *in vitro* inhibition of DNA gyrase, topo IV, and protein synthesis. Remarkably, compounds **131**, **132** and **133** displayed potent inhibition of both DNA gyrase (73 nM, 85 nM 41 nM, respectively) and topo IV (0.58 μM, 0.55 μM and 7.90 μM) with better efficacy than ciprofloxacin (1.3 μM, 10.8 μM). They also showed good inhibition of protein synthesis (2.20 μM, 16.7 μM and 18.1 μM, respectively) when compared to neoB (10.5 μM). Compound **132** performed better in all three assays compared to the parent antibiotics. It should be stated that ciprofloxacin is inactive in the protein synthesis assay and neoB is inactive in the DNA gyrase and topoIV assay. These results eloquently highlight the steric bulk that can be accommodated at the C7 piperazine position and still result in DNA gyrase inhibition. Moreover, these hybrids displayed enhanced efficacy for DNA gyrase and topo IV over the highly successful commercial drug, ciprofloxacin. It should be observed that the ciprofloxacin molecule used has a free carboxylic acid and no esterified hybrids were synthesised in this study. This is important because previous SAR has shown the free acid is essential for effective formation of the water-metal ion bridge that stabilises the quinolones during their intercalation into double strand breaks (as discussed in chapter 1).[18]

4.03 Coumarin-quinolone hybrids

Two publications have described the synthesis and biological evaluation of novel coumarin-quinolone hybrids.[260,261] The first study combined the structural features of N-(2-arylethyl) piperazinyl quinolones and a simple unfunctionalised coumarin to give novel N-[2-(coumarin-3-yl)ethyl]piperazinyl quinolones. The synthetic strategy used converted acetyl coumarin into its bromine or α-bromo oxime derivative. This was coupled directly to the quinolone derivative in the presence of a mild base at room temperature to give the desired product. This provided a brief and efficient synthesis. Subsequently, the coumarin-quinolone hybrids were evaluated *in vitro* for their potential antibacterial activity. The control comparator drugs were norfloxacin, ciprofloxacin and enoxacin; these compounds were assessed using the agar dilution method.[262] The strains tested were *S. aureus*, *B. subtilis*, *Klebsiella pneumonia*, *P. aeruginosa*, *Staphylococcus epidermidis*, and *MRSA*.

The most potent compound, **134**, contained a cyclopropyl moiety at the N1 position, consistent with quinolone SAR (Figure 47). Three of the four worst performing compounds had a naphthyridine core, and the most effective hybrid **134** contained the quinoline scaffold. The MIC was 0.19 μg/mL which was comparable to the quinolone controls for *S. aureus*. All of the hybrids had some activity against *B. subtilis*, but none of the hybrids demonstrated improved activity against Gram-negative pathogens compared to the controls.

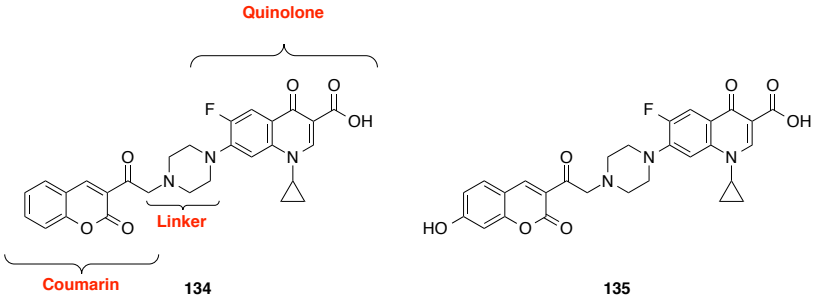

Figure 47. Structures of efficacious coumarin-quinolone hybrids.

In this study the linker used is short, and the coumarin is linked through a ketone or oxime not an amide. This publication predates the first quinolone and SD8 crystal structures and highlights the usefulness of the quinolone scaffold. Also, this indicates the presence of a coumarin does not abrogate activity against gyrase. Supplementing this work, a similarly conjugated coumarin-gatifloxacin and coumarin-ciprofloxacin hybrids were synthesised and probed for biological evaluation.[261] The asymmetric compounds were obtained using the bromine or bromo-oxime coumarin derivative combined with the appropriately substituted quinolone. In contrast to the first study, additional substitutions were explored on the coumarin at the 7' position as well as the piperazine ring. *In vitro* activity was assessed against *M. segmentis* and *M. tuberculosis*. All of the hybrids demonstrated good activity against *M. segmentis*. However, this was no better than the control gatifloxacin, ciprofloxacin, rifampicin and moxifloxacin compounds. The best performing compound against *M. tuberculosis* was **135** (0.5 μg/mL), a 7-hydroxycoumarin derivative joined to ciprofloxacin. This outperformed ciprofloxacin (1.0 μg/mL), and rifampicin (2.0 μg/mL), and was equally as effective as 8-methoxy ciprofloxacin and moxifloxacin. No benefit was seen from substitution on the piperazine ring. Furthermore, no relationship was observed between the calculated logP values and antimicrobial activity. No supercoiling assays were performed for these compounds.

4.04 Crystal structure data and rational design

The previously discussed structures provide a justification of the usefulness of creating quinolone hybrids. Furthermore, the work provides insight into the suitable locations for conjugation to quinolone molecules. These results combined with the 2014 crystal structure of GyrA55-SD8 formed the foundation from which our hypothesis was derived.[184] The GyrA55-SD8 structure revealed that two molecules of SD8 were responsible for binding to DNA gyrase. The mode of action of the natural product is to 'staple' across the surface of the GyrA homodimer interface at the DNA gate. Consequently, this prevents DNA strand passage and precludes the conformational changes necessary in order for the enzyme to bind DNA. The aminocoumarin and the polyketide of SD8 occupy well defined pockets. The polyketide portion spans both surfaces of the gyrase homodimer (Figure 48). Interestingly, the GyrA55-SD8 structure showed the orientation of the coumarin was different from the previous GyrA59-SD8 structure (Figure 49). The consequence of this alternative conformation on the angle that the linker exits the aminocoumarin pocket is pronounced. This highlights some of the limitations of x-ray crystallography. Careful interpretation is required when evaluating data, as the resultant structure could be an artefact of the crystallisation process and not representative of the conformation adopted in solution. Furthermore, what is presented is a 'snap shot' in time. Published crystal structures for both SD8 and quinolones are available. However, the most recent structures of SD8 and quinolones are supported by *in vitro* mutational data that substantiates the observed conformations. Thus, the latest SD8 crystal structure is likely a true reflection of the conformation adopted by SD8 at low concentrations in solution.

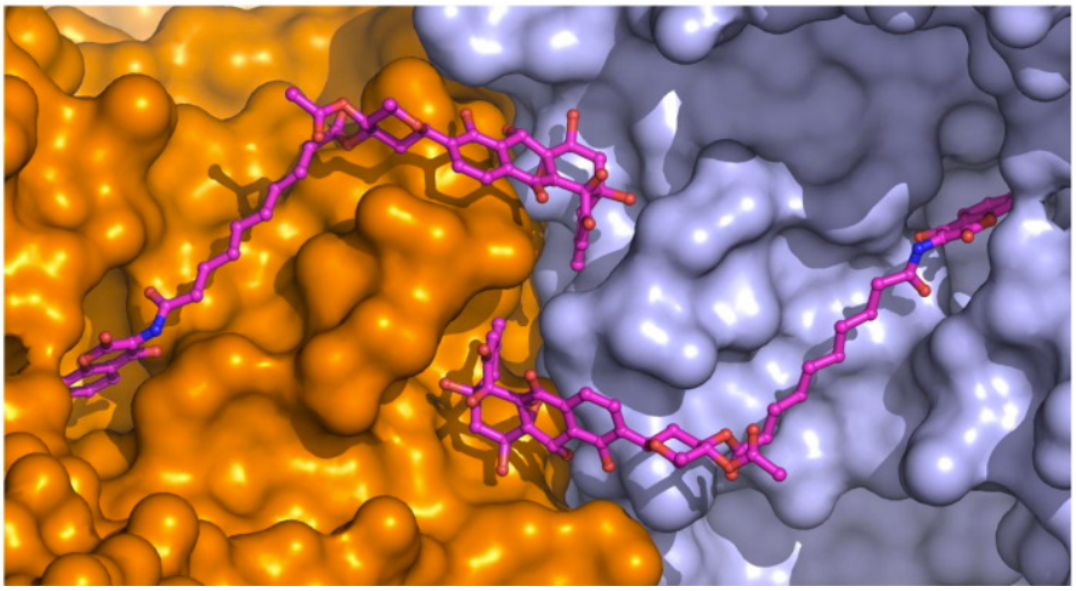

Figure 48. Crystal structure of the GyrA55-SD8 complex (PDB 4CKL). Two SD8 molecules (magenta) span different GyrA homodimers, one is shown in orange the other in blue.[184]

It has also been shown that close sequence similarity occurs between *S. aureus* and *E. coli* gyrase.[263] This has suggested that the binding site of the N-terminal domain of SD8 bound to *E. coli* gyrase (PDB ref 4CKL) and the interaction between ciprofloxacin, DNA and *S. aureus* gyrase (PDB ref 2XCT) warranted further investigation.[88] Analysis revealed that the quinolone binding pocket is in close proximity to the D-olivose sugar of SD8 (Hearnshaw unpublished data), this is shown in Figure 50 below. Inspired by the bi-functional structure of SD8 we sought to take advantage of both binding pockets using a fragment based approach to develop a novel class of gyrase inhibitor. No coumarins with low affinity for gyrase were identified in chapter 2, thus we reasoned to use the most simplistic scaffold in order that we could probe future SAR.

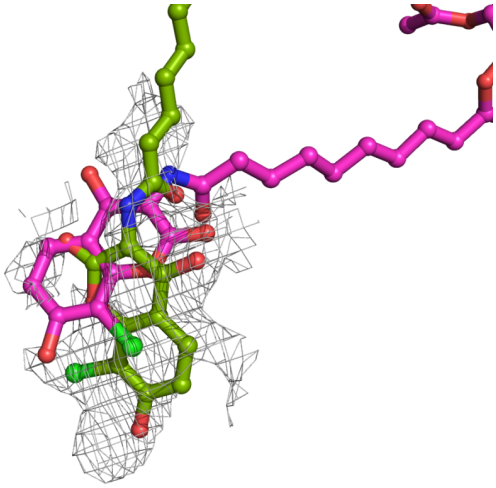

Figure 49. Different orientations of the aminocoumarin bound to GyrA. The GyrA55-SD8 structure is shown in magenta, the GyrA59-SD8 structure is shown in green.[184]

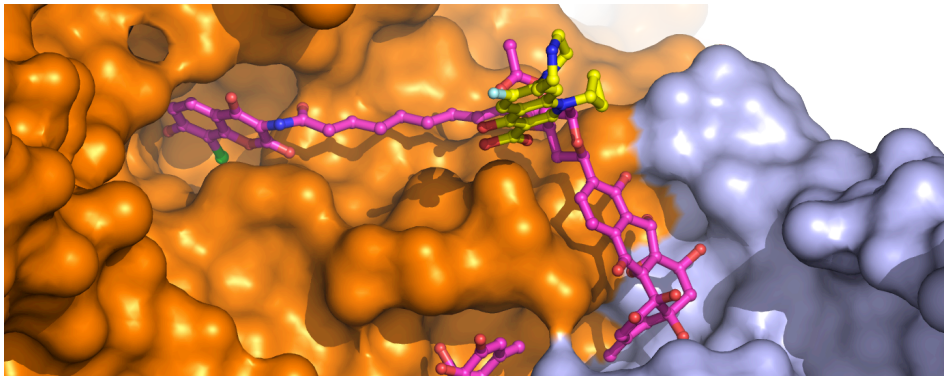

Figure 50. Crystal structure of SD8 (magenta) in complex with GyrA55.[184] The position of ciprofloxacin (yellow), from the *S. aureus* gyrase structure, is obtained by superposition of the *E. coli* and *S. aureus* gyrase structures (Hearnshaw unpublished data).[88] One GyrA monomer is shown in orange, the other in blue.

It was envisaged that a simple coumarin could be tethered to a ciprofloxacin molecule using a 15 Å linker that would generate an asymmetric hybrid. The unfunctionalised coumarin was predicted to still be able to maintain hydrogen bonds with Arg91 via the lactone in the aminocoumarin pocket. Furthermore, it was hypothesised that the linker would preserve hydrophobic interactions with Ser171. It has previously been shown that dual hybrids can successfully overcome resistance and exert a bi-modal action on their therapeutic targets. As a strong body of literature existed for quinolone hybrids, we chose the validated ciprofloxacin structure. From SAR it has been well established that the largest accommodation of steric bulk is in the C7 position for quinolones, thus setting a precedent. Furthermore, efficacious targeting of gyrase would likely require a free carboxylic acid. Based on the information from Figure 50 it was theorised that the synthetic analogue **136** would be able to adopt a favourable conformation to take advantage of the two identified binding sites (Figure 51).

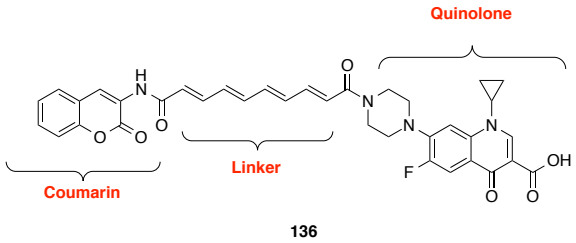

Figure 51. Structure of the target hybrid **136**.

4.05 Synthesis

With a rational starting point for the generation of asymmetric analogues, the focus turned to developing a viable synthetic route. Preliminary work with ciprofloxacin as a commercially available free acid proved unfruitful. Ciprofloxacin **137** is only soluble in aqueous acid, thus limiting the scope of chemistry available for downstream reactions. To surmount this problem, the carboxylic acid was masked as an ester. This conferred the advantage of reducing unwanted side products, and made the compound easier to handle in organic solvents. This was achieved using $SOCl_2$ to form the reactive acyl chloride. Both MeOH and EtOH were tried as protecting alcohols, EtOH was found to be more favourable with higher yields and cleaner reactions, consonant with previous work (Scheme 75).[264] Often, a white solid was filtered off during the work up, and this was not soluble in either aqueous or organic solvent and was predicted to be polymerised ciprofloxacin. The acid chloride is free to react with the secondary amine present on another ciprofloxacin molecule in an intermolecular fashion. Furthermore, the secondary amine of the piperazine heterocycle has the capacity to form a sulphonamide. These unwanted side products could account for the moderate yields observed.

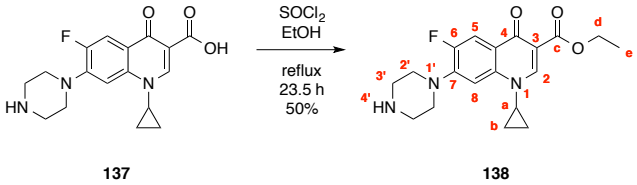

137 138

Scheme 75. Synthesis of ethyl 1-cyclopropyl-6-fluoro-4-oxo-7-(piperazine-1-yl)-1,4 dihydroquinoline-3-carboxylate.

Compound **138** was isolated as a colourless powder (Scheme 75). The ^{1}H NMR spectrum showed a deshielded singlet at 8.42 ppm for the 2-H proton, the downfield signal was due to conjugation with both the ketone and carbonyl of the ester. A doublet at 7.88 ppm with a J_{HF}= 12.0 Hz value, was ascribed as the proton *ortho* to the fluorine group. These observations were confirmed by a ^{19}F decoupling experiment, whereby the doublet was transformed into a singlet . The remaining doublet at 7.20 ppm was the aromatic proton *meta* to the fluorine group with J_{HF}= 8.0 Hz. A quartet at 4.32 ppm with an integration of 2 H was indicative of the CH_2 group adjacent to the CH_3 of the ester. A multiplet at 3.43-3.38 ppm represented the a-H of the cyclopropyl. Further upfield the piperazine alkyl groups displayed a distinguishing high order splitting pattern 'roofing effect' at 3.21-3.05 ppm due to a plane of symmetry from the C1' to C4' position. A prominent triplet at 1.35 ppm integrating for 3 H was the CH_3 portion of the ester. Lastly, the CH_2 groups of the cyclopropyl moiety formed disparate upfield multiplets at 1.30-1.25 ppm and 1.11-1.07 ppm respectively. COSY analysis confirmed the interaction between the CH of the cyclopropyl and the ascribed CH_2 groups. ^{13}C NMR showed the most downfield signal at 173.1 ppm (J_{CF} = 2.0 Hz) as a doublet for the C4 position; it was split due to the presence of fluorine. The next doublet appeared at 153.4 ppm with a large coupling constant of 247.0 Hz, this could easily be mistaken for two separate carbons, but was the C6 position experiencing the strongest effect of the halogen. Subsequently, a doublet occurred at 144.9 ppm (J_{CF} = 10.0 Hz) for the C7 whereas the C4a appeared at 122.8 ppm (J_{CF} = 7.0 Hz). The *ortho* C5 signal was at 113.0 ppm (J_{CF} = 23.0 Hz) with the *meta* C8 at 104.8 ppm having a much smaller coupling constant (J_{CF} = 3.0 Hz). The last doublet was at 51.4 ppm (J_{CF} = 4.0 Hz) assigned to both the piperazine C2' substituents. The piperazine C2' and C3' ring had equivalence showing only two signals for the four carbons, as did the cyclopropyl group Cb atoms with a single upfield signal at 8.2 ppm. A further 9 resolved carbons were present, giving a total of 16 carbons which is correct for a compound with the formula $C_{19}H_{22}FN_3O_3$. ^{19}F{^{1}H} NMR proton de-coupled showed a single peak at -123.7 ppm indicating a single fluorinated compound was present. IR analysis showed absorptions between 2942-2820 cm^{-1} for the CH_2 and CH_3 groups, two carbonyl absorptions occurred at 1716 cm^{-1} and 1617 cm^{-1}. A high-resolution accurate mass of 360.1720 $[M+H]^+$ was observed.

The synthesis of the tetraene linker has been previously described in the literature.[265] However, this stereoselective synthesis is complex and time consuming. It was noted that usable quantities of the linker could be obtained from the hydrolysis of the commercially available fumagillin **139**.[266,267] This compound could be used to circumvent the requirement for a total synthesis.

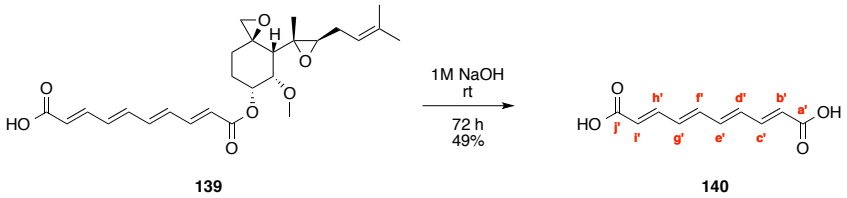

139 **140**

Scheme 76. Synthesis of (2E, 4E, 6E, 8E)-deca-2, 4, 6, 8-tetraenedioic acid.

Compound **140** was isolated as a pale yellow powder in 49% yield (Scheme 76). ^{1}H NMR showed a broad singlet at 12.28 ppm (2 H) assigned to the carboxylic acid protons. Next, appeared a doublet of doublets at 7.25 ppm (J_1 = 16.0 Hz, J_2 = 12.0 Hz) integrating for 2 protons. This was ascribable to the c' and h'-H. The splitting pattern was due to the adjacent b'/i-H and the d'/g'-H protons. The remaining core of the linker appeared as two multiplets between 6.82-6.75 ppm (2H) and 6.66-6.56 ppm (2H). Lastly, a doublet appeared at an upfield region of 5.99 ppm (J = 16.0 Hz), attributed to the b' and i'-H signals. The reciprocal coupling to the c' and h'-H was evident from the coupling constant. This signal was the most upfield of the protons, this was unexpected. It was predicted adjacent electronegative atoms would de-shield the b' and i'-H protons and result in a downfield signal. One explanation is that the overlapping *p*-orbitals of the unsaturated linker allow the delocalisation of electrons. The electron density is then drawn towards the carboxylic acid termini via induction. ^{13}C NMR showed 6 resolved signals due to the chemical equivalence present in the molecule. IR analysis showed two broad signals at 2818 cm^{-1} and 2534 cm^{-1} assigned as O-H stretches. A high-resolution accurate mass of 193.0505 $[M-H]^-$ was found.

With the successful isolation of the unsaturated linker, attempts were made to couple this to a simple coumarin. Initial efforts were made to convert the diacid into the corresponding acyl chloride facilitating the coupling of the free amino coumarin (Scheme 77). These attempts failed to give the desired compound. Instead, a sticky insoluble mass was obtained that was difficult to work with. We turned to an alternative approach using standard peptide coupling conditions EDC and 30% pyridine in DCM. However, similar to the acid chloride product an insoluble sticky mass was obtained. Proton ^{1}H NMR analysis provided little insight, other than the presence of multiple products. Unsuccessful attempts were made to remove impurities by triturating with solvents that the starting materials were known to be soluble in (DCM, MeOH, EtOAc).

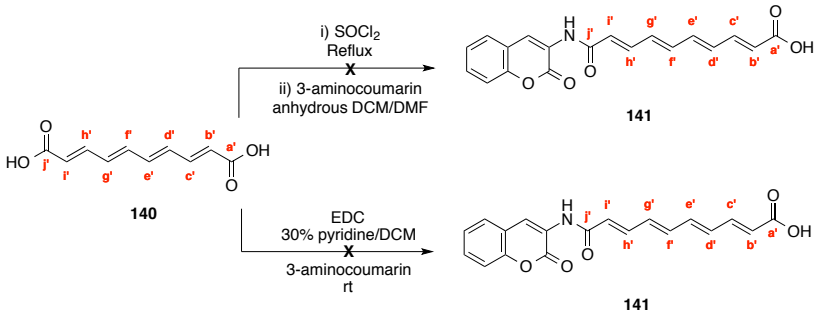

Scheme 77. Attempted synthesis of 9-[(2-oxo-2H-chromen-3-yl) carbamoyl].

Empirically, it was noted that the isolated tetraene linker was very insoluble, with the NMR only obtainable in DMSO. This property; combined with the poor solubility of the parent coumarin, could account for the unsuccessful coupling. Moreover, due to the free diacid being utilised there would be a high possibility of dimer formation, particularly with the acid chloride methodology. Alternative approaches that could have been pursued included selective esterification of one end of the diacid followed by selective mono-coupling. However, reflecting on the poor physiochemical properties of the linker, it was decided to try using a commercially available saturated linker as previously a successful mono-coupling to a coumarin had been described.[268]

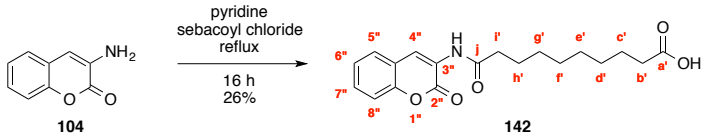

Scheme 78. Synthesis of 9-[(2-oxo-2H-chromen-3-yl) carbamoyl] nonanoic acid.

3-Aminocoumarin **104** was synthesised as described previously. In order to access the asymmetric hybrid it was necessary to obtain a mono-coupled product **142**. This was achieved using a previously reported procedure whereby coumarin is refluxed in the presence of sebacoyl chloride.[268] Compound **142** was isolated as an off-white powder after purification by flash column chromatography (Scheme 78). ^{1}H NMR showed a carboxylic acid peak downfield at 11.97 ppm, a broader singlet at 9.66 ppm represented the NH peak of the amide bond. HSQC analysis confirmed no carbon was correlated to the proton signal. The 4"-H of the coumarin appeared as a singlet at 8.64 ppm. The four aromatic protons were non-equivalent, creating a complex splitting pattern termed an ABCD spin system. A doublet of doublets occurred at 7.70 ppm (1 H) and two multiplets between 7.52-7.48 ppm (1 H) and 7.40-7.32 ppm (2 H) respectively. ^{13}C NMR showed 19 resolved carbon signals. IR analysis showed a broad OH signal at 3289 cm^{-1} which was overlapped by a sharp CONH stretch. The alkyl signals appeared at 2920-2843 cm^{-1}. Furthermore, three carbonyl absorptions were seen at 1728 cm^{-1} for the lactone, as well as 1685 cm^{-1} and 1682 cm^{-1} for the

carboxylic acid and amide. Due to their similar values they could not be differentiated. A confirmatory high-resolution accurate mass of 346.1649 $[M+H]^+$ was found. Reaction yields were moderate; this can be accounted for by the low reactivity of the aniline type nitrogen found on the coumarin, and competing dimer formation during the reaction. However, in order to circumvent a deprotection and purification step, a free diacid was intentionally utilised during the synthesis of the mono-coupled aminocoumarin. This approach had the advantage of allowing the product to be directly carried forward to the coupling reaction with the ciprofloxacin-ester fragment **138**. Previously described methods successfully use 30% pyridine in DCM with EDC to partner aliphatic linkers with aminocoumarin scaffolds.[269,270] Consequently these conditions proved fruitful for promoting amide bond formation to the secondary amine of the C7 piperazine group of the ciprofloxacin-ester fragment. Attempts to couple both fragments together via an acid chloride where unsuccessful. A significant disadvantage of the acid chloride methodology is the harsh reaction conditions, which limits its utility. In contrast, carbodiimides are a versatile class of activating agents for promoting amide and ester formation. Highly reactive *O*-acylisourea intermediates can be generated from the interaction between a carboxylic acid and the two basic nitrogen atoms found in carbodiimides. The active species readily couples with amine derivatives to form an amide bond. A consequence of the highly reactive nature of carbodiimides is the unwanted formation of side products. *O*-acylisoureas can undergo an intramolecular reaction to acetylate the nitrogen atom of the carbodiimide to form the inactive species. Additionally, cyclisation can occur to form an oxazolone heterocycle; whilst this can be ring opened to form the desired product, it also allows for racemisation to take place (Scheme 79).[271,272]

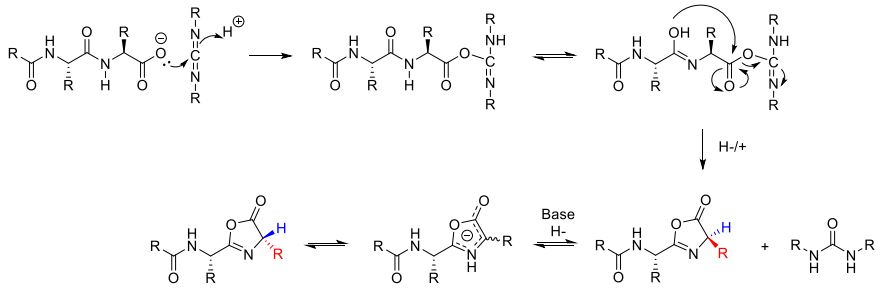

Scheme 79. Inversion of stereochemistry via oxazolone intermediate highlighted in red and blue.

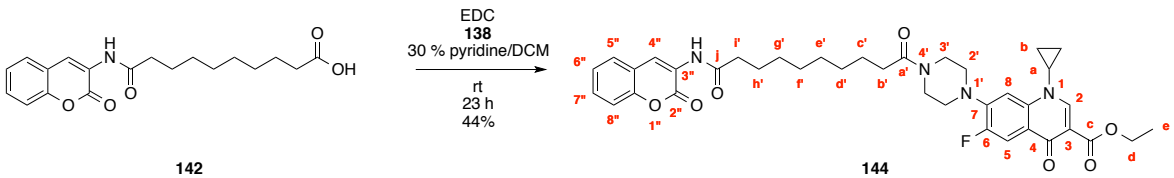

Scheme 80. Synthesis of 1-cyclopropyl-6-fluoro-4-oxo-7-(4-{9-[(2-oxo-2H-chromen-3-yl)carbamoyl]nonanoyl}piperazin-1-yl)-1,4-dihydroquinoline-3-carboxylate.

EDC and its by-products possess the added advantage of being water soluble and thus can easily be removed from the reaction mixtures by performing an aqueous/organic work up. With no stereocenters in the coumarin-quinolone hybrid there was no capacity for racemisation to occur. The mild peptide coupling conditions yielded the asymmetric protected coumarin-quinolone hybrid in a viable yield of 44%. Compound **144** was isolated as a colourless powder (Scheme 80). ^{1}H NMR showed two singlets at 8.68 ppm and 8.50 ppm corresponding to the 4"-H and 2-H protons. The NH singlet at 8.06 ppm was broad and overlapped one of the aromatic ciprofloxacin doublets at 8.02 ppm. The aromatic protons for the simple coumarin appeared as multiplets between 7.50-7.41 ppm (2 H) and 7.32-7.24 ppm (3 H), the latter multiplet also overlaid the remaining ciprofloxacin doublet signal and this accounted for the integration of 3. A quartet occurred at 4.38 ppm for the d-H_2 signal and was a defining feature of this compound. Two apparent triplets at 3.84 ppm and 3.69 ppm corresponded to the 3'-H_2 signals of the piperazine ring. It should be noted that these were significantly broadened; and have been reported as they appear (Figure 52). They were not true triplets by virtue of the fact that the coupling constants were not the same. They did serve as a useful indicator of successful coupling to the secondary amine as there was no longer a plane of symmetry from the C1'-C4' position. Thus, while the preceding compound had two signals, the product had four. These peaks were more deshielded due to the adjacent carbonyl group, compared to the sister 2' signals. The HSQC data showed that the carbons correlated to these signals were not split by fluorine, supporting the assignment described here.

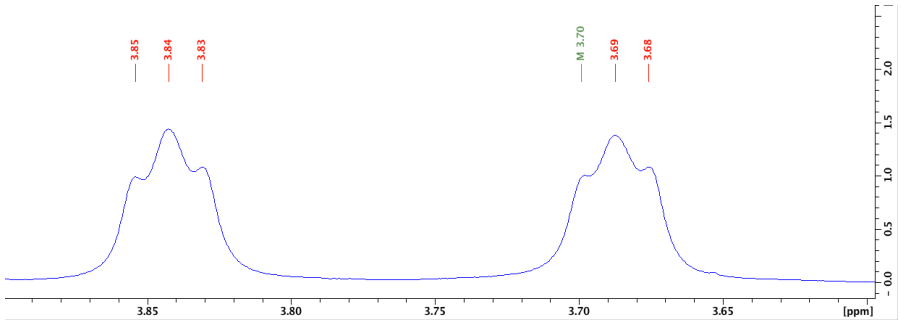

Figure 52. Piperazine signals for compound **144**.

A multiplet between 3.44-3.39 ppm for the a-H signal of the cyclopropyl preceded the remaining two apparent triplets at 3.26 and 3.20 ppm assigned for the 2'-H_2 protons. The b' and i'-H_2 alkyl groups appeared as an intermingled multiplet between 2.44-2.35 ppm integrating for 4. Similarly, the c' and h'-H_2 groups were sufficiently different from the main alkyl chain to appear as a separate multiplet between 1.74-1.64 ppm. The remaining d', e', f', and g'-H_2 signals overlapped the e-H_3 and one of the cyclopropyl b-H_2 signals to form a large coalesced multiplet between 1.41-1.30 ppm integrating for 13 protons. ^{13}C NMR showed a deshielded doublet at 173.1 ppm (J_{CF} = 1.0 Hz) that

appeared for the carbonyl of the C4, followed by four non-split signals at 172.7 ppm, 171.9 ppm, 165.9 ppm, and 159.0 ppm for the remaining carbonyl groups. A doublet occurred at 153.5 ppm (J_{CF} = 247.0 Hz) for the C6 position, whilst another doublet occurred at 144.2 ppm (J_{CF} = 10.0 Hz) for the C7 position followed by 123.6 ppm (J_{CF} = 7.0 Hz) for the C4a quaternary carbon. A further doublet at 113.6 ppm (J_{CF} = 23.0 Hz) indicated the aromatic C5 whilst a doublet at 105.2 ppm (J_{CF} = 3.0 Hz) was allocated to the C8 position. The piperazine ring carbon atoms were distinct as the C2' experienced effects from the F atom whereas the C3' carbon atoms did not. The C2' piperazine ring generated two doublets at 50.8 ppm (J_{CF} = 6.0 Hz) and 49.7 ppm (J_{CF} = 3.0 Hz) respectively. In total, 37 carbons were observed (counting doublets as one). This was correct for a compound with the formula $C_{38}H_{43}FN_4O_7$ where the cyclopropyl Cb signals were equivalent and thus showed only as a single observable peak. The $^{19}F\{^1H\}$ spectral data contained a single peak at -123.9 ppm, as expected for the proton decoupled NMR. This indicated that only one fluorine containing product had been isolated after purification. IR showed an absorption at 2928 cm^{-1} and 2851 cm^{-1} for the CH_2 and CH_3 groups, followed by strong bands at 1720 cm^{-1}, 1682 cm^{-1} and 1615 cm^{-1} for three of the five the carbonyl groups. The spectrum was complex, as expected, and it was highly likely the remaining carbonyl groups were hidden under the aforementioned absorptions. A high-resolution accurate mass of 697.3189 $[M+H]^+$ was obtained. RP-HPLC alongside the NMR evidence indicated that the product had 97% purity.

To liberate the carboxylic acid moiety, lithium hydroxide (LiOH) monohydrate was used as a strong base to hydrolyse the ester, releasing methanol as the side product. The hydroxide anion acts as a nucleophile to attack the electropositive carbonyl of the ester. The tetrahedral intermediate loses the methoxide ion to reform the carbonyl bond and generate the acid. The methoxide anion is a good leaving group due to its ability to stabilise the negative charge. The anion can rapidly pick up a proton from the environment to form its corresponding alcohol.

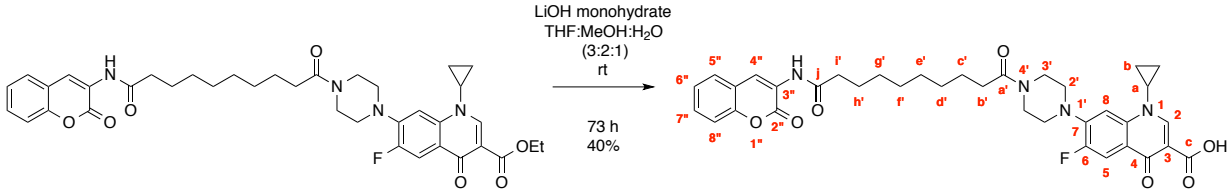

Scheme 81. Synthesis of 1-cyclopropyl-6-fluoro-4-oxo-7-(4-{9-[2-oxo-2H-chromen-3-yl)carbamoyl]nonanoyl}piperazin-1-yl)-1,4-dihydroquinoline-3-carboxylic acid.

Compound **145** was isolated as a cream powder in 40% yield (Scheme 81). ^{1}H NMR showed a downfield singlet at 14.9 ppm ascribed to the carboxylic acid, indicating that the deprotection was successful. Further evidence was provided by the lack of a quartet and triplet in the spectra. A second singlet occurred at 8.76 ppm and was attributable to the 2-H, followed closely by the coumarin 4"-H at 8.69 ppm. The NH showed itself as a broad singlet at 8.06 ppm. The remaining aromatic protons appeared as a doublet at 8.03 ppm (1 H), and two multiplets at 7.50-7.42 ppm (2 H) and 7.37-7.28 ppm (3 H) and accounted for all 6 aromatic protons present in the final product. As observed with the parent compound, the 3'-H_2 piperazine signals appeared as apparent triplets at 3.87 ppm and 3.72 ppm followed by the a-H of the cyclopropyl group as a multiplet at 3.57-3.51 ppm. The remaining 2'-H_2 apparent triplets occurred at 3.35 ppm and 2.39 ppm. Two triplets were seen for the b' / i'-H_2 at 2.43 ppm and 2.38 ppm. The c' and h'-H_2 signals were merged due to their similar environment and produced a multiplet at 1.75-1.67 ppm. The remaining alkyl chain was a coalesced multiplet at 1.42-1.33 ppm accounting for the d', e', f', g'-H_2 which overlapped a b-H_2 signal of the cyclopropyl group to give a total integration of 10 protons. The remaining b-H2 signal was assigned to an upfield multiplet at 1.22-1.18 ppm. ^{13}C NMR showed the C4 carbonyl was a doublet at 177.3 ppm (J_{CF} = 2.0 Hz) and the remaining carbonyls were accounted for at 172.7 ppm, 172.0 ppm, 167.0 ppm, and 159.0 ppm, a characteristic region for this type of signal. The C6 showed itself as a doublet at 153.7 ppm (J_{CF} = 248.0 Hz), followed by the C7 doublet at 145.6 ppm (J_{CF} = 10.0 Hz) and the C4a position at 120.5 ppm (J_{CF} = 8.0 Hz). The aromatic C5 position was ascribed to a doublet at 112.8 ppm (J_{CF} = 23.0 Hz) and the C8 at 105.2 ppm. The final piperazine C2' signals were split at 50.5 ppm (J_{CF} = 6.0 Hz) and 49.6 ppm (J_{CF} = 3.0 Hz). The remaining carbons were well resolved giving a total of 36, with the Cb carbons being equivalent. This accounted for all the carbon atoms in a compound with the formula $C_{36}H_{39}FN_4O_7$. ^{19}F{^{1}H} NMR proton decoupled showed a singlet at -121.1 ppm which indicated only one fluorine containing product had been obtained. This was very similar to the antecedent compound. Due to the need to conserve this sample for biological testing no IR or melting point analysis was performed. A corroborating high-resolution accurate mass of 659.2874 was found $[M+H]^+$. The purity as judged by RP-HPLC was 98%.

To establish the effect, if any, of the coumarin on DNA gyrase activity it was necessary to synthesise two control compounds. Aniline **146** was selected to confirm whether the binding affinity was driven by the ability of the aminocoumarin to bind to GyrA. It was predicted hydrogen bonding from the exocyclic carbonyl group would be crucial for this binding to the aminocoumarin pocket. There also was a need to establish the effect of linker introduction on quinolone activity. Consequently, this would allow us to attribute any observed activity to the aminocoumarin scaffold as opposed to a non-specific aromatic effect.

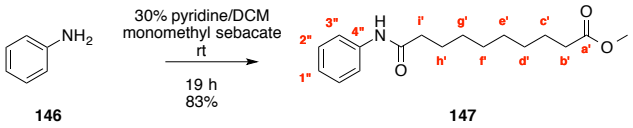

Scheme 82. Synthesis of methyl 9-(phenylcarbamoyl)nonanoic acid.

Commercially available aniline **146** was coupled to monomethyl sebacate using the previously validated peptide coupling conditions (Scheme 82).[273] This procedure worked well with a high yield of 83%. Compound **147** was isolated as a colourless powder. ^{1}H NMR showed a singlet integrating for 1 H at 7.57 ppm for the NH proton, as indicated by HSQC analysis. The remaining signals in this region were for the aromatic protons. Interestingly, they appeared as apparent triplets at 7.29 ppm and 7.07 ppm. The signals were broad, indicating a dynamic self-association, most likely with the linker (Figure 53) which due to its flexible nature, can wrap back on itself.

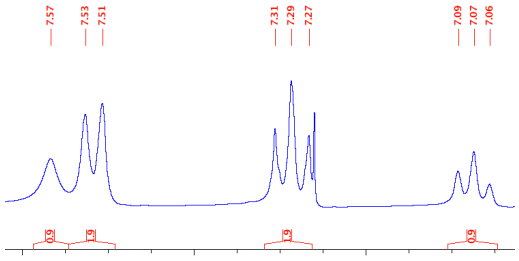

Figure 53. Inter/intra molecular hydrogen bonding phenomenon.

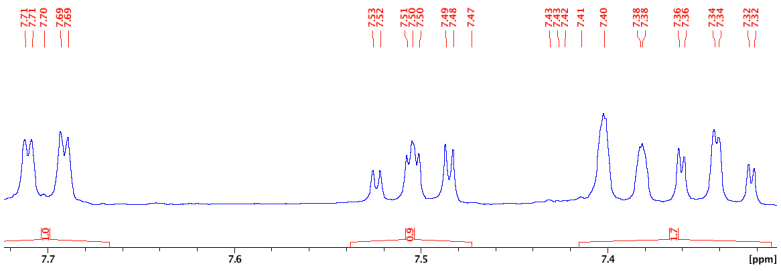

Figure 54. Improved resolution of peaks using wet DMSO solvent.

Alternatively, the compound could have been aggregating with other molecules of itself i.e. in an intermolecular fashion. The broad signals were reduced in the presence of wet DMSO compared to anhydrous $CDCl_3$ (Figure 54). This was ascribable to the presence of water as indicated by the proton NMR at 3.33 ppm. Water molecules can hydrogen bond to the compound and diminish the inter/intra-molecular hydrogen bonding phenomenon from occurring. Although chloroform itself is hygroscopic, the spectrum was obtained using a dry ampoule. However, the spectrum indicated that no water was present. Consequently, the broadened signals were therefore not true triplets.

Averaging of the spectra by the experimental parameters caused the loss of resolution due to the exchange phenomenon. Due to second order coupling effects, the true splitting pattern was highly complex being an AA'BB'C system with similar chemical shifts for each coupled interacting nuclei. The aromatic had a plane of symmetry running through the C1' and C4' positions. Assignments have been made according to how the signals appeared in the NMR spectra. The remaining portion of the compound in $CDCl_3$ can be assigned as a prominent singlet at 3.65 ppm for the methyl group. The alkyl chains formed overlapping multiplets between 2.36-2.28 ppm (4 H), 1.73-1.66 ppm (2 H), 1.62-1.56 ppm (2 H) and 1.36-1.26 ppm (8H). The ^{13}C NMR displayed 15 resolved signals, the aromatic core had equivalence and thus, only 4 signals instead of 6 were observed. Lastly, two carbons of the alkyl chain were also chemically and magnetically equivalent. This was attributed to the Cf' and Ce' in the centre of the chain which experienced an identical environment giving a single isochronous chemical shift. IR analysis showed a strong absorption at 3359 cm^{-1} assigned to the CONH, the CH_2 and CH_3 appearing between 2927-2849 cm^{-1} and two carbonyl signals were observed at 1713 cm^{-1} and 1682 cm^{-1}. A correct high-resolution accurate mass of 292.1905 was found $[M+H]^+$.

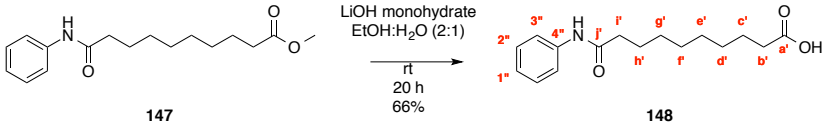

Scheme 83. Synthesis of 9-(phenylcarbamoyl)nonanoic acid.

The methyl ester **147** was de-protected using lithium hydroxide monohydrate similar to the previously synthesised coumarin hybrid (Scheme 83). A slight modification was made to the solvent system with EtOH and water being utilised in a 2:1 ratio. Similar compounds have been successfully de-protected with these conditions.[274] Compound **148** was isolated as a colourless solid after being recrystalised from EtOH and washed with hexane (66%). Having observed the broadened signals for the parent compound, MeOD was intentionally chosen as a protic NMR solvent to try and obtain the best resolution of the aromatic signals. ^1H NMR showed complex multiplets for the aromatic AA'BB'C system at 7.54-7.52 ppm (2H), 7.31-7.26 ppm (2 H) and 7.09-7.05 ppm (1 H). The loss of the methyl peak was apparent with no singlet integrating for 3 H, indicating the successful removal. Two triplets appeared at 2.36 ppm and 2.27 ppm (J = 8.0 Hz), attributed to the b' and i'-H_2 positions of the linker. Two multiplets appeared at 1.73-1.66 ppm (2 H) and 1.64-1.56 ppm (2 H) for the c' and h'-H_2 peaks. The remaining alkyl signals were under one large multiplet at 1.41-1.32 ppm (8 H). ^{13}C NMR showed 14 resolved signals as anticipated. IR showed the CONH at 3300 cm^{-1} overlapping a broad OH absorption. Furthermore, CH_2 signals appeared between 2916-2848 cm^{-1}. Lastly, two carbonyl signals showed themselves at 1689 cm^{-1}

and 1659 cm^{-1}. A corroborating high-resolution accurate mass of 276.1600 $[M-H]^-$ was found using electrospray ionisation in negative mode.

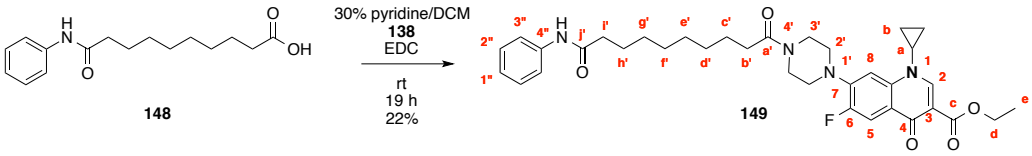

Scheme 84. Synthesis of Ethyl 1-cyclopropyl-6-fluoro-4-oxo-7-{4-[9-(phenylcarbamoyl)nonanoyl]piperazine-1-yl}-1, 4-dihydroquinoline-3-carboxylate.

With the free carboxylic acid terminus available, it was possible to couple the ester-protected ciprofloxacin fragment **138** to form the penultimate aromatic control compound. After purification by flash column chromatography, compound **149** was obtained as a cream solid (Scheme 84). ^{1}H NMR in $CDCl_3$ showed the most deshielded proton was the 2-H position at 8.54 ppm as a singlet followed by an aromatic proton in the 5-H position. This was *ortho* to the fluorine and has a large coupling constant of 16.0 Hz. Subsequently, signals from the aniline aromatic moiety appeared as an apparent doublet at 7.52 ppm for the 3”-H, and an apparent triplet at 7.31 ppm for the 2”-H, which overlapped the NH signal. The remaining ciprofloxacin aromatic 8-H signal appeared at 7.26 ppm (J = 8.0 Hz), consistent for *para* coupling. The last aromatic proton was correlated to the 1”-H aniline aromatic, and appeared as an apparent triplet at 7.09 ppm. The d-H_2 group of the ester occurred, as expected, as a prominent quartet at 4.38 ppm. This was followed by the two 3’-H_2 groups of the piperazine ring as very broadened apparent triplets at 3.85 ppm and 3.69 ppm. Next appeared a multiplet for the a-H of the cyclopropyl ring between 3.44-3.38 ppm. Subsequently, the remaining 2’-H_2 alkyl groups of the piperazine appeared as another set of broadened apparent triplets at 3.26 ppm and 3.21 ppm. The linker showed as multiplets between 2.39-2.32 ppm (4 H) and 1.74-1.62 ppm (4 H). These were in the correct downfield region for alkyl chains, and were interspersed with a true triplet at 1.41 ppm (J = 8.0 Hz) for the e-H_3 portion of the ethyl ester. The signals for the remaining core of the linker all overlapped due to their very similar environment to form a large coalesced multiplet between 1.38-1.29 ppm (d’, e’, f’, g’-H_2). Crucially, one of the cyclopropyl b-H_2 groups was also under this multiplet accounting for the integration of 10 H. The remaining cyclopropyl d-H_2 was assigned to the upfield multiplet between 1.15-1.11 ppm. The $^{19}F\{^1H\}$ NMR showed one singlet at -124.0 ppm indicating only one fluorinated product was present. The most deshielded signal in the ^{13}C NMR at 173.2 ppm was ascribable to the carbonyl of the C4 position which was split to give a doublet (J_{CF} = 2.0 Hz). The amide carbonyl groups were at 172.0 ppm and 171.9 ppm. The least deshielded carbonyl was the Cc of the ciprofloxacin fragment at 165.6 ppm. The C6 position was characteristic at 153.3 ppm with its large J_{CF} of 247.0 Hz. The C7 was a doublet at 144.1 ppm (J_{CF} = 10.0 Hz), whereas the C4a doublet appeared at 123.4 ppm (J_{CF} = 7.0 Hz). The C5 and C8 positions were assigned based on their relative

positions in the ^{1}H NMR, *J* values and observed coupling in the HSQC. The more upfield C5 was at 113.3 ppm (J_{CF} = 23.0 Hz) whereas the C8 position appeared at 105.2 ppm with a much smaller coupling (J_{CF} = 2.0 Hz). Lastly, the two piperazine signals of 2' were also split at 50.5 ppm (J_{CF} = 4.0 Hz) and 49.7 ppm J_{CF} = 3.0 Hz.). The linker, as expected for the C5" and C6" carbons was equivalent, giving a single peak at 29.2 ppm. The protons for the cyclopropyl group, were not in different environments, thus the carbons are equivalent, giving a single signal at 8.2 ppm. A further 20 resolved carbon signals, as expected, are seen giving a total of 31 carbons. Taking into account splitting (counted as one) and equivalent environments this was the correct number for a molecule with 35 carbons. IR analysis showed an absorption at 3286 cm^{-1} for the CONH, with alkyl groups appearing between 2923-2853 cm^{-1}. Only two carbonyl absorptions could be seen clearly, at 1732 cm^{-1} and 1615 cm^{-1}. A high-resolution accurate mass of 619.3290 $[M+H]^+$ was observed.

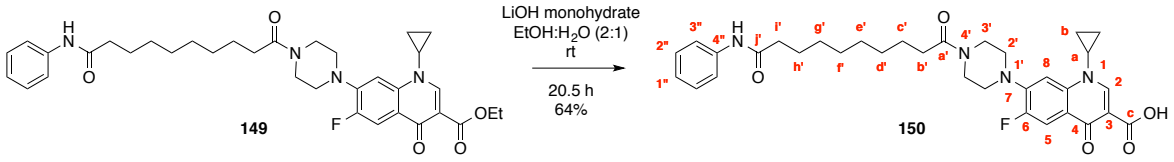

Scheme 85. Synthesis of 1-cyclopropyl-6-fluoro-4-oxo-7-{4-[9-(phenylcarbamoyl)nonanoyl]piperazin-1-yl}-1,4-dihydroquinoline-3-carboxylic acid.

Deprotection of the **149** using a mixture of ethanol and water with lithium hydroxide monohydrate gave the desired final compound **150** as a cream powder in 64% with no further purification necessary (Scheme 85). ^{1}H NMR in DMSO showed a very downfield signal at 15.19 ppm (1 H) typical of a carboxylic acid, followed by the NH (1 H) as a broad singlet at 9.84 ppm. The 2-H occurred as a singlet at 8.67 ppm. The remaining aromatic protons occured in the appropriate region; a true doublet appeared at 7.94 ppm (J_{CF} = 13.2 Hz) for the 5-H signal. An apparent doublet at 7.58 ppm (3 H), was comprised of two signals from the aniline and one from the 8-H ciprofloxacin. The apparent triplet at 7.27 ppm (2 H) and 7.01 ppm (1 H) are consigned to the remaining aniline protons. Extra validation of the successful deprotection comes from the lack of a quartet and triplet for the ester. A multiplet appeared at 3.85-3.79 ppm for 1 H indicative of the a-H of the cyclopropyl moiety. The piperazine 3'-H_2 were represented by a broadened apparent triplet at 3.68 ppm. This was poorly resolved and integrated for 4 H. The remaining portion of the 2'-H_2 piperazine overlaped a residual water signal, and showed as a broad multiplet from 3.36-3.29 ppm. The alkyl linker had well resolved triplets at 2.37 ppm and 2.29 ppm for the b' and i'-H_2 positions. The c' and h'-H_2 positions were multiplets from 1.61-1.51 ppm (4 H) with the remaining central core of the linker forming the larger coalesced multiplet at 1.35-1.28 ppm. Also, a b-H_2 signal from the cyclopropyl group was concealed by this multiplet, accounting for the total integration of 10 H. The last multiplet at 1.21-1.17 ppm for 2 H, was ascribed to the remaining protons of the cyclopropyl

group. Proton decoupled $^{19}F\{^{1}H\}$ NMR gave one singlet at -121.8 ppm, indicating only one fluorine containing product was present. ^{13}C NMR showed the C4 as a doublet at 176.3 ppm (J_{CF} = 8.0 Hz), subsequently this was followed by the C6 signal at 153.0 ppm with its characteristically large *J* value (J_{CF} = 250.0 Hz). The next doublet carbon occurred at 144.9 ppm and this was ascribable to the C7 position (J_{CF} = 10.0 Hz). The C4a doublet was next at 118.8 ppm (J_{CF} = 8.0 Hz), followed by the C5 *ortho* to the fluorine at 111.0 (J_{CF} = 23.0 Hz). The C8, consistent with the previous NMR, appeared at 106.6 ppm (J_{CF} = 2.0 Hz), followed by the piperazine C2' as doublets at 49.7 ppm and 49.3 ppm (J_{CF} = 4.0 Hz). The central linker C5" and C6" were equivalent and thus showed as a double height signal at 28.8 ppm. The cyclopropyl b-H_2 gave a single signal at 7.6 ppm. The remaining 20 carbons were well resolved giving a total of 28, taking into account split doublets (counted as one) and the equivalence of the molecule. This was one short of the 29 carbons expected for a compound with the formula $C_{33}H_{40}FN_4O_5$. The DEPT 135 data accounts for all of the protonated signals. Therefore, the missing carbon was a quaternary signal. A high-resolution accurate mass of 659.2874 $[M+H]^+$ was observed. Due to the value of the final sample, with 38 mg synthesised, IR and destructive MP analysis were not performed as the compound was conserved for biological testing. RP-HPLC and NMR data indicated the product had 98% purity.

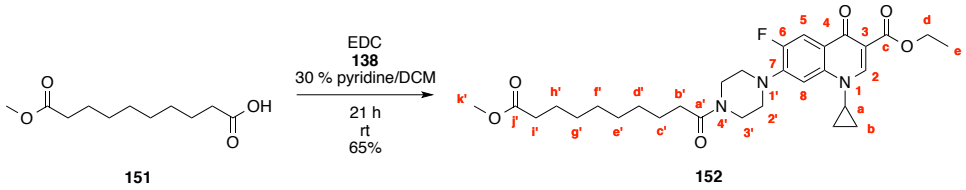

Scheme 86. Synthesis of Ethyl 1-cyclopropyl-6-fluoro-7-[4-(10-methoxy-10-oxodecanoyl)piperazin-1-yl]-4-oxo-1,4-dihydroquinoline-3-carboxylate.

The final control compound to synthesise was a ciprofloxacin fragment with the commercially available alkyl linker **151** attached at the 7'-position but without the secondary fragment (Scheme 86). This would allow us to evaluate the consequence of attaching this substituent to the activity of the quinolone. Moreover, combined with the data from the aromatic control and contrasting with the effect of the coumarin moiety, this would allow analysis of the impact of different parts of the hybrid. Compound 1**52** was isolated after purification by flash column chromatography as a cream powder (65%). ^{1}H NMR showed the 2-H proton as a very downfield singlet at 8.50 ppm, followed by a doublet for the 5-H proton *ortho* to the fluorine at 8.02 ppm (J_{HF} = 13.2 Hz). The second aromatic *meta* to fluorine at 7.25 ppm (J_{HF} = 8.0 Hz) assigned to the 5-H position also appeared as a doublet overlapping the residual solvent peak ($CDCl_3$). The d-H_2 of the ester appeared as a prominent quartet at 4.37 ppm, followed by two apparent triplets for the 3'-H_2 piperazine at 3.84 ppm and 3.68 ppm respectably. A lone singlet at 3.65 ppm (3 H) for the f-H_3 of the linker was prominent, followed by a multiplet at 3.47-3.38 ppm ascribed to the a-H of the cyclopropyl ring. The remaining

two multiplets of the 2'-H_2 piperazine ring showed as apparent triplets at 3.25 ppm and 3.20 ppm. The b' and i'-H_2 protons appeared as triplets at 2.36 ppm and 2.29 ppm (J = 8.0 Hz). A multiplet integrating for 4 H from 1.68-1.57 ppm represented the c' and h'-H_2. A large triplet at 1.39 ppm with a correct J value of 8.0 Hz for reciprocal coupling to the d-H_2 signal, was attributed to the remaining CH_3 of the ethyl ester. A large coalesced multiplet occurred at 1.35-1.29 ppm (10 H) for the remaining alkyl chain of the linker and one of the b-H_2 signals of the cyclopropyl group. The last signal was assigned as the remaining b-H_2 signal showed as a multiplet at 1.15-1.11 ppm. Proton decoupled $^{19}F\{^{1}H\}$ NMR gave one singlet at -124.01 ppm indicating that only one fluorine containing product was present. ^{13}C NMR showed the C10" carbonyl group of the ester at 174 ppm was the most deshielded atom. A doublet followed at 173.1 ppm (J_{CF} = 2.0 Hz) for the C4 position. The C6 atom was also a doublet at 153.5 ppm (J_{CF} = 250.0 Hz) consonant with previously synthesised analogues. The C7 doublet signal appeared at 144.2 ppm (J_{CF} = 10.0 Hz), while the quaternary C4a signal occurred at 123.7 ppm (J_{CF} = 10.0 Hz) and the remaining aromatic C5 at 113.6 ppm (J_{CF} = 20.0 Hz). The remaining two doublets were ascribed to the C2' atoms at 50.7 ppm and 49.7 ppm (J_{CF} = 2.0 Hz). A further 20 individually resolved signals appeared in the spectrum giving a total of 29 carbons which when accounting for the split doublets and the equivalence of the cyclopropyl carbons was correct for a compound with the formula $C_{30}H_{41}FN_3O_6$. Unlike previously analysed compounds, the central d', e', f', g'-H_2 carbons were in sufficiently different environments to be individually resolved and non equivalent in the carbon NMR. IR gave strong carbonyl signals at 1713 cm^{-1}, 1646 cm^{-1} and 1615 cm^{-1}. A high-resolution mass of 558.2959 was observed $[M+H]^+$. RP-HPLC showed the compounds had 96% purity.

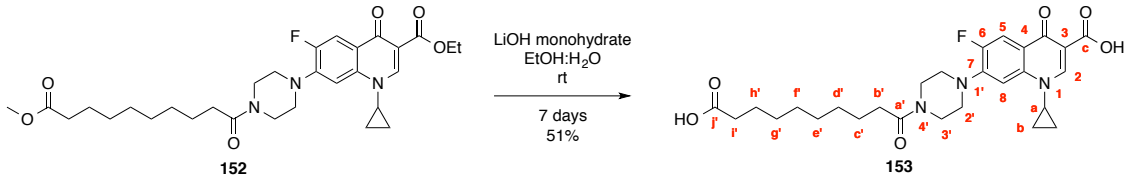

Scheme 87. Synthesis of 7-[4-(9-carboxynonanoyl)piperazin-1-yl]-1-cyclopropyl-6-fluoro-4-oxo-1,4-dihydroquinoline-3-carboxylic acid.

The final step was to deprotect both esters of **152** simultaneously using lithium hydroxide monohydrate to give compound **153** in a 51% yield (Scheme 87). ^{1}H NMR showed two singlets at 15.18 ppm and 11.96 ppm ascribed to the carboxylic acids. HSQC confirmed neither peak was correlated with a carbon signal. The 2-H followed at 8.66 ppm as a further singlet integrating for 1 H. A doublet at 7.92 ppm (J_{HF} = 12.0 Hz) and 7.57 ppm (J_{HF} = 8.0 Hz) was characteristic of the 5-H and 8-H protons respectively. The a-H of the cyclopropyl ring occurred as a multiplet between 3.84-3.79 ppm (1 H). Followed by one apparent triplet at 3.68 ppm assigned to the piperazine ring 3'-H_2 groups and a multiplet at 3.35-3.38 ppm ascribed to the 2'-H_2 that overlapped the water peak.

Two triplets at 2.36 ppm and 2.18 ppm (J = 8.0 Hz) were the b' and i'-H_2 of the linker. A multiplet between 1.53-1.47 ppm was for the c' and h'-H_2 of the linker. A large coalesced multiplet between 1.33-1.24 ppm integrating for 10 H, was the d', e', f' and g'-H_2 signals as well as an overlapping b-H_2 of the cyclopropyl group. The disappearance of a singlet for 3 H, as well as a quartet (2 H) and triplet (3 H) highlighted that the strong base had been successful in de-protecting both esters simultaneously to form the final compound. ^{13}C NMR showed a doublet at 176.2 ppm (J_{CF} = 2.0 Hz) ascribed to the C4 carbonyl group. The C6 carbon maintained its large J value of 248.0 Hz and appeared as a doublet at 152.9 ppm. The C7 group was also remained a doublet at 144.9 ppm (J_{CF} = 10.0 Hz), whilst the quaternary C4a doublet was at 118.7 ppm (J_{CF} = 8.0 Hz). The C5 aromatic showed as doublet at 110.9 ppm (J_{CF} = 20.0 Hz) whilst the C8 signal was at 106.4 ppm (J_{CF} = 2.0 Hz). The remaining piperazine C2' carbons which were not equivalent, as demonstrated by all the analogues, still gave two doublets at 49.7 ppm (J_{CF} = 5.0 Hz) and 49.2 ppm (J_{CF} = 3.0 Hz). The Ce' and Cf' of the linker were in sufficiently similar environments to show as an equivalent peak at 28.8 ppm. The two Cb carbons were also equivalent at their normal 7.6 ppm. The remaining 17 carbons were well resolved giving a total of 25 (counting doublets as one) that accounted for all of the signals in a product comprised of 27 carbon atoms. ^{19}F{^{1}H} NMR gave a single peak at -124.0 Hz indicating a single fluorinated product had been isolated. IR showed a broad absorption between 3600-2400 cm^{-1}, and three carbonyl absorptions at 1715 cm^{-1}, 1626 cm^{-1}, and 1614 cm^{-1}. A high-resolution accurate mass of 516.2497 $[M+H]^+$ was observed. RP-HPLC showed the purified compound had 96% purity.

4.06 Biological evaluation

Having completed the synthesis of the target hybrids it was necessary to evaluate their *in vitro* biological activity using the previously described supercoiling assay with *E. coli* gyrase. In the previous chapter no coumarins displayed any significant activity. The most simplistic aminocoumarin fragment had been screened at 50 μM. Therefore, the supercoiling assay was repeated at higher, although physiologically irrelevant, concentrations to determine the effect, if any, the coumarin fragment had on gyrase. Figure 55 below shows the results. Aminocoumarin **104** did not cause any detectable inhibition of enzyme supercoiling activity at a maximal concentration of 300 μM.

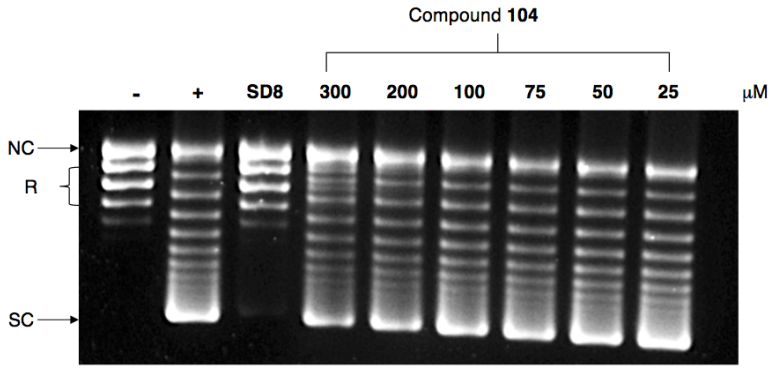

Figure 55. Effect of Compound **104** on DNA supercoiling by wild type *E. coli* gyrase. Relaxed pBR322 plasmid DNA is used as a negative control (-), and incubated in the presence of gyrase as a positive control (+). SD8 is used as a comparator at a concentration of 1 μM. NC indicates nicked circle DNA; R, relaxed DNA; SC, supercoiled DNA.

Subsequently, the ester-protected analogues **138**, **144**, **149** and **152** were evaluated (Figure 56). Only the ester protected ciprofloxacin **138** was able to inhibit supercoiling, albeit at a concentration of 50 μM to 10 μM with compared to its normal IC_{50} of ~0.5 μM. This demonstrates that whilst activity is retained, it is attenuated. It has been shown that in order for the quinolones to intercalate into DNA, the carboxylic acid portion forms vital contacts with serine and aspartic/glutamic acid residues as discussed in Chapter 1. This is mediated via a non-catalytic magnesium ion with an octahedral co-ordination sphere comprised of two oxygen and four water molecules. This phenomenon is termed the water-metal ion bridge. Efficacious binding is attributed to the free carboxylic acid that can delocalise a negative charge across the carbonyl group through resonance stabilisation. This effect is not possible with an ester. However, the presence of two carbonyl groups is predicted to retain a degree of co-ordination. The noted attenuated activity displayed by **138** supports this theory. The hybrid esters **144**, **149** and **152** show no effect on wild type *E. coli* gyrase at a maximal concentration of 100 μM.

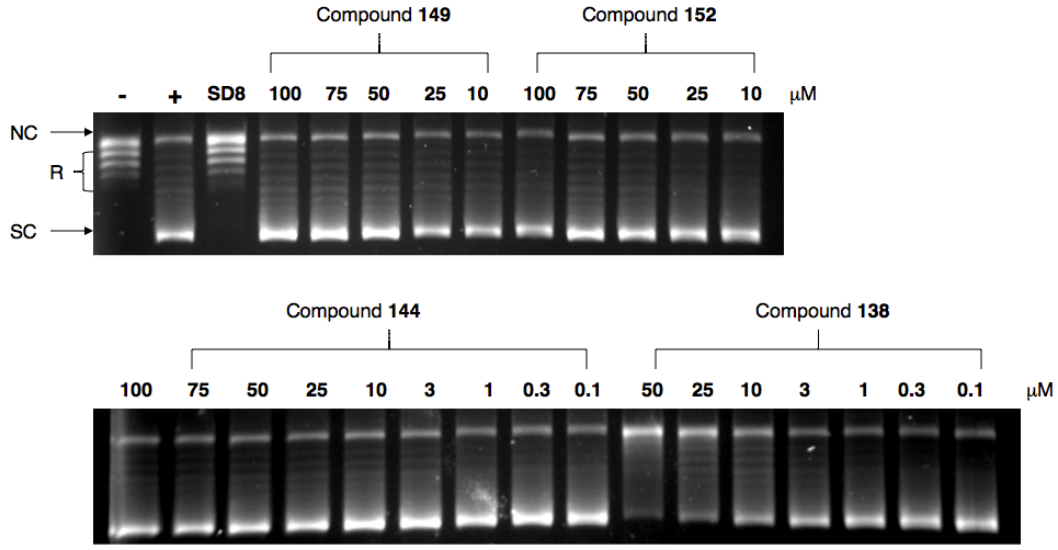

Figure 56. Effects of Compounds, **138**, **144**, **149** and **152** on DNA supercoiling by wild type *E. coli* gyrase. Relaxed pBR322 plasmid DNA is used as a negative control (-), and incubated in the presence of gyrase as a positive control (+). SD8 is used as a comparator at a concentration of 1 μM. NC indicates nicked circle DNA; R, relaxed DNA; SC, supercoiled DNA.

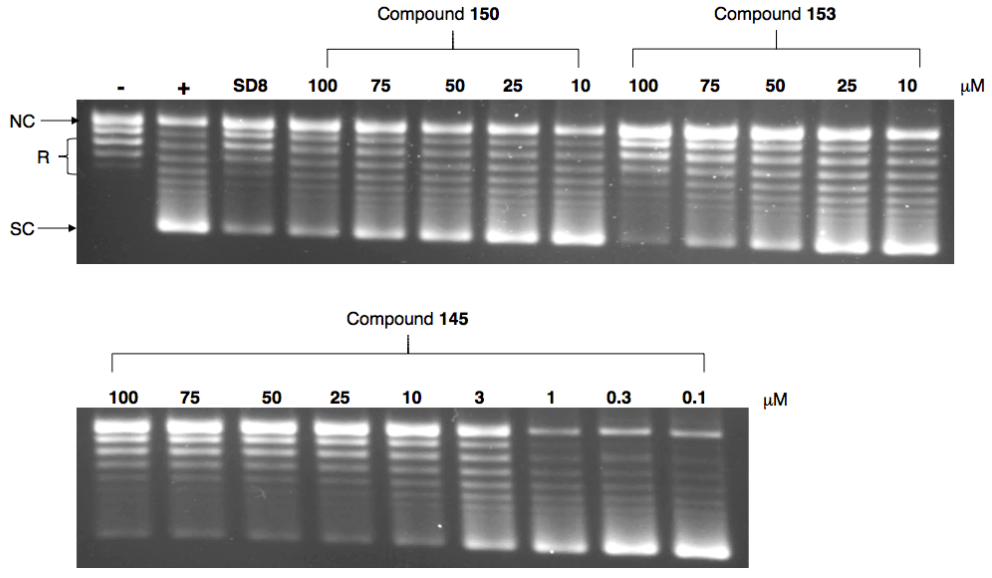

Figure 57. Effects of Compounds, **150**, **153** and **145** on DNA supercoiling by wild type *E. coli* gyrase. Relaxed pBR322 plasmid DNA is used as a negative control (-), and incubated in the presence of gyrase as a positive control (+). SD8 is used as a comparator at a concentration of 1 μM. NC indicates nicked circle DNA; R, relaxed DNA; SC, supercoiled DNA.

The effects of the compounds **145**, **150** and **153** on the supercoiling activity are shown in Figure 57. The aniline compound **150** has activity only at high concentrations from 100 μM to 75 μM when comparing the intensity of the supercoiling band to the negative control (-). This is a minor improvement over the ester protected sister analogue (**149**), suggesting that **150** cannot make favourable contacts in the coumarin binding site. Similarly, a moderate improvement in activity of the ciprofloxacin linker control **153** is observed with inhibition occurring from 100 to 50 μM. Strikingly, the introduction of a coumarin scaffold in compound **145** dramatically restores inhibitory activity. Potent inhibition can be seen from 100 μM to 10 μM, as exhibited by the lack of a supercoiling band. The compound has an IC_{50} of 3 μM, with complete supercoiling apparent at 0.3 μM. This assay data unequivocally attributes the restored activity to the coumarin moiety. These results demonstrate a favourable interaction when fragments **104** and **143** are combined that is not seen when a simple aromatic ring **146** is combined to **143**. This is in contrast to the poor inhibition displayed by each fragment individually. This implies that a synergistic effect is vital for the observed activity. After repeated freeze thawing, compound **145** degraded, losing its ability to inhibit gyrase. To confirm the results, the compound was re-synthesised and the assays repeated with same results observed.

Noting that the coumarin scaffold contributes to the inhibitory activity of the hybrid compound, it was necessary to explore the mode of action. The effect of the compounds **145**, **150** and **153** on the gyrase cleavage-religation equilibrium was investigated (Figure 58). The assay is carried out as previously described for the supercoiling reaction, with the addition of a termination step. Cessation of a reaction between gyrase and DNA in the presence of a quinolone inhibitor like ciprofloxacin by the addition of SDS and proteinase K results in cleaved DNA. The SDS and proteinase K denature the gyrase protein and cause the separation of the enzyme from the DNA. The cleaved DNA is a manifestation of the covalent bonds formed between the enzyme and DNA that are stabilised by a drug (such as ciprofloxacin), as described in the introduction. Experimentally, when supercoiled DNA is used as the substrate, this is represented by the appearance of a linear band. SD8 was used as a negative control, its ability to block DNA binding and prevent strand passage cycle taking place by stapling across the surface of the enzyme resulted in no linear band being visible. Ciprofloxacin **137** was used as positive control for comparison with strong linear bands visible from 3 μM to 0.3 μM. Linear bands are visible only at 100 μM to 75 μM for **150** and from 100 μM to 50 μM for **153.** Conversely, compound **145** displays a consistent linear band from 100 μM to 3 μM. The results demonstrate the ability of all the hybrids to stabilise cleaved DNA. The loss of the linear band occurs at approximately the same concentration as inhibition in the corresponding supercoiling assay. This is consistent with observations with ciprofloxacin which shows a correlation between supercoiling and cleavage stabilisation inhibitory concentrations.

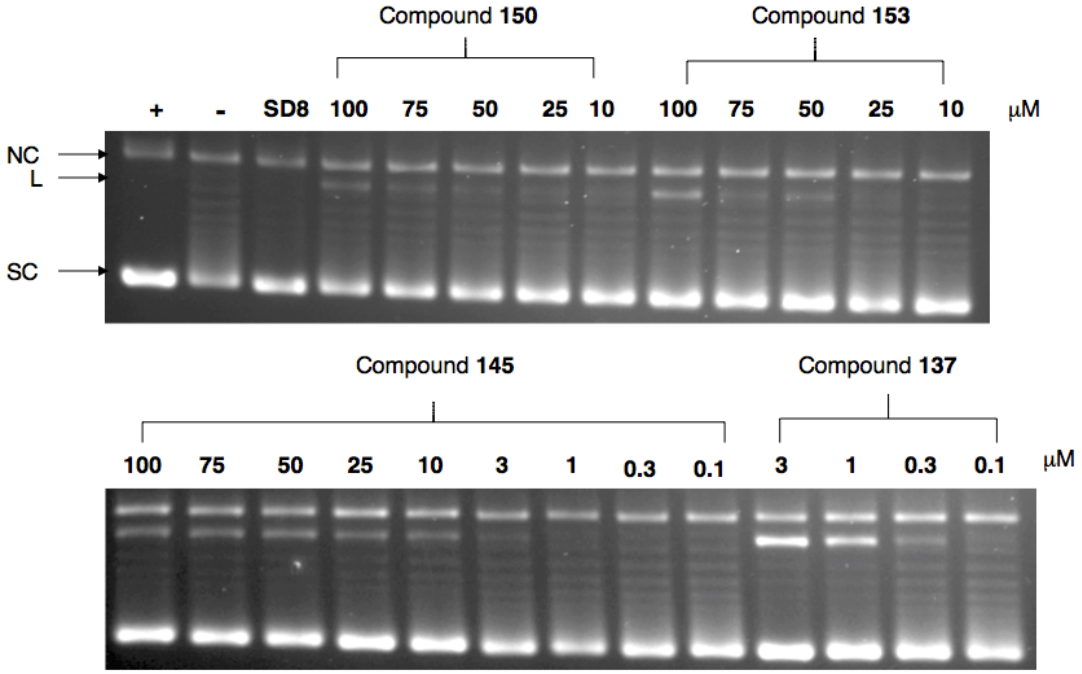

Figure 58. Effects of compounds **145**, **150** and **153** on cleavage complex formation by wild type *E. coli* gyrase in the absence of ATP. Supercoiled pBR322 plasmid DNA is used as a positive control (+), and incubated in the presence of gyrase as a negative control (-). SD8 is used as an additional control at a concentration of 1 μM. Ciprofloxacin **137** is used as a comparator. NC, nicked circle; L, linear band; SC, supercoiled DNA.

Lastly, the final compounds **145**, **150** and **153** were tested against DNA gyrase with a substitution from lysine42 to alanine. It was anticipated that a decrease in activity would be observed with the mutant enzyme, due to impaired binding by the coumarin chromophore. As a control experiment, the wild type and mutant enzymes were tested at the same time using the same serial dilutions. The results are shown in Figure 59 and Figure 60. Ciprofloxacin **137** and SD8 were used as comparators from 50 μM to 0.1 μM. There is inhibition from the asymmetric hybrid compound only at 50 μM and 25 μM. This is the same for both the wild type and mutant enzyme. Ciprofloxacin is unaffected by the mutant enzyme, as would be expected; conversely SD8 has less efficacy at inhibiting the lysine mutant with an IC_{50} of 3 μM compared to 0.3 μM in this wild type assay. This is consistent with previous reported observations. The decreased activity in both the wild type and the mutant is a strong indication that the stock solution of compound **145** had started to degrade. Thus the conclusions drawn from this data must be considered alongside future work.

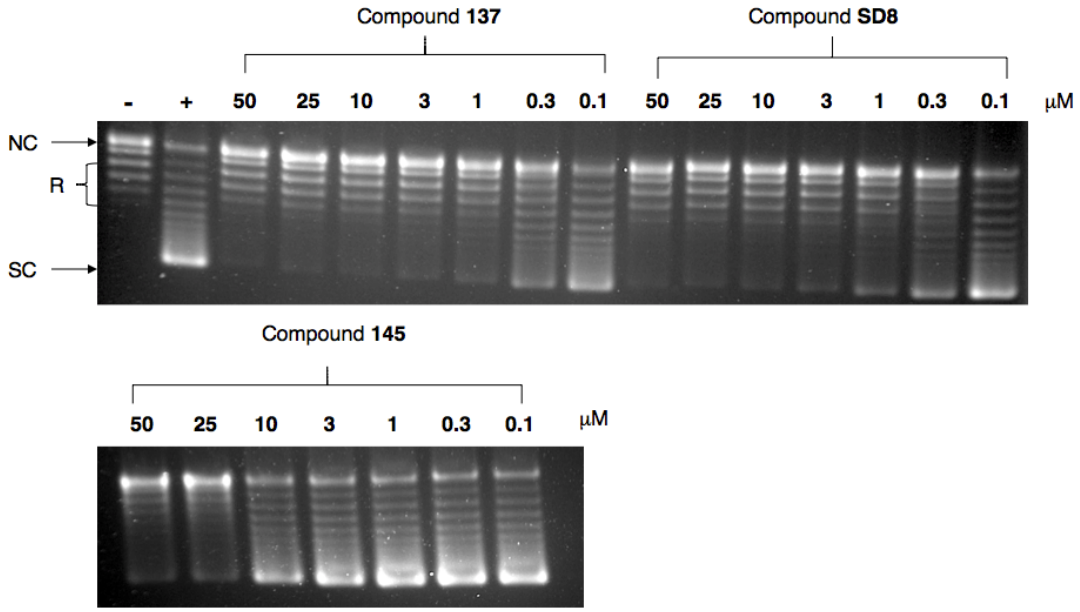

Figure 59. Effects of Compound **145** on DNA supercoiling by wild type *E. coli* gyrase. Relaxed pBR322 plasmid DNA is used as a negative control (-), and incubated in the presence of gyrase as a positive control (+). Ciprofloxacin **137** and **SD8** are used as comparators. NC indicates nicked circle DNA; R, relaxed DNA; SC, supercoiled DNA.

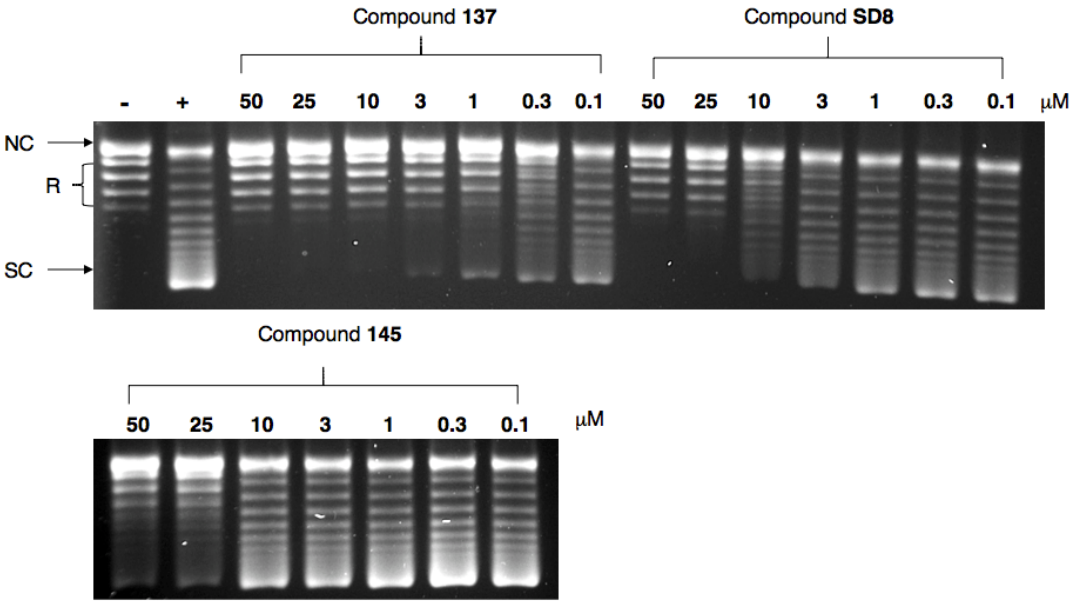

Figure 60. Effects of Compound **145** on DNA supercoiling by Lys42Ala mutant *E. coli* gyrase. Relaxed pBR322 plasmid DNA is used as a negative control (-), and incubated in the presence of gyrase as a positive control (+). Ciprofloxacin **137** and **SD8** are used as comparators. NC indicates nicked circle DNA; R, relaxed DNA; SC, supercoiled DNA.

4.07 Conclusions

Ten analogues were synthesised, purified and characterised with seven being biologically evaluated for their effects on DNA gyrase. The rational fragment based strategy utilised simple chemistry to generate six novel hybrids not previously described in the literature, driven by crystal structure data and inspired by SD8. This body of work supports findings that modification of the carboxylic acid is detrimental to quinolone activity. This is in agreement with the quinolones mode of action via a water-metal ion stabilisation with key amino acid residues from the carboxylic acid miety. Not unexpectedly, the ester protected ciprofloxacin fragment **138** retains some activity against gyrase. A degree of co-ordination of metal ions would still be permitted to take place from the two carbonyl groups. However, the results presented substantiate the favourable effect of having a free acid present. This extends to all final asymmetric hybrids tested, as seen with **145**, **150** and **153**. Strikingly, a coumarin moiety on its own possesses no intrinsic inhibition, but when coupled to ciprofloxacin via a 15 Å linker contributes to a significant restoration of inhibitory activity when included in the hybrid. This is the first example of a coumarin demonstrating an ability to have a synergistic effect on a quinolone inhibitory activity. Moreover, we have revealed this effect is, in part, mediated through stabilisation of ligated DNA. Thus all de-protected hybrids retained an ability to stabilise cleaved DNA and is noteworthy. Preliminary attempts were made towards screening these compounds against DNA gyrase with a mutation in the aminocoumarin pocket. However, due to possible degradation with the final compound further work is required. That said, as the inhibition is the same in both wild type and mutant, albeit at reduced efficacy, the change in one hydrogen-bonding residue may not be enough to drastically alter the effect of the hybrid. Furthermore, it highlights that it would be prudent to screen a wider concentration range as well as trying multiple mutant enzymes. Commensurate with previous coumarin-quinolone antibiotics, these results build upon earlier findings by investigating the effects on cleavage stabilisation. The lack of inhibition with the aniline and ciprofloxacin controls is rationalised as a function of poor binding to the coumarin pocket. However, to substantiate this theory more experimental data is required. A number of areas warrant further attention, this will be discussed in Chapter 5.

Chapter 5. Conclusions and future work

5.1 Overall conclusion and future work

The publication of the new crystal structure of SD8 bound to DNA gyrase provided an unprecedented level of information regarding the bonding interactions made to the target enzyme.[145] This thesis focused on efforts towards the structural components of SD8 as well as generating and screening a range of coumarin analogues. The eventual aim was to take a lead compound forward and produce a hybrid inhibitor.

The synthesis of a novel isomerised pericyclic adduct **62** provides a crucial platform from which further enatioselective synthesis can take place. A natural progression is to continue efforts towards the total synthesis of the PK. The reported biological evaluation of the novel 7-oxo-SD8 illustrates that changing a single functional group on the PK has a deleterious effect on inhibitory activity.[146] The noted good inhibition of SD4, which has structural parity with SD8 except for the chlorine substituent, indicates a halogen is not a prerequisite for efficacious binding to the AC site. This should be carefully considered when designing future rational inhibitors.

A diverse set of 23 AC compounds were synthesised and evaluated using an enzyme supercoiling assay. It was demonstrated that a wide variety of salicylaldehydes can be used as starting reagents in the modified Perkin reaction. Furthermore, the widespread resilience of the AC chromophore to highly acidic conditions provides a streamlined route to accessing a free amine via deacetylation.

Using the well-studied inhibitor ciprofloxacin a novel coumarin hybrid **145** was successfully synthesised and evaluated alongside appropriate controls **150** and **153**. This work shows for the first time that the introduction of the coumarin chromophore **104** unequivocally contributes to observed inhibition of DNA gyrase. The exact mode of action needs further investigation. Preliminary results indicated that cleavage stabilisation is still able to take place. This is an exciting step towards the development of inhibitors of DNA gyrase and represents a proof of principle fragment based approach to the design of novel compounds. The basic coumarin framework provides a starting point from which future SAR can now be undertaken. The work can progress in two fundamental directions. Firstly, to investigate linker length and its contribution to activity. Secondly, to investigate substitution of the basic coumarin for functionalised coumarins.

Elucidation of the mechanism of action and an exploration of the hybrids ability to overcome quinolone resistance could be achieved through testing against mutant DNA gyrase enzymes. Mutations to Arg91, Lys42, His45 and Ser172 should provide substantial evidence of weather or not the coumarin binds to the same pocket as SD8. Whilst mutations to the serine/glutamic acid residues in the QRDR would check for an ability to overcome quinolone resistance. The biological assays conducted so far are *in vitro*, examination using an *in vivo* model would provide insights as

to the lead compounds ability to traverse cell membranes. Whilst the hybrid is potent in the supercoiling assays, this may not necessarily translate into *in vivo* activity. The molecule is of a medium molecular weight, and relatively hydrophobic. This work would be crucial alongside the SAR for optimising the hybrid.

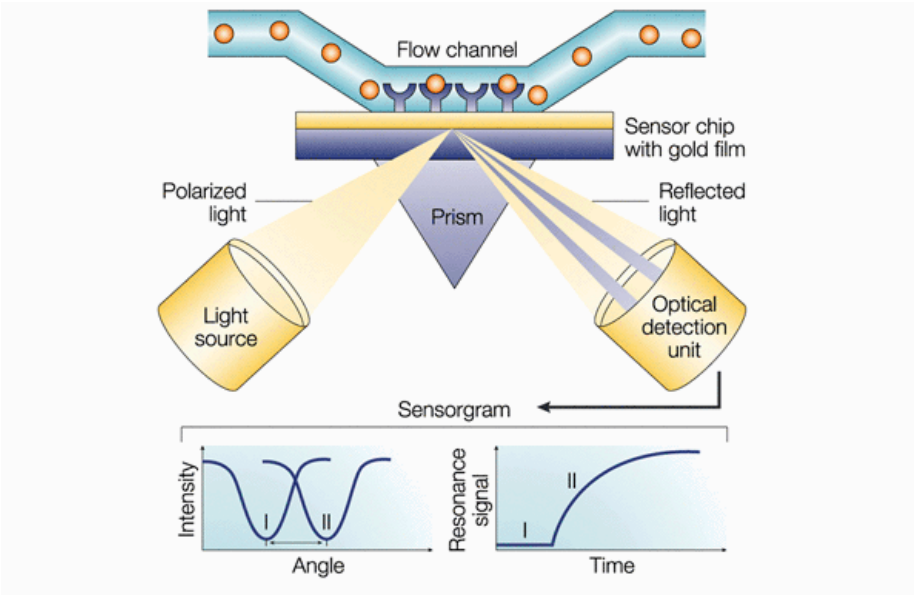

Figure 61. Surface plasmon resonance.[275]

A technique that could facilitate the mechanistic understanding of the hybrid compound is to use surface plasmon resonance (SPR). This is a real time experiment whereby polarised light is focused onto a gold-coated glass sensor (Figure 61). The light is reflected off the surface and hits a photo-detector. An enzyme can be immobilised to the surface of the gold and a drug flowed across the surface of the enzyme. If the drug binds to the enzyme a change in mass of the surface will take place at the interface resulting in a change in the reflected signal.[275] This is measured and plotted as a function of time to give a sensorgram. Thus, a binding event can be seen. This is a very sensitive technique and even small changes at the molecular surface will shift the SPR curve.

Finally, efforts towards obtaining a crystal structure of the hybrid bound to the target DNA gyrase enzyme could be pursued. This would provide detailed information of the binding orientation of the hybrid and would expedite the design of analogues based on the lead compound.

Chapter 6. Experimental

^{1}H and ^{13}C NMR spectra were obtained in Fourier Transform mode on a Bruker™ Ultrashield PLUS 400 spectrometer operating at a normal frequency of 400 MHz using the specified deuterated solvent. All spectra have been calibrated to the residual deuterated solvent peak and chemical shifts reported in ppm. All fluorine NMR experiments are externally referenced to trichlorofluoromethane. Spectra were analysed and processed using Topspin 3.2 software. Multiplicities in the NMR are described as: br s = broad singlet, d = doublet, dd = doublet of doublets, t = triplet, td = triplet of doublets, q = quartet, m = multiplet, br = broad, app = apparent; coupling constants are reported in Hz. Melting points were recorded using capillary tubes on a Mel-Temp™ electro thermal melting point apparatus. Infrared spectra were recorded from neat samples using a Perkin-Elmer Spectrum BX FT-IR spectrometer and analysed using Spectrum v5.3.1 software. RP-HPLC were obtained using a Agilent 1200 apparatus with a Eclipse XDB-C18 column (5 μM, 4.6 x 15 mm) running a gradient over 20 minutes. MeOH:H_2O (5:95) to MeOH:H_2O (95:5) at a flow rate of 1mL/min. Wavelength of detection as a 214 nm and 254 nm. Accurate masses were provided by the EPSRC National Mass Spectrometry Service in Swansea.

6.1 Chromatography

Thin layer chromatography was performed using Merck aluminium plates coated with 0.2 mm silica gel-60 F_{254}. After elution TLC plates were visualised under UV light. Flash chromatography was performed using silica gel (particle size 60 μM) unless otherwise specified all samples were dry loaded onto silica prior to separation. Chromatography was performed using a Biotage Isolera ACI™ with wave monitoring set to 254 nm and 214 nm.

6.2 Reagents and Glassware

All chemicals used were purchased from Sigma-Aldrich or Thermo-Fisher Scientific. All glassware was oven dried prior to use. Anhydrous solvents were commercially purchased and assumed to conform to manufacturers specifications. All water for reagents, reactions and assays was purified using a Merk Millipore Milli-Q direct water purification system.

6.3 Biological Procedures

E. coli gyrase supercoiling and cleavage assay kits were purchased from Inspiralis. Gyrase was prepared from overexpressing strains JMtacA and JMtacB and supplied as an A_2B_2 complex in dilution buffer. Dilution buffer consisted of 50 mM Tris.HCl (pH 7.5), 100 nM KCl, 2 mM DTT, 1 mM EDTA and 50% (w/v) glycerol. Supercoiling assay buffer consisted of 35 mM Tris.HCl (pH 7.5), 24 mM KCl, 4 mM $MgCl_2$, 2 mM DTT, 1.8 mM spermidine, 1 mM ATP. The same dilution buffer was utilised for cleavage stabilisation assays. Cleavage assay buffer consisted of 35 mM Tris.HCl (pH 7.5), 24 mM KCL, 4 mM $MgCl_2$, 2 mM DTT, 1.8 mM spermidine, 6.5% (w/v) glycerol, 0.1 mg/mL

albumin. All enzymes were stored at -80°C. Supercoiled or relaxed pBR322 DNA was supplied with the assay kits. TAE buffer was used for electrophoresis containing 40 mM Tris acetate and 1 mM EDTA.

6.4 Agarose gel electrophoresis

1% (w/v) agarose was added to TAE buffer and brought to the boil until the agarose had completely dissolved. The gel was allowed to cool for 5 minutes prior to being cast into a rack with a comb. The gel was allowed to solidify for 45 minutes and the comb removed; the gel was placed into an electrophoresis tank and covered with TAE buffer. Experimental samples were then loaded into the wells.

6.5 Supercoiling assay

The inhibitory effect of compounds on gyrase supercoiling activity was assessed using the Inspiralis assay kits and following the manufacturers instructions. Compounds were weighed into an eppendorf tube and dissolved in DMSO. Serial dilutions were performed using water. For each compound a master mix (MM) was prepared using 0.5 μL of relaxed pBR322 DNA, 6 μL of dilution buffer, 6 μL of assay buffer and 15.5 μL of water. Diluted samples and MM were prepared whilst in ice prior to incubation to minimise intrinsic supercoiling activity. A 28 μL aliquot of MM was used for the negative control and the volume made up to 30 μL with water. Subsequently 1 μL of enzyme was added for every compound to be tested including the positive control, the MM was homogenised. Afterwards 29 μL of MM was dispensed into an eppendorf, with 1 μL of compound added to each eppendorf. Samples were centrifuged at 13,200 RPM, for 5 seconds prior to incubation at 37°C for 30 minutes. To arrest the reaction 30 μL of a mixture of iso-amyl alcohol and chloroform (1:24) and 15 μL of 40% (w/v) sucrose, 0.1 M Tris.HCl (pH 8.0), 0.1 M EDTA, 0.5 mg/mL bromophenol blue (STEB buffer) were added. The samples were centrifuged at 13,200 RPM, for 5 minutes, and 15 μL of aqueous layer loaded onto a 1% agarose gel. The topoisomers and supercoiled DNA were separated by electrophoresis. The gel was stained in mixture of TAE and ethidium bromide (1 μg/mL) for 15 minutes before being distained using TAE buffer for 15 minutes. The gel was then visualised under UV light.

6.6 Cleavage stabilisation assay

Compounds were weighed into an eppendorf tube and dissolved in DMSO. Serial dilutions were carried out using water. For each compound a master mix (MM) was prepared using 0.3 μL of supercoiled pBR322 DNA, 6 μL of dilution buffer, 6 μL of cleavage assay buffer and 15.7 μL of water. Diluted samples and MM were prepared whilst on ice prior to incubation to minimise intrinsic supercoiling activity. A 28 μL aliquot of MM was used for the negative control and the volume made

up to 30 μL with water. Subsequently 1 μL of enzyme was added for every compound to be tested including the positive control, the MM was homogenised. Afterwards 29 μL of MM was dispensed into an eppendorf tube, with 1 μL of compound added to each eppendorf. Samples were centrifuged at 13,200 RPM, for 5 seconds prior to incubation at 37°C for 30 minutes. After which, 0.3 μL of 20% SDS and 0.5 μL of proteinase K were added to each sample, a further incubation was performed for an additional 30 minutes. To arrest the reaction, a mixture of 30 μL iso-amyl alcohol and chloroform (1:24) and 15 μL of 40% (w/v) sucrose, 0.1 M Tris.HCl (pH 8.0), 0.1 M EDTA, 0.5 mg/mL bromophenol blue (STEB buffer) were added. The samples were centrifuged at 13,200 RPM, for 5 minutes, and 15 μL of aqueous layer loaded onto a 1% agarose gel. The topoisomers and supercoiled DNA were separated by electrophoresis. The gel was stained in mixture of TAE and ethidium bromide (1 μg/mL) for 15 minutes before being distained using pure TAE buffer for 15 minutes. The gel was then visualised under UV light.

6.7 Experimental procedures and characterisation

1,3-diethyl 2-{[(tert-butoxy) carbonyl] amino} propanedioate (17)

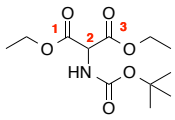

Diethyl aminomalonate hydrochloride (25 g, 118 mmol) was dissolved in a mixture of 1 M NaOH (119 mL) and 1,4 dioxane (100 mL). Subsequently Boc_2O (28.5 g, 130.73 mmol) dissolved in 1,4 dioxane (50 mL) was added dropwise to the solution of starting material. The reaction was stirred at rt for 17 h before the solvent was removed under reduced pressure. The residue was taken up into EtOAc and the organic layer washed with 5% $KHSO_4$, sat. $NaHCO_3$ and brine. The organic layer was dried over $MgSO_4$ and the solvent removed under reduced pressure to give the desired product as a colourless oil (24.7 g, 76%). ^{1}H NMR (400 MHz, DMSO-d6) δ_H ppm: 7.63 (d, *J* = 8.0 Hz, 1 H, NH), 4.86 (d, *J* = 8.0 Hz, 1 2-H), 4.22-4.11 (m, 4 H, CH_2), 1.39 (s, 9 H, Boc), 1.20 (t, *J* = 8.0 Hz, 6 H, CH_3). ^{13}C NMR (100 MHz, DMSO-d6) δ_c ppm: 166.6, 155.1, 79.0, 61.5, 57.4, 28.0, 13.8. IR ν_{max} (neat) / cm^{-1} 3371 (N-H), 2979 (CH_2/CH_3) 2941 (CH_2/CH_3), 1745 (C=O), 1714 (C=O), 1368 (C-N), 1182 (C-O) 1158 (C-O). HRMS (ESI+) calculated for $C_{12}H_{22}NO_6$ $[M+H]^+$ 276.1442 found 276.1442.

2-{[(tert-butoxy) carbonyl] amino}-3-ethoxy-3-oxopropanoic acid (18)

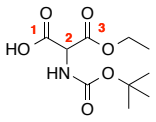

Compound **17** (5 g, 18.18 mmol) was added to a solution of KOH (1 g, 17.82 mmol) in EtOH (20 mL). The mixture was stirred at room temperature for 3 hours before 90% of the solvent was removed under pressure. EtOAc was added and the organic extract removed to eliminate unreacted starting material. Consequently the aqueous layer was acidified with 1 M $NaHCO_3$ and extracted with EtOAc. The organic layer was dried over $MgSO_4$ and the solvent removed under vacuum to furnish a white solid (2.56 g, 57%). ^{1}H NMR (400 MHz, DMSO-d6) δ_H ppm: 7.47 (d, *J* = 8.1 Hz, 1 H, NH), 4.71 (d, *J* = 8.1 Hz, 1 H, 2-H), 4.18-4.10 (m, 2 H, CH_2), 1.38 (s, 9 H, Boc), 1.19 (t, *J* = 7.2 Hz, 3 H, CH_3) .^{13}C NMR (100 MHz, DMSO-d6) δ_C ppm: 167.8, 167.3, 155.1, 79.0, 61.4, 57.6, 28.1, 14.0. IR ν_{max} (neat) / cm^{-1} 3272 (CON-H), 2980 (Ar-H), 2933 (Ar-H), 1747 (C=O), 1723 (C=O), 1650 (C=O), 1182 (C-O), 1154 (C-O). HRMS (ESI+) calculated for $C_{10}H_{18}NO_6$ $[M+H]^+$ 248.1129 found 248.1130. Mp. 75-79°C.

2,4-bis(actyloxy) benzoic acid (20)

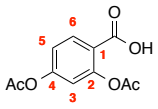

Commercially available 2,4-dihydroxybenzoic acid (500 mg, 3.24 mmol) was dissolved in a mixture of pyridine (3 mL) and DMAP (5 mg, 0.04 mmol). Subsequently acetic anhydride (1.53 mL, 16.19 mmol) was added drop wise to the reaction mixture. The reaction vessel was flushed with nitrogen, covered in foil and stirred for 4 h at rt. To quench the reaction ice was added and the mixture acidified with 3 M HCl causing a precipitate to form. The mixture was washed with EtOAc three times and the organic layer dried over $MgSO_4$ the solvent was removed under reduced pressure immediately to give the desired product as a white powder (0.74 g, 97%). ^{1}H NMR (400 MHz, DMSO-d6) δ_H ppm: 13.13 (s, 1 H, OH), 7.92 (d, *J* = 8.0 Hz, 1 H, ArH), 7.18 (dd, J_1 = 8.8 Hz, J_2 = 2.4 Hz, 1 H, ArH), 7.08 (d, *J* = 2.4 Hz, 1 H, ArH) 2.29 (s, 3 H, CH_3), 2.24 (s, 3 H, CH_3). ^{13}C NMR (100 MHz, DMSO-d6) δ_C ppm: 168.9, 168.6, 164.9, 154.0, 151.0, 132.4, 121.6, 119.6, 117.6, 20.82, 20.77. IR ν_{max} (neat) / cm^{-1} 2981 (C-H_3), 2941 (C-H_3), 2645 (Ar-H), 2539 (Ar-H), 1773 (C=O), 1681 (C=O), 1607 (C=O). HRMS calculated for $C_{11}H_9O_6$ $[M-H]^-$ 237.0405 found 237.0405. Mp. 149-150°C.

3-(acetyloxy)-4-(carbonochloridoyl) phenyl acetate (21)

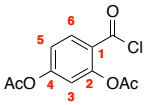

Compound **20** (4 g, 16.79 mmol) was taken up in anhydrous DCM (40 mL) and added to $SOCl_2$ (24 mL). The mixture was refluxed for 4 h after which the reagent and solvent was evaporated under reduced pressure to give a sticky oil, this was taken up into anhydrous DCM and used directly in the next procedure.

Ethyl 3-[2,4-bis(acetyloxy)phenyl]-2-{[(tert-butoxy) carbonyl] amino}-3-oxopropanoate (22)

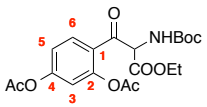

Compound **18** (4.45 g, 23.51 mmol) was added to a mixture of anhydrous THF (45 mL), triethylamine (14.63 mL, 105 mmol) and $MgCl_2$ (5.44 g, 57.1 mmol). The slurry was stirred vigorously for 2.5 h before crude **21** was added dropwise to the mixture. Upon addition a colour change was noted from grey suspension to an orange brown suspension. The mixture was stirred at rt for 15.5 h after which the reaction was quenched with sat. NH_4Cl causing the mixture to clarify. The solution was extracted three times with EtOAc and the organic layer dried over $MgSO_4$. The solvent was removed under reduced pressure to give a crude brown oil (7.08 g). The product was used directly in the following reaction without further purification.

***Tert*-butyl N-(4,7-dihydroxy-2-oxo-2H-chromen-3-yl) carbamate (23)**

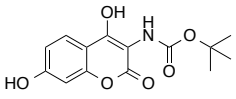

A mixture of MeOH (40 mL) and 1.5 M NaOH (50 mL) was added to crude compound **22** (7.08 g). The mixture was stirred for 3.5 h after which the reaction was acidified with 1 M HCl causing a precipitate to form. The reaction was extracted three times with EtOAc and the organic fraction dried over $MgSO_4$ and the solvent removed under reduced pressure to give a crude orange brown solid (4.04 g). This was used directly in the next step without further purification.

4,7-dihydroxy-2-oxo-2H-chromen-3-aminium chloride (24)

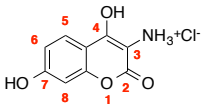

Crude compound **23** (4.04 g) was added to a mixture of ethereal 1M HCl (30 mL) and MeOH (20 mL) and stirred at rt for 29 h after which the solid precipitate was filtered and washed with a small amount of EtOAc to give the desired compound as a brown solid (881 mg, 23% over 3 steps). ^{1}H NMR (400 MHz, CD_3OD) δ_H ppm: 7.88 (d, J = 8.0 Hz, 1 H, ArH), 6.90 (dd, J_1 = 8.8 Hz, J_2 = 2.4 Hz, 1 H), 6.77 (d, J = 2.0 Hz, 1 H, ArH). ^{1}H NMR (100 MHz, CD_3OD) δ_c ppm: 164.5, 161.9, 161.4, 155.7, 126.1, 115.0, 108.0, 104.0, 96.5. IR ν_{max} (neat) / cm^{-1} 3345 (O-H), 2929 (O-H), 1710 (C=O), 1639 (N-H bend), 1564 (C=C), 1526 (C=C). HRMS (ESI-) calculated for $C_9H_6NO_4$ $[M-H]^-$ 192.0302 found 192.0303. Mp. 237-238°C.

3-chloro-2,4-dihydroxybenzaldehyde (27)

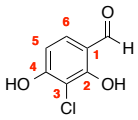

2,4-dihydroxybenzaldehyde (2 g, 14.49 mmol) was suspended in H_2O (10 mL) and dissolved in a solution of KOH (2 g, 35.71 mmol) in H_2O (15 mL). Subsequently commercial NaOCl 10-15% (20 mL) was added dropwise to the vigorously stirred solution that turned dark brown on addition. After 1 hour stirring at room temperature the reaction was acidified with 1 M HCl and extracted with EtOAc and the organic layer dried over $MgSO_4$. The crude extract was purified by flash column chromatography (EtOAc/Hexanes 1:1) and recrystallized from DCM to give the product as an off white solid (1.12 g, 45%). ^{1}H NMR (400 MHz, CD_3OD) δ_H ppm: 9.69 (s, 1 H, COH), 7.49 (d, J = 8.6 Hz, 1 H, ArH), 6.59 (d, J = 8.6 Hz, 1 H, ArH). ^{13}C NMR (100 MHz, CD_3OD) δ_C ppm: 195.8, 162.6, 160.8, 134.3, 116.2, 109.6, 108.7. IR ν_{max} (neat) / cm^{-1} 3294 (O-H), 3084 (C-H), 2878 (C-H), 1618 (C=O). HRMS (APCI+) calculated for $C_7H_5ClO_3H$ $[M+H]^+$ 173.0000 found 173.0000. Mp. 156-158°C, (Lit 146-148°C).[210]

3,5-dichloro-2,4-dihydroxybenzaldehyde (28)

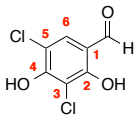

2,4-dihydroxybenzaldehyde (2 g, 14.49 mmol) was suspended in H_2O (10 mL) and dissolved in a solution of KOH (2 g, 35.71 mmol) in H_2O (15 mL). Subsequently commercial NaOCl 10-15% (20 mL) was added dropwise to the vigorously stirred solution that turned dark brown on addition. After

3 hours stirring at room temperature the reaction was acidified with 6 M HCl and extracted three times with EtOAc and the organic layer dried over $MgSO_4$. The crude was purified by flash column chromatography (EtOAc/hexanes) to give the product as an off white solid (0.83 g, 28%). ^{1}H NMR (400 MHz, DMSO-d6) δ_H ppm: 11.48 (br s, 1 H, OH), 9.88 (s, 1 H, COH), 7.77 (s, 1 H, 6-H). (100 MHz, DMSO-d6) δ_C ppm: 192.6, 156.9, 156.1, 130.8, 115.5, 113.3, 109.6. . IR ν_{max} (neat) / cm^{-1} 2941 (C-H), 1623 (C=O), 741 (C-Cl), 714 (C-Cl). HRMS (ESI-) calculated for $C_7H_3Cl_2O_3$ $[M-H]^-$ 204.9465 found 204.9461. Mp. 203-205°C.

3-chloro-2,4-dimethoxybenzaldehyde (34)

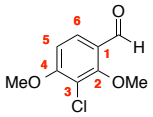

Compound **27** (3.56 g, 20.70 mmol) was added to a suspension of K_2CO_3 (14.21 g, 102.17 mmol) in acetone (50 mL). Iodomethane (14.59 g, 103.47 mmol) was added dropwise and the suspension refluxed for 2 hours. The solvent was removed under vacuum and the residue dissolved in water (50 mL). The remaining solid was filtered and dried in a desiccator to yield a white solid (4.14 g, 100%). ^{1}H NMR (400 MHz, $CDCl_3$) δ_H ppm: 10.17 (s, 1 H, COH), 7.72 (d, *J* = 8.80 Hz, 1 H, ArH) 6.79 (d, *J* = 8.80 Hz, 1 H, ArH) 3.94 (s, 3 H, CH_3), 3.93 (s, 1 H, CH_3). ^{13}C NMR (100 MHz, $CDCl_3$) δ_C ppm: 188.0, 161.2, 160.6, 127.9, 123.9, 116.7, 107.8, 63.0, 56.7. IR ν_{max} (neat) / cm^{-1} 2950 (O-CH_3), 2869 (O-CH3), 1673 (C=O). HRMS (ES+) calculated for $C_9H_{10}O_3Cl$ $[M+H]^+$ 201.0313 found 201.0309. Mp. 109-111°C, (Lit 109-111°C).[276]

3-chloro-2,4-dimethoxybenzoic acid (35)

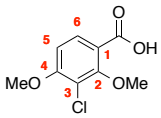

Compound **34** (8.39 g, 41.95 mmol) was dissolved in anhydrous acetonitrile (100 mL). Subsequently Cu(II)Br (467 mg, 2.09 mmol) was added and the reaction flask purged with nitrogen. Luperox 70%™ TBH70X (15.12 g, 167.80 mmol) was added dropwise and a colour change observed from a clear green to brown and finally to a green suspension. After 25 hours at room temperature an additional aliquot of Luperox was added (1.80 g, 20 mmol) and the mixture left for a further 3 hours. The suspension was filtered through activated charcoal, the solvent removed under vacuum and the product recrystallized from EtOAc to furnish a white solid (3.99 g, 44%). ^{1}H NMR (400 MHz, DMSO-d6) δ_H ppm: 12.82 (s, 1 H, OH), 7.75 (d, *J* = 8.8 Hz, 1 H, ArH), 6.99 (d, *J* = 8.9 Hz, 1 H, ArH), 3.90 (s, 3 H, CH_3), 3.80 (s, 3 H, CH_3). ^{13}C NMR (100 MHz, DMSO-d6) δ_C ppm: 165.8, 158.7, 156.9, 130.8, 118.9, 116.5, 107.7, 61.4, 56.7. IR ν_{max} (neat) / cm^{-1} 2950 (C-H), 2564

(O-H), 1664 (C=O), 1583 (C-C), 1284 (C-O), 1221 (C-O). HRMS (ES+) calculated for $C_9H_{10}ClO_4$ $[M+H]^+$ 217.0262 found 217.0261. Mp. 171-172°C, (Lit 168-170°C).[210]

3-chloro-2,4-dihydroxybenzoic acid (33)

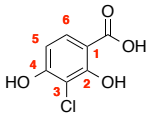

To a suspension of compound **35** (3.58 g, 16.57 mmol) in anhydrous DCM (35 mL) under nitrogen at reduced temperature (-78°C) was added BBr_3 dropwise (16.57 g, 66.28 mmol). The reaction was stirred for 1 h and then allowed to warm to room temperature and stirred overnight. The suspension was poured onto crushed ice and extracted with EtOAc, a white residue was filtered off. The remaining solution was dried under reduced pressure and the residue dissolved in MeOH (25 mL). This was left overnight forming a red solution before being evaporated off and purified by flash column chromatography (MeOH/DCM 2:8) to give the product as a white powder (2.17 g, 70%). ^{1}H NMR (400 MHz, CD_3OD) δ_H ppm: 7.64 (d, *J* = 8.0 Hz, 1 H, ArH), 6.46 (d, *J* = 8.0 Hz, 1 H, ArH). ^{13}C NMR (100 MHz, CD_3OD) δ_C ppm: 173.4, 160.9, 160.8, 130.4, 108.7, 108.3, 106.6 IR ν_{max} (neat) / cm^{-1} 3445 (O-H), 3056 (COO-H), 1643 (C=O). HRMS (APCI+) calculated for $C_7H_6ClO_4$ $[M+H]^+$ 188.9949 observed 188.9947. Mp. 208-210°C.

2,4-bis(acetyloxy)-3-chlorobenzoic acid (39)

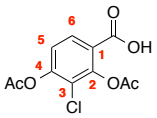

To a light protected and cooled solution of compound **33** (50 mg, 0.27 mmol) in pyridine (1 mL) was added DMAP (5 mg, 0.04 mmol). The flask was purged with nitrogen and Ac_2O (0.5 mL, 5.14 mmol) added dropwise. After 4 hours at room temperature crushed ice was added to the reaction mixture forming a precipitate. The suspension was extracted with EtOAc and the organic layer dried over $MgSO_4$. The solvent was removed under pressure to furnish the labile product as a brown solid (62.42 mg, 85%). The solid was used directly in the next step without further purification. ^{1}H NMR (400 MHz, DMSO-d6) δ_H ppm: 7.96 (d, *J* = 8.7 Hz, 1 H, ArH), 7.40 (d, *J* = 8.6 Hz, 1 H, ArH), 2.37 (s, 3 H, CH_3), 2.33 (s, 3 H, CH_3). HRMS calculated for $C_{11}H_8ClO_6$ $[M-H]^-$ 271.0015 found 271.0016.

4-hydroxy-2H-chromen-2-one (48)

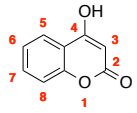

Sodium (2.11 g, 91.91 mmol) in mineral oil was washed with hexane and added portion wise to a vigorously stirred mixture of 2-hydroxyacetaphenone (5 g, 36.76 mmol) and diethyl carbonate (13 g, 110.28 mmol). The mixture was brought to 160°C and diluted with xylene (30 mL). After 1 hour the mixture was allowed to cool to room temperature and quenched with H_2O. Sodium Hydroxide (2 M) was added and the aqueous extracted once with diethyl ether. This was discarded and the remaining aqueous layer acidified with HCl. The resultant precipitate was filtered; dissolved in MeOH and the solvent removed under reduced pressure. The remaining solid was triturated with diethyl ether and filtered to give the desired product as a cream powder (4.34 g, 73%). ^{1}H NMR (400 MHz, DMSO-d6) δ_H ppm: 12.62 (s, 1 H, OH), 7.82 (dd, J_1 = 8.0 Hz, J_2 = 1.6 Hz, 1 H, 5-H), 7.66-7.62 (m, 1 H, 6-H), 7.37-7.32 (m, 2 H, 7 and 8-H), 5.65 (s, 1 H, 3-H). ^{13}C NMR (100 MHz, DMSO-d6) δ_C ppm: 165.7, 161.9, 153.5, 132.7, 123.9, 123.2, 116.4, 115.8, 91.0. IR ν_{max} (neat) / cm^{-1}. 2941-2555 (Ar-H overlapping broad OH), 2896 (O-H), 1608 (C=O), 1556 (C=C), 1562 (C=C), 1504 (C=C), 1273 (O-H bending). HRMS (ES) calculated for found. HRMS (ESI-) calculated for $C_9H_5O_4$ [M-H]$^-$ 161.0244 found 161.0244. Mp. 212-214°C, (Lit 213-215°C).[277]

4-hydroxy-3-nitro-2H-chromen-2-one (51)

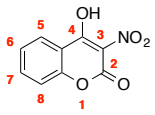

70% HNO_3 (0.78 mL, 18.52 mmol) was added carefully to conc. H_2SO_4 (0.82 mL, 15.43 mmol) at 0°C. The nitrating mixture was then added dropwise to compound **48** (1 g, 6.17 mmol) suspended in $CHCl_3$ (40 mL) at room temperature. After 5 minutes the reaction mixture turned to a brown clear solution. After 1 hour the reaction was poured onto crushed ice. The resultant solution was extracted three times with $CHCl_3$ and the organic fractions dried over $MgSO_4$. The solvent was removed under reduced pressure and the product recrystallized from MeOH to furnish the product as orange needles (345 mg, 27%). ^{1}H NMR (400 MHz, DMSO-d6) δ_H ppm: 7.89 (dd, J_1 = 8.0 Hz, J_2 = 1.6 Hz, 1 H, ArH), 7.55-7.50 (m, 2 H, ArH), 7.24-7.17 (m, 2 H, ArH). ^{13}C NMR (100 MHz, DMSO-d6) δ_C ppm: 166.8, 157.3, 152.5, 132.6, 125.6, 123.3, 121.5, 120.7, 116.2. IR ν_{max} (neat) / cm^{-1} 2941 (Ar-H), 2555 (Ar-H, overlapping OH), 1605 (C=O), 1422 (N-O), 1144 9 (N-O). HRMS (ESI-) calculated for $C_9H_4NO_5$ [M-H]$^-$ 206.0095 found 206.0092. Mp. 176-178°C, (Lit 174-175°C).[278]

1-[4-(benzyloxy)- 2-hydroxyphenyl] ethan-1-one (53)

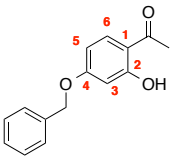

2,4-dihydroxyacetaphenone (10 g, 65.79 mmol) was added to a mixture of K_2CO_3 (10.89 g, 78.91 mmol) in acetone (200 mL). The mixture was brought to reflux for 2 hours before benzyl bromide (7.86 mL, 65.79 mmol) was added dropwise. The mixture was refluxed for a further 3 hours before being cooled to room temperature. The mixture was filtered and the solvent removed under reduced pressure. The title compound was recrystalised from MeOH to give magenta crystals (15.5 g, 97%). ^{1}H NMR (400 MHz, DMSO-d6) δ_H ppm: 12.63 (s, 1H, OH), 7.84 (d, J_1 = 8.0 Hz, 1 H, ArH), 7.46-7.32 (m, 5 H, ArH), 6.60 (dd, J_1 = 8.8 Hz, J_2 = 2.4 Hz, 1 H, ArH), 6.56 (d, J = 2.4 Hz, 1 H, ArH), 5.19 (s, 2 H, CH_2), 2.55 (s, 3 H, CH_3). ^{13}C NMR (100 MHz, DMSO-d6) δ_C ppm: 203.1, 164.7, 164.0, 136.3, 133.3, 128.5, 128.0, 127.8, 113.9, 107.8, 101.7, 69.6, 26.6. IR ν_{max} (neat) / cm^{-1} 3026 (Ar-H), 3002 (Ar-H), 2937 (Ar-H), 1617 (C=O), 1363 (C-O). HRMS (ESI+) calculated for $C_{15}H_{15}O_3$ $[M+H]^+$ 243.1016 found 243.1018. Mp. 107-108°C, (Lit 104-105 °C).[279]

1-[4-(benzyloxy)-3-chloro-2-hydroxyphenyl] ethan-1-one (54)

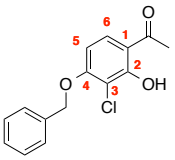

Compound **53** (1 g, 4.13 mmol) was added to a mixture of KOH (850 mg), THF (150 mL) and water (25 mL). Subsequently, NaOCl (5.5 mL) was added dropwise to the vigorously stirred solution. After 1.5 h the solution was acidified with 6 M HCl and the organic solvent removed under reduced pressure to cause the crude product to precipitate in the remaining aqueous fraction. The precipitate was filtered and dried. The desired compound was recrystalised from MeOH as colourless crystals (217 mg, 19%). ^{1}H NMR (400 MHz, DMSO-d6) δ_H ppm: 13.14 (s, 1 H, OH), 7.94 (d, J = 8.0 Hz, 1 H, ArH), 7.49-7.33 (m, 5 H, ArH), 6.91 (d, J = 9.2 Hz, 1 H, ArH), 5.36 (s, 2 H, CH_2), 2.62 (s, 3 H, CH_3). ^{13}C NMR (100 MHz, DMSO-d6) δ_c ppm: 204.1, 159.7, 158.8, 136.0, 131.6, 128.6, 128.1, 127.5, 114.6, 104.9, 70.4, 26.6. IR ν_{max} (neat) / cm^{-1} 3048 (Ar-H), 3029 (Ar-H), 2940 (Ar-H), 2881 (Ar-H), 1627 (C=O), 1277 (C-O), 1055 (C-O), 919 (O-H bend), 840 (C-Cl). HRMS (ESI+) calculated for $C_{15}H_{14}ClO_3$ $[M+H]^+$ 277.0626 found 277.0628. Mp. 127-129°C.

(±) 3-ethoxy-5-methylcyclohex-2-en-1-one (58)

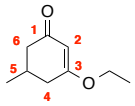

p-Toluenesulfonic acid (340 mg, 1.98 mmol) was added to a solution of 5-methyl-1,3-cyclohexanedione (4 g, 31.75 mmol) in EtOH (100 mL). The reaction was heated to 60°C for 70 h, subsequently the solvent was removed under pressure and the crude product purified by flash column chromatography (EtOAc/Hexanes 4:6) to give the title compound as a clear yellow oil (3.32 g, 68%). ^{1}H NMR (400 MHz, $CDCl_3$) δ_H ppm: 5.30 (s, 1 H, 2-H), 3.90-3.83 (m, 2 H), 2.41-2.39 (m, 1 H), 2.37-2.35 (m, 1 H), 2.25-2.16 (m, 1 H), 2.15-2.08 (m, 1 H, CH_2), 2.03-1.96 (m, 1 H, CH_2), 1.33 (t, 3 H, CH_3), 1.04 (dd, *J* = 6.36 Hz, 3 H, CH_3). ^{13}C NMR (100 MHz, $CDCl_3$) δ_C ppm: 199.9, 177.4, 102.4, 64.3, 45.2, 37.3, 28.9, 21.0, 14.2. IR ν_{max} (neat) / cm^{-1} 2973-2872 (C-H_3 and C-H_2), 1650 (C=O), 1597 (C=C). HRMS (ESI+) calculated for $C_9H_{15}O_2$ $[M+H]^+$ 155.1067 found 155.1063.

(±) 3-ethynyl-5-methylcyclohex-2-en-1-one (59)

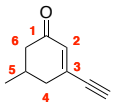

Compound **58** (2 g, 12.99 mmol) was dissolved in anhydrous THF (3 mL) and added dropwise to a vigorously stirred solution of ethynylmagnesium chloride in THF (1 M, 39 mL, 19.49 mmol). The reaction mixture was stirred at room temperature for 25 h before being acidified with 1 M HCl and extracted with DCM. The organic layer was dried over $MgSO_4$ and the solvent evaporated under pressure to furnish the crude product as a dark brown oil. The product was purified via flash column chromatography (EtOAc/hexanes 4:6) to give the title compound as a pale yellow oil (1.27 g, 73%). ^{1}H NMR (400 MHz, $CDCl_3$) δ_H ppm: 6.25 (s, 1 H, α,βH), 3.52 (s, 1 H, alkyne-H), 2.52-2.50 (m, 1 H, CH_2), 2.48-2.46 (m, 1 H, CH_2), 2.28-2.20 (m, 1 H, C-H), 2.19-2.05 (m, 2 H, CH_2), 1.07 (d, *J* = 6.36, 3 H, CH_3) ^{13}C NMR (100 MHz, $CDCl_3$) δ_C ppm: 199.0, 141.6, 133.8, 87.2, 82.6, 45.6, 38.4, 30.2, 21.0. IR ν_{max} (neat) / cm^{-1} 3242 (alkyne-H), 2956-2876 (C-H_3 and C-H_2), 2092 (alkyne stretch) 1658 (C=O), 1592 (C=C). HRMS (APCI+) calculated for $C_9H_{11}O_1$ $[M+H]^+$ 135.0804 found 135.0803

(±) 3-[(E)-2-methoxyethenyl]-5-methylcyclohex-2-en-1-one (60)

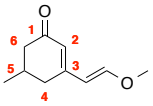

4-methylmorpholine (75.86 mg, 0.75 mmol) was added to a solution of compound **59** (100 mg, 0.75 mmol) and MeOH (95.80 mg, 2.99 mmol) in anhydrous toluene (3 mL). The reaction was stirred at

room temperature for 24 h, after which an additional aliquot of 4-methylmorpholine (75.86 mg, 0.75 mmol) and MeOH (95.80 mg, 2.99 mmol) was added. The reaction was stirred for a further 5 h before the solvent was removed under pressure and the crude was purified by flash column chromatography immediately (EtOAc/hexanes 3:7) to furnish the labile diene product as a clear, yellow oil (58 mg, 46%). ^{1}H NMR (400 MHz, $CDCl_3$) δ_H ppm: 7.03 (d, *J* = 12.88, 1 H, C=CH), 5.83 (s, 1 H, α,β-H) 5.64 (d, *J* = 12.84, 1 H, C=CH), 3.70 (s, 3 H, CH_3), 2.54-2.43 (m, 2 H, CH_2), 2.27-2.15 (m, 1 H, CH), 2.11-2.00 (m, 2 H, CH_2), 1.09 (d, *J* = 6.48, 3 H, CH_3) ^{13}C NMR (100 MHz, $CDCl_3$) δ_C ppm: 199.8, 156.4, 154.4, 123.9, 107.1, 57.2, 45.8, 33.8, 30.0, 21.5. IR ν_{max} (neat) / cm^{-1} 2952-2835 (C-H_2) 1613 (C=O) 1227 (C=C-O-C).

8-hydroxy-3-methyl-1,2,3,4,7,12-hexahydrotetraphene-1,7,12-trione (Ochromycinone)

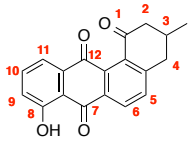

Compound **60** (537 mg, 3.23 mmol) was added dropwise to a light protected mixture of commercially available 5-hydroxy-1,4-naphthoquinone (500 mg, 2.87 mmol) and tetraacetoxy diboroxane (881 mg, 0.66 mmol) in anhydrous DCM (10 mL) at 0°C. The reaction was stirred vigorously for 2 minutes before being quenched with ice water to form a black sticky solid. The mixture was extracted with DCM, dried over $MgSO_4$ and purified by flash column chromatography immediately (EtOAc/Hexanes 3:7) to furnish the product as an orange solid (63 mg, 7%). ^{1}H NMR (400 MHz, $CDCl_3$) δ_H ppm: 12.28 (s, 1 H, OH), 8.28 (d, *J* = 8.0, 1 H, ArH), 7.69-7.64 (m, 2 H, ArH), 7.55 (d, *J* = 8.00, 1 H, ArH), 7.27 (dd, J_1 = 7.2, J_2 = 2.4, 1 H, ArH), 3.06-2.97 (m, 2 H, CH_2), 2.61 (dd, J_1 = 16.0 Hz, J_2 = 4.0 Hz, 1 H) 2.50 (dd, J_1 = 16.0 Hz, J_2 = 4.0 Hz, 1 H), 2.52-2.42 (m, 1 H, CH), 1.21 (d, *J* = 6.5, 3 H, CH_3). (100 MHz, $CDCl_3$) δ_C ppm: 199.3, 187.7, 183.2, 162.2, 150.5, 137.2, 136.8, 136.1, 135.3, 133.6, 133.2, 129.1, 123.8, 119.7, 115.6, 47.6, 38.5, 30.9, 21.6. IR ν_{max} (neat) / cm^{-1} 2955-2872 (C-H_2 and C-H_3 and O-H overlapping), 1698 (C=O), 1666 (C=O), 1631 (C=O). HRMS (ESI+) calculated for $C_{19}H_{15}O_4$ $[M+H]^+$ 307.0965 found 307.0965 found 307.0964. Mp. 145-148°C.

8-hydroxy-6-methoxy-3-methyl-1,2,3,4,5,6,6a,7,12,12a-decahydrotetraphene-1,7,12-trione (62)

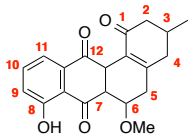

Compound **60** (110 mg, 0.66 mmol) was added to commercially available 5-hydroxy-1,4-naphthoquinone (115 mg, 0.66 mmol) and tetraacetoxy diboroxane (180 mg, 0.66 mmol) in anhydrous DCM (3 mL). After stirring at room temperature for 5 minutes the reaction was quenched with water and extracted three times with DCM. The organic layer was dried onto silica and columned (EtOAc-Hexanes 4:6). The crude oil was re-purified by flash column chromatography (DCM 100%) and the product recrystallized from hexane and diethyl ether (1:1) to give the product as an orange brown solid. (16 mg, 8%). ^{1}H NMR (400 MHz, $CDCl_3$) δ_H ppm: 12.20 (s, 1 H, OH), 7.61 (t, J = 8.0 Hz, 1 H, ArH), 7.47 (dd, J_1 = 8.0 Hz, J_2 = 1.16, 1 H, ArH), 7.19 (dd, J_1 = 8.36, J_2 = 1.12, 1 H, ArH), 4.34 (dd, J = 6.92, 1 H, CH), 4.0-3.98 (m, 1 H, CH), 3.07 (dd, J = 6.90, 1 H, CH), 3.00 (s, 3 H, OCH_3), 2.61-2.42 (m, 4 H, CH_2), 2.33-2.22 (m, 3 H, CH_2 and CH overlapping), 1.13 (d, J = 5.92, 3 H, CH_3). (100 MHz, $CDCl_3$) δ_C ppm: 205.0, 197.8, 193.4, 161.7, 152.6, 137.33, 137.26, 128.6, 122.5, 118.5, 118.0, 76.8, 57.6, 52.3, 45.8, 42.5, 39.4, 35.1, 30.6, 21.7. IR ν_{max} (neat) / cm^{-1} 2953-2871 (C-H_3 and C-H_2 & O-H overlapping), 1698 (C=O), 1667 (C=O), 1633 (C=O). HRMS (ESI+) calculated for $C_{20}H_{21}O_5$ $[M+H]^+$ 341.1384 found 341.1381. Mp. 155-156°C.

N-(2-oxo-2H-chromen-3-yl) acetamide (77)

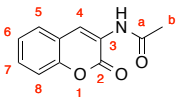

Salicylaldehyde (6.1 g, 50 mmol) was added to N-acetylglycine (5.85 g, 50 mmol), anhydrous NaOAc (16 g, 195 mmol) and Ac_2O (30 mL). The mixture was heated to reflux for 5 hours. After which the mixture was allowed to cool to room temperature before being quenched and triturated with ice water. Small portions of EtOAc were added and the precipitated solid collected and washed with small aliquots of EtOAc to furnish the product as a yellow powder (1.39 g, 14%). ^{1}H NMR (400 MHz, DMSO-d6) δ_H ppm: 9.76 (s, 1 H, NH), 8.60 (s, 1 H, 4-H), 7.69 (dd, J_1 = 8.0 Hz, J_2 = 1.6 Hz, 1 H, ArH), 7.50 (td, 1 H, J_1 = 8.0 Hz, J_2 = 1.6 Hz, 1 H, ArH), 7.38 (app d, J = 8.0 Hz, 1 H, ArH), 7.33 (td, J_1 = 8.0 Hz, J_2 = 1.6 Hz, 1 H, ArH), 2.16 (s, 3 H, b-H_3). ^{13}C NMR (100 MHz, DMSO-d6) δ_C ppm: 170.2, 157.4, 149.6, 129.5, 127.8, 124.9, 124.6, 123.5, 119.5, 115.8, 23.9. IR ν_{max} (neat) / cm^{-1} 3328 (N-H), 1707 (C=O), 1680 (C=O). HRMS (ESI+) calculated for $C_{11}H_9NO_3H$ $[M+H]^+$ 204.0655 found 204.0655. Mp. 205-207°C, (Lit 203-204°C).[280]

N-(8-methoxy-2-oxo-2H-chromen-3-yl) acetamide (79)

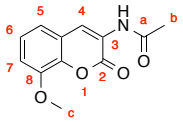

A mixture of *O*-vanillin (3.8 g, 25.0 mmol), N-acetylglycine (2.9 g, 24.76 mmol), anhydrous sodium acetate (8.2 g, 100 mmol) and acetic anhydride (12.5 mL) was brought to reflux for 3.5 hours. After this the reaction was allowed to cool to room temperature before being triturated with water. EtOAc was added to cause the product to precipitate into the organic layer. The solid was collected and washed well with small aliquots of EtOAc to furnish the desired product as a yellow powder (1.05 g, 18%). ^{1}H NMR (400 MHz, $CDCl_3$) δ_H ppm: 8.65 (s, 1 H, 4-H), 8.08 (br s, 1 H, NH), 7.23 (t, J = 8.0 Hz, 1 H, ArH), 7.09 (dd, J_1 = 8.0 Hz, J_2 = 1.2 Hz, 1 H, ArH), 7.01 (dd, J_1 = 8.0 Hz, J_2 = 1.2 Hz, 1 H, ArH), 3.97 (s, 3 H, c-H_3), 2.23 (s, 3, b-H_3). ^{13}C NMR (100 MHz, $CDCl_3$) δ_C ppm: 169.4, 158.5, 147.0, 139.5, 125.1, 124.4, 123.4, 120.7, 119.5, 111.8, 56.3, 24.8. IR ν_{max} (neat) / cm^{-1} 3333 (CON-H), 3087-2839 (Ar-H), 1707 (C=O), 1676 (C=O). HRMS (ESI+) calculated for $C_{12}H_{11}NO_4H$ $[M+H]^+$ 234.0761 found 234.0756. Mp. 240-242°C, (Lit 237-238°C).[248]

N-(7-methoxy-2-oxo-2H-chromen-3-yl) acetamide (81)

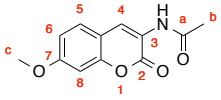

4-Methoxysalicylaldehyde (3.8 g, 25 mmol), was added to N-acetylglycine (2.9 g, 24.79 mmol), anhydrous NaOAc (8.2 g, 100 mmol) and Ac_2O (15.5 mL). The mixture was refluxed for 24 hours, after which it was allowed to cool to room temperature. The reaction was quenched and triturated with water. Subsequently EtOAc was added, the resultant precipitate was filtered and washed with a small amount of EtOAc to furnish the product as a yellow powder (666 mg, 11%). ^{1}H NMR (400 MHz, $CDCl_3$) δ_H ppm: 8.63 (s, 1 H, 4-H), 7.98 (br s, 1 H, NH), 7.40 (d, J = 8.4, 1 H, 5-H), 6.88 (dd, J_1 = 8.4, J_2 = 2.4, 1 H, 6-H), 6.81 (d, J = 2.0, 1 H, 8-H), 3.86 (s, 3 H, c-H_3), 2.22 (s, 3 H, b-H_3). ^{13}C NMR (100 MHz, $CDCl_3$) δ_C ppm: 169.3, 161.4, 159.2, 151.6, 128.8, 124.2, 121.7, 113.3, 113.2, 100.9, 55.9, 24.8. IR ν_{max} (neat) / cm^{-1} 3347 (CON-H), 3060 (CO-CH_3), 2949-2843 (C-H_3), 1702 (C=O), 1676 (C=O), 1523 (C=C), 1519 (C=C), 1504 (C=C). HRMS (ESI+) calculated for $C_{12}H_{12}NO_4$ $[M+H]^+$ 234.0761 found 234.0762 Mp 237-240 °C, (Lit 234-235 °C).[248]

N-(6-chloro-2-oxo-2H-chromen-3-yl) acetamide (83)

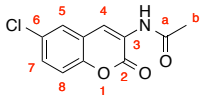

A mixture of 2-hydroxy-5-chlorobenzaldehyde (5 g, 32.05 mmol), N-acetylglycine (3.75 g, 32.05 mmol), anhydrous sodium acetate (10.51 g, 128 mmol) and acetic anhydride (15.13 mL) was refluxed for 3.5 hours before being allowed to cool to room temperature. The resultant yellow solid was triturated with water and then EtOAc added to precipitate the product in the organic layer. The solid was filtered and washed with small aliquots of EtOAc to give the desired compound as a yellow powder (2.65 g, 35%). ^{1}H NMR (400 MHz, DMSO-d6) δ_H ppm: 9.82 (s, 1 H, NH), 8.60 (s, 1 H, 4-H), 7.87 (d, J = 2.4 Hz, 1 H, ArH), 7.52 (dd, J_1 = 8.8 Hz, J_2 = 2.8 Hz, 1 H, ArH), 7.42 (d, J = 8.8 Hz, 1 H, ArH), 2.17 (s, 3 H, b-H_3). ^{13}C NMR (100 MHz, CDCl3) δ_C ppm: 169.5, 158.4, 148.3, 130.7, 129.7, 127.1, 125.0, 121.9, 121.1, 117.9, 24.9. IR ν_{max} (neat) / cm^{-1} 3337 (CON-H), 3093 (Ar-H) 3056 (Ar-H), 3030 (Ar-H), 1711 (C=O), 1676 (C=O), 1568 (C=C), 1537 (C=C), 1524 (C=C), 828 (C-Cl). HRMS (APCI+) calculated for $C_{11}H_9ClNO_3$ $[M+H]^+$ 238.0265 found 238.0269. Mp 263-264°C.

N-(8-chloro-2-oxo-2H-chromen-3-yl) acetamide – (85)

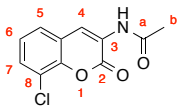

A mixture of 3-chlorosalicylaldeyde (1 g, 6.41 mmol), N-acetylglycine (750 mg, 6.41 mmol), anhydrous sodium acetate (2.1 g, 25.64 mmol), and acetic anhydride (16 mL) was refluxed for 4 hours before being allowed to cool to room temperature. Ice was added to quench the reaction and the solid triturated with water. EtOAc was added to precipitate the product and the filtered solid was washed with small aliquots of EtOAc. The organic filtrate had the solvent removed under pressure and the crude was purified by flash column chromatography (EtOAc/hexanes 3:7) to give a white powder (0.68 g, combined yield 45%). ^{1}H NMR (400 MHz, DMSO-d6) δ_H ppm: δ 9.87 (s, 1 H, NH), 8.64 (s, 1 H, 4-H), 7.66 (dd, J_1 = 7.6 Hz, J_2 = 1.2, 1 H, ArH), 7.61 (dd, J_1 = 8.0 Hz, J_2 = 1.6 Hz, 1 H, ArH), 7.33 (t, J = 8.0 Hz, 1 H, ArH), 2.18 (s, 3 H, b-H_3). ^{13}C NMR (DMSO-d6, 100 MHz) δ_C ppm: 170.4, 156.7, 144.9, 129.4, 126.8, 125.5, 125.3, 122.6, 121.4, 119.2, 24.0. IR ν_{max} (neat) / cm^{-1} 3337 (CON-H), 1711 (C=O), 1676 (C=O), 767 (C-Cl). HRMS (ESI+) calculated for $C_{11}H_9O_3N_1Cl_1$ $[M+H]^+$ 238.0265 found 238.0265. Mp. 248-249°C.

3-acetamido-2-oxo-2H-chromen-8-yl acetate (87)

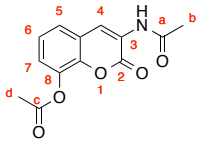

A mixture of 2,3-dihydroxybenzaldehyde (4.5 g, 32.60 mmol), N-acetylglycine (3.81 g, 32.60 mmol), anhydrous sodium acetate (10.69 g, 130 mmol) and acetic anhydride (12 mL) was refluxed for 3 hours. After this the mixture was allowed to cool to room temperature. The crude solid was triturated with water and EtOAc added to precipitate the product. The solid was filtered and washed with small aliquots of EtOAc to furnish the desired compound as a off white powder (3.57 g, 42%). ^{1}H NMR (400 MHz, $CDCl_3$) δ_H ppm: 8.68 (s, 1 H, 4-H), 8.06 (br s, 1 H, NH), 7.39 (dd, J_1 = 8.0 Hz, J_2 = 1.6 Hz, 1 H, ArH), 7.28 (t, J = 8.0 Hz, 1 H, ArH), 7.20 (dd, J_1 = 8.0 Hz, J_2 = 1.6 Hz, 1 H, ArH), 2.42 (s, 3 H, d-CH_3), 2.25 (s, 3 H, b-CH_3). ^{13}C NMR (100 MHz, $CDCl_3$) δ_C ppm: 169.6, 168.7, 157.9, 141.7, 137.7, 125.4, 125.2, 124.5, 123.3, 123.0, 121.4, 24.9, 20.8. IR ν_{max} (neat) / cm^{-1} 3284 (CON-H), 1773 (C=O), 1711 (C=O), 1676 (C=O). HRMS (ESI+): calculated for $C_{13}H_{11}NO_5H$ $[M+H]^+$ 262.0710 found 262.0712. Mp 215-217°C.

3-acetamido-7-acetoxy-2H-chromen-2-one (88)

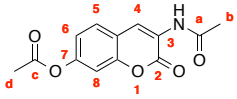

A mixture of 2,4-dihydroxybenzaldehyde (13.82 g, 100 mmol), N-acetylglycine (11.70 g, 100 mmol), anhydrous sodium acetate (32.8 g, 400 mmol) and acetic anhydride (60 mL) was refluxed for 3.5 hours before being cooled to room temperature and quenched with crushed ice. The mixture was triturated well with water and then EtOAc added to precipitate the product. The solid was filtered and washed with small aliquots of EtOAc to furnish the desired product as a pale yellow powder (10.44 g, 40%). ^{1}H NMR (400 MHz, $CDCl_3$) δ_H ppm: δ 8.67 (s, 1 H, 4-H), 8.03 (br s, 1 H, NH), 7.51 (d, J = 8.0 Hz, 1 H, ArH), 7.13 (d, J = 2.4 Hz, 1 H, ArH), 7.07 (dd, J_1 = 8.4 Hz, J_2 = 2.0 Hz, 1 H, ArH), 2.34 (s, 3 H, d-H_3), 2.25 (s, 3 H, b-H_3). ^{13}C NMR (100 MHz, $CDCl_3$) δ_C ppm: 169.5, 169.0, 158.6, 151.5, 150.3, 128.5, 123.7, 122.9, 119.3, 117.8, 110.2, 24.9, 21.2. IR ν_{max} (neat) / cm^{-1} 3340 (CON-H), 3079 (C=O overtone ester) 1757 (C=O), 1716 (C=O), 1678 (C=O), 1532 (C=C), 1200 (C-O stretch ester). HRMS (ESI+) calculated for $C_{13}H_{11}NO_5H$ $[M+H]^+$ 262.0710 found 262.0714. Mp. 238-239°C, (Lit 234-236°C).[248]

N-(6-nitro-2-oxo-2H-chromen-3-yl) acetamide (90)

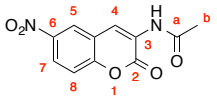

A mixture of 5-nitrosalicylaldhyde (5 g, 29.94 mmol), N-acetylglycine (3.50 g, 29.94 mmol), anhydrous sodium acetate (1119.76 mmol) and Ac_2O (14.13 mL) was refluxed for 3.5 hours. After which the mixture was allowed to cool to room temperature. The solid was triturated with water and EtOAc added to precipitate the product in the organic layer. The solid was filtered and washed with small aliquots of EtOAc to furnish the desired product as a pale yellow solid (3.71 g, 50%). ^{1}H NMR (400 MHz, $CDCl_3$) δ 8.76 (s, 1 H, 4-H), 8.44 (d, J = 2.6 Hz, 1 H, ArH), 8.30 (dd, J_1 = 8.0 Hz, J_2 = 2.4 Hz, 1 H, ArH), 8.08 (br s, 1 H, NH), 7.46 (d, J = 8.0 Hz, 1 H, ArH), 2.28 (s, 3H, c-H_3). ^{13}C NMR (100 MHz, $CDCl_3$) δ_C ppm: 169.6, 157.7, 153.1, 145.0, 125.7, 124.4, 123.5, 121.4, 120.5, 117.6, 24.9. IR ν_{max} (neat) / cm^{-1} 3372 (CON-H), 3096-3080 (Ar-H), 1722 (C=O), 1686 (C=O), 1519 (C=C), 1515 (C=C), 1504 (C=C), 1332 (C-NO_2). HRMS (ESI+) calculated for $C_{11}H_9N_2O_5$ $[M+H]^+$ 249.0506 found 249.0509. Mp. 277-278°C, (Lit 274-277°C).[248]

***Tert*-butyl N-(2-oxo-2H-chromen-3-yl) carbamate (95)**

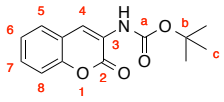

To a mixture of compound **77** (1 g, 4.92 mmol) and DMAP (60 mg, 0.49 mmol) in THF (15 mL) was added Boc_2O (3.21 g, 14.72 mmol). The mixture was stirred vigorously at room temperature for 1 hour before hydrazine hydrate (0.78 g, 24.63 mmol) and methanol (10 mL) were added. The reaction was allowed to stir for a further 3 hours after which the solvent was removed under vacuum. The crude was then dissolved in DCM, washed with 1M HCl, Cu(II)SO_4 and sat. $NaHCO_3$. The organic layer was dried over $MgSO_4$ the solvent removed under pressure and the product purified by flash column chromatography (ethyl acetate/hexanes 1:9) to furnish the product as a white powder (0.64 g, 50%). ^{1}H NMR (400 MHz, $CDCl_3$) δ_H ppm: 8.27 (br s, 1 H, 4-H) 7.45 (dd, J_1 = 7.6 Hz, J_2 = 1.6 Hz, 1 H, ArH) 7.41 (td, J_1 = 7.2 Hz, J_2 = 1.6 Hz, 2 H, ArH overlapping NH), 7.31-7.25 (m, 2 H, 7 and ArH), 1.54 (s, 9 H, c-H_3). ^{13}C NMR ($CDCl_3$ 100 MHz) δ_C ppm: 158.7, 152.6, 149.6, 129.1, 127.4, 125.1, 124.7, 120.5, 120.1, 116.4, 81.8, 28.3. IR ν_{max} (neat) / cm^{-1} 3415 (CON-H), 3321 (CON-H), 2997-2924 (Ar-H), 1702 (C=O) 1698 (C=O), 1519 (C=C). HRMS (ESI+) calculated for $C_{14}H_{15}NO_4H$ $[M+H]^+$ 262.1074 found 262.1071. Mp. 96-98°C, (Lit 85-86 °C).[248]

Tert-butyl N-(8-methoxy-2-oxo-2H-chromen-3-yl) carbamate (96)

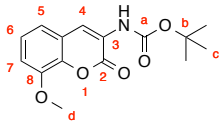

To a mixture of compound **79** (0.5 g , 2.15 mmol) and DMAP (26.23 mg, 0.22 mmol) in THF was added Boc_2O (1.87 g, 8.58 mmol). The reaction mixture was stirred at rt for 19 hours after which hydrazine was added (345 mg, 10.75 mmol) followed by MeOH (6 mL). The reaction was stirred for a further 50 minutes before the solvent was removed under pressure. The crude was dissolved in DCM, washed once with 1M HCl, $Cu(II)SO_4$ and sat. $NaHCO_3$. The organic layer was then dried over $MgSO_4$, the solvent removed under pressure and the product purified by flash column chromatography (EtOAc/hexanes 3:17) to give a yellow powder (0.3 g, 48%). ^{1}H NMR (400 MHz, $CDCl_3$) δ_H ppm: 8.22 (br s, 1 H, 4-H), 7.42 (br s, 1 H, NH), 7.18 (t, J = 8.0 Hz, 1 H, ArH), 7.02 (dd, J_1 = 8.0 Hz, J_2 = 1.2 Hz, 1 H, ArH), 6.95 (dd, J_1 = 8.0 Hz, J_2 = 1.2 Hz, 1 H, ArH), 3.94 (s, 3 H, d-H_3), 1.52 (s, 9 H, c-H_3). ^{13}C NMR (100 MHz, $CDCl_3$) δ_C ppm: 158.2, 152.6, 147.1, 139.1, 125.0, 124.9, 120.9, 120.5, 119.0, 111.2, 81.8, 56.3, 28.3. IR ν_{max} (neat) / cm^{-1} 3317 (CON-H), 2984 (Ar-H), 1728 (C=O), 1698 (C=O). HRMS (ESI+) calculated for $C_{15}H_{18}NO_5$ $[M+H]^+$ 292.1179 found 292.1178. Mp. 145-147°C, (Lit 97-99°C).[248]

Tert-butyl N-(7-methoxy-2-oxo-2H-chromen-3-yl) carbamate (97)

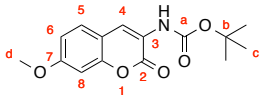

To a mixture of compound **81** (1 g, 4.29 mmol), and DMAP (2.62 g, 21.46 mmol) in THF (30 mL) was added Boc_2O (4.68 g, 21.46 mmol). After 2 hours hydrazine monohydrate (1.06 g, 21.17 mmol) followed by 15 mL of MeOH was added and the reaction stirred vigorously for a further hour before the reaction solvent was removed under vacuum. The crude residue was dissolved in DCM and washed once with 1M HCl, 1M $Cu(II)SO_4$ and sat. $NaHCO_3$. The organic layer was dried over $MgSO_4$ and the solvent removed under reduced pressure. The product was isolated by flash column chromatography (EtOAc/hexanes 1:4) to furnish the product as a white powder (372 mg, 30%). ^{1}H NMR (400 MHz, $CDCl_3$) δ_H ppm: 8.23 (s, 1 H, 4-H), 7.35 (d, J = 8.0 Hz, 1 H, ArH), 7.28 (s, 1 H, NH), 6.86 (dd, J_1 = 8.0 Hz, J_2 = 2.4 Hz, 1 H, ArH), 6.81 (d, J = 2.4 Hz, 1 H, ArH), 3.85 (s, 3 H, d-H_3), 1.52 (s, 9 H, c-H_3). ^{13}C NMR (100 MHz, $CDCl_3$) δ_C ppm: 160.9, 159.0, 152.7, 151.1, 128.2, 122.3, 121.4, 113.4, 113.2, 100.8, 81.6, 55.8, 28.4. IR ν_{max} (neat) / cm^{-1} 3423 (CON-H), 2985 (Ar-H), 2939 (Ar-H), 2831 (Ar-H), 1713 (C=O), 1615 (C=O). HRMS (ESI+) calculated for $C_{15}H_{18}NO_5$ $[M+H]^+$ 292.1179 found 2921182. Mp.119-120°C, (Lit 117-118°C).[248]

Tert-butyl N-(6-chloro-2-oxo-2H-chromen-3-yl) carbamate (98)

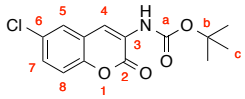

To a mixture of compound **83** (250 mg, 0.52 mmol) and DMAP (64 mg, 1.05 mmol) in THF (4 mL) was added Boc_2O (0.9 g, 4.13 mmol). The reaction mixture was stirred for 18 hours at room temperature. Subsequently hydrazine monohydrate (254 μL, 10.5 mmol) and MeOH (4 mL) were added and the reaction left for 1 hour before the solvent was removed under reduced pressure. The crude residue was dissolved in DCM, washed with 1M HCl, sat. $CuIISO_4$, Sat. $NaHCO_3$ and dried over $MgSO_4$. The product was purified by flash column chromatography (EtOAc/hexanes 1:1) to give the desired compound as a white powder (62 mg, 20%). ^{1}H NMR (400 MHz, $CDCl_3$) δ_H ppm: 8.13 (br s, 1 H, 4-H), 7.39 (br s, 1 H, NH), 7.37 (d, J = 2.4 Hz, 1 H, ArH), 7.29 (dd, J_1 = 8.8 Hz, J_2 = 2.4 Hz, 1 H, ArH), 7.19 (d, J = 8.8 Hz, 1 H, ArH), 1.50 (s, 9 H, c-H_3). ^{13}C NMR (100 MHz, $CDCl_3$) δ_C ppm: 158.1, 152.3, 147.8, 130.4, 128.8, 126.4, 125.6, 121.4, 118.8, 117.7, 82.0, 28.2. IR ν_{max} (neat) / cm^{-1} 3403 (CON-H), 3095 (Ar-H), 2986 (C-H_3), 2929 (C-H_3) 1706 (C=O), 1507 (C=O), 767 (C-Cl). HRMS (ESI+) calculated for $C_{14}H_{15}ClNO_4$ $[M+H]^+$ 296.0684 found 296.0688. Mp.113-114°C.

Tert-butyl N-(8-chloro-2-oxo-2H-chromen-3-yl) carbamate (99)

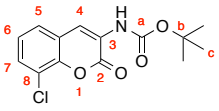

To a mixture of compound **85** (1 g, 4.22 mmol) and DMAP (257 mg, 2.11 mmol) in THF (15 mL) was added Boc_2O (3.68 g, 16.88 mmol). The mixture was stirred at room temperature for 28 h after which hydrazine monohydrate (1.06 g, 21.10 mmol) was added followed by MeOH (15 mL). After a further 2 hours of vigorous stirring the solvent was removed under pressure and the crude dissolved in DCM. The organic layer was washed once with 1M HCl, sat. $Cu(II)SO_4$, sat. $NaHCO_3$ and dried over $MgSO_4$. The product was purified by flash column chromatography (EtOAc/hexanes 1:9) to furnish the product as a white powder (320 mg, 26%). ^{1}H NMR (400 MHz, $CDCl_3$) δ_H ppm: 8.26 (br s, 1 H, 4-H), 7.45 (dd, J_1 = 8.0 Hz, J_2 = 1.6 Hz, 1 H, ArH), 7.43 (br s, 1 H, NH), 7.36 (dd, J_1 = 8.0 Hz, J_2 = 1.6 Hz, 1 H, ArH), 7.21 (t, J = 8.0 Hz, 1 H, ArH), 1.53 (s, 9 H, c-H_3). ^{13}C NMR ($CDCl_3$, 100 MHz) δ_C ppm: 157.9, 152.5, 145.2, 129.5, 125.9, 125.4, 125.3, 121.6, 121.4, 119.8, 82.2, 28.3. IR ν_{max} (neat) / cm^{-1} 3326 (CON-H), 2983-2924 (Ar-H), 1731 (C=O), 1702 (C=O), 1597 (C=C), 1567 (C=C), 1526 (C=C), 759 (C-Cl). HRMS (ESI+) calculated for $C_{14}H_{15}ClNO_4$ $[M+H]^+$ 296.0684 observed 296.0686. Mp. 145-147°C.

Tert-butyl N-(8-hydroxy-2-oxo-2H-chromen-3-yl) carbamate (100)

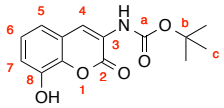

To a mixture of compound **87** (0.5 g, 1.92 mmol) and DMAP (117 mg, 0.96 mmol) in THF (8 mL) was added Boc_2O (1.67 g, 7.68). The mixture was stirred for 2 hours at room temperature after which hydrazine monohydrate (460 mg, 9.60 mmol) was added followed by MeOH (8 mL). The reaction mixture was stirred for a further 4 hours before the solvent was removed under vacuum. The residue was dissolved in DCM and washed once with 1M HCl, $Cu(II)SO_4$, sat. $NaHCO_3$ and brine. The organic layer was dried over $MgSO_4$, the solvent removed under pressure, and the product was purified by flash column chromatography (EtOAc/hexanes 3:7) to give a white powder (111 mg, 21%). ^{1}H NMR (400 MHz, $CDCl_3$) δ_H ppm: 8.30 (br s, 1 H, 4-H), 7.37 (br s, 1 H, NH), 7.04 (dd, J_1 = 8.0 Hz, J_2 = 1.6 Hz, 1 H, ArH), 7.01 (dd, J_1 = 8.0 Hz, J_2 = 1.6 Hz, 1 H, ArH), 1.54 (s, 9 H, c-H_3). ^{13}C NMR (100 MHz, $CDCl_3$) δ_C ppm: 157.9, 152.5, 143.1, 137.5, 125.7, 124.7, 121.1, 120.6, 119.0, 115.7, 82.0, 28.4. IR ν_{max} (neat) / cm^{-1} 3419 (CON-H), 3398 (O-H), 2970 (Ar-H), 1707 (C=O). HRMS (ESI+) calculated for $C_{14}H_{15}NO_5Na$ $[M+Na]^+$ 300.0842 found 300.0845. Mp. 165-167°C.

Tert-butyl N-(7-hydroxy-2-oxo-2H-chromen-3-yl) carbamate (101)

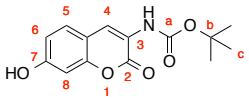

To a mixture of compound **88** (2.17 g, 8.25 mmol) and DMAP (250 mg, 2.04 mmol) in THF (85 mL) was added Boc_2O (7.19 g, 32.96 mmol). The reaction mixture was stirred at room temperature for 45 minutes after which hydrazine monohydrate (2.06 g, 41.20 mmol) was added followed by MeOH (40 mL). After a further 40 minutes the solvent was removed under reduced pressure and the residue taken up in DCM. The organic layer was washed once with 1M HCl, 1M $Cu(II)SO_4$ and sat. $NaHCO_3$. The organic layer was dried over $MgSO_4$ the solvent removed. The product was purified by flash column chromatography (EtOAc/hexane 3:17) to give the desired compound as a white powder (480 mg, 21%). ^{1}H NMR (400 MHz, CD_3OD) δ_H ppm: δ 8.14 (br s, 1 H, 4-H), 7.34 (d, J = 8.0 Hz, 1 H, ArH), 6.77 (dd, J_1 = 8.0 Hz, J_2 = 2.4 Hz, 1 H, ArH), 6.68 (d, J = 2.4 Hz, 1 H, ArH), 1.52 (s, 9 H, c-H_3). ^{13}C NMR (100 MHz, CD_3OD) δ_C ppm: 160.8, 160.2, 154.5, 152.8, 129.6, 124.5, 122.8, 114.8, 113.4, 103.2, 82.1, 28.5. IR ν_{max} (neat) / cm^{-1} 3316 (O-H), 3079 (C-H_3 and C-H_2), 2978 (C-H_3 and C-H_2) 1702 (C=O), 1684 (C=O), 1607 (C=C), 1534 (C=C), 1510 (C=C). HRMS (ESI+) calculated for $C_{14}H_{15}NO_5H$ $[M+H]^+$ 278.1028 found 278.1028. Mp. 174-176°C, (Lit 177-178°C).[248]

Tert-butyl-N-(6-nitro-2-oxo-2H-chromen-3-yl) carbamate (102)

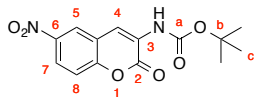

To a mixture of compound **90** (1 g, 4.03 mmol) and DMAP (245 mg, 2.01 mmol) in THF (50 mL) was added Boc_2O (3.51 g, 16.12 mmol). The reaction mixture was stirred at room temperature for 19 h after which hydrazine monohydrate (1 g, 20.15 mmol) was added followed by MeOH (25 mL). After a further 2 hours of vigorous stirring at room temperature the solvent was removed under reduced pressure and the crude dissolved in DCM. The organic layer was washed once with 1M HCl, sat. $Cu(II)SO_4$ and sat. $NaHCO_3$. Subsequently the organic layer was dried over $MgSO_4$ and the solvent removed to furnish crude compound. The desired product was obtained by flash column chromatography (EtOAc/hexanes 1:9) as an off white powder (228 mg, 18%). ^{1}H NMR (400 MHz, $CDCl_3$) δ_H ppm: 8.38 (d, J = 2.4 Hz, 1 H, ArH), 8.35 (s, 1 H, 4-H), 8.25 (dd, J_1 = 8.0 Hz, J_2 = 2.4 Hz, 1 H, ArH), 7.43 (d, J = 8.0 Hz, 2 H, ArH overlapping NH), 1.54 (s, 9 H, c-H_3). ^{13}C NMR (100 MHz, $CDCl_3$) δ_C ppm: 157.5, 152.7, 152.2, 144.9, 126.5, 123.8, 123.0, 120.8, 118.5, 117.5, 82.6, 28.3. IR ν_{max} (neat) / cm^{-1} 3409 (CON-H), 3075 (C-H_3), 2976 (Ar-H), 1715 (C=O), 1526 (C=C) 1509 (C=C), 1338 (C-NO_2). HRMS (ACPI+) calculated for $C_{14}H_{15}N_2O_6$ $[M+H]^+$ 307.0925 found 307.0920. Mp. 145-146°C, (Lit 132-134).[248]

3-amino-2H-chromen-2-one (104)

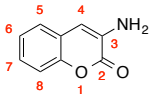

Compound **77** (1.99 g, 9.08 mmol) was added to a mixture of conc. HCl and EtOH (2:1) and refluxed for 5 hours. Subsequently the solution was allowed to cool to room temperature. The pH was adjusted with NaOH to pH 7 and the precipitate filtered and desiccated to furnish the product as a yellow powder (866 mg, 54%). ^{1}H NMR (400 MHz, DMSO-d6) δ_H ppm: 7.42-7.40 (m, 1 H, ArH), 7.28-7.24 (m, 1 H, ArH), 7.22-7.17 (m, 2 H, ArH), 6.71 (s, 1 H, 4-H), 5.69 (s, 2 H, NH_2). ^{13}C NMR (DMSO-d6, 100 MHz) δ_C ppm: 158.6, 147.9, 133.3, 125.3, 124.8, 124.5, 121.8, 115.4, 107.6. IR ν_{max} (neat) / cm^{-1} 3425 (N-H), 3313 (N-H), 3054 (Ar-H), 3022 (Ar-H), 1702 (C=O), 1633 (N-H_2 scissor), 1331 (C-N), 888 (N-H_2 wag). HRMS (APCI+) calculated for $C_9H_7NO_2H$ $[M+H]^+$ 162.0550 found 162.0548. Mp. 136-138°C, (Lit 138-140°C).[281]

3-amino-8-methoxy-2H-chromen-2-one (106)

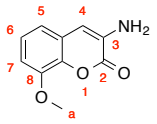

A mixture of conc. HCl (5 mL) and EtOH (5 mL) was added to compound **79** (1.2 g, 5.15 mmol). The suspension was refluxed for 3 hours before being allowed to cool to room temperature. The pH was adjusted to neutral with NaOH. The resultant precipitate was filtered and washed with small aliquots of EtOH to furnish the desired product (0.49 g, 50%). ^{1}H NMR (400 MHz, DMSO-d6) δ_H ppm: 7.13 (t, J = 8.0 Hz, 1 H, ArH), 6.97 (dd, J_1 = 8.0 Hz, J_2 = 1.3 Hz, 1 H, ArH), 6.92 (dd, J_1 = 8.0 Hz, J_2 = 1.2 Hz, 1 H, ArH) 6.68 (s, 1 H, 4-H), 5.69 (br s, 2 H, NH_2), 3.86 (s, 3 H, a-H_3). ^{13}C NMR (100 MHz, DMSO-d6) δ_C ppm: 158.3, 146.3, 137.0, 133.5, 124.4, 122.4, 116.6, 108.3, 107.8, 55.8. IR ν_{max} (neat) / cm^{-1} 3360 (N-H), 3338 (N-H), 2997 (C-H_3), 2969 (C-H_3), 2941 (C-H_3), (Ar-H) 1686 (C=O), 1633 (N-H_2 scissor), 1608 (C=C), 1593 (C=C), 1571 (C=C), 763 (N-H_2 wag). HRMS (ESI+) calculated for $C_{10}H_9NO_3H$ $[M+H]^+$ 192.0655 found 192.0654. Mp. 133-135 °C, (Lit 124-125 °C).[281]

3-amino-7-methoxy-2H-chromen-2-one (107)

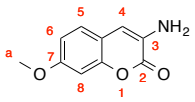

Compound **81** (1 g, 4.29 mmol) was added to a mixture of conc. HCl and EtOH (2:1) and refluxed for 18 hours. Subsequently the solution was allowed to cool to room temperature and quenched with H_2O. The pH was adjusted with KOH to pH 8 and the aqueous phase extracted three times with chloroform. The organic fractions were pooled, dried over $MgSO_4$ and the solvent removed under vacuum. The crude was purified by flash column chromatography using a gradient (EtOAc/Hexanes 1:9 to 1:4) to furnish the product as a yellow powder (213 mg, 26%). ^{1}H NMR (400 MHz, $CDCl_3$) δ_H ppm: 7.19 (d, J = 8.0 Hz, 1 H, ArH), 6.83-6.80 (m, 2 H, ArH), 6.70 (s, 1 H, 4-H), 4.06 (br s, 2 H, NH_2). ^{13}C NMR (100 MHz, $CDCl_3$) δ_C ppm: 159.9, 159.2, 150.5, 129.9, 126.0, 114.5, 112.7, 112.4, 100.9, 55.8. IR ν_{max} (neat) / cm^{-1} 3419 (N-H), 3355 (N-H), 3091 (Ar-H), 3006 (Ar-H), 2745-2498 (C-H_3), 1707 (C=O), 1607 (N-H_2 scissor), 1556 (C=C), 1543 (C=C), 1510 (C=C), 1250 (C-N), 753 (N-H_2 wag). HRMS (ESI+) calculated for $C_{10}H_{10}NO_3$ $[M+H]^+$ 192.0655 found 192.0653. Mp. 220-222°C, (137-139°C).[248]

3-amino-6-chloro-2H-chromen-2-one (108)

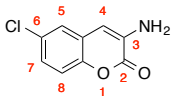

A suspension of compound **83** (1 g, 4.22 mmol), in conc. HCl and EtOH (2:1) was refluxed for 3.5 hours. After which it was allowed to cool to room temperature and the suspension cooled to zero degrees. The pH was adjusted with KOH to neutral. A cream solid was filtered, washed with small aliquots of EtOH and subsequently desiccated to give the desired compound (735 mg, 90%). ^{1}H NMR (400 MHz, DMSO-d6) δ_H ppm: 7.54 (d, J = 2.4 Hz, 1 H, ArH), 7.29 (d, J = 8.4 Hz, 1 H, ArH), 7.21 (dd, J_1 = 8.8 Hz, J_2 = 2.4 Hz, 1 H, ArH), 6.66 (s, 1 H, 4-H), 5.94 (br s, 2 H, NH_2). ^{13}C NMR (100 MHz, DMSO-d6) δ_C ppm: 158.2, 146.3, 134.2, 128.4, 124.5, 123.7, 123.6, 117.2, 105.8. IR ν_{max} (neat) / cm^{-1} 3407 (N-H), 3322 (N-H), 1708 (C=O), 810 (C-Cl). HRMS (APCI+) calculated for C_9H_7NOCl $[M+H]^+$ 196.0160 found 196.0159. Mp. 213-215°C, (Lit 204-206°C).[282]

3-amino-8-chloro-2H-chromen-2-one (109)

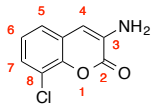

A mixture of conc. HCl and EtOH (2:1) was added to compound **85** (1 g, 4.22 mmol). The suspension was refluxed for 3.5 hours after which the reaction was cooled to 0 °C and taken to a neutral pH with KOH. The solvent was removed under reduced pressure. The product was purified by flash chromatography (EtOAc/hexanes 2:3) to give the product as white solid. (59 mg, 7%). ^{1}H NMR (400 MHz, $CDCl_3$) δ_H ppm: 7.32 (dd, J_1 = 8.0 Hz, J_2 = 1.6 Hz, 1 H, ArH), 7.19 (dd, J_1 = 8.0 Hz, J_2 = 1.6 Hz, 1 H, ArH), 7.13 (t, J = 8.0 Hz, 1 H, ArH) 6.67 (s, 1 H, 4-H), 4.35 (br s, 2 H, NH_2). ^{13}C NMR ($CDCl_3$, 100 MHz) δ_C ppm: 158.6, 144.7, 132.6, 127.2, 125.0, 123.6, 122.8, 121.2, 110.1. IR ν_{max} (neat) / cm^{-1} 3416 (N-H), 3334 (N-H), 1712 (C=O), 1638 (N-H_2 scissor), 15591 (C=C), 1556 (C=C), 1152 (C-N), 898 (N-H_2 wag) 764 (C-Cl). HRMS (ESI+) calculated for $C_9H_7ClNO_2$ $[M+H]^+$ 196.0160 found 196.0160. Mp. 127-128°C.

3-amino-8-hydroxy-2H-chromen-2-one (110)

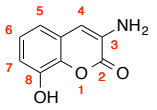

A mixture of conc. HCl (3 mL) and EtOH (3mL) was added to compound **87** (1 g, 3.83 mmol). The suspension was refluxed for 3 hours before being allowed to cool to room temperature. The suspension was taken to pH 7 with NaOH and the solid filtered and washed with a small aliquot of

EtOH to furnish the desired product as a brown solid (0.27 g, 40%). ^{1}H NMR (400 MHz, DMSO-d6) δ_H ppm: 9.94 (s, 1 H, OH) 6.68 (t, J = 8.0 Hz, 1 H, ArH), 6.80 (dd, J_1 = 8.0 Hz, J_2 = 1.6 Hz, 1 H, ArH), 6.75 (dd, J_1 = 8.0 Hz, J_2= 1.6 Hz, 1 H, ArH), 6.66 (s, 1 H, 4-H), 5.62 (br s, 2 H, NH_2). ^{13}C NMR (100 MHz, DMSO-d6) δ_C ppm: 158.5, 144.2, 136.6, 133.2, 124.4, 122.7, 115.0, 112.4, 108.2. IR ν_{max} (neat) / cm^{-1} 3454 (N-H), 3456 (N-H), 3364 (OH), 1704 (C=O), 1697 (N-H scissor), 1611 (C=C), 1594 (C=C), 1567 (C=C), 1174 (C-O), 1144 (C-N). HRMS: (ESI+) calculated for $C_9H_7NO_3H$ $[M+H]^+$ 178.0499 found 178.0496. Mp. 203-204°C, (Lit 192°C).[283]

3-amino-7-hydroxy-2H-chromen-2-one (111)

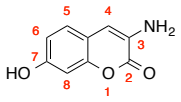

A suspension of compound **88** (4.13 g, 15.82 mmol) in conc. HCl and EtOH (2:1) was heated to reflux for 2 hours. The reaction was allowed to cool to room temperature before the pH was adjusted to neutral with 10% NaOH. The resultant solid was filtered and washed with small aliquot of EtOH to give the desired compound (0.87 g, 31%). ^{1}H NMR (400 MHz, CD_3OD) δ_H ppm: δ 7.33 (d, J = 8.0 Hz, 1 H, ArH), 7.26 (s, 1 H, 4-H), 6.80 (dd, J_1 = 8.0 Hz, J_2 = 2.4 Hz, 1 H, ArH), 6.73 (d, J = 2.4, 1 H, ArH). ^{13}C NMR (100 MHz, CD_3OD) δ_C ppm: 168.5, 165.9, 159.1, 139.1, 135.5, 122.9, 122.5, 120.6, 111.4. IR ν_{max} (neat) / cm^{-1} 3435 (N-H stretch), 3344 (N-H stretch), 3214 (O-H), 1678 (C=O). HRMS (ESI+) calculated for $C_9H_7NO_3H$ $[M+H]^+$ 178.0499 found 178.0498. Mp. 240-241°C, (Lit 237-238°C).[248]

Ethyl 1-cyclopropyl-6-fluoro-4-oxo-7-(piperazine-1-yl)-1,4-dihydroquinoline-3-carboxylate (138)

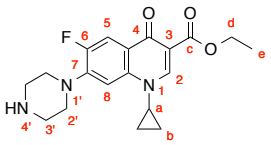

Thionyl chloride (8 mL, 13 g, 109.67 mmol) was added to ciprofloxacin (2 g, 6.04 mmol) at room temperature. Subsequently EtOH (30 mL) was added dropwise whilst vigorously stirring. Care was taken as the reaction was very exothermic. The reaction mixture went from a suspension to a clear orange solution, it was then refluxed for 30 h before being allowed to cool to room temperature. The crude was taken up into sat. $NaHCO_3$ and extracted three times with DCM, dried over $MgSO_4$ and the solvent removed under pressure. The product was obtained as a white powder (1.3 g, 60%). ^{1}H NMR (400 MHz, $CDCl_3$) δ_H ppm: 8.42 (s, 1 H, 2-H), 7.88 (d, J_{HF} = 12.0 Hz, 1 H, 5-H), 7.2 (d, J_{HF} = 7.2 Hz, 1 H, 8-H), 4.32 (q, J = 7.1 Hz, 2 H, d-H_2), 3.43-3.38 (m, 1 H, a-H), 3.21-3.19 (m, 4 H, 2' or 3'-H_2), 3.07-3.05 (m, 4 H, 2' or 3'-H_2), 2.35 (br s, 1 H, NH), 1.35 (t, J = 7.1 Hz, 3 H, e-H_3),

1.30-1.25 (m, 2 H, b-H_2), 1.11-1.07 (m, 2 H, b-H_2). ^{13}C NMR (100 MHz, $CDCl_3$) δ_C ppm: 173.1 (d, J_{CF} = 2.0 Hz), 165.6, 153.4 (d, J_{CF} = 247.0 Hz), 148.1, 144.9 (d, J_{CF} = 10.0 Hz), 138.0, 122.8 (d, J_{CF} = 7.0 Hz), 113.0 (d, J_{CF} = 23.0 Hz), 110.2, 104.8 (d, J_{CF} = 3.0 Hz), 60.8, 51.4 (d, J_{CF} = 4.0 Hz), 46.0, 34.6, 14.5, 8.2. ^{19}F NMR (376 MHz, $CDCl_3$) δ_F ppm: -123.7 (s). IR ν_{max} (neat) / cm^{-1} 2942-2820 cm^{-1} (C-H_2 and C-H_3), 1716 cm^{-1} (C=O), 1617 cm^{-1} (C=O). HRMS (ESI+) calculated for $C_{19}H_{23}FN_3O_3$ $[M+H]^+$ 360.1718 found 360.1720. Mp. 218-223°C, (Lit 179-180).[284] RP-HPLC showed 99% purity at 254 nm.

(2E, 4E, 6E, 8E)-deca-2, 4, 6, 8-tetraenedioic acid (140)

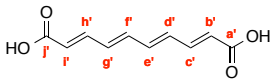

Commercially available Fumadil B^{TM} (1 g, 2.18 mmol) was added to EtOAc (200 mL) and washed three times with an equal volume of water to remove unwanted excipients. The organic layer was dried over $MgSO_4$ and the solvent removed under reduced pressure. The resultant product was added to 100 mL of 1M NaOH and stirred at rt for 72 h. Subsequently the mixture was washed three times with diethyl ether to remove any unreacted starting material. The remaining aqueous fraction was acidified with conc. HCl until pH 1 causing a yellow precipitate to form. This was filtered, and desiccated to give the desired product as a yellow powder (207 mg, 49%). ^{1}H NMR (400 MHz, DMSO-d6) δ_H ppm: 12.28 (br s, 2 H, OH), 7.25 (dd, J_1 = 16.0 Hz, J_2 = 12.0 Hz, 2 H, c'/h'-H), 6.82-6.75 (m, 2 H, d'-H), 6.66-6.56 (m, 2 H, c'-H), 5.99 (d, J = 16.0 Hz, b'/i'-H). ^{13}C NMR (100 MHz, DMSO-d6) δ_C ppm: 167.4, 143.4, 139.2, 133.8, 123.6, 69.8. IR ν_{max} (neat) / cm^{-1} 2818 (COO-H), 2534 (COO-H), 1659 (C=O), 1614 (C=O). HRMS (ESI-) calculated for $C_{10}H_9O_4$ $[M-H]^-$ 193.0506 found 193.0505. Mp. 240-245°C, (Lit 271-280°C).[285]

9-[(2-oxo-2H-chromen-3-yl) carbamoyl] nonanoic acid (142)

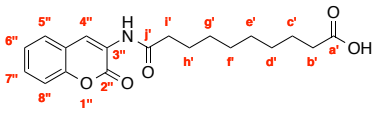

3-aminocoumarin (1 g, 5.07 mmol) in pyridine (15 mL) was added to a mixture of refluxing sebacoyl chloride (1.46 g, 6.09 mmol) in pyridine (15 mL) and stirred for 16 h before being cooled to rt. The reaction mixture was quenched with water and taken to pH 7 with 1 M HCl. Subsequently the product was extracted three times with EtOAc and washed with 10% Cu(II)SO_4 to remove pyridine. The organic layer was then dried over $MgSO_4$ and the solvent removed under reduced pressure. The product was purified by flash column chromatography by running a gradient from 1-10% MeOH in DCM. The desired compound was obtained as a white powder (0.45 g, 26%). ^{1}H NMR (400 MHz, DMSO-d6) δ_H ppm: 11.97 (s, 1 H, OH), 9.66 (s, 1 H, NH), 8.64 (s, 1 H, 4"-H), 7.70 (dd,

J_1 = 7.7, J_2 = 1.60, 1 H, ArH), 7.52-7.48 (m, 1 H, ArH), 7.40-7.32 (m, 2 H, ArH), 2.48-2.46 (t, 2 H, b' or i'-H_2, overlaps DMSO), 2.18 (t, 2 H, b' or i'-H_2), 1.58-1.55 (m, 2 H, c' or h'-H_2), 1.50-1.47 (m, 2 H, c' or h'-H_2) 1.29-1.23 (m, 8 H, d', e', f', g'-H_2). ^{13}C NMR (100 MHz, DMSO-d6) δ_C ppm: 174.5, 173.2, 157.5, 149.6, 129.5, 127.8, 124.9, 124.5, 123.6, 119.6, 115.8, 35.9, 33.7, 28.7, 28.6, 28.54, 28.53, 25.0 24.5. IR v_{max} (neat) / cm^{-1} 3289 (O-H & CON-H overlapping), 2920-2843 (C-H_2), 1728 (C=O), 1685 (C=O), 1682 (C=O). HRMS (ESI+) calculated for $C_{19}H_{24}N_1O_5$ $[M+H]^+$ 346.1649 found 346.1652. Mp 149-152°C.

1-cyclopropyl-6-fluoro-4-oxo-7-(4-{9-[(2-oxo-2H-chromen-3-yl)carbamoyl]nonanoyl}piperazin-1-yl)-1,4-dihydroquinoline-3-carboxylate (144)

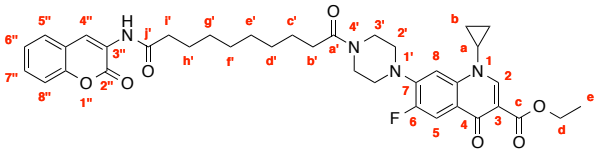

EDC (56.72 mg, 0.29 mmol) was added to a solution of compound **142** (94 mg, 0.27 mmol) in 30% pyridine/ DCM (10 mL) and stirred vigorously for 5 minutes to allow activation of the carboxylic acid. Subsequently compound **138** (96 mg, 0.27 mmol) was added and the reaction stirred for 23 h. After which it was acidified with 1 M HCl, extracted three times with EtOAc and the organic layer dried over $MgSO_4$. The solvent was removed under reduced pressure and the resultant product triturated with diethyl ether and DCM. The product was purified by flash chromatography using a gradient (EtOAc/hexanes 1:1 to 100% EtOAc). The product was obtained as a white solid (81.50 mg, 44%). ^{1}H NMR (400 MHz, $CDCl_3$) δ_H ppm: 8.68 (s, 1H, H, 4'-H), 8.50 (s, 1 H, 2-H), 8.06 (br s, 1 H, NH, overlaps doublet), 8.02 (d, J = 13.2 Hz, 1 H, ArH), 7.50-7.41 (m, 2 H, ArH), 7.32-7.24 (m, 3 H, ArH overlapping CDCl3 peak), 4.38 (q, J = 8.0 Hz, 2 H, d-H_2), 3.84 (app t, 2 H, 2' or 3'-H_2), 3.69 (app t, 2 H, 2' or 3'-H_2), 3.44-2.38 (m, 1 H, a-H), 3.26 (app t, 2 H, 2' or 3'-H_2), 3.20 (app t, 2 H, 2' or 3'-H_2), 2.44-2.35 (m, 4 H, b' or i'-H_2), 1.74-1.64 (m, 4 H, c' or h'-H_2), 1.41-1.30 (m, 13 H, d', e', f', g', overlapping, b-H_2 and e-H_3), 1.15-1.11 (m, 2 H, b-H_2). ^{13}C NMR (100 MHz, $CDCl_3$) δ_C ppm: 173.1 (d, J_{CF} = 1.0 Hz), 172.7, 171.9, 165.9, 159.0, 153.5 (d, J_{CF} = 247.0 Hz), 150.0, 148.4, 144.2 (d, J_{CF} = 10.0 Hz), 138.1, 129.8, 127.9, 125.3, 124.1, 123.6 (d, J_{CF} = 7.0 Hz), 123.3, 120.0, 116.5, 113.6 (d, J_{CF} = 23.0 Hz), 110.7, 105.2 (d, J_{CF} = 3.0 Hz), 61.1, 50.8 (d, J_{CF} = 6.0 Hz), 49.7 (d, J_{CF} = 3.0 Hz), 45.7, 41.4, 37.8, 33.6, 33.4, 29.5, 29.31 29.28, 29.19, 25.40, 25.37, 14.6, 8.3.^{19}F NMR (376 MHz, $CDCl_3$) δ_F ppm: -123.9 (s). IR v_{max} (neat) / cm^{-1} 2928-2851 (C-H_2 and C-H_3), 1720 (C=O), 1682 (C=O), 1615 (C=O). HRMS (ESI+) calculated for $C_{38}H_{44}FN_4O_7$ $[M+H]^+$ 687.3189 found 687.3181. RP-HPLC showed 97% purity at 214 nm.

1-cyclopropyl-6-fluoro-4-oxo-7-(4-{9-[2-oxo-2H-chromen-3-yl)carbamoyl]nonanoyl}piperazin-1-yl)-1,4-dihydroquinoline-3-carboxylic acid (145)

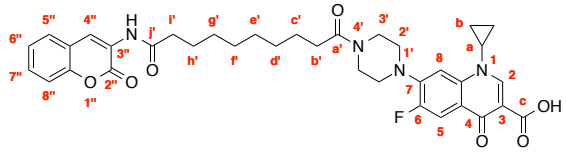

Compound **144** (39 mg, 0.057 mmol) was added to a solution of lithium hydroxide monohydrate (7.1 mg, 0.17 mmol) in a mixture of THF:MeOH:H_2O (3:2:1). The solution was stirred vigorously, after 23 hours another portion of lithium hydroxide monohydrate was added (7 mg, 0.017 mmol) and the solution stirred for a further for a further 50 hours at room temperature, after which 1 M HCl was added to form a precipitate. The suspension was extracted once with $CHCl_3$ and twice with DCM. The organic fractions were pooled and dried over $MgSO_4$. The crude orange solid was purified by flash column chromatography (DCM/MeOH 95:5) to give the desired product as a white powder (15 mg, 40%). ^{1}H NMR (400 MHz, $CDCl_3$) δ_H ppm: 14.9 (s, 1 H, OH), 8.76, (s, 1 H, 2-H), 8.69 (s, 1 H, 4"-H), 8.06 (br s, 1 H, NH), 8.03 (d, *J* = 12.0 Hz, 1 H, ArH), 7.50-7.42 (m, 2 H, ArH), 7.37-7.28 (m, 3 H, ArH), 3.87 (app t, 2 H, 3'-H_2), 3.72 (app t, 2 H, 3'-H_2), 3.57-3.51 (m, 1 H, a-H), 3.35 (app t, 2 H, 2'-H_2), 3.29 (app t, 2 H, 2'-H_2), 2.43 (t, *J* = 8.0 Hz, 2 H, b' or i'-H_2), 2.38 (t, 2 H, b' or l'-H_2), 1.75-1.67 (m, 4 H, c' and h'-H_2), 1.42-1.33 (m, 10 H, c', d', e', f', g'-H_2 overlapping b-H_2), 1.22-1.18 (m, 2 H, b-H_2). ^{13}C NMR (100 MHz, $CDCl_3$) δ_C ppm: 177.3 (d, J_{CF} = 2.0 Hz), 172.7, 172.0, 167.0, 159.0, 153.7 (J_{CF} = 248.0 Hz), 150.0, 147.8, 145.6 (d, J_{CF} = 10.0 Hz), 139.2, 129.8. 127.9, 125.4, 124.1, 123.4, 120.5 (d, J_{CF} = 8.0 Hz), 120.0, 116.5, 112.8 (d, J_{CF} = 23.0 Hz), 108.5, 105.2 (d, J_{CF} = 3.0 Hz), 50.5 (d, J_{CF} = 6.0 Hz), 49.6 (d, J_{CF} = 3.0 Hz), 45.4, 41.2, 37.9, 35.4, 33.3, 29.5, 29.30, 29.28, 29.19, 25.4, 25.3, 8.4. ^{19}F NMR (376 MHz, $CDCl_3$) δ_F ppm: -121.1 (s). HRMS (ESI+) calculated for $C_{36}H_{40}FN_4O_7$ $[M+H]^+$ 659.2876 found 659.2874. RP-HPLC showed 98% purity at 214 nm.

Methyl 9-(phenylcarbamoyl) nonanoic acid (147)

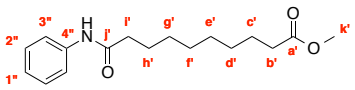

EDC (884 mg, 5.56 mmol) was added to a stirred solution of sebacic acid monomethyl ester (1 g, 4.63 mmol) in 30% pyridine/DCM solution. After 5 minutes, aniline (430.5 mg, 4.63 mmol) was added and the reaction stirred at room temperature for 19 h. Subsequently the reaction mixture was acidified with 1 M HCl and extracted three times with DCM. The organic layers were dried over $MgSO_4$ and the solvent removed under pressure. The crude product was taken up into sat. $NaHCO_3$ and extracted three times with DCM. The organic layers were pooled together, dried over $MgSO_4$ and the solvent removed to furnish the title product as a white solid (1.13 g, 83%). ^{1}H NMR

(400 MHz, $CDCl_3$) δ_H ppm: 7.57 (s, 1 H, NH), 7.51 (app d, *J* = 7.9 Hz, 1 H, ArH), 7.29 (app t, 2 H, ArH), 7.07 (app t, 2 H, ArH), 3.66 (s, 3 H, k'-H_3), 2.35-2.27 (m, 4 H, b' or i'-H_2), 1.73-1.66 (m, 2 H, c' or h'-H_2), 1.62-1.56 (m, 2 H, c' or h'-H_2), 1.36-1.26 (m, 8 H, overlapping d', e', f', g'-H_2). ^{13}C NMR (100 MHz, $CDCl_3$) δ_C ppm: 174.5, 171.7, 138.2, 129.0, 124.2, 119.9, 51.6, 37.8, 34.2, 29.25, 29.20, 29.12, 25.7, 25.0. IR ν_{max} (neat) / cm^{-1} 3359 cm^{-1} (CON-H), 2927-2849 cm^{-1} (C-H_2 and C-H_3), 1713 cm^{-1} (C=O), 1682 cm^{-1} (C=O). HRMS (ESI+) calculated for $C_{17}H_{26}NO_3$ $[M+H]^+$ 292.1907 found 292.1905. Mp. 70-73 °C.

9-(phenylcarbamoyl) nonanoic acid (148)

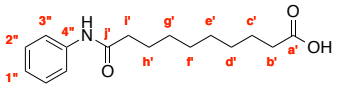

Compound **147** (1g, 3.44 mmol) was added to a solution of LiOH monohydrate (422 mg, 10.31 mmol) in EtOH and H_2O (2:1). The reaction was stirred at room temperature for 20 h after which sat. $NaHCO_3$ was added and extracted once with DCM. The remaining aqueous layer was acidified with 1 M HCl, extracted three times with DCM and dried over $MgSO_4$. The solvent was removed under pressure and hot EtOAc added; the product was allowed to recrystallize at room temperature, filtered off and washed with cold hexane to furnish the desired compound as a white solid (626 mg, 66%). ^1H NMR (400 MHz, CD_3OD) δ_H ppm: 7.54-7.52 (m, 2 H, ArH), 7.31-7.26 (m, 2 H, ArH), 7.09-7.05 (m, 1 H, ArH), 2.36 (t, *J* = 8.0 Hz, 2 H, 2, b' or i'-H_2), 2.27 (t, *J* = 8.0 Hz, 2 H, 2, b' or i'-H_2), 1.73-1.66 (quint, 2 H, c' or d'-H_2), 1.62-1.56 (quint, 2 H, c' or d'-H_2), 1.41-1.32 (m, 8 H, overlapping e', f', g', h'-H_2). ^{13}C NMR (100 MHz, CD_3OD) δ_C ppm: 177.7, 174.7, 139.9, 129.8, 125.1, 121.3, 38.0, 35.0, 30.28, 30.26, 30.17, 26.9, 26.1. IR ν_{max} (neat) / cm^{-1} 3300 cm^{-1} (CON-H overlapping O-H), 2916-2848 cm^{-1} (C-H_2), 1689 cm^{-1} (C=O), 1659 cm^{-1} (C=O). HRMS (ESI-) calculated for $C_{16}H_{22}NO_3$ $[M-H]^-$ 276.1605 found 276.1600. Mp: 120-123°C.

Ethyl 1-cyclopropyl-6-fluoro-4-oxo-7-{4-[9-(phenylcarbamoyl)nonanoyl]piperazine-1-yl}-1, 4-dihydroquinoline-3-carboxylate (149)

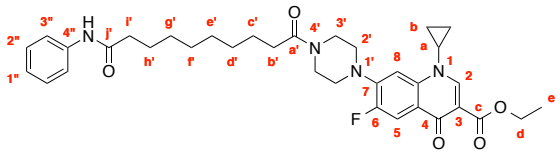

A mixture of **148** (500 mg, 1.81 mmol) and EDC (414 mg, 2.17 mmol) was added to a solution of 30% pyridine/DCM. The mixture was stirred vigorously for 5 minutes after which compound **138** (649 mg, 1.81 mmol) was added. The mixture was stirred at room temperature for 19 hours then acidified with 1 M HCl, extracted three times DCM and the organic fractions dried over $MgSO_4$. The dried organic fraction was azeotroped with toluene to furnish an orange solid. The product was

purified by flash column chromatography (DCM/MeOH 95:5) to remove major impurities and the desired product recrystallized from the eluent using EtOAc and Hexane to give a cream solid (247 mg, 22%). ^{1}H NMR (400 MHz, $CDCl_3$) δ_H ppm: 8.54 (s, 1 H, 2-H), 8.10 (d, J = 16.0 Hz, 5-H), 7.52 (app d, 2 H, ArH), 7.31 (app t, 3 H, ArH overlapping NH), 7.26 (d, J = 8.0 Hz, 1 H, 8-H), 7.09 (app t, 1 H, ArH), 4.38 (q, J = 8.0 Hz, 1 H, d-H_2), 3.85 (app t, 2 H, 3'-H_2), 3.69 (app t, 2 H, 3'-H_2), 3.44-3.38 (m, 1 H, a-H), 3.26 (app t, 2 H, 2'-H_2), 3.21 (app t, 2 H, 2'-H_2), 2.39-2.32 (m, 4 H, b' or i'-H_2), 1.74-1.62 (m, 4 H, c or h'-H_2), 1.41 (t, J = 8.0 Hz, 3 H, e-H_3 overlapping multiplet), 1.38-1.29 (m, 10 H, (d', e', f', g' overlapping b-H_2), 1.15-1.11 (m, 2 H, b-H_2). ^{13}C NMR (100 MHz, $CDCl_3$) δ_C ppm: 173.2 (d, J_{CF} = 2.0 Hz), 172.0, 171.9, 165.6, 153.3 (d, J_{CF} = 247.0 Hz), 148.3, 144.1 (d, J_{CF} = 10.0 Hz), 138.4, 138.0, 128.9, 124.0, 123.4 (d, J_{CF} = 7.0 Hz), 119.9, 113.3 (d, J_{CF} = 23.0 Hz), 110.4, 105.2 (d, J_{CF} = 2.0 Hz), 60.8, 50.5 (d, J_{CF} = 4.0 Hz), 49.7 (d, J_{CF} = 3.0 Hz), 45.6, 41.3, 37.6, 34.7, 33.3, 29.4, 29.2, 25.6, 25.3, 29.1, 14.5, 8.2. ^{19}F NMR (376 MHz, $CDCl_3$) δ_F ppm: -124.0 (s). IR ν_{max} (neat) / cm^{-1} 3286 (CON-H), 2923-2853 (C-H_2 and C-H_3), 1732 (C=O), 1615 (C=O). HRMS (ESI+) calculated for $C_{35}H_{44}FN_4O_5$ 619.3290 $[M+H]^+$ found 619.3275. Mp. 145-147°C. RP-HPLC showed 95% purity at 214 nm.

1-cyclopropyl-6-fluoro-4-oxo-7-{4-[9-(phenylcarbamoyl)nonanoyl]piperazin-1-yl}-1,4-dihydroquinoline-3-carboxylic acid (150)

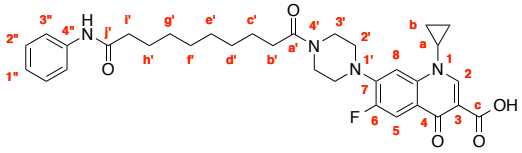

Compound **149** (50 mg, 0.08 mmol) was added to a mixture of LiOH monohydrate (14 mg, 0.34 mmol) in 1.5 mL EtOH/H_2O (2:1) and stirred vigorously at room temperature for 20.5 hours. After which sat. $NaHCO_3$ was added, the mixture was extracted with DCM, dried over $MgSO_4$ and evaporated under reduced pressure. The resultant film was triturated with ether and a few drops of DCM to furnish a cream powder (38 mg, 64%). ^{1}H NMR (400 MHz, DMSO-d6) δ_H ppm: 15.19 (s, 1 H, OH), 9.83 (br s, 1 H, NH), 8.67 (s, 1 H, 2-H) 7.94 (d, J_{HF} = 13.2 Hz, 1 H, 5-H), 7.58 (app d, 3 H, ArH overlapping 8-H), 7.27 (app t, 2 H, ArH), 7.01 (app t, 1 H, ArH), 3.85-3.79 (m, 1 H, a-H), 3.68 (app t, 4 H, 3'-H_2), 3.36-3.27 (m, 4 H, 2'-H_2 overlapping water peak), 2.36 (t, J = 8.0 Hz, 2 H, b' or i'-H_2), 2.29 (t, J = 8.0 Hz, 2 H, b' or i'-H_2), 1.60-1.50 (m, 4 H, c' or h'-H_2), 1.33-1.28 (m, 10 H, (d', e', f', g'-H_2 overlapping b-H_2), 1.21-1.17 (m, 2 H, b-H_2). ^{13}C NMR (100 MHz, DMSO-d6) δ_C ppm: 176.3 (d, J_{CF} = 8.0 Hz), 171.2, 170.8, 165.9, 152.95 (d, J_{CF} = 250.0 Hz), 148.07, 144.94 (d, J_{CF} = 10.0 Hz), 139.3, 139.1, 128.6, 122.9, 119.0, 118.81 (d, J_{CF} = 8.0 Hz), 111.0, 106.8, 106.63 (d, J_{CF} = 3.0 Hz), 49.7 (d, J_{CF} = 4.0 Hz), 49.3 (d, J_{CF} = 4.0 Hz), 44.6, 40.60, 36.4 35.9, 32.2, 28.8, 28.6, 25.1, 24.7, 7.6. ^{19}F NMR (376 MHz, DMSO-d6) δ_F ppm: -121.8 (s). HRMS (ESI+) calculated for $C_{33}H_{40}FN_4O_5$ $[M+H]^+$ 591.2977 found 591.2970. RP-HPLC trace showed 98% purity at 214 nm.

Ethyl 1-cyclopropyl-6-fluoro-7-[4-(10-methoxy-10-oxodecanoyl)piperazin-1-yl]-4-oxo-1,4-dihydroquinoline-3-carboxylate (152)

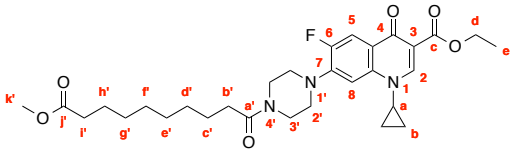

EDC (382 mg, 2 mmol) was added to monomethyl sebacate (360 mg, 1.69 mmol) in 30% pyridine/DCM and stirred vigorously for 5 minutes. Compound **138** (600 mg, 1.67 mmol) was added to the solution and stirred for 21 h at room temperature after which sat. $NaHCO_3$, was added and extracted three times with DCM. The organic layers were dried over $MgSO_4$ and the solvent removed under pressure. The crude was purified by flash column chromatography (EtOAc 100%) to give the product as a white solid (612 mg, 65%). ^{1}H NMR (400 MHz, $CDCl_3$) δ_H ppm: 8.50 (s, 1 H, 2-H), 8.02 (d, J_{HF} = 13.2, 5-H), 7.25 (d, overlaps solvent peak, J_{HF} = 8.0 Hz, 1 H, 8-H), 4.37 (q, J = 7.1 Hz, 2 H, d-H_2), 3.84 (app t, 2 H, 3'-H_2), 3.68 (app t, 2 H, 3'-H_2), 3.65 (s, 3 H, k'-H_3), 3.44-3.38 (m, 1 H, a-H), 3.25 (app t, 2 H, 2'-H_2), 3.20 (app t, 2 H, 2'-H_2), 2.38-2.34 (t, J = 8.0 Hz, 2 H, b'-H_2), 2.31-2.27 (t, J = 8.0 Hz, 2 H, i'-H_2), 1.66-1.59 (m, 4 H, c' and h'-H_2), 1.39 (t, J = 8.0 Hz, 3 H, e-H_3) 1.35-1.29 (m, 10 H, d', e', f', g'-H_2 overlapping b-H_2), 1.15-1.11 (m, b-H_2). ^{13}C NMR (100 MHz, $CDCl_3$) δ_C ppm: 174.4, 173.1 (d, J_{CF} = 2.0 Hz), 171.9, 165.9, 153.5 (d, J_{CF} = 250.0 Hz), 148.3, 144.2 (d, J_{CF} = 10.0 Hz), 138.1, 123.7 (d, J_{CF} = 10.0 Hz), 113.6 (C5, J_{CF} = 20.0 Hz), 110.7, 105.2 (d, J_{CF} = 2.0 Hz), 61.03, 51.6, 50.7 (d, J_{CF} = 5.0 Hz) , 49.7 (d, J_{CF} = 2.0 Hz), 45.7, 41.4, 34.6, 34.2, 33.4, 29.5, 29.3, 29.2, 29.18, 25.4, 25.0, 14.6, 8.3. ^{19}F NMR (376 MHz, $CDCl_3$) δ_F ppm: -124.0 (s). IR ν_{max} (neat) / cm^{-1} 2973-2850 cm^{-1} (C-H_2 and C-H_3), 1713 cm^{-1} (C=O), 1646 cm^{-1} (C=O), 1615 cm^{-1} (C=O). HRMS (ESI+) calculated for $C_{30}H_{41}FN_3O_6$ $[M+H]^+$ 558.2974 found 558.2959. Mp: 104-105°C. RP-HPLC showed 96% purity at 254 nm.

7-[4-(9-carboxynonanoyl)piperazin-1-yl]-1-cyclopropyl-6-fluoro-4-oxo-1,4-dihydroquinoline-3-carboxylic acid (153)

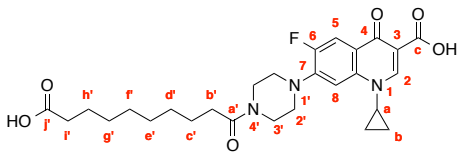

Compound **152** (262 mg, 0.47 mmol) was added to a solution of LiOH monohydrate (58 mg, 1.4 mmol) in EtOH and H_2O (2:1) and stirred vigorously at room temperature for 7 days. After which the solution was acidified with 1 M HCl and extracted three times with DCM. The organic phases were pooled together and dried over $MgSO_4$, the solvent was removed under reduced pressure to furnish the crude product. This was purified by flash column chromatography (DCM/MeOH 95:5) to give

the desired compound as a cream solid (123 mg, 51%). ^{1}H NMR (400 MHz, DMSO-d6) δ_H ppm: 15.18 (s, 1 H, OH), 11.96 (s, 1 H, OH), 8.66 (s, 1 H, 2-H), 7.92 (d, J_{HF} = 12.0 Hz, 5-H), 7.57 (d, 1 H, J_{HF} = 8.0 Hz, 8-H), 3.84-3.79 (m, 1 H, a-H), 3.68 (app t, 4 H, 3'-H_2), 3.35-3.38 (m, 4 H, 2'-H_2 overlaps water peak), 2.36 (t, J = 8.0 Hz, 2 H, b'-H_2), 2.18 (t, J = 8.0 Hz, 2 H, i'-H_2), 1.53-1.47 (m, 4 H, c' and h'-H_2), 1.33-1.24 (m, 10 H, d', e', f', g'-H_2 overlapping b-H_2), 1.20-1.16 (m, 2 H, b-H_2). ^{13}C NMR (100 MHz, DMSO-d6) δ_C ppm: 176.2 (d, J_{CF} = 2.0 Hz), 174.5, 170.8, 165.8, 152.9 (d, J_{CF} = 248.0 Hz), 147.8, 144.89 (d, J_{CF} = 10.0 Hz), 139.0, 118.67 (d, J_{CF} = 8.0 Hz), 110.9 (d, J_{CF} = 20.0 Hz), 106.7, 106.43 (d, J_{CF} = 2.0 Hz), 49.7 (d, J_{CF} = 5.0 Hz), 49.2 (d, J_{CF} = 3.0 Hz), 44.6, 40.6, 35.8, 33.7, 32.2, 28.8, 28.73, 28.66, 28.6, 24.8, 24.5, 7.60. ^{19}F NMR (376 MHz, DMSO-d6) δ_F ppm: -121.8 (s). IR ν_{max} (neat) / cm^{-1} 3600-2400 cm^{-1} (O-H), 2923-2852 cm^{-1} (C-H_2 and C-H_3), 1715 cm^{-1} (C=O), 1626 cm^{-1} (C=O), 1614 cm^{-1} (C=O). HRMS (ESI+) calculated for $C_{27}H_{35}FN_3O_6$ $[M+H]^+$ 516.2504 found 516.2497. Mp. 190-192 °C. RP-HPLC showed 96% purity at 214 nm.

References

(1) Vollmer, W.; Blanot, D.; de Pedro, M. A. Peptidoglycan structure and architecture. *FEMS Microbiol. Rev.* **2008**, *32* (2), 149–167.

(2) Wilke, M. S.; Lovering, A. L.; Strynadka, N. C. J. β-Lactam antibiotic resistance: a current structural perspective. *Curr. Opin. Microbiol.* **2005**, *8* (5), 525–533.

(3) Glauert, A. M.; Thornley, M. J. The topography of the bacterial cell wall. *Annu. Rev. Microbiol.* **1969**, *23*, 159–198.

(4) Kamio, Y.; Nikaido, H. Outer membrane of Salmonella typhimurium: accessibility of phospholipid head groups to phospholipase C and cyanogen bromide activated dextran in the external medium. *Biochemistry* **1976**, *15* (12), 2561–2570.

(5) Raetz, C. R.; Whitfield, C. Lipopolysaccharide endotoxins. *Annu. Rev. Biochem.* **2002**, *71*, 635–700.

(6) Silhavy, T. J.; Kahne, D.; Walker, S. The bacterial cell envelope. *Cold Spring Harb. Perspect. Biol.* **2010**, *2* (5), 1–17.

(7) Fleming, A. On the antibacterial action of cultures of a penicillium, with special reference to their use in the isolation of B. influenzae. *Br. J. Exp. Pathol.* **1929**, *10* (3), 226–236.

(8) Balsalobre, L. C.; Dropa, M.; Matte, M. H. An overview of antimicrobial resistance and its public health significance. *Braz. J. Microbiol.* **2014**, *45* (1), 1–5.

(9) World Health Organization. *Antimicrobial Resistance: Global Report on Surveillance*; Geneva, Switzerland, **2014**, 1–256.

(10) Boucher, H. W.; Talbot, G. H.; Bradley, J. S.; Edwards, J. E.; Gilbert, D.; Rice, L. B.; Scheld, M.; Spellberg, B.; Bartlett, J. Bad Bugs, No Drugs: No ESKAPE! An update from the Infectious Diseases Society of America. *Clin. Infect. Dis.* **2009**, *48* (1), 1–12.

(11) Blair, J. M. A.; Webber, M. A.; Baylay, A. J.; Ogbolu, D. O.; Piddock, L. J. V. Molecular mechanisms of antibiotic resistance. *Nat. Rev. Micro.* **2015**, *13* (1), 42–51.

(12) Randall, C. P.; Mariner, K. R.; Chopra, I.; O'Neill, A. J. The target of daptomycin is absent from Escherichia coli and other gram-negative pathogens. *Antimicrob. Agents Chemother.* **2013**, *57* (1), 637–639.

(13) Tsuchido, T.; Takano, M. Sensitization by heat treatment of Escherichia coli K-12 cells to

hydrophobic antibacterial compounds. *Antimicrob. Agents Chemother.* **1988**, *32* (11), 1680–1683.

(14) Abraham, E. P.; Chain, E. An enzyme from bacteria able to destroy penicillin. 1940. *Rev. Infect. Dis.* **1988**, *10* (4), 677–678.

(15) Philippon, A.; Labia, R.; Jacoby, G. Extended-spectrum beta-lactamases. *Antimicrob. Agents Chemother.* **1989**, *33* (8), 1131–1136.

(16) Lautenbach, E.; Strom, B. L.; Bilker, W. B.; Patel, J. B.; Edelstein, P. H.; Fishman, N. O. Epidemiological investigation of fluoroquinolone resistance in infections due to extended-spectrum β-lactamase—producing Escherichia coli and Klebsiella pneumoniae. *Clin. Infect. Dis.* **2001**, *33* (8), 1288–1294.

(17) Rawat, D.; Nair, D. Extended-spectrum β-lactamases in gram negative bacteria. *J. Glob. Infect. Dis.* **2010**, *2* (3), 263–274.

(18) Aldred, K. J.; Kerns, R. J.; Osheroff, N. Mechanism of quinolone action and resistance. *Biochemistry* **2014**, *53* (10), 1565–1574.

(19) Ito, H.; Yoshida, H.; Bogaki-Shonai, M.; Niga, T.; Hattori, H.; Nakamura, S. Quinolone resistance mutations in the DNA gyrase gyrA and gyrB genes of Staphylococcus aureus. *Antimicrob. Agents Chemother.* **1994**, *38* (9), 2014–2023.

(20) Yoshida, H.; Bogaki, M.; Nakamura, M.; Nakamura, S. Quinolone resistance-determining region in the DNA gyrase gyrA gene of Escherichia coli. *Antimicrob. Agents Chemother.* **1990**, *34* (6), 1271–1272.

(21) Lavigne, J. P.; Sotto, A.; Nicolas-Chanoine, M. H.; Bouziges, N.; Pages, J. M.; Davin-Regli, A. An adaptive response of Enterobacter aerogenes to imipenem: regulation of porin balance in clinical isolates. *Int. J. Antimicrob. Agents* **2013**, *41* (2), 130–136.

(22) Baroud, M.; Dandache, I.; Araj, G. F.; Wakim, R.; Kanj, S.; Kanafani, Z.; Khairallah, M.; Sabra, A.; Shehab, M.; Dbaibo, G.; et al. Underlying mechanisms of carbapenem resistance in extended-spectrum beta-lactamase-producing Klebsiella pneumoniae and Escherichia coli isolates at a tertiary care centre in Lebanon: role of OXA-48 and NDM-1 carbapenemases. *Int. J. Antimicrob. Agents* **2013**, *41* (1), 75–79.

(23) Bornet, C.; Saint, N.; Fetnaci, L.; Dupont, M.; Davin-Régli, A.; Bollet, C.; Pagès, J.-M. Omp35, a new Enterobacter aerogenes porin Involved in selective susceptibility to cephalosporins. *Antimicrob. Agents Chemother.* **2004**, *48* (6), 2153–2158.

(24) Edqvist, L.-E.; Pedersen, K. B. Antimicrobials as growth promoters: resistance to common sense. *Late lessons from early Warnings the precautionary Principle.* **2001**, 93, 1896–2000.

(25) Appendix 2 Specialist Advisory Committee on Antimicrobial Resistance (SACAR) Antimicrobial Framework. *J. Antimicrob. Chemother.* **2007**, *60*, 87–90.

(26) Levy, S. B.; FitzGerald, G. B.; Macone, A. B. Changes in intestinal flora of farm personnel after introduction of a tetracycline-supplemented feed on a farm. *N. Engl. J. Med.* **1976**, *295* (11), 583–588.

(27) Hummel, R.; Tschäpe, H.; Witte, W. Spread of plasmid-mediated nourseothricin resistance due to antibiotic use in animal husbandry. *J. Basic Microbiol.* **1986**, *26* (8), 461–466.

(28) Sarmah, A. K.; Meyer, M. T.; Boxall, A. B. A. A global perspective on the use, sales, exposure pathways, occurrence, fate and effects of veterinary antibiotics (VAs) in the environment. *Chemosphere* **2006**, *65* (5), 725–759.

(29) Mellon, M.; Benbrook, C.; Benbrook, K. L. Hogging it. *Estimates of Antimicrobial Abuse in Livestock* **2001**, 1–14.

(30) Davies, J.; Davies, D. Origins and evolution of antibiotic resistance. *Microbiol. Mol. Biol. Rev.* **2010**, *74* (3), 417–433.

(31) Bell, B. G.; Schellevis, F.; Stobberingh, E.; Goossens, H.; Pringle, M. A systematic review and meta-analysis of the effects of antibiotic consumption on antibiotic resistance. *BMC Infect. Dis.* **2014**, *14*, 1–25.

(32) Policy statement on antimicrobial stewardship by the Society for Healthcare Epidemiology of America (SHEA), the Infectious Diseases Society of America (IDSA), and the Pediatric Infectious Diseases Society (PIDS). *Infect. Control Hosp. Epidemiol.* **2012**, *33* (4), 322–327.

(33) Pulcini, C.; Gyssens, I. C. How to educate prescribers in antimicrobial stewardship practices. *Virulence* **2013**, *4* (2), 192–202.

(34) Sosa, A. de J. *Antimicrobial resistance in developing countries*; Springer: New York, **2010**, 1–548

(35) Sauermann, R.; Rothenburger, M.; Graninger, W.; Joukhadar, C. Daptomycin: a review 4 years after first approval. *Pharmacology* **2007**, *81* (2), 79–91.

(36) Lewis, K. Platforms for antibiotic discovery. *Nat. Rev. Drug Discov.* **2013**, *12* (5), 371–387.

(37) Waxman, D. J.; Strominger, J. L. Penicillin-binding proteins and the mechanism of action of

beta-lactam antibiotics. *Annu. Rev. Biochem.* **1983**, *52*, 825–869.

(38) Papp-Wallace, K. M.; Endimiani, A.; Taracila, M. A.; Bonomo, R. A. Carbapenems: past, present, and future. *Antimicrob. Agents Chemother.* **2011**, *55* (11), 4943–4960.

(39) Hashizume, T.; Ishino, F.; Nakagawa, J.; Tamaki, S.; Matsuhashi, M. Studies on the mechanism of action of imipenem (N-formimidoylthienamycin) in vitro: binding to the penicillin-binding proteins (PBPs) in Escherichia coli and Pseudomonas aeruginosa, and inhibition of enzyme activities due to the PBPs in E. coli. *J. Antibiot.* **1984**, *37* (4), 394–400.

(40) Nieto, M.; Perkins, H. R. Modifications of the acyl-D-alanyl-D-alanine terminus affecting complex-formation with vancomycin. *Biochem. J.* **1971**, *123* (5), 789–803.

(41) Reynolds, P. E. Structure, biochemistry and mechanism of action of glycopeptide antibiotics. *Eur. J. Clin. Microbiol. Infect. Dis.* **1989**, *8* (11), 943–950.

(42) Hansen, J. L.; Ippolito, J. A.; Ban, N.; Nissen, P.; Moore, P. B.; Steitz, T. A. The structures of four macrolide antibiotics bound to the large ribosomal subunit. *Mol. Cell* **2002**, *10* (1), 117–128.

(43) Tenson, T.; Lovmar, M.; Ehrenberg, M. The mechanism of action of macrolides, lincosamides and streptogramin B Reveals the nascent peptide exit path in the ribosome. *J. Mol. Biol.* **2003**, *330* (5), 1005–1014.

(44) Douthwaite, S. Interaction of the antibiotics clindamycin and lincomycin with Escherichia coli 23S ribosomal RNA. *Nucleic Acids Res.* **1992**, *20* (18), 4717–4720.

(45) Poulsen, S. M.; Kofoed, C.; Vester, B. Inhibition of the ribosomal peptidyl transferase reaction by the mycarose moiety of the antibiotics carbomycin, spiramycin and tylosin. *J. Mol. Biol.* **2000**, *304* (3), 471–481.

(46) Mao, J. C. H.; Robishaw, E. E. Erythromycin, a peptidyltransferase effector. *Biochemistry* **1972**, *11* (25), 4864–4872.

(47) Cocito, C.; Di Giambattista, M.; Nyssen, E.; Vannuffel, P. Inhibition of protein synthesis by streptogramins and related antibiotics. *J. Antimicrob. Chemother.* **1997**, *39*, 7–13.

(48) Wolfe, A. D.; Hahn, F. E. Mode of action of chloramphenicol IX. Effects of chloramphenicol upon a ribosomal amino acid polymerization system and its binding to bacterial ribosome. *Biochim. Biophys. Acta - Nucleic Acids Protein Synth.* **1965**, *95* (1), 146–155.

(49) Schlunzen, F.; Zarivach, R.; Harms, J.; Bashan, A.; Tocilj, A.; Albrecht, R.; Yonath, A.;

Franceschi, F. Structural basis for the interaction of antibiotics with the peptidyl transferase centre in eubacteria. *Nature* **2001**, *413* (6858), 814–821.

(50) Yoshizawa, S.; Fourmy, D.; Puglisi, J. D. Structural origins of gentamicin antibiotic action. *EMBO J.* **1998**, *17* (22), 6437–6448.

(51) Lioy, V. S.; Goussard, S.; Guerineau, V.; Yoon, E.-J.; Courvalin, P.; Galimand, M.; Grillot-Courvalin, C. Aminoglycoside resistance 16S rRNA methyltransferases block endogenous methylation, affect translation efficiency and fitness of the host. *RNA* **2014**, *20* (3), 382–391.

(52) Chopra, I.; Roberts, M. Tetracycline antibiotics: mode of action, applications, molecular biology, and epidemiology of bacterial resistance. *Microbiol. Mol. Biol. Rev.* **2001**, *65* (2), 232–260.

(53) Brodersen, D. E.; Clemons Jr, W. M.; Carter, A. P.; Morgan-Warren, R. J.; Wimberly, B. T.; Ramakrishnan, V. The structural basis for the action of the antibiotics tetracycline, pactamycin, and hygromycin B on the 30S Ribosomal Subunit. *Cell* **2000**, *103* (7), 1143–1154.

(54) Bozdogan, B.; Appelbaum, P. C. Oxazolidinones: activity, mode of action, and mechanism of resistance. *Int. J. Antimicrob. Agents* **2004**, *23* (2), 113–119.

(55) Lin, A. H.; Murray, R. W.; Vidmar, T. J.; Marotti, K. R. The oxazolidinone eperezolid binds to the 50S ribosomal subunit and competes with binding of chloramphenicol and lincomycin. *Antimicrob. Agents Chemother.* **1997**, *41* (10), 2127–2131.

(56) Zhou, C. C.; Swaney, S. M.; Shinabarger, D. L.; Stockman, B. J. 1H nuclear magnetic resonance study of oxazolidinone binding to bacterial ribosomes. *Antimicrob. Agents Chemother.* **2002**, *46* (3), 625–629.

(57) Floss, H. G.; Yu, T.-W. Rifamycin mode of action, resistance, and biosynthesis. *Chem. Rev.* **2005**, *105* (2), 621–632.

(58) Wehrli, W.; Knüsel, F.; Schmid, K.; Staehelin, M. Interaction of rifamycin with bacterial RNA polymerase. *Proc. Natl. Acad. Sci.* **1968**, *61* (2), 667–673.

(59) Watson, J. D.; Crick, F. H. Molecular structure of nucleic acids; a structure for deoxyribose nucleic acid. *Nature* **1953**, *171* (4356), 737–738.

(60) Bates, A. D.; Maxwell, A. *DNA Topology*; Oxford University Press: Oxford, **2005**, 1–198.

(61) Neidle, S. *DNA Structure and Recognition*; IRL Press at Oxford University Press, **1994**, 1–

108.

(62) Franklin, R. E.; Gosling, R. G. Molecular configuration in sodium thymonucleate. *Nature* **1953**, *171* (4356), 740–741.

(63) Berg, J. M.; Tymoczko, J. L.; Stryer, L. *Biochemistry, Fifth Edition*; W.H. Freeman, **2002**.

(64) OpenStaxCollege. *DNA Replication in Prokaryotes*; CNX, O., Ed.; OpenStax CNX, **2013** https://www.boundless.com/biology/textbooks/boundless-biology-textbook/dna-structure-and-function-14/dna-replication-101/dna-replication-in-prokaryotes-436-12940/images/dna-replication-in-prokaryotes-97b3199a-6138-42ea-bd48-382479ee4bd3/ (accessed August 2015).

(65) Wang, J. C. Interaction between DNA and an Escherichia coli protein ω. *J. Mol. Biol.* **1971**, *55* (3), 523–533.

(66) Champoux, J. J.; Dulbecco, R. An activity from mammalian cells that untwists superhelical DNA—a possible swivel for DNA replication. *Proc. Natl. Acad. Sci.* **1972**, *69* (1), 143–146.

(67) Forterre, P.; Gribaldo, S.; Gadelle, D.; Serre, M.-C. Origin and evolution of DNA topoisomerases. *Biochimie* **2007**, *89* (4), 427–446.

(68) Lima, C. D.; Wang, J. C.; Mondragon, A. Three-dimensional structure of the 67K N-terminal fragment of E. coli DNA topoisomerase I. *Nature* **1994**, *367* (6459), 138–146.

(69) Brown, P. O.; Cozzarelli, N. R. Catenation and knotting of duplex DNA by type 1 topoisomerases: a mechanistic parallel with type 2 topoisomerases. *Proc. Natl. Acad. Sci.* **1981**, *78* (2), 843–847.

(70) Tse, Y. C.; Kirkegaard, K.; Wang, J. C. Covalent bonds between protein and DNA. Formation of phosphotyrosine linkage between certain DNA topoisomerases and DNA. *J. Biol. Chem.* **1980**, *255* (12), 5560–5565.

(71) Terekhova, K.; Gunn, K. H.; Marko, J. F.; Mondragón, A. Bacterial topoisomerase I and topoisomerase III relax supercoiled DNA via distinct pathways. *Nucleic Acids Res.* **2012**, *40* (20), 10432–10440.

(72) Kikuchi, A.; Asai, K. Reverse gyrase - a topoisomerase which introduces positive superhelical turns into DNA. *Nature* **1984**, *309* (5970), 677–681.

(73) Hsieh, T. S.; Plank, J. L. Reverse gyrase functions as a DNA renaturase: annealing of complementary single-stranded circles and positive supercoiling of a bubble substrate. *J.*

Biol. Chem. **2006**, *281* (9), 5640–5647.

(74) Redinbo, M. R.; Stewart, L.; Kuhn, P.; Champoux, J. J.; Hol, W. G. Crystal structures of human topoisomerase I in covalent and noncovalent complexes with DNA. *Science (80).* **1998**, *279* (5356), 1504–1513.

(75) Koster, D. A.; Croquette, V.; Dekker, C.; Shuman, S.; Dekker, N. H. Friction and torque govern the relaxation of DNA supercoils by eukaryotic topoisomerase IB. *Nature* **2005**, *434* (7033), 671–674.

(76) Forterre, P. DNA topoisomerase V: a new fold of mysterious origin. *Trends Biotechnol.* **2006**, *24* (6), 245–247.

(77) Slesarev, A. I.; Stetter, K. O.; Lake, J. A.; Gellert, M.; Krah, R.; Kozyavkin, S. A. DNA topoisomerase V is a relative of eukaryotic topoisomerase I from a hyperthermophilic prokaryote. *Nature* **1993**, *364* (6439), 735–737.

(78) Taneja, B.; Patel, A.; Slesarev, A.; Mondragon, A. Structure of the N-terminal fragment of topoisomerase V reveals a new family of topoisomerases. *EMBO J.* **2006**, *25* (2), 398–408.

(79) Peng, H.; Marians, K. J. The interaction of Escherichia coli topoisomerase IV with DNA. *J. Biol. Chem.* **1995**, *270* (42), 25286–25290.

(80) Bergerat, A.; de Massy, B.; Gadelle, D.; Varoutas, P.-C.; Nicolas, A.; Forterre, P. An atypical topoisomerase II from archaea with implications for meiotic recombination. *Nature* **1997**, *386* (6623), 414–417.

(81) Dutta, R.; Inouye, M. GHKL, an emergent ATPase/kinase superfamily. *Trends Biochem. Sci.* **2000**, *25* (1), 24–28.

(82) Nichols, M. D.; DeAngelis, K.; Keck, J. L.; Berger, J. M. Structure and function of an archaeal topoisomerase VI subunit with homology to the meiotic recombination factor Spo11. *EMBO J.* **1999**, *18* (21), 6177–6188.

(83) Roca, J.; Wang, J. C. DNA transport by a type II DNA topoisomerase: evidence in favor of a two-gate mechanism. *Cell* **1994**, *77* (4), 609–616.

(84) Reece, R. J.; Maxwell, A.; Wang, J. C. DNA gyrase: structure and function. *Crit. Rev. Biochem. Mol. Biol.* **1991**, *26* (3-4), 335–375.

(85) Costenaro, L.; Grossmann, J. G.; Ebel, C.; Maxwell, A. Small-angle X-ray scattering reveals the solution structure of the full-length DNA gyrase A subunit. *Structure* **2005**, *13* (2), 287–

296.

(86) Costenaro, L.; Grossmann, J. G.; Ebel, C.; Maxwell, A. Modular structure of the full-length DNA gyrase B subunit revealed by small-angle X-ray scattering. *Structure* **2007**, *15* (3), 329–339.

(87) Thornton, M.; Armitage, M.; Maxwell, A.; Dosanjh, B.; Howells, A. J.; Norris, V.; Sigee, D. C. Immunogold localization of GyrA and GyrB proteins in Escherichia coli. *Microbiology* **1994**, *140* (9), 2371–2382.

(88) Bax, B. D.; Chan, P. F.; Eggleston, D. S.; Fosberry, A.; Gentry, D. R.; Gorrec, F.; Giordano, I.; Hann, M. M.; Hennessy, A.; Hibbs, M.; et al. Type IIA topoisomerase inhibition by a new class of antibacterial agents. *Nature* **2010**, *466* (7309), 935–940.

(89) Liu, L. F.; Wang, J. C. Micrococcus luteus DNA gyrase: active components and a model for its supercoiling of DNA. *Proc. Natl. Acad. Sci.* **1978**, *75* (5), 2098–2102.

(90) Orphanides, G.; Maxwell, A. Evidence for a conformational change in the DNA gyrase-DNA complex from hydroxyl radical footprinting. *Nucleic Acids Res.* **1994**, *22* (9), 1567–1575.

(91) Corbett, K. D.; Shultzaberger, R. K.; Berger, J. M. The C-terminal domain of DNA gyrase A adopts a DNA-bending β-pinwheel fold. *Proc. Natl. Acad. Sci.* **2004**, *101* (19), 7293–7298.

(92) Kramlinger, V. M.; Hiasa, H. The “GyrA-box” Is Required for the ability of DNA Gyrase to wrap DNA and catalyze the supercoiling reaction. *J. Biol. Chem.* **2006**, *281* (6), 3738–3742.

(93) Ali, J. A.; Jackson, A. P.; Howells, A. J.; Maxwell, A. The 43-kilodalton N-terminal fragment of the DNA gyrase B protein hydrolyzes ATP and binds coumarin drugs. *Biochemistry* **1993**, *32* (10), 2717–2724.

(94) Wigley, D. B.; Davies, G. J.; Dodson, E. J.; Maxwell, A.; Dodson, G. Crystal structure of an N-terminal fragment of the DNA gyrase B protein. *Nature* **1991**, *351* (6328), 624–629.

(95) Hockings, S. C.; Maxwell, A. Identification of four GyrA residues involved in the DNA breakage–reunion reaction of DNA gyrase. *J. Mol. Biol.* **2002**, *318* (2), 351–359.

(96) Noble, C. G.; Maxwell, A. The role of GyrB in the DNA cleavage-religation reaction of DNA gyrase: a proposed two metal-ion mechanism. *J. Mol. Biol.* **2002**, *318* (2), 361–371.

(97) Sissi, C.; Chemello, A.; Vazquez, E.; Mitchenall, L. A.; Maxwell, A.; Palumbo, M. DNA gyrase requires DNA for effective two-site coordination of divalent metal ions: further insight into the mechanism of enzyme action. *Biochemistry* **2008**, *47* (33), 8538–8545.

(98) Bates, A. D.; Maxwell, A. Energy coupling in type II topoisomerases: why do they hydrolyze ATP? *Biochemistry* **2007**, *46* (27), 7929–7941.

(99) Collin, F.; Karkare, S.; Maxwell, A. Exploiting bacterial DNA gyrase as a drug target: current state and perspectives. *Appl. Microbiol. Biotechnol.* **2011**, *92* (3), 479–497.

(100) Fedorko, J.; Katz, S.; Allnoch, H. In vitro activity of Coumermycin A(1). *Appl. Microbiol.* **1969**, *18* (5), 869–873.

(101) Berger, J.; Schocher, A. J.; Batcho, A. D.; Pecherer, B.; Keller, O.; Maricq, J.; Karr, A. E.; Vaterlaus, B. P.; Furlenmeier, A.; Speigelberg, H. Production, isolation, and synthesis of the coumermycins (sugordomycins), a new streptomycete antibiotic complex. *Antimicrob. Agents Chemother.* **1965**, *5*, 778–785.

(102) Kawaguchi, H.; Naito, T.; Tsukiura, H. Studies on coumermycin a new antibiotic. II Structure of coumermycin A1. *J. Antibiot.* **1965**, *18*, 11–25.

(103) Hinman, J. W.; Hoeksema, H.; Caron, E. L.; Jackson, W. G. The partial structure of novobiocin (streptonivicin). II. *J. Am. Chem. Soc.* **1956**, *78* (5), 1072–1074.

(104) Hoeksema, H.; Bergy, M. E.; Jackson, W. G.; Shell, J. W.; Hinman, J. W.; Fonken, A. E.; Boyack, G. A.; Caron, E. L.; Ford, J. H.; Devries, W. H.; et al. Streptonivicin, a new antibiotic. II. Isolation and characterization. *Antibiot. Chemother.* **1956**, *6* (2), 143–148.

(105) Smith, C. G.; Dietz, A.; Sokolski, W. T.; Savage, G. M. Streptonivicin, a new antibiotic. I. Discovery and biologic studies. *Antibiot. Chemother.* **1956**, *6* (2), 135–142.

(106) Maxwell, A. The interaction between coumarin drugs and DNA gyrase. *Mol. Microbiol.* **1993**, *9* (4), 681–686.

(107) Wishnow, R. M.; Stroming.Jl; Birge, C. H.; Threnn, R. H. Biochemical effects of novobiocin on staphylococcus aureus. *J. Bacteriol.* **1965**, *89* (4), 1117-1123.

(108) Smith, D. H.; Davis, B. D. Mode of action of novobiocin in Escherichia coli. *J. Bacteriol.* **1967**, *93* (1), 71–79.

(109) Brock, T. Novobiocin. In *Mechanism of Action*; Gottlieb, D., Shaw, P., Eds.; Springer Berlin Heidelberg, **1967**, (1),651–665.

(110) Ryan, M. J. Coumermycin A1: a preferential inhibitor of replicative DNA synthesis in Escherichia coli. I. In vivo characterization. *Biochemistry* **1976**, *15* (17), 3769–3777.

(111) Brock, T. D. Effects of magnesium ion deficency on Escherichia coli and possible relation to

the mode of action of novobiocin. *J. Bacteriol.* **1962**, *84* (4), 679–682.

(112) Fairweather, N. F.; Orr, E.; Holland, I. B. Inhibition of deoxyribonucleic acid gyrase: effects on nucleic acid synthesis and cell division in Escherichia coli K-12. *J. Bacteriol.* **1980**, *142* (1), 153–161.

(113) Gellert, M.; O'Dea, M. H.; Itoh, T.; Tomizawa, J. Novobiocin and coumermycin inhibit DNA supercoiling catalyzed by DNA gyrase. *Proc. Natl. Acad. Sci.* **1976**, *73* (12), 4474–4478.

(114) Mizuuchi, K.; O'Dea, M. H.; Gellert, M. DNA gyrase: subunit structure and ATPase activity of the purified enzyme. *Proc. Natl. Acad. Sci.* **1978**, *75* (12), 5960–5963.

(115) Sugino, A.; Higgins, N. P.; Brown, P. O.; Peebles, C. L.; Cozzarelli, N. R. Energy coupling in DNA gyrase and the mechanism of action of novobiocin. *Proc. Natl. Acad. Sci.* **1978**, *75* (10), 4838–4842.

(116) Gilbert, E. J.; Maxwell, A. The 24 kDa N-terminal sub-domain of the DNA gyrase B protein binds coumarin drugs. *Mol. Microbiol.* **1994**, *12* (3), 365–373.

(117) Lewis, R. J.; Singh, O. M.; Smith, C. V; Skarzynski, T.; Maxwell, A.; Wonacott, A. J.; Wigley, D. B. The nature of inhibition of DNA gyrase by the coumarins and the cyclothialidines revealed by X-ray crystallography. *EMBO J.* **1996**, *15* (6), 1412–1420.

(118) Tsai, F. T. F.; Singh, O. M. P.; Skarzynski, T.; Wonacott, A. J.; Weston, S.; Tucker, A.; Pauptit, R. A.; Breeze, A. L.; Poyser, J. P.; O'Brien, R.; et al. The high-resolution crystal structure of a 24-kDa gyrase B fragment from E. coli complexed with one of the most potent coumarin inhibitors, clorobiocin. *Proteins Struct. Funct. Bioinforma.* **1997**, *28* (1), 41–52.

(119) Confreres, A.; Maxwell, A. GyrB mutations which confer coumarin resistance also affect DNA supercoiling and ATP hydrolysis by Escherichia coli DNA gyrase. *Mol. Microbiol.* **1992**, *6* (12), 1617–1624.

(120) Gormley, N. A.; Orphanides, G.; Meyer, A.; Cullis, P. M.; Maxwell, A. The Interaction of coumarin antibiotics with fragments of the DNA gyrase B Protein. *Biochemistry* **1996**, *35* (15), 5083–5092.

(121) Maxwell, A.; Lawson, D. M. The ATP-binding site of type II topoisomerases as a target for antibacterial drugs. *Curr. Top. Med. Chem.* **2003**, (3), 283–303.

(122) Mullins, J. D.; Macek, T. J. Some pharmaceutical properties of novobiocin. *J. Am. Pharm. Assoc.* **1960**, *49* (4), 245–248.

(123) Lesher, G. Y.; Froelich, E. J.; Gruett, M. D.; Bailey, J. H.; Brundage, R. P. 1,8-naphthyridine derivatives. A new class of chemotherapeutic agents. *J. Med. Pharm. Chem.* **1962**, *5* (5), 1063–1065.

(124) Butler, M. S.; Buss, A. D. Natural products — The future scaffolds for novel antibiotics? *Biochem. Pharmacol.* **2006**, *71* (7), 919–929.

(125) Harvey, A. L.; Edrada-Ebel, R.; Quinn, R. J. The re-emergence of natural products for drug discovery in the genomics era. *Nat. Rev. Drug Discov.* **2015**, *14* (2), 111–129.

(126) Berdy, J. Thoughts and facts about antibiotics: Where we are now and where we are heading. *J. Antibiot. (Tokyo).* **2012**, *65* (8), 385–395.

(127) Schelhorn, C.; Andriole, V. T. Classification of quinolones by V. Andriole. *Infection* **1998**, *26* (1), 64.

(128) Andriole, V. T. The quinolones: past, present, and future. *Clin. Infect. Dis.* **2005**, *41*, 113–119.

(129) Barlow, A. M. Nalidixic acid in infections of urinary tract. *Br. Med. J.* **1963**, *2* (5368), 1308–1310.

(130) Barry, A. L.; Jones, R. N.; Thornsberry, C.; Ayers, L. W.; Gerlach, E. H.; Sommers, H. M. Antibacterial activities of ciprofloxacin, norfloxacin, oxolinic acid, cinoxacin, and nalidixic acid. *Antimicrob. Agents Chemother.* **1984**, *25* (5), 633–637.

(131) Maigaard, S.; Frimodt-Möller, N.; Welling, P. G.; Madsen, P. O. Cinoxacin: pharmacokinetics and tolerance in patients with normal and impaired renal function. *Antimicrob. Agents Chemother.* **1979**, *16* (3), 411–416.

(132) Oliphant, C. M.; Green, G. M. Quinolones: a comprehensive review. *Am. Fam. Physician* **2002**, *65* (3), 455–464.

(133) Rohlfing, S. R.; Gerster, J. F.; Kvam, D. C. Bioevaluation of the antibacterial flumequine for urinary tract use. *Antimicrob. Agents Chemother.* **1976**, *10* (1), 20–24.

(134) Ball, P. Quinolone generations: natural history or natural selection? *J. Antimicrob. Chemother.* **2000**, *46*, 17–24.

(135) Brown, S. A. Fluoroquinolones in animal health. *J. Vet. Pharmacol. Ther.* **1996**, *19* (1), 1–14.

(136) Hansen; Horsberg. Single-dose pharmacokinetics of flumequine in halibut (Hippoglossus

hippoglossus) and turbot (Scophthalmus maximus). *J. Vet. Pharmacol. Ther.* **1999**, *22* (2), 122–126.

(137) Delmas, J. M.; Chapel, A. M.; Gaudin, V.; Sanders, P. Pharmacokinetics of flumequine in sheep after intravenous and intramuscular administration: bioavailability and tissue residue studies. *J. Vet. Pharmacol. Ther.* **1997**, *20* (4), 249–257.

(138) Domagala, J. M. Structure-activity and structure-side-effect relationships for the quinolone antibacterials. *J. Antimicrob. Chemother.* **1994**, *33* (4), 685–706.

(139) Domagala, J. M.; Hanna, L. D.; Heifetz, C. L.; Hutt, M. P.; Mich, T. F.; Sanchez, J. P.; Solomon, M. New structure-activity relationships of the quinolone antibacterials using the target enzyme. The development and application of a DNA gyrase assay. *J. Med. Chem.* **1986**, *29* (3), 394–404.

(140) Wolfson, J. S.; Hooper, D. C. The fluoroquinolones: structures, mechanisms of action and resistance, and spectra of activity in vitro. *Antimicrob. Agents Chemother.* **1985**, *28* (4), 581–586.

(141) Yamane, N.; Jones, R. N.; Frei, R.; Hoban, D. J.; Pignatari, A. C.; Marco, F. Levofloxacin in vitro activity: results from an international comparative study with ofloxacin and ciprofloxacin. *J. Chemother.* **1994**, *6* (2), 83–91.

(142) Hooper, D. C.; Wolfson, J. S. Mode of action of the quinolone antimicrobial agents: review of recent information. *Rev. Infect. Dis.* **1989**, *11,* 902–911.

(143) Pucci, M. J.; Podos, S. D.; Thanassi, J. A.; Leggio, M. J.; Bradbury, B. J.; Deshpande, M. In vitro and in vivo profiles of ACH-702, an isothiazoloquinolone, against bacterial pathogens. *Antimicrob. Agents Chemother.* **2011**, *55* (6), 2860–2871.

(144) Wang, Q.; Lucien, E.; Hashimoto, A.; Pais, G. C. G.; Nelson, D. M.; Song, Y.; Thanassi, J. A.; Marlor, C. W.; Thoma, C. L.; Cheng, J.; et al. Isothiazoloquinolones with enhanced antistaphylococcal activities against multidrug-resistant strains: effects of structural modifications at the 6-, 7-, and 8-Positions. *J. Med. Chem.* **2007**, *50* (2), 199–210.

(145) Kim, H. Y.; Wiles, J. A.; Wang, Q.; Pais, G. C. G.; Lucien, E.; Hashimoto, A.; Nelson, D. M.; Thanassi, J. A.; Podos, S. D.; Deshpande, M.; et al. Exploration of the activity of 7-pyrrolidino-8-methoxyisothiazoloquinolones against methicillin-resistant Staphylococcus aureus (MRSA). *J. Med. Chem.* **2011**, *54* (9), 3268–3282.

(146) Huband, M. D.; Cohen, M. A.; Zurack, M.; Hanna, D. L.; Skerlos, L. A.; Sulavik, M. C.; Gibson, G. W.; Gage, J. W.; Ellsworth, E.; Stier, M. A.; et al. In vitro and in vivo activities of

PD 0305970 and PD 0326448, new bacterial gyrase/topoisomerase inhibitors with potent antibacterial activities versus multidrug-resistant gram-positive and fastidious organism groups. *Antimicrob. Agents Chemother.* **2007**, *51* (4), 1191–1201.

(147) Laponogov, I.; Sohi, M. K.; Veselkov, D. A.; Pan, X. S.; Sawhney, R.; Thompson, A. W.; McAuley, K. E.; Fisher, L. M.; Sanderson, M. R. Structural insight into the quinolone-DNA cleavage complex of type IIA topoisomerases. *Nat. Struct. Mol. Biol.* **2009**, *16* (6), 667–669.

(148) Gellert, M.; Mizuuchi, K.; O'Dea, M. H.; Itoh, T.; Tomizawa, J. I. Nalidixic acid resistance: A second genetic character involved in DNA gyrase activity. *Proc. Natl. Acad. Sci.* **1977**, *74* (11), 4772–4776.

(149) Ferrero, L.; Cameron, B.; Manse, B.; Lagneaux, D.; Crouzet, J.; Famechon, A.; Blanche, F. Cloning and primary structure of Staphylococcus aureus DNA topoisomerase IV: a primary target of fluoroquinolones. *Mol. Microbiol.* **1994**, *13* (4), 641–653.

(150) Sugino, A.; Peebles, C. L.; Kreuzer, K. N.; Cozzarelli, N. R. Mechanism of action of nalidixic acid: Purification of Escherichia coli nalA gene product and its relationship to DNA gyrase and a novel nicking-closing enzyme. *Proc. Natl. Acad. Sci.* **1977**, *74* (11), 4767–4771.

(151) Heddle, J.; Maxwell, A. Quinolone-binding pocket of DNA gyrase: role of GyrB. *Antimicrob. Agents Chemother.* **2002**, *46* (6), 1805–1815.

(152) Laponogov, I.; Pan, X.-S.; Veselkov, D. A.; McAuley, K. E.; Fisher, L. M.; Sanderson, M. R. Structural basis of gate-DNA breakage and Resealing by Type II Topoisomerases. *PLoS One* **2010**, *5* (6), e11338.

(153) Wohlkonig, A.; Chan, P. F.; Fosberry, A. P.; Homes, P.; Huang, J.; Kranz, M.; Leydon, V. R.; Miles, T. J.; Pearson, N. D.; Perera, R. L.; et al. Structural basis of quinolone inhibition of type IIA topoisomerases and target-mediated resistance. *Nat. Struct. Mol. Biol.* **2010**, *17* (99), 1152–1153.

(154) Aldred, K. J.; McPherson, S. A.; Turnbough, C. L.; Kerns, R. J.; Osheroff, N. Topoisomerase IV-quinolone interactions are mediated through a water-metal ion bridge: mechanistic basis of quinolone resistance. *Nucleic Acids Res.* **2013**, *41* (8), 4628–4639.

(155) Aldred, K. J.; McPherson, S. A.; Wang, P.; Kerns, R. J.; Graves, D. E.; Turnbough, C. L.; Osheroff, N. Drug Interactions with Bacillus anthracis topoisomerase IV: biochemical basis for quinolone action and resistance. *Biochemistry* **2012**, *51* (1), 370–381.

(156) Aldred, K. J.; Schwanz, H. A.; Li, G.; McPherson, S. A.; Turnbough, C. L.; Kerns, R. J.; Osheroff, N. Overcoming target-mediated quinolone resistance in topoisomerase IV by

introducing metal ion-independent drug-enzyme interactions. *ACS Chem. Biol.* **2013**, *8* (12), 2660–2668.

(157) Khodursky, A. B.; Cozzarelli, N. R. The mechanism of inhibition of topoisomerase IV by quinolone Antibacterials. *J. Biol. Chem.* **1998**, *273* (42), 27668–27677.

(158) Goss, W. A.; Deitz, W. H.; Cook, T. M. Mechanism of action of nalidixic acid on Escherichia coli II. Inhibition of deoxyribonucleic acid synthesis. *J. Bacteriol.* **1965**, *89* (4), 1068–1074.

(159) Chen, C.-R.; Malik, M.; Snyder, M.; Drlica, K. DNA Gyrase and topoisomerase IV on the bacterial chromosome: quinolone-induced DNA cleavage. *J. Mol. Biol.* **1996**, *258* (4), 627–637.

(160) Lewin, C. S.; Howard, B. M.; Smith, J. T. Protein- and RNA-synthesis independent bactericidal activity of ciprofloxacin that involves the A subunit of DNA gyrase. *J. Med. Microbiol.* **1991**, *34* (1), 19–22.

(161) Malik, M.; Hussain, S.; Drlica, K. Effect of anaerobic growth on quinolone lethality with Escherichia coli. *Antimicrob. Agents Chemother.* **2007**, *51* (1), 28–34.

(162) Drlica, K.; Hiasa, H.; Kerns, R.; Malik, M.; Mustaev, A.; Zhao, X. Quinolones: action and resistance updated. *Curr. Top. Med. Chem.* **2009**, *9* (11), 981–998.

(163) Dwyer, D. J.; Kohanski, M. A.; Hayete, B.; Collins, J. J. Gyrase inhibitors induce an oxidative damage cellular death pathway in Escherichia coli. *Mol. Syst. Biol.* **2007**, *3*, 91, 1–15.

(164) Wang, X.; Zhao, X. Contribution of oxidative damage to antimicrobial lethality. *Antimicrob. Agents Chemother.* **2009**, *53* (4), 1395–1402.

(165) Wang, X.; Zhao, X.; Malik, M.; Drlica, K. Contribution of reactive oxygen species to pathways of quinolone-mediated bacterial cell death. *J. Antimicrob. Chemother.* **2010**, *65* (3), 520–524.

(166) Schimana, J.; Fiedler, H. P.; Groth, I.; Sussmuth, R.; Beil, W.; Walker, M.; Zeeck, A. Simocyclinones, novel cytostatic angucyclinone antibiotics produced by Streptomyces antibioticus Tu 6040 I. Taxonomy, fermentation, isolation and biological activities. *J. Antibiot. (Tokyo).* **2000**, *53* (8), 779–787.

(167) Rohr, J.; Thiericke, R. Angucycline group antibiotics. *Nat. Prod. Rep.* **1992**, *9* (2), 103–137.

(168) Tarbell, D. S.; Carman, R. M.; Chapman, D. D.; Huffman, K. R.; McCorkindale, N. J. The

structure of fumagillin 1. *J. Am. Chem. Soc.* **1960**, *82* (4), 1005–1007.

(169) Shirling, E. B.; Gottlieb, D. Methods for characterization of Streptomyces species. *Int. J. Syst. Bacteriol.* **1966**, *16* (3), 313–340.

(170) Theobald, U.; Schimana, J.; Fiedler, H. P. Microbial growth and production kinetics of Streptomyces antibioticus Tu 6040. *Antonie Van Leeuwenhoek Int. J. Gen. Mol. Microbiol.* **2000**, *78* (3-4), 307–313.

(171) Holzenkampfer, M.; Walker, M.; Zeeck, A.; Schimana, J.; Fiedler, H. P. Simocyclinones, novel cytostatic angucyclinone antibiotics produced by Streptomyces antibioticus Tu 6040 - II. Structure elucidation and biosynthesis. *J. Antibiot. (Tokyo).* **2002**, *55* (3), 301–307.

(172) Flatman, R. H.; Howells, A. J.; Heide, L.; Fiedler, H. P.; Maxwell, A. Simocyclinone D8, an inhibitor of DNA gyrase with a novel mode of action. *Antimicrob. Agents Chemother.* **2005**, *49* (3), 1093–1100.

(173) Willmott, C. J.; Maxwell, A. A single point mutation in the DNA gyrase A protein greatly reduces binding of fluoroquinolones to the gyrase-DNA complex. *Antimicrob. Agents Chemother.* **1993**, *37* (1), 126–127.

(174) Sadiq, A. A.; Patel, M. R.; Jacobson, B. A.; Escobedo, M.; Ellis, K.; Oppegard, L. M.; Hiasa, H.; Kratzke, R. A. Anti-proliferative effects of simocyclinone D8 (SD8), a novel catalytic inhibitor of topoisomerase II. *Invest. New Drugs* **2010**, *28* (1), 20–25.

(175) Oppegard, L. M.; Thuy, N.; Ellis, K. C.; Hiasa, H. Inhibition of human topoisomerases I and II by simocyclinone D8. *J. Nat. Prod.* **2012**, *75* (8), 1485–1489.

(176) Edwards, M. J.; Flatman, R. H.; Mitchenall, L. A.; Stevenson, C. E. M.; Le, T. B. K.; Clarke, T. A.; McKay, A. R.; Fiedler, H.-P.; Buttner, M. J.; Lawson, D. M.; et al. A crystal structure of the bifunctional antibiotic simocyclinone D8, bound to DNA Gyrase. *Science.* **2009**, *326* (5958), 1415–1418.

(177) Cabral, J. H. M.; Jackson, A. P.; Smith, C. V; Shikotra, N.; Maxwell, A.; Liddington, R. C. Crystal structure of the breakage-reunion domain of DNA gyrase. *Nature* **1997**, *388* (6645), 903–906.

(178) Cole, J. L.; Lary, J. W.; Moody, T.; Laue, T. M. Analytical ultracentrifugation: sedimentation velocity and sedimentation equilibrium. *Methods Cell Biol.* **2008**, *84*, 143–179.

(179) Ruiz, N.; Falcone, B.; Kahne, D.; Silhavy, T. J. Chemical conditionality: a genetic strategy to probe organelle assembly. *Cell* **2005**, (2), 307–317.

(180) Edwards, M. J.; Williams, M. A.; Maxwell, A.; McKay, A. R. Mass spectrometry reveals that the antibiotic simocyclinone D8 binds to DNA gyrase in a “bent-over” conformation: evidence of positive cooperativity in binding. *Biochemistry* **2011**, *50* (17), 3432–3440.

(181) Rodger, A.; Marrington, R.; Roper, D.; Windsor, S. Circular dichroism spectroscopy for the study of protein-ligand interactions. In *Protein-Ligand Interactions*; Ulrich Nienhaus, G., Ed.; Humana Press, **2005**; (305), 343–363.

(182) Sissi, C.; Vazquez, E.; Chemello, A.; Mitchenall, L. A.; Maxwell, A.; Palumbo, M. Mapping simocyclinone D8 interaction with DNA gyrase: evidence for a new binding site on GyrB. *Antimicrob. Agents Chemother.* **2010**, *54* (1), 213–220.

(183) Sissi, C.; Perdonà, E.; Domenici, E.; Feriani, A.; Howells, A. J.; Maxwell, A.; Palumbo, M. Ciprofloxacin affects conformational equilibria of DNA gyrase A in the presence of magnesium ions. *J. Mol. Biol.* **2001**, *311* (1), 195–203.

(184) Hearnshaw, S. J.; Edwards, M. J.; Stevenson, C. E.; Lawson, D. M.; Maxwell, A. A new crystal structure of the bifunctional antibiotic simocyclinone D8 bound to DNA gyrase gives fresh insight into the mechanism of inhibition. *J. Mol. Biol.* **2014**, *426* (10), 2023–2033.

(185) Schäfer, M.; Le, T. B. K.; Hearnshaw, S. J.; Maxwell, A.; Challis, G. L.; Wilkinson, B.; Buttner, M. J. SimC7 is a novel NAD(P)H-dependent ketoreductase essential for the antibiotic activity of the DNA gyrase inhibitor simocyclinone. *J. Mol. Biol.* **2015**, *427* (12), 2192–2204.

(186) Macarron, R. Critical review of the role of HTS in drug discovery. *Drug Discov. Today* **2006**, *11* (7-8), 277–279.

(187) Oprea, T. I.; Matter, H. Integrating virtual screening in lead discovery. *Curr. Opin. Chem. Biol.* **2004**, *8* (4), 349–358.

(188) Brown, D.; Superti-Furga, G. Rediscovering the sweet spot in drug discovery. *Drug Discov Today* **2003**, *8* (23), 1067–1077.

(189) Mahajan, R.; Gupta, K. Food and drug administration’s critical path initiative and innovations in drug development paradigm: challenges, progress, and controversies. *J. Pharm. Bioallied Sci.* **2010**, *2* (4), 307–313.

(190) Jencks, W. P. On the attribution and additivity of binding energies. *Proc. Natl. Acad. Sci.* **1981**, *78* (7), 4046–4050.

(191) Andrews, P. R.; Craik, D. J.; Martin, J. L. Functional group contributions to drug-receptor

interactions. *J. Med. Chem.* **1984**, *27* (12), 1648–1657.

(192) Wenlock, M. C.; Austin, R. P.; Barton, P.; Davis, A. M.; Leeson, P. D. A Comparison of physiochemical property profiles of development and marketed oral drugs. *J. Med. Chem.* **2003**, *46* (7), 1250–1256.

(193) Feyfant, E.; Cross, J.; Paris, K.; Tsao, D. H. Fragment-based drug design. In *Chemical Library Design*; Zhou, J. Z., Ed.; Humana Press, **2011**; (685), 241–252.

(194) Kuntz, I. D.; Chen, K.; Sharp, K. A.; Kollman, P. A. The maximal affinity of ligands. *Proc. Natl. Acad. Sci.* **1999**, *96* (18), 9997–10002.

(195) Fedorov, A. Y.; Nyuchev, A. V; Beletskaya, I. P. Catalytic methods of creation and functionalization of the coumarin skeleton. *Chem. Heterocycl. Compd. (New York, NY, United States)(Translation Khimiya Geterotsiklicheskikh Soedin.* **2012**, *48* (1), 166–178.

(196) Jain, P. K.; Himanshu, J. Coumarin: chemical and pharmacological profile. *J. Appl. Pharm. Sci.* **2012**, *2* (6), 236–240.

(197) Smyth, T.; Ramachandran, V. N.; Smyth, W. F. A study of the antimicrobial activity of selected naturally occurring and synthetic coumarins. *Int. J. Antimicrob. Agents* **2009**, *33* (5), 421–426.

(198) Pratap, R.; Ram, V. J. Natural and synthetic chromenes, fused chromenes, and versatility of dihydrobenzo[h]chromenes in organic synthesis. *Chem. Rev.* **2014**, *114* (20), 10476–10526.

(199) Bhat, S. V; Nagasampagi, B. A.; Sivakumar, M. Coumarin classification. In *Chemistry of Natural Products*; Springer-Verlag Berlin and Heidelberg GmbH & Co. KG, **2005**; 613.

(200) Venugopala, K. N.; Rashmi, V.; Odhav, B. Review on natural coumarin lead compounds for their pharmacological activity. *Biomed. Res. Int.* **2013**, 1–14.

(201) Sethna, S. M.; Shah, N. M. The chemistry of coumarins. *Chem. Rev.* **1945**, *36* (1), 1–62.

(202) Tao, J.; Hu, S.; Pacholec, M.; Walsh, C. T. Synthesis of proposed oxidation–cyclization–methylation intermediates of the coumarin antibiotic biosynthetic pathway. *Org. Lett.* **2003**, *5* (18), 3233–3236.

(203) Stecher, H.; Tengg, M.; Ueberbacher, B. J.; Remler, P.; Schwab, H.; Griengl, H.; Gruber-Khadjawi, M. Biocatalytic friedel–crafts alkylation using non-natural cofactors. *Angew. Chemie Int. Ed.* **2009**, *48* (50), 9546–9548.

(204) Okubo, T.; Yoshikawa, R.; Chaki, S.; Okuyama, S.; Nakazato, A. Design, synthesis, and

structure–activity relationships of novel tetracyclic compounds as peripheral benzodiazepine receptor ligands. *Bioorg. Med. Chem.* **2004**, *12* (13), 3569–3580.

(205) Suzuki, N.; Suzuki, T.; Ota, Y.; Nakano, T.; Kurihara, M.; Okuda, H.; Yamori, T.; Tsumoto, H.; Nakagawa, H.; Miyata, N. Design, synthesis, and biological activity of boronic acid-based histone deacetylase inhibitors. *J. Med. Chem.* **2009**, *52* (9), 2909–2922.

(206) Schneider, H.; Sigmund, G.; Schricker, B.; Thirring, K.; Berner, H. Synthesis of modified partial structures of the bacterial cell wall. Lipopeptides containing nonproteinogenic amino acids. *J. Org. Chem.* **1993**, *58* (3), 683–689.

(207) Pullar, J. M.; Vissers, M. C.; Winterbourn, C. C. Living with a killer: the effects of hypochlorous acid on mammalian cells. *IUBMB Life* **2000**, *50* (4-5), 259–266.

(208) Reger, D.; Goode, S.; Ball, D. *Chemistry: principles and practice*; Cengage Learning, **2009**.

(209) Nicolaou, K. C.; Boddy, C. N. Atropselective macrocyclization of diaryl ether ring systems: application to the synthesis of vancomycin model systems. *J. Am. Chem. Soc.* **2002**, *124* (35), 10451–10455.

(210) Tan, J. S.; Ciufolini, M. A. Total synthesis of topopyrones B and D. *Org. Lett.* **2006**, *8* (21), 4771–4774.

(211) Pham, A. N.; Xing, G.; Miller, C. J.; Waite, T. D. Fenton-like copper redox chemistry revisited: hydrogen peroxide and superoxide mediation of copper-catalyzed oxidant production. *J. Catal.* **2013**, *301* (0), 54–64.

(212) Das, R.; Chakraborty, D. Cu(II) bromide catalyzed oxidation of aldehydes and alcohols. *Appl. Organomet. Chem.* **2011**, *25* (6), 437–442.

(213) Musso, H. Phenol oxidation reactions. *Angew. Chemie Int. Ed. English* **1963**, *2* (12), 723–735.

(214) Gammon, D. W.; Hunter, R.; Wilson, S. A. An efficient synthesis of 7-hydroxy-2,6-dimethylchromeno[3,4-d] oxazol-4-one - a protected fragment of novenamine. *Tetrahedron* **2005**, *61* (45), 10683–10688.

(215) Rao, M. L. N.; Kumar, A. Pd-catalyzed chemo-selective mono-arylations and bis-arylations of functionalized 4-chlorocoumarins with triarylbismuths as threefold arylating reagents. *Tetrahedron* **2014**, *70* (39), 6995–7005.

(216) Gaskell, L. M.; Ellis, K. C. Defining a simplified pharmacophore for simocyclinone D8

inhibition of DNA gyrase, Virginia Commonwealth University, **2013**, M.Sc, 1–132.

(217) Frank, R. L.; Hall, H. K. Monocyclic terpenes from cyclic 1,3-diketones. *J. Am. Chem. Soc.* **1950**, *72* (4), 1645–1648.

(218) Khojasteh, S. C.; Oishi, S.; Nelson, S. D. Metabolism and toxicity of menthofuran in rat Liver slices and in rats. *Chem. Res. Toxicol.* **2010**, *23* (11), 1824–1832.

(219) Larsen, D. S.; O'Shea, M. D. Synthetic approaches to the angucycline antibiotics: the total syntheses of (+/-)-rubiginone B1 and B2, (+/-)-emycin A, and related analogues. *J. Chem. Soc. Perkin Trans. 1* **1995**, (8), 1019–1028.

(220) Guingant, A.; Manuel Barreto, M. A new route for the efficient synthesis of (±)ochromycinone, a naturally occurring benz[a] anthraquinone. *Tetrahedron Lett.* **1987**, *28* (27), 3107–3110.

(221) Perkin, W. H. On the hydride of aceto-salicyl. *J. Chem. Soc.* **1868**, (21), 181–186.

(222) Perkin, W. H. On the artificial production of coumarin and formation of its homologues. *J. Chem. Soc.* **1868**, (21), 53–63.

(223) Crawford, M.; Shaw, J. A. M. The course of the Perkin coumarin synthesis. Part I. *J. Chem. Soc.* **1953**, 3435–3439.

(224) Breslow, D. S.; Hauser, C. R. Condensations brought about by bases V. The condensation of the anhydride with the aldehyde in the Perkin synthesis. *J. Am. Chem. Soc.* **1939**, *61* (4), 786–792.

(225) Hauser, C. R.; Breslow, D. S. Condensations brought about by bases VI. The mechanism of the Perkin synthesis. *J. Am. Chem. Soc.* **1939**, *61* (4), 793–798.

(226) Chandrasekhar, S.; Karri, P. Revised mechanism and improved methodology for the Perkin condensation. Resuscitation of the mechanism involving benzal acetate and the improbability of the enolate of acetic anhydride. *Tetrahedron Lett.* **2006**, *47* (13), 2249–2251.

(227) Kochhar, K. S.; Bal, B. S.; Deshpande, R. P.; Rajadhyaksha, S. N.; Pinnick, H. W. Protecting groups in organic synthesis. Part 8. Conversion of aldehydes into geminal diacetates. *J. Org. Chem.* **1983**, *48* (10), 1765–1767.

(228) Man, E. H.; Sanderson, J. J.; Hauser, C. R. Boron fluoride catalyzed addition of aliphatic anhydrides to aldehydes. *J. Am. Chem. Soc.* **1950**, *72* (2), 847–848.

(229) Robertson, A.; Sandrock, W. F.; Hendry, C. B. Hydroxy-carbonyl compounds Part V. The preparation of coumarins and 1 : 4-pyrones from phenol, p-cresol, quinol, and α-naphthol. *J. Chem. Soc.* **1931**, No. 0, 2426–2432.

(230) Sethna, S. M.; Shah, R. C. 203. Aluminium chloride, a new reagent for the condensation of β-ketonic esters with phenols. Part II. The condensation of 2 : 4-dihydroxy-5-ethylbenzoic acid and its methyl ester with ethyl acetoacetate. *J. Chem. Soc.* **1938**, 1066–1069.

(231) Zafaruddin Ahmad, S.; Desai, R. D. Heterocyclic compounds. Part III. The synthesis of cyclopenteno- (1': 2': 2: 3)-chromones, and a discussion on the mechanism of the Pechmann and the Simonis reactions. *Proc. Indian Acad. Sci.* **1937**, *6* (1), 6–11.

(232) Daru, J.; Stirling, A. Mechanism of the Pechmann reaction: a theoretical study. *J. Org. Chem.* **2011**, *76* (21), 8749–8755.

(233) Clayden, J.; Greeves, N.; Warren, S. Organic Chemistry; Oxford University Press, **2012**, 1–1234.

(234) Bogdal, D. Coumarins: fast synthesis by Knoevenagel condensation under microwave irradiation. *J. Chem. Res. Synopses* **1998**, (8), 468–469.

(235) Song, A.; Wang, X.; Lam, K. S. A convenient synthesis of coumarin-3-carboxylic acids via Knoevenagel condensation of Meldrum's acid with ortho-hydroxyaryl aldehydes or ketones. *Tetrahedron Lett.* **2003**, *44* (9), 1755–1758.

(236) Bigi, F.; Chesini, L.; Maggi, R.; Sartori, G. Montmorillonite KSF as an inorganic, water stable, and reusable catalyst for the Knoevenagel synthesis of coumarin-3-carboxylic acids. *J. Org. Chem.* **1999**, *64* (3), 1033–1035.

(237) Chimenti, F.; Secci, D.; Bolasco, A.; Chimenti, P.; Bizzarri, B.; Granese, A.; Carradori, S.; Yáñez, M.; Orallo, F.; Ortuso, F.; et al. Synthesis, molecular modeling, and selective inhibitory activity against human monoamine oxidases of 3-carboxamido-7-substituted coumarins. *J. Med. Chem.* **2009**, *52* (7), 1935–1942.

(238) Watson, B. T.; Christiansen, G. E. Solid phase synthesis of substituted coumarin-3-carboxylic acids via the Knoevenagel condensation. *Tetrahedron Lett.* **1998**, *39* (33), 6087–6090.

(239) Iles, A.; Fortt, R.; de Mello, A. J. Thermal optimisation of the Reimer-Tiemann reaction using thermochromic liquid crystals on a microfluidic reactor. *Lab Chip* **2005**, *5* (5), 540–544.

(240) Akselsen, Ø. W.; Skattebøl, L.; Hansen, T. V. Ortho-formylation of oxygenated phenols.

Tetrahedron Lett. **2009**, *50* (46), 6339–6341.

(241) Hofsløkken, N.; Skattebøl, L. Convenient method for the ortho-formylation of phenols. *Acta Chem. Scand.* **1999**, *53*, 258–262.

(242) Buckle, D. R.; Cantello, B. C. C.; Smith, H.; Spicer, B. A. Antiallergic activity of 4-hydroxy-3-nitrocoumarins. *J. Med. Chem.* **1975**, *18* (4), 391–394.

(243) Perrella, F. W.; Chen, S.-F.; Behrens, D. L.; Kaltenbach III, R. F.; Seitz, S. P. Phospholipase C inhibitors: a new class of agents. *J. Med. Chem.* **1994**, *37* (14), 2232–2237.

(244) Matos, M. J.; Santana, L.; Uriarte, E.; Serra, S.; Corda, M.; Fadda, M. B.; Era, B.; Fais, A. Tyrosine-like condensed derivatives as tyrosinase inhibitors. *J. Pharm. Pharmacol.* **2012**, *64* (5), 742–746.

(245) Dean, F. M.; Park, B. K. Activating groups for the ring expansion of coumarin by diazoethane: benzoyl, pivaloyl, arylsulphonyl, arylsulphinyl, and nitro. *J. Chem. Soc. Perkin Trans. 1* **1976**, (11), 1260–1268.

(246) Díaz, U.; García, T.; Velty, A.; Corma, A. Synthesis and catalytic properties of hybrid mesoporous materials assembled from polyhedral and bridged silsesquioxane monomers. *Chem. A Eur. J.* **2012**, *18* (28), 8659–8672.

(247) Kumar, S. An efficient one pot synthesis of 3-cyanocoumarins using phase transfer catalysis. *Orient. J. Chem.* **2009**, *25* (4), 1145–1148.

(248) Kudale, A. A.; Kendall, J.; Warford, C. C.; Wilkins, N. D.; Bodwell, G. J. Hydrolysis-free synthesis of 3-aminocoumarins. *Tetrahedron Lett.* **2007**, *48* (29), 5077–5080.

(249) Li, H. Y.; Gao, S.; Xi, Z. A colorimetric and “turn-on” fluorescent chemosensor for Zn(II) based on coumarin Shiff-base derivative. *Inorg. Chem. Commun.* **2009**, *12* (4), 300–303.

(250) Hallett, P.; Grimshaw, A. J.; Wigley, D. B.; Maxwell, A. Cloning of the DNA gyrase genes under tac promoter control: overproduction of the gyrase A and B proteins. *Gene* **1990**, *93* (1), 139–142.

(251) Osheroff, N.; Bjornsti, M.-A. DNA topoisomerase protocols . In *Methods in Molecular Biology*; Walker, J., Ed.; Humana Press, **2001**; (95), 25–33.

(252) Gordeev, M. F.; Hackbarth, C.; Barbachyn, M. R.; Banitt, L. S.; Gage, J. R.; Luehr, G. W.; Gomez, M.; Trias, J.; Morin, S. E.; Zurenko, G. E.; et al. Novel oxazolidinone-quinolone

hybrid antimicrobials. *Bioorg. Med. Chem. Lett.* **2003**, *13* (23), 4213–4216.

(253) Fung, H. B.; Kirschenbaum, H. L.; Ojofeitimi, B. O. Linezolid: an oxazolidinone antimicrobial agent. *Clin. Ther.* **2001**, *23* (3), 356–391.

(254) Paladino, J. A. Linezolid: an oxazolidinone antimicrobial agent. *Am. J. Helth. Syst. Pharm.* **2002**, *59* (24), 2413–2425.

(255) National Committe for Clinical Laboratory Standards. Methods for dilution antimicrobial susceptibility tests for bacteria that grow aerobically. 5th ed. **2000**.

(256) Hubschwerlen, C.; Specklin, J.-L.; Sigwalt, C.; Schroeder, S.; Locher, H. H. Design, synthesis and biological evaluation of oxazolidinone–quinolone Hybrids. *Bioorg. Med. Chem.* **2003**, *11* (10), 2313–2319.

(257) Fajdetić, A.; Čipčić Paljetak, H.; Lazarevski, G.; Hutinec, A.; Alihodžić, S.; Đerek, M.; Štimac, V.; Andreotti, D.; Šunjić, V.; Berge, J. M.; et al. 4″-O-(ω-quinolylamino-alkylamino)propionyl derivatives of selected macrolides with the activity against the key erythromycin resistant respiratory pathogens. *Bioorg. Med. Chem.* **2010**, *18* (17), 6559–6568.

(258) Pavlović, D.; Mutak, S. Discovery of 4′′-ether linked azithromycin-quinolone hybrid series: influence of the central linker on the antibacterial activity. *ACS Med. Chem. Lett.* **2011**, *2* (5), 331–336.

(259) Pokrovskaya, V.; Belakhov, V.; Hainrichson, M.; Yaron, S.; Baasov, T. Design, synthesis, and evaluation of novel fluoroquinolone–aminoglycoside hybrid antibiotics. *J. Med. Chem.* **2009**, *52* (8), 2243–2254.

(260) Emami, S.; Foroumadi, A.; Faramarzi, M. A.; Samadi, N. Synthesis and antibacterial activity of quinolone-based compounds containing a coumarin moiety. *Arch. der Pharm. (Weinheim, Ger.* **2008**, *341* (1), 42–48.

(261) Guo, Q.; Liu, M.-L.; Feng, L.-S.; Lv, K.; Guan, Y.; Guo, H.-Y.; Xiao, C.-L. Synthesis and In-vitro antimycobacterial activity of fluoroquinolone derivatives containing a coumarin moiety. *Arch. der Pharm. (Weinheim, Ger.* **2011**, *344* (12), 802–809.

(262) European Committee for Antimicrobial Susceptibility Testing of the European Society of Clinical Microbiology and Infectious Diseases. Determination of minimum inhibitory concentrations (MICs) of antibacterial agents by agar dilution. *Clinical Microbiology and Infection Eucast Definitive Document E.* **2000**, 509–515.

(263) Hopewell, R.; Oram, M.; Briesewitz, R.; Fisher, L. M. DNA cloning and organization of the Staphylococcus aureus gyrA and gyrB genes: close homology among gyrase proteins and implications for 4-quinolone action and resistance. *J. Bacteriol.* **1990**, *172* (6), 3481–3484.

(264) Ambrus, J. I. Development of potential dual-action antibacterial agents. Ph.D. Thesis, University of Wollongong: Australia , **2008**, PhD, 1–259.

(265) Vosburg, D. A.; Weiler, S.; Sorensen, E. J. Concise stereocontrolled routes to fumagillol, fumagillin, and TNP-470. *Chirality* **2003**, *15* (2), 156–166.

(266) Landquist, J. K. 815. Some degradation products of fumagillin. *J. Chem. Soc.* **1956**, 4237–4245.

(267) Schenck, J. R.; Hargie, M. P.; Tarbell, D. S.; Hoffman, P. Decatetraenedioic acid, a fumagillin degradation product. *J. Am. Chem. Soc.* **1953**, *75* (9), 2274.

(268) Gaskell, L. M.; Thuy, N.; Ellis, K. C. Defining a minimum pharmacophore for simocyclinone D8 disruption of DNA gyrase binding to DNA. *Med. Chem. Res.* **2014**, *23* (8), 3632–3643.

(269) Hadden, M. K.; Blagg, B. S. Dimeric approaches to anti-cancer chemotherapeutics. *Anticancer Agents Med. Chem.* **2008**, *8* (7), 807–816.

(270) Burlison, J. A.; Blagg, B. S. Synthesis and evaluation of coumermycin A1 analogues that inhibit the Hsp90 protein folding machinery. *Org. Lett.* **2006**, *8* (21), 4855–4858.

(271) Montalbetti, C. A. G. N.; Falque, V. Amide bond formation and peptide coupling. *Tetrahedron* **2005**, *61* (46), 10827–10852.

(272) El-Faham, A.; Albericio, F. Peptide coupling reagents, more than a letter soup. *Chem. Rev. (Washington, DC, United States)* **2011**, *111* (11), 6557–6602.

(273) Kusuma, B. R.; Peterson, L. B.; Zhao, H.; Vielhauer, G.; Holzbeierlein, J.; Blagg, B. S. Targeting the heat shock protein 90 dimer with dimeric inhibitors. *J. Med. Chem.* **2011**, *54* (18), 6234–6253.

(274) Anandan, S.-K.; Ward, J. S.; Brokx, R. D.; Bray, M. R.; Patel, D. V; Xiao, X. X. Mercaptoamide-based non-hydroxamic acid type histone deacetylase inhibitors. *Bioorg. Med. Chem. Lett.* **2005**, *15* (8), 1969–1972.

(275) Cooper, M. A. Optical biosensors in drug discovery. *Nat. Rev. Drug Discov.* **2002**, *1* (7), 515–528.

(276) Plattner, J. J.; Fung, A. K.; Parks, J. A.; Pariza, R. J.; Crowley, S. R.; Pernet, A. G.; Bunnell,

P. R.; Dodge, P. W. Substituted 5,6-dihydrofuro[3,2-f]-1,2-benzisoxazole-6-carboxylic acids: high-ceiling diuretics with uricosuric activity. *J. Med. Chem.* **1984**, *27* (8), 1016–1026.

(277) Kasabe, A.; Mohite, V.; Ghodake, J.; Vidhate, J. Synthesis, characterization and primary antimicrobial, antifungal activity evaluation of schiff bases of 4-chloro-(3-substituted-phenylimino) - methyl-[2H] - chromene-2-one. *Eur. J. Chem.* **2010**, *7* (2), 377–382.

(278) Iaroshenko, V. O.; Mkrtchyan, S.; Gevorgyan, A.; Vilches-Herrera, M.; Sevenard, D. V; Villinger, A.; Ghochikyan, T. V; Saghiyan, A.; Sosnovskikh, V. Y.; Langer, P. Synthesis of heteroannulated 3-nitro- and 3-aminopyridines by cyclocondensation of electron-rich aminoheterocycles with 3-nitrochromone. *Tetrahedron* **2012**, *68* (11), 2532–2543.

(279) Jung, S. H.; Cho, S. H.; Dang, T. H.; Lee, J. H.; Ju, J. H.; Kim, M. K.; Lee, S. H.; Ryu, J. C.; Kim, Y. Structural requirement of isoflavonones for the inhibitory activity of interleukin-5. *Eur. J. Med. Chem.* **2003**, *38* (5), 537–545.

(280) Dakin H., D. The condensation of aromatic aldehydes with glycine and acetylglycine. *J. Biol. Chem.* **1929**, *82*, 429–433.

(281) Das, D. K.; Sarkar, S.; Khan, M.; Belal, M.; Khan, A. T. A mild and efficient method for large scale synthesis of 3-aminocoumarins and its further application for the preparation of 4-bromo-3-aminocoumarins. *Tetrahedron Lett.* **2014**, *55* (35), 4869–4874.

(282) Messaoudi, S.; Brion, J.-D.; Alami, M. An Expeditious copper-catalyzed access to 3-aminoquinolinones, 3-aminocoumarins and anilines using sodium azide. *Adv. Synth. Catal.* **2010**, *352* (10), 1677–1687.

(283) Costa, M.; Rodrigues, A. I.; Proença, F. Synthesis of 3-aminochromenes: the Zincke reaction revisited. *Tetrahedron* **2014**, *70* (33), 4869–4875.

(284) Koga, H.; Itoh, A.; Murayama, S.; Suzue, S.; Irikura, T. Structure-activity relationships of antibacterial 6,7- and 7,8-disubstituted 1-alkyl-1,4-dihydro-4-oxoquinoline-3-carboxylic acids. *J. Med. Chem.* **1980**, *23* (12), 1358–1363.

(285) Cantrell, T. S. Carboxylation of cyclooctatetraene dianion. Structures and reactions of the dicarboxylic acids produced. *J. Am. Chem. Soc.* **1970**, *92* (18), 5480–5483.